Characterization and Exploitation of the Glycocalyx for Drug Delivery

by

Michael Joseph Palte

A dissertation submitted in partial fulfillment

of the requirements for the degree of

Doctor of Philosophy

(Molecular and Cellular Pharmacology)

at the

UNIVERSITY OF WISCONSIN–MADISON

2012

Date of final oral examination: 05/04/12
The dissertation is approved by the following members of the Final Oral Committee:
Ronald T. Raines, *Henry Lardy Professor of Biochemistry*, Biochemistry and Chemistry
Sandro Mecozzi, Associate Professor, Pharmaceutical Sciences
Deane Mosher, Professor, Biomolecular Chemistry
Arnold E. Ruoho, Professor, Neuroscience
Jamey Weichert, Associate Professor, Radiology

Characterization and Exploitation of the Glycocalyx for Drug Delivery

Michael Joseph Palte

Under the supervision of Professor Ronald T. Raines

at the University of Wisconsin–Madison

Of the 30,000 or so genes encoded by the human genome, approximately 10% are druggable by small molecules. Hence, the majority of disease states are likely intractable to modulation by small molecule therapeutics. Macromolecular biologics, such as DNA, RNA, and proteins, have shown great promise as curative therapies. Nevertheless, this class of drugs is not readily translatable into clinical treatments. The main hurdle for clinical use of biologics is efficient delivery to their site of action. This thesis describes ways to address the issues of inefficient biologic delivery.

In Chapter Two, I detail the characterization of the interactions of nucleic acids with the glycocalyx, which is one of the main barriers to entry inside the cell. In Chapters Three and Four, I describe a method to take advantage of the anionic glycocalyx for a timed-release prodrug strategy. By attaching a ribonucleoside 3′-phosphate to a drug of interest, the biodistribution into the cytoplasm of cells is prevented until the parent drug is released by a ribonuclease, which occurs in a time-dependent fashion. This strategy allows for greater temporal modulation of the concentration of active drug. Finally, in

Chapter Five I describe a method to take advantage of the glycocalyx to enhance the delivery of proteins. Since protein therapeutics can be delivered into cells by endocytosis, the delivery of a protein can be enhanced by increasing the affinity of that protein for the cell surface. Boronic acids readily form boronate esters with the 1,2- and 1,3-diols of saccharides, such as those that coat the surface of mammalian cells. Here, pendant boronic acids are shown to enhance the cytosolic delivery of a protein toxin. Thus, boronates are a non-cationic carrier that can deliver a polar macromolecule into mammalian cells.

Acknowledgments

I would like to express my deepest gratitude to everyone who has provided me with guidance, advice, and assistance throughout my graduate career and prior to entrance into graduate school. First and foremost, I am grateful to my advisor, Professor Ron T. Raines. While interviewing at several biochemistry departments thoughout the country, I was enthralled by the diversity of research conducted in the Raines Lab. I wanted to learn the fundamentals of both organic chemistry and biochemistry during graduate school. I specifically enrolled in the MSTP program at the University of Wisconsin to join the Raines Lab. My experiences in the Raines Lab have made me into the scientist I am today, and have substantially molded my vision on how I want to run my own lab someday. I am extreamely grateful for the collaborative environment of the Raines Lab and the freedom Ron gives us to pursue and develop our own ideas. After joining the lab, I viewed it as a "scientific playground" where I was free to try any technique or assay that was remotely applicable to my projects. Consequently, I was constantly exposed to new science that has enabled me to have a wide breadth of experiences that most graduate students do not acquire. I am extremely grateful for these scientific experiences, which is a direct consequence of having joined a lab of multidisiplanary science. Finally, I'd like to especially thank Ron for superbly editing our manuscripts and taking great care to present our science in a straightforward and easily comprehensible way.

Throughout my entire life, I have strived to continually surround myself with people who are smarter than me and I continued this practice in graduate school. The diversity of science attracted me to the Raines Lab, but what sold me on joining the Raines Lab was the opportunity to work with incredible graduate students and postdocs with a wide array of expertise. I can say with sincerity that everyone I overlapped with during graduate school, both inside and outside the lab, significantly contributed to my development as a scientist. Within the Raines Lab, I have had the privilege to work alongside Tom Rutkoski, Jeet Kalia, Annie Tam, Luke Lavis, Cindy Chao, Kelly Gorres, Nicole McElfresh, Mariëlle Delville, Joe Binder, Margie Borra, Daniel Gottlieb, Rex Watkins, Katrina Jensen, Christine Bradford, Chelcie Eller, Sean Johnston, Mike Levine, Joelle Lomax, Nadia Sundlass, Langdon Martin, Greg Jakubczak, Matt Shoulders, Rebecca Turcotte, Sayani Chattopadhyay, Kristen Andersen, Trish Hoang, Rob Presler, Jim Vasta, Matt Aronoff, Rob Newberry, Thom Smith, Ian Windsor, Raso Biswas, Ho-Hsuan Chou, Kevin Desai, Caglar Tanrikulu, and Brett VanVeller. I am especially grateful to Amit Choudhary for his friendship, teaching me the fundamental techniques of organic chemistry when I first joined the lab, and always giving me valuable advice on pursuing a career in academia. Likewise, I am extremely grateful to Eddie Myers for always taking the time to discuss my science, encouraging me to pursue my own ideas, collaborating with me, and his friendship. Lastly, I am exceptionally grateful for the friendships and collaborations with Greg Ellis, Ben Caes, Nick McGrath, and John Lukesh III. Without Amit, Eddie, Greg, Ben, Nick, and John, graduate school would have been much more difficult. Special thanks are due to the high school and undergraduate

students I was able to mentor: Eric Thornton, Amy Davis, Wes Maier, Rachel Kean, and Emily Fox.

I am grateful for the helpful advice of my thesis committee: Professors Sandro Mecozzi, Deane Mosher, Arnold E. Ruoho, and Jamey Weichert. I am also thankful for the many invaluable discussions I have had with Dr. Darrell McCaslin, Dr. Martha Vestling, Dr. Mark Anderson, Dr. Milo Westler, Dr. Charlie Fry, and Matt Morgan. I am also appreciative of the mentorship of my undergraduate advisors at the University of Michigan, Professors Yehoash Raphael and Blake Roessler, who taught me the fundamentals of research, which helped me to succeed as a graduate student.

I owe many thanks to the Medical Scientist Training Program, especially the director Deane Mosher and administrator Paul Cook. Additionally, I am grateful to the MSTP students that have offered me great advice and friendship throughout my time in Madison. I am grateful to my clinical mentors, Dr. Bennett Vogelman and Dr. Azita Hamedani, for their invaluable medical insight and willingness to advise me throughout graduate school.

Lastly and most importantly, I am eternally grateful for my family, current and future. I would not be a MD/PhD student if it were not for the constant support (both emotionally and financially) and encouragement from my parents, Suzanne and Larry Palte, to pursue a career in science. I was fortunate to grow up in the shadows of my two brothers, Chris and Eric Palte, both of which provided me with great examples on how to excel in scientific careers. I would like to thank my future family, the Kubiaks and

Soukups for welcoming me into their family. Above all, I am grateful for my greatest achievement during graduate school, having found my soulmate and future wife, Rachel Kubiak. Words cannot express my gratitude and excitement towards starting our lives together. I couldn't have finished graduate school and I can't imagine my future without her. To her, all I can say is "stuck with me!"

Table of Contents

List of Tables

List of Schemes

List of Figures

List of Abbreviations

ε	extinction coefficient
5-IAF	5-iodoacetamidofluorescein
6-FAM	6-carboxyfluorescein
6-TAMRA	6-carboxytetramethylrhodamine
A	adenosine
A	anisotropy
A_B	anisotropy of bound species
A_F	anisotropy of free species
A_{OBS}	anisotropy observed (sample)
ADEPT	antibody-directed enzyme prodrug therapy
ADME	absorption, distribution, metabolism, and excretion
Ala or A	alanine
ALS	amyotrophic lateral sclerosis, Lou Gehrig's disease
ANG	angiogenin
Arg or R	arginine
Asp or D	aspartate or aspartic acid
ATCC	American Type Culture Collection
B	boronic acid
BCA	bicinchoninic acid
Benzoboroxole	2-hydroxymethylphenylboronic acid

BSA	bovine serum albumin
BS-RNase	bovine seminal ribonuclease
ca.	circa, approximately
cDNA	complementary deoxyribonucleic acid
CHO	Chinese hamster ovary
CPP	cell-penetrating peptide
d	day
Da	Dalton
ddH_2O	distilled, deionized water
DCM	dichloromethane
DEPC	diethylpyrocarbonate
DEF	2′,7′-diethylfluorescein
DEFIA	2′,7′-diethylfluorescein-5-iodoacetamide
DMEM	Dulbecco's modified Eagle's medium
DMF	dimethylformamide
DMSO	dimethylsulfoxide
DNA	deoxyribonucleic acid
DOPC	1,2-dioleoyl-*sn*-glycero-3-phosphocholine
DPBS	Dulbecco's phosphate-buffered saline
DRNG RNase A	D38R/R39D/N67R/G88R variant of RNase A
DTNB	5,5′-dithiobis(2-nitrobenzoic acid)
DTT	dithiothreitol

E	enzyme
ECP	eosinophilic cationic protein; RNase 3
EDC	*N*-(3-dimethylaminopropyl)-*N*′-ethylcarbodiimide hydrochloride
EDN	eosinophil-derived neurotoxin; RNase 2
EDTA	ethylenediaminetetraacetic acid
F	fluorescence
F_{SB}	fraction bound
FACS	fluorescence-activated cell sorting
FBS	fetal bovine serum
FDA	United States Food and Drug Administration
FPLC	fast performance liquid chromatography
FRET	Förster resonance energy transfer
GFP	green fluorescent protein
GSH	reduced glutathione
GSSH	oxidized glutathione
h	hour
HCl	hydrochloric acid
HEPES	2[4-(2-hydroxyethyl)-1-piperazinyl]ethanesulfonic acid
His, H	histidine
HIV	human immunodeficiency virus
HPLC	high performance (pressure) liquid chromatography
HSPG	heparan sulfate proteoglycan

HT	4-hydroxytamoxifen
I	inhibitor
IC_{50}	half maximal inhibitory concentration
IPTG	isoproyl-1-thio-β-D-galactopyranoside
k_{cat}	first-order enzymatic rate constant
K_d	equilibrium dissociation constant
kDa	kilodalton
K_i	inhibitor dissociation constant
K_M	Michaelis constant
λ_{em}	emission wavelength
λ_{ex}	excitation wavelength
LB	Luria–Bertani medium
logD	distribution coefficient
logP	partition coefficient
MALDI–TOF	matrix-assisted laser desorption/ionization time-of-flight
MEM	minimum essential medium
MeOH	methanol
MES	2-(N-morpholino)-ethanesulfonic acid
Met	metronidazole
MHz	megahertz
microRNA	micro ribonucleic acid
min	minute

mRNA	messenger ribonucleic acid
MW	molecular weight
MWCO	molecular weight cutoff
NaCl	sodium chloride
NaOH	sodium hydroxide
NBS	non-binding surface
Neu5Ac	*N*-acetylneuraminic acid
NMR	nuclear magnetic resonance
OD	optical density
OVS	oligo(vinylsulfonic acid)
p value	probability value
PBA	phenylboronic acid
PBS	phosphate-buffered saline
PCR	polymerase chain reaction
PDB	protein data bank
PEG	poly(ethylene glycol)
p*I*	isoelectric point
pK_a	log of the acid dissociation constant
PMSF	phenylmethane sulfonyl fluoride
PPI	protein–protein interaction
pRI	porcine ribonuclease inhibitor
PTD	protein transduction domains; cell-penetrating peptide

Q	ratio of fluorescence intensities of bound and free species
R_9, Arg_9	nonaarginine
RGD	arginine-glycine-aspartate tripeptide
Rh_{110}	rhodamine 110
RI	ribonuclease inhibitor
RNA	ribonucleic acid
RNAi	ribonucleic acid interference
RNase A	bovine pancreatic ribonuclease
RNase 1	human pancreatic ribonuclease
RPMI	Roswell Park Memorial Institute medium
rRNA	ribosomal ribonucleic acid
S	saccharide
s	second
SDS-PAGE	sodium dodecyl sulfate polyacrylamide gel electrophoresis
Ser or S	serine
SMSF	Small Molecule Screening Facility
STP	4-sulfo-2,3,5,6-tetrafluorophenol, sodium salt
t	time
TAT	residues 47–57 of the HIV-1 trans-activator of transcription
TB	terrific broth
T_m	temperature at the midpoint of the denaturation curve
TLC	thin-layer chromatography

THF	tetrahydrofuran
TML	trimethyl lock
TMS	tetramethylsilane
TNB	2-nitro-5-thiobenzoate
Tris	2-amino-2-(hydroxymethyl)-1,3-propanediol
U	uridine
U>p	uridine 2′,3′-cyclic phosphate
Up	uridine 3'-phosphate
uPa, urokinase	urokinase-type plasmogen activator
UpHT	uridine 3'-(4-hydroxytamoxifen phosphate)
UV	ultraviolet
UW	University of Wisconsin
UWCCC	University of Wisconsin Carbone Cancer Center
v/v	volume per volume
w/v or wt/vol	weight per volume
Z	net molecular charge (Arg + Lys – Asp – Glu

Chapter One

Characterization and Exploitation of the Glycocalyx for Drug Delivery

Abstract: Of the 30,000 or so genes encoded by the human genome, approximately 10% are druggable by small molecules. Hence, the majority of disease states are likely intractable to modulation by small molecule therapeutics. Macromolecular biologics, such as DNA, RNA, and proteins, have shown great promise as curative therapies. Nevertheless, this class of drugs is ot readiliy translatable into clinical treatments. The main hurdle for clinical use of biologics is efficient delivery to their site of action. This thesis describes ways to address the issues of inefficient biologic delivery.

In Chapter Two, I detail the characterization of the interactions of nucleic acids with the glycocalyx, which is one of the main barriers to entry inside the cell. In Chapters Three and Four, I describe a method to take advantage of the anionic glycocalyx for a timed-release prodrug strategy. By attaching a ribonucleoside 3′-phosphate to a drug of interest, the biodistribution into the cytoplasm of cells is prevented until the parent drug is released by a ribonuclease, which occurs in a time-dependent fashion. This strategy allows for greater temporal modulation of the concentration of active drug. Finally, in Chapter Five I describe a method to take advantage of the glycocalyx to enhance the delivery of proteins. Since protein therapeutics can be delivered into cells by endocytosis, the delivery of a protein can be enhanced by increasing the affinity of that protein for the cell surface. Boronic acids readily form boronate esters with the 1,2- and 1,3-diols of saccharides, such as those that coat the surface of mammalian cells. Here, pendant

boronic acids are shown to enhance the cytosolic delivery of a protein toxin. Thus, boronates are a non-cationic carrier that can deliver a polar macromolecule into mammalian cells.

1.1 The Need for Biologic Therapeutics

Modern medicine is dominated by small-molecule drugs for the treatment of disease. Yet, numerous disease states are undruggable by small molecules. The basic components of life, and therefore the basic components of a diseased state, can be broken down into five classes of molecules: carbohydrates, lipids, proteins, nucleic acids, and metabolites. Generally, small molecules are only able to modulate the activity of proteins, significantly limiting their utility towards most disease processes. Of the approximate 30,000 genes in the human genome it is estimated that only 10% of those genes encode a protein that are "druggable," meaning that the protein has a predicted fold amenable to interacting with a small molecule.[3,4] Consequently, only a small fraction of the biomolecules that compose a diseased state are actually tractable to modulation by a small molecule. To expand the arsenal of therapeutics for medicine, macromolecular drugs need to be developed and enlisted for clinical use. In the past thirty years, significant progress has been made towards improving the properties of biologics for therapeutic use. Nevertheless, inefficient delivery of these macromolecular compounds into cells precludes them from the clinic.[5-7]

1.2 The Advent of Gene Therapy

A little over 50 years ago, Francis Crick walked into the Eagle Pub in Cambridge, UK and declared, "We have found the secret of life."[8,9] He was referring to having just discovered

that DNA is a double helix. This was the final puzzle to be solved in understanding the basic components of genetic inheritance. That same year, the Hershey–Chase experiment was published, providing substantial evidence that DNA was the genetic material of a cell.[10] Shortly thereafter, in 1956, Vernon Ingram published the first description of a genetic disease by demonstrating that sickle cell anemia was caused by a single point mutation.[11] Consequently, the race to treat genetic diseases through proper gene expression began.

The first attempts at gene therapy required two essential components: an efficient method for gene transfer, and the ability to synthesize or clone genes. During the 1960s and 1970s, the genetic code was deciphered, the first gene was synthesized, and modern cloning techniques were developed.[12-14] In 1973, calcium phosphate-mediated gene transfer was invented and led to the second attempt at inserting a gene into a human for therapeutic benefit.[13] Nevertheless, due to the inefficiency of calcium phosphate transfection, this human gene therapy trial was ultimately doomed for failure.[13,15-17] The 1990s saw a renewed interest in gene therapy trials. During this era of biotechnology, viral vectors were the most efficient method for inserting genes into mammalian cells.[13] Unfortunately, the use of viral vectors was shown to induce life-threatening and sometimes lethal immunological responses,[18] and at times, oncogenesis in the target cells.[19] Only in recent years was the first successful gene therapy trial completed wherein two out of three patients were cured of chronic lymphoid leukemia, with the third patient having a partial remission.[20] In summary, the promise of gene therapy as a therapeutic technique is quite enticing, but a safe and efficient method of transferring genes into target cells continues to be the primary hurdle towards its clinical adoption.

1.3 Chemical Transfection Reagents

In 1973, calcium phosphate became the first effective chemical transfection reagent.[21,22] During the 1980s, efficient delivery of DNA using cationic lipids[23] and cationic polymers[24] was first reported. This technology still persists today and most contemporary transfection reagents are some form of poly-cationic polymer. The currently understood mechanism of delivery is described as a condensation of DNA by the cationic polymer, giving the overall complex a net positive charge. This DNA-polymer complex can then associate with the anionic glycocalyx, allowing for endocytosis and eventual delivery of the DNA inside the cell.[25] Generally, reports focus on the amount of positive charge required to mask the negative charge of the nucleic acid.[26-29] Prior to the publication described in Chapter Two, there was not a thorough analysis of the unfavorable interaction between DNA and the glycocalyx.[29]

1.4 Barriers to Cytosolic Nucleic Acid Delivery

The "cell coat," now commonly referred to as a glycocalyx, was first described by electron microscopists as a carbohydrate-rich layer on the surface of cells containing acidic groups.[30] It is well established that sialic acids, which contain a carboxylic acid functional group, and glycosaminoglycans (GAGs), which have carboxylic acid and sulfate functional groups, are ubiquitously expressed in mammalian cells and impart a negative charge throughout the glycocalyx.[31,32] Although this anionic barrier is one of the major hindrances for efficient delivery of anionic nucleic acids into cells, a thorough characterization of nucleic acid–glycocalyx interactions had not yet been reported.

Due to the significant Coulombic repulsive forces between nucleic acids and the cellular surface, it is difficult to analyze any interaction between them. To characterize DNA–glycocalyx interactions, one must imbue DNA with a greater affinity for the cell surface. As further described in Chapter Two, I synthesized fluorescently-labeled lipid–oligonucleotide (LO) conjugates (Figure 1.1) to create a sensitive probe to characterize glycocalyx–nucleic acid interactions. I demonstrated that both sialic acids and GAGs provide a formidable barrier for the uptake of nucleic acids by mammalian cells. This conclusion has implications for genomic stability, as well as the delivery of genes and RNAs into mammalian cells.

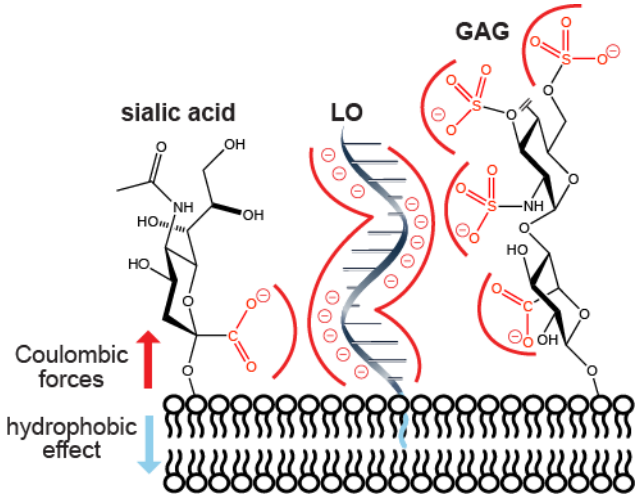

Figure 1.1 Characterization of the interactions of nucleic acids with the glycocalyx. Depiction of forces that govern the interaction of a LO conjugate with mammalian cells. The hydrophobic effect mediated by the lipid tails stabilizes a LO in a cellular membrane, enabling analysis of the consequences of Coulombic repulsion between an anionic nucleic acid and anionic sialic acid and GAGs.

1.5 Anionic Glycocalyx Mediates Biodistribution of Drugs

As described in Chapter Two, due to Coulomb's Law[33,34] the anionic glycocalyx and anionic phosphoryl groups of nucleic acids repel each other substantially.[35] This has significant implications for the biodistribution of drugs inside and outside of cells (Figure 1.2). Not only

does a negative charge prevent passive diffusion across the hydrophobic lipid-bilayer of the plasma membrane, but it also causes repulsion from the cell surface due to the anionic glycocalyx.[35] For example, phosphorylated drugs are not absorbed by the gut epithelial cells until alkaline phosphatase dephosphorylates the molecule.[36,37] If the drug then becomes neutrally charged, it would be free to diffuse into the cells. Previous work had focused primarily on masking the anionic phosphoryl groups of drugs to make phosphorylated drugs bioavailable inside the cytoplasm of the cell.[38-41] I envisioned a system in which prevention of a phosphorylated drug's uptake would be advantageous for the pharmacokinetics of anti-cancer therapeutics.

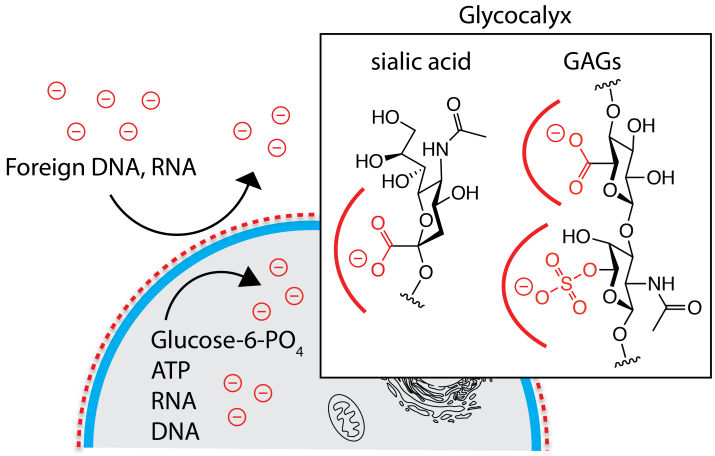

Figure 1.2 The anionic glycocalyx and the plasma membrane compartmentalize anionic molecules between the extracellular space and the cytoplasm of the cell.

Cancer is defined as the uncontrolled growth of a subset of cells in the human body. There is only a subtle difference between the biology of healthy cells and malignant cells in any given patient.[42] Consequently, chemotherapeutic agents for cancer have little selection for cancer cell death versus healthy cell death/toxicity, causing this class of drugs to have a narrow therapeutic index.[43] Since all pharmacological responses, including side effects, are relative to

the dose given, maintaining tight control over the concentrations of antineoplastic drugs in the body should help ameliorate the toxicities associated with this class of pharmaceuticals.

The ideal method to tightly control the plasma concentration of a drug would be to have a continuous parenteral administration of the drug throughout the duration of treatment. Having a constant intravenous (IV) administration of a drug for extended periods of time is, however, inpractical from a financial standpoint (requiring expert caregivers to constantly monitor the equipment), a patient safety standpoint (IV catheters are typical routes for bacteriemia, which can lead to sepsis), and a patient compliance standpoint (most patients detest undergoing IV administration of a drug for even a 2–5 h duration). By installing a pro-moiety, the pharmacokinetics of a constant IV administration of a drug can be simulated by slowly activating the drug over time. The ideal pro-moiety for timed release of an antineoplastic drug would be negatively charged to prevent the uptake of the prodrug into the cytoplasm of cells (sight of action of most drugs), easily and cheaply synthesized, and would be released slowly over time by an endogenous, promiscuous enzyme in the plasma.

Fulfilling these criteria is difficult, as few enzymes have adequate plasma concentrations and many that do have high specificity for a native substrate. Human pancreatic ribonuclease (RNase 1[44]; EC 3.1.27.5) is an exception. Contrary to its name, RNase 1 is expressed in tissues other than the pancreas[45] and circulates in human plasma at a concentration of ~0.4 mg/L.[46] Moreover, like its renowned homolog bovine pancreatic ribonuclease (RNase A[47,48]), RNase 1 catalyzes the cleavage of RNA by a transphosphorylation reaction[49-51] and has little specificity for its leaving group.[52-56] Due to the promiscuous activity of ribonucleases, I reasoned that a chemotherapeutic drug condensed with a ribonucleoside 3′-phosphate pro-moiety would be

released upon cleavage by RNase 1 slowly over time. In Chapters Three and Four, I outline a method for taking advantage of the repulsive effects of the glycocalyx with anionic ribonucleoside 3′-phosphate moieties for a timed-release prodrug strategy (Figure 1.3).

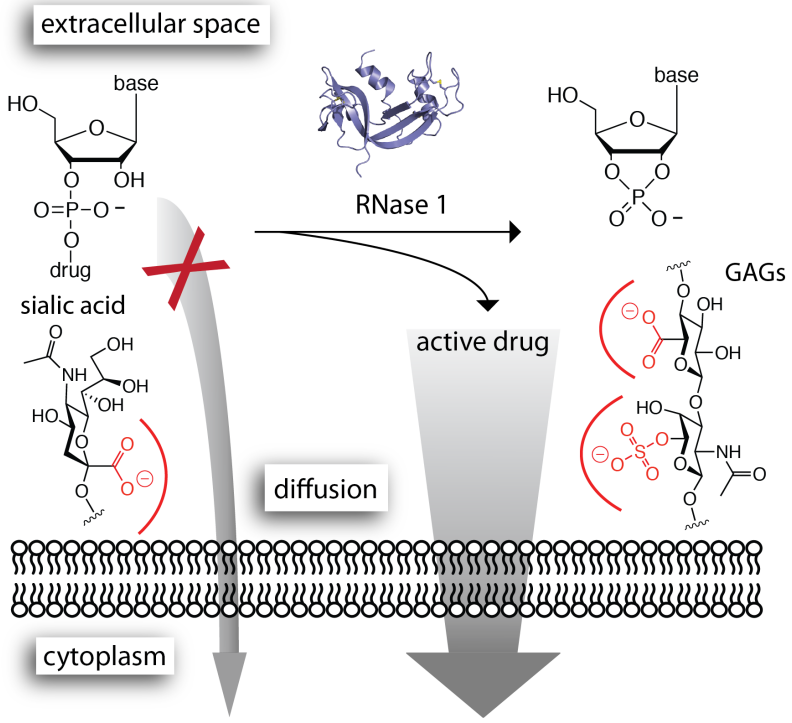

Figure 1.3 Rationale of the ribonucleoside 3′-phosphate pro-moiety to enhance the pharmacokinetics of a parent drug. Attaching a ribonucleoside 3′-phosphate to a drug prevents the drug's cytoplasmic delivery until endogenous RNAse 1 liberates it. This process occurs slowly over time, permitting this strategy to allow for the timed release of the parent drug.

1.6 Methods for Protein Delivery

The glycocalyx can not only prevent the delivery of molecules into a cell, but also be used as a "receptor" to enhance the delivery of drugs into cells. Macromolecular therapeutics are predominantly delivered into the cell by endocytosis. Therefore, increasing the affinity of the therapeutic for the cell surface, which increases its rate of endocytosis, will ultimately enhance

its cellular delivery.[23,57-62] Previous efforts have focused on enhancing endocytotic delivery by increasing cell-surface binding. For example, cationic polymers (peptidic: HIV TAT, nonaarginine; and non-peptidic: dendrimers, polyethylimine) have been used to facilitate Coulombic attraction between therapeutic agents and the anionic cell surface.[60,62-64] Natural ligands (*e.g.*, folate, substance P, and the RGD tripeptide) have also been used to target therapeutic agents to cell-surface protein receptors.[65-67] While some of these methods have had moderate clinical success, additional delivery strategies are needed. Due to the abundance of glycans on the cell surface, I reasoned that targeting therapeutic agents to these abundant saccharides would enhance their cellular delivery.

1.7 Boronic Acids Complex with Glycans

I envisioned using boronic acids to target a therapeutic to the saccharides that compose the glycocalyx. Aryl boronic acids readily form boronic esters with the 1,2- and 1,3-diols found in saccharides. Boronic acid complexation with diols is best illustrated by the thermodynamic cycle depicted in Figure 1.4.[68]

The pK_a of the labile hydroxyl (green) dictates whether boronates are in the tetrahedral or trigonal planar geometry. Upon binding a diol (an entropically driven process) the 5-membered cyclic boronic ester prefers a O-B-O angle of 113°. Therefore a sp^3 hybridized boron, which prefers a O-B-O angle of 109.5°, forms a more stable boronic ester than a sp^2 hybridized center, which prefers a O-B-O angle of 120°. From an enthalpy viewpoint, boronic acids prefer binding to diols in the sp^3 hybridization state versus the sp^2 hybridization state. The enhancement of sp^3 hybridization stabilization upon binding diols is reflected by a shift in the pK_a of the labile

hydroxyl, where $pK_a > pK_{a'}$. For example, the pK_a of the labile hydroxyl of phenyl boronic acid (PBA) is 8.8, but upon complexation with fructose, the $pK_{a'}$ shifts to 5.3.[68]

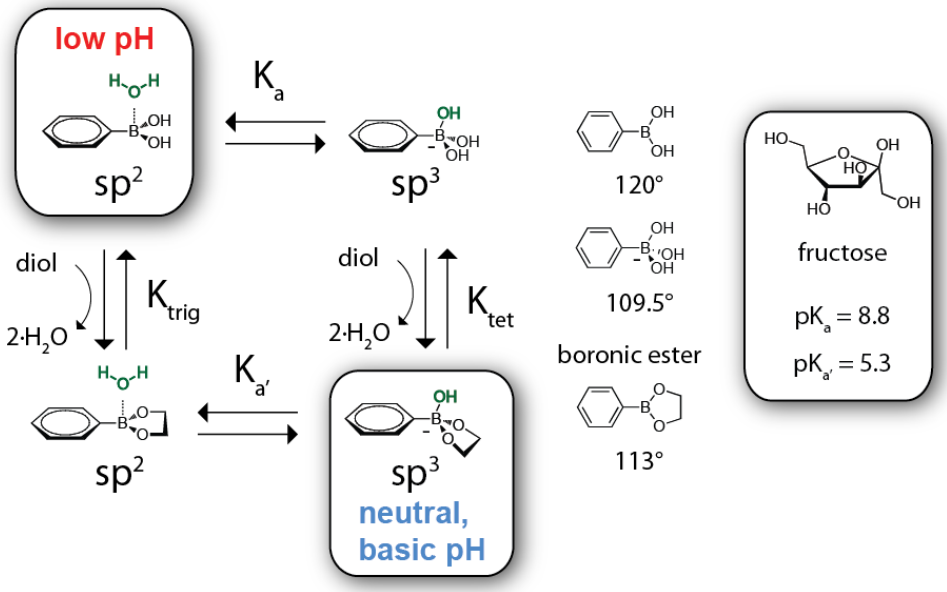

Figure 1.4 Boronic acid–diol complexation. The labile hydroxyl group is colored green.

This ability for boronic acids to bind to diols in neutral and basic conditions, but release the diol in acidic conditions, makes them perfect mediators for enhancing the cellular delivery of cargo. The boronic acid should first complex with the glycocalyx saccharides in the neutral extracellular environment. Upon endocytosis of the cargo, the endosomes will acidify to a pH of 4–5. I hypothesized that this acidification would encourage the dissociation of the boronic acid, freeing the cargo to translocate into the cytosol. A further benefit is that these acidified boronic acids would have a trigonal planar geometry and lose the formal negative charge, which is known to increase their hydrophobicity,[69] potentially allowing for them to destabilize the endosomal lipid bilayer and enhance endosomal escape.

The vast majority of biologically relevant boronic acid research has been aimed at either developing high-affinity sensors for glycans or towards developing boron neutron capture therapies for cancer.[68,70,71] Additional studies have utilized boronic acids to transport nucleotides across liposomal bilayers,[72] to label liposomes for increased affinity for erythrocyte ghosts,[73] to fluorescently label tumor-specific glycans on cells,[74] to enhance PEI–DNA complexation for transfection reagents,[75] and to function as glucose sensors for the controlled release of insulin.[76] Furthermore, boronic acid polymers have been shown to inhibit HIV entry into cells,[77] while boronate-coated surfaces have demonstrated a high affinity for cell surfaces and have been used as cancer cell detection devices.[78-81] In Chapter Five, I describe the first use of boronic acids as reagents for protein delivery (Figure 1.5).

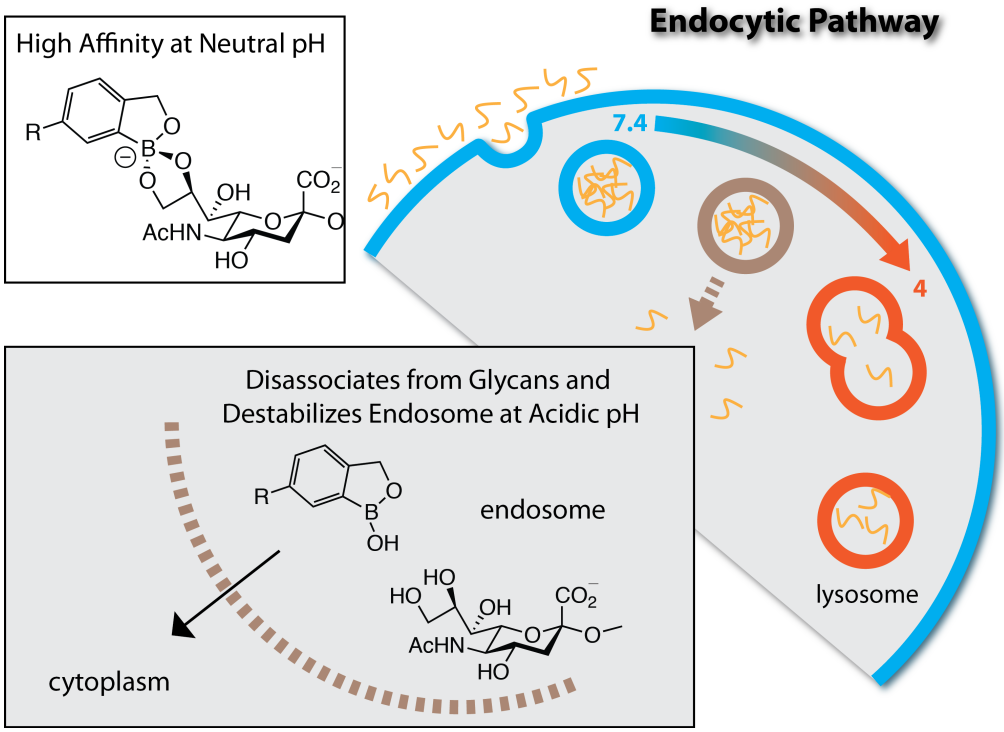

Figure 1.5 Premise for boronate-mediated biologic delivery. At the cell surface, boronates bind to cell surface glycans and mediate the enhancement of their endocytosis. Upon acidification of endosomes along the endocytotic pathway, boronates disassociate from glycans and become hydrophobic due to the loss of a formal negative charge and adoption of sp^2 hybridization. This increase in hydrophobicity could destabilize endosomes, permitting the cargo of interest to more readily escape from the endosome.

Chapter Two

Interaction of Nucleic Acids with the Glycocalyx*

* This chapter has been published in part, under the same title. Reference: Palte, M.J. & Raines, R.T. Interaction of nucleic acids with the glycocalyx. *J. Am. Chem. Soc*. 134 6218–6223 (2012).

2.1 Abstract

Mammalian cells resist the uptake of nucleic acids. The lipid bilayer of the plasma membrane presents one barrier. Here we report on a second physicochemical barrier for uptake. To create a sensitive probe for nucleic acid–cell interactions, we synthesized fluorescent conjugates in which lipids are linked to DNA oligonucleotides. We found that these conjugates incorporate readily into the plasma membrane but are not retained there. Expulsion of lipid–oligonucleotide conjugates from the plasma membrane increases with oligonucleotide length. Conversely, the incorporation of conjugates increases markedly in cells that lack the major anionic components of the glycocalyx—sialic acid and glycosaminoglycans, and in cells that had incorporated highly cationic lipids into their plasma membrane. We conclude that anionic oligosaccharides provide a formidable barrier to the uptake of nucleic acids by mammalian cells. This conclusion has implications for genomic stability, as well as the delivery of genes and siRNAs into mammalian cells.

2.2 Author Contributions

M.J.P. proposed using LOs to characterize the interaction of nucleic acids with the glycocalyx. M.J.P. performed the research and drafted the manuscript and figures. M.J.P. and R.T.R. designed experiments, analysed data, and edited the manuscript and figures.

2.3 Introduction

The efficient delivery of genes into cells could engender re-parative therapies for genetic diseases.[5,82] The advent of RNAi technology[83,84] has provoked additional interest in the cellular delivery of nucleic acids.[85-87] Delivering genes and siRNAs into cells requires that nucleic acids traverse the plasma membrane. A thorough understanding of the interaction of nucleic acids with cell-surface molecules could inspire new strategies for efficient cellular internalization.[88-93]

The mammalian cell surface is analogous to a forest, wherein phospholipid head groups are the floor, extracellular domains of transmembrane proteins are the understory, and oligosaccharides of glycolipids and glycoproteins are the canopy. These oligosac-charides, known collectively as the glycocalyx, constitute the bulk of the material on a cell surface.[94] The glycoca-lyx is highly anionic, due largely to the presence of sialic acid, which contains a carboxylate group, and glycosaminoglycans (GAGs), which contain both carboxylate and sulfate groups. As expected from Coulomb's law,[33,34] cationic and neutral molecules are delivered more readily into cells than are anionic molecules.[40,95-101] Masking the anionic charge of DNA with a highly cationic lipid (such as Lipofectamine™) facilitates the delivery of DNA into cells.[102]

To analyze the interaction of nucleic acids with the cell surface, we sought to create an equilibrating system in which nucleic acids could be localized near the glycocalyx without disrupting the biophysical characteristics of either the nucleic acids or the cell surface. We reasoned that the conjugation of a lipid tail onto a DNA oligonucleotide would enable such a system (Figure 2.1). Here, we use fluorescently labeled lipid–oligonucleotide conjugates (LOs) to characterize DNA–glycocalyx interactions. Such conjugates are known to incorporate into the

plasma mem-brane.[103-108] Our findings pro-vide insight on evolutionary imperatives and suggest new strategies for the cellular delivery of nucleic acids.

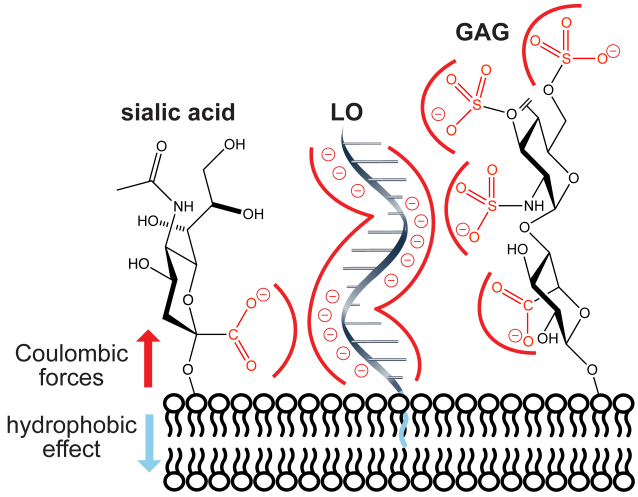

Figure 2.1 Depiction of forces that govern the interaction of a lipid–oligonucleotide conjugate (LO) with mammalian cells. The hydro-phobic effect mediated by the lipid tails stabilizes an LO in a cellular membrane, enabling analysis of the consequences of Coulombic repulsion between an anionic nucleic acid and anionic sialic acid and glycosaminoglycans (GAGs).

2.4 Results and Discussion

2.4.1 LO and Medium Attributes that Affect Incorporation.

Our initial experiments used confocal microscopy to observe the interaction of synthetic LOs (Table 2.1) with live mammalian cells. We found that LOs were incorporated into the plasma membrane in a concentration-dependent manner that relied on the presence of the lipid tail (Figure 2.2, panel A). LO-incorporation occurred within an hour of incubation, regardless of the presence of serum in the medium (Figure 2.2, panel B).

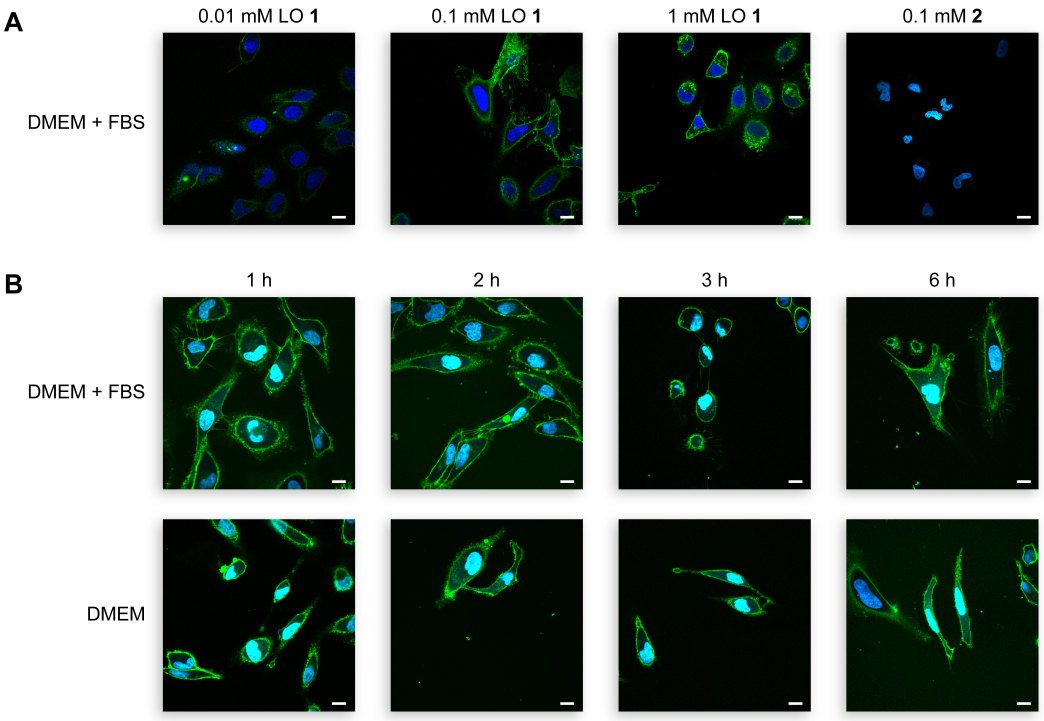

Figure 2.2 Images of LOs incorporated into cell membranes. Cells incorporate a LO but not a lipid-free oligonucleotide in their plasma membrane. Images were obtained by confocal microscopy. LO (1) and oligonucleode 2 are green (fluorescein); cell nuclei are blue (Hoechst 33342). (A) LO (1) was suspended in DMEM containing 10% v/v FBS and incubated with HeLa cells at the indicated concentration for 12 h. Oligonucleotide 2 was likewise incubated with HeLa cells for 4 h. (B) LO (1) (0.1 mM) was incubated with or without 10% v/v FBS for the indicated times. Scale bars: 10 μm.

Next, we used flow cytometry to obtain quantitative data on the interaction of LOs with cells. We found the concentration-dependence of LO-incorporation to be indistinguishable in two distinct cell types (Figure 2.3) and the rate of LO incorporation to decrease with time, indicative of steady-state equilibration (Figure 2.4). The extent of LO-incorporation depends on the medium, decreasing in the order: phosphate-buffered saline (PBS) > Dulbecco's modified

Table 2.1 Synthetic DNA oligonucleotides used in this work

	Sequence (5′→3′)
LO **1**	L_{18}AAAAAAAAAAAAAAAAAAF
2	AAAAAAAAAAAAAAAAAAF
LO **3**	L_{18}GCGGCTAGCAAAAAAAAAAAAAF
LO **4**	L_{18}AAAAAAAAAAAAAAAAAAAAAAAAAAAAAAAAAF
LO **5**	L_{18}AAAAAAAAAF
LO **6**	L_{18}AAAAAAAAAAAAAAF
LO **7**	L_{18}AAGAACGAAAGAAAAGTAACCAAAF
LO **8**	L_{18}ATCTTAGGGAATCTATGCTCCTTGGGACAGAAACACTF
9	GCGGCTAGCAAAAAAAAAAAAAAF
LO **10**	L_{12}GCGGCTAGCAAAAAAAAAAAAAAF
LO **11**	L_{26}GCGGCTAGCAAAAAAAAAAAAAAF
LO **12**	TTTTTTTTTTTTTTCCAAGCCGCL_{18}
13	GCGGCTTGGAAAAAAAAAAAAAF

F = 6-carboxyfluorescein; L_n = alkyl chain with n carbons.

Eagle's medium (DMEM) > PBS containing fetal bovine serum (FBS) (10% v/v) > DMEM containing FBS (10% v/v) (Figure 2.5). To confirm that LOs partition between the aqueous phase and the cell surface, we replaced the medium from LO-labeled cells and observed a gradual loss of LO incorpo-rated/cell as LOs diffused out of the plasma membrane and into the fresh medium to establish a new equilibrium (Figure 2.6). A LO containing 24 nucleotides and a 1,2-O-dioctadecyl-rac-glycerol lipid (which contains two C18 tails) was retained only ~3-fold longer by HeLa cells than was LO3 (data not shown). We note that this intrinsic instability could confound efforts to exploit LOs incorporated into cellular membranes.[103-108]

We sought to discern whether the anionic components of the cell surface repel LOs. We did so by measuring the dependence of LO-incorporation on the length of the oligonucleotide. Regardless of its sequence, the incorporation of a LO correlates inversely with the number of its phosphoryl groups (Figure 2.7). Tan and coworkers observed a similar trend, concluding that longer LOs form larger micelles and that larger micelles fuse less well with the cell surface.[104]

We favor an alternative explanation—longer oligonucleotides contain more anionic phosphoryl groups that are repelled by the anionic glycocalyx. For example, we observed this correlation for duplex oligonucleotides formed by preincubation of a LO (12) with its reverse-complement oligonucleotide (13) (Figure 2.7).

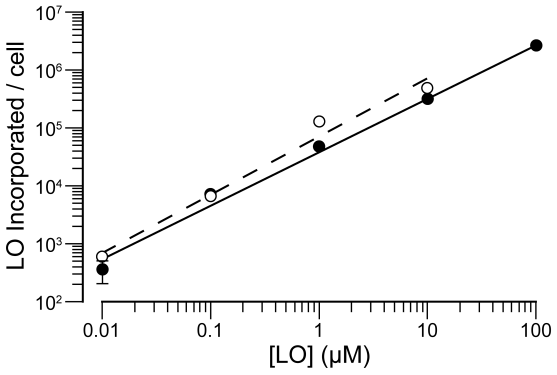

Figure 2.3 Cellular incorporation of a LO depends on concentration. Fluoresent LO 3 was incubated with HeLa cells (●; n = 3) and K-562 cells (○; n = 1) for 15 min, and incorporation was measured by flow cytometry. Error bars: ±SD (which were all smaller than the "○" symbols).

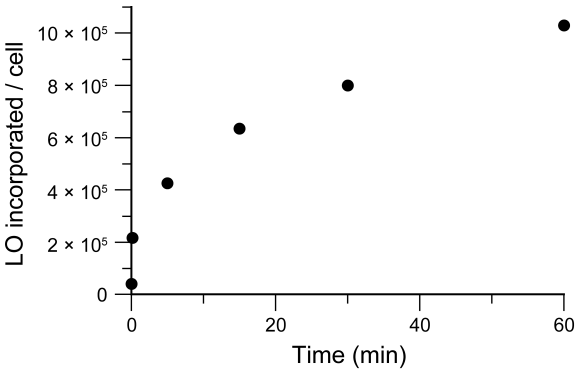

Figure 2.4 Cellular incorporation of a LO depends on time. LO (3) (10 mM) was incubated with HeLa cells for the indicated times, and incorporation was measured by flow cytometry.

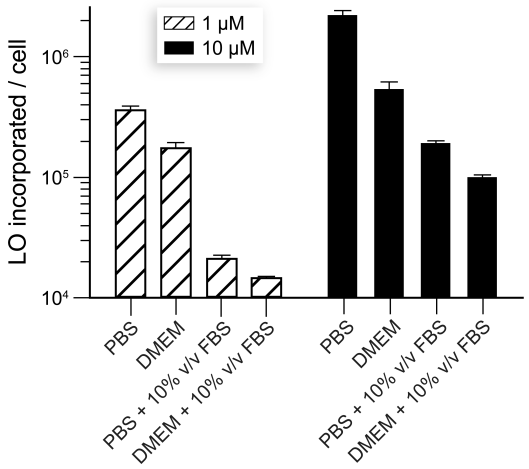

Figure 2.5 Cellular incorporation of a LO is affected by the medium. LO (3) (1 or 10 μM) was incubated with HeLa cells for 15 min in the indicated media, and incorporation was measured by flow cytometry. n = 3; error bars: ±SD.

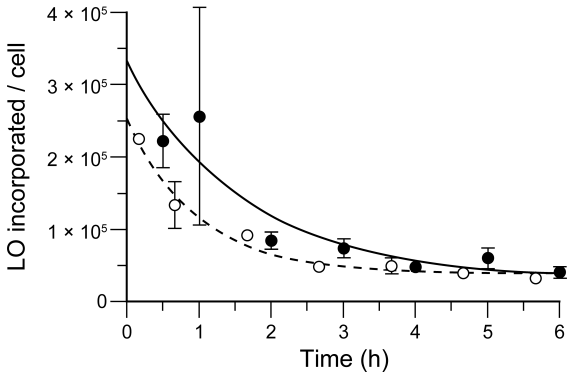

Figure 2.6 Cells release a LO after incorporation. Fluorescent LO (3) (10 μM) was incorporated into the plasma membrane of HeLa cells (●; n = 3) and K-562 cells (○; n = 3). The cells were then washed and incubated with cell medium containing FBS (10% v/v) for the indicated time. Cellular retention was measured by flow cytometry. Error bars: ±SD.

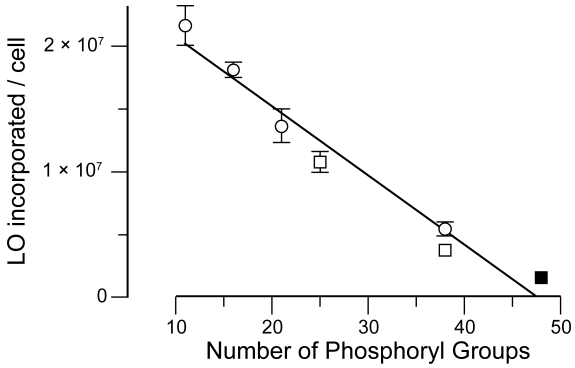

Figure 2.7 Cellular incorporation of LOs depends on charge but not sequence. LOs (10 μM, n = 3) of varying length and sequence were incubated with HeLa cells. (○) LOs (5), (6), (1), and (4) contained poly(2′ deoxyadenylic acid) sequences of 10, 15, 20, and 37 nucleotides, respectively. (□) LOs (7) and (8) contained random sequences of 24 and 37 nucleotides, respectively. (■) LO (12) was co-incubated with oligonucleotide 13 to give a duplex with 48 phosphoryl groups. Error bars: ±SD.

We also sought to determine whether the hydrophobic effect[109,110] drives LO incorporation into the plasma membrane. We found that LO-incorporation correlates strongly with lipid length: no lipid < C12 < C18 << C26 (Figure 2.8). Moreover, an LO (11) containing a long lipid tail (C26) still displays characteristic re-equilibration after medium replacement (Figure 2.9).

2.4.2 Cellular Attributes that Affect Incorporation.

The major anionic components of the glycocalyx are sialic acid and GAGs. To assess their effect on LO-incorporation into cellular membranes, we used mutant cell lines deficient in sialic acid and GAG expression (Figure 2.10). Lec-2 cells are Pro-5 CHO cells with a mutation in the gene encoding a sialyltransferase, the transporter of CMP–sialic acid from the cytosol to

Golgi vesicle.[111] These cells have diminished sialic acid in their glycans. As shown in Figure 2.10A, sialic acid hinders LO incorporation into

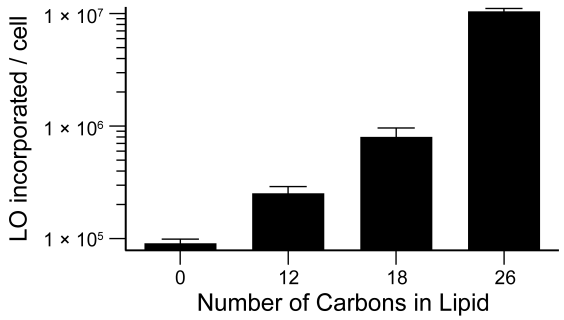

Figure 2.8 Cellular incorporation of LOs is affected by hydrophobicity. LO (9) (no lipid), LO (10) (C12), LO (3) (C18), and LO (11) (C26) at 10 μM were incubated with HeLa cells for 15 min, and incorporation was measured by flow cytometry. Error bars: ±SD.

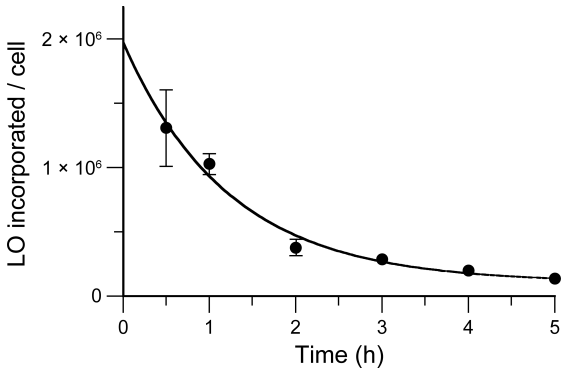

Figure 2.9 Cells release a long LO after incorporation. Fluorescent LO 11 (10 μM), which has a C26 lipid tail, was incorporated into the plasma membrane of HeLa cells, and retention was measured by flow cytometry. Error bars: ±SD.

cells.[112] Likewise, CHO-745 cells have lowered expression of heparan sulfate and chondroitin sulfate due to a mutation in xylosyltransferase, the enzyme that initiates the bio-synthesis of these GAGs.[113-115],[116] As shown in Figure 2.10B, these GAGs diminish LO incorporation.[112]

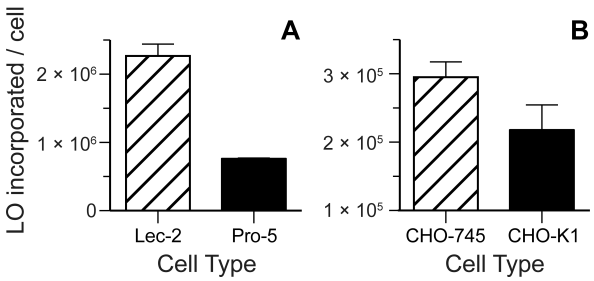

Figure 2.10 Cellular incorporation of LOs is deterred by cell-surface sialic acid and GAGs. (A) LO (4) (10 μM, n = 3) was incubated with CHO cells deficient in sialic acid (Lec-2) and wild-type cells (Pro-5). (B) LO (3) (10 μM, n = 3) was incubated with CHO cells deficient in heparan sulfate and chondroitin sulfate (CHO-745) and wild-type cells (CHO-K1). Error bars: ±SD. Student's t-test gave two-tailed p-values of 0.0001 and 0.0371 for panels A and B, respectively.

To validate that the anionic glycocalyx repels LOs from the cell surface, we used a chemical approach. Specifically, we reduced the net anionic charge of the glycocalyx by preincubating HeLa cells with varying amounts of Lipofectamine™ 2000, and then observed LO incorporation (Figure 2.11). We observed a direct correlation between the amounts of Lipofectamine™ 2000 pre-incubated with the cells and LO incorporation.[112] The results of this chemical experiment, in addition to those from the genetic experiment, led us to conclude that the anionic components of the glycocalyx deter nucleic acids from mammalian cells.

Finally, we were aware that cell-surface GAGs are known to diminish the efficiency of transfection.[116] To complete our analysis, we investigated the effect of sialic acid on the efficiency of siRNA delivery. Even though these experiments were performed in the presence of

a transfection reagent that masks deleterious Coulombic interactions, we found that sialic acid, like GAGs (Figure 2.10), diminishes the efficiency of transfection (Figure 2.12).[112]

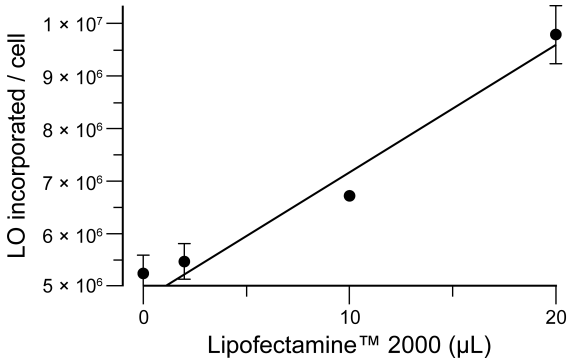

Figure 2.11 Cellular incorporation of LOs is facilitated by increasing the cationicity of the glycocalyx. HeLa cells were incubated with various volumes of Lipofectamine™ 2000, a highly cationic lipid. Then, the cells were washed with PBS and incubated with LO (4) (●; 10 μM, n = 3). Error bars: ±SD.

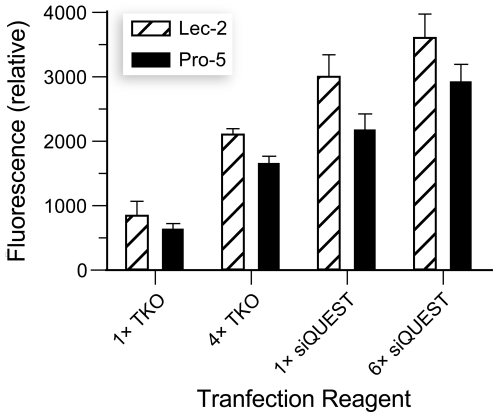

Figure 2.12 Sialic acid hinders siRNA delivery. Delivery of fluorescently labeled siRNA was assessed with CHO cells deficient in sialic acid (Lec-2) and wild-type cells (Pro-5) using the TransIT-TKO and TransIT-siQUEST transfection reagents, each tested in triplicate at two concentrations. Error bars: ±SD.

Many important biomolecules contain phosphoryl groups, which are hydrophilic and anionic.[117] The plasma membrane of mammalian cells presents two potential barriers to the entry of such groups: a bilayer of lipids and anionic glycans (Figure 2.1). Our data indicate that the anionic glycocalyx repels the phosphoryl groups of nucleic acids.

The "double barrier" encountered by extracellular DNA and RNA could serve to facilitate the evolution and maintenance of stable genomes. Conversely, organisms that do not express anionic components of the glycocalyx could have more vulnerable genomes and should be more susceptible to gene knockdown by RNAi. Interestingly, *Caenorhabditis elegans* nematodes do not express the enzymes necessary for sialic acid production. They also do not express keratan sulfate, dermatan sulfate, or hyaluronan, and they lack the sulfotransferases and epimerases necessary to add sulfuryl groups to chondroitin sulfate.[94] Thus, the cells of *C. elegans* could have a substantially less anionic glycocalyx than those of mammals. *C. elegans* is the prototypical organism for gene knockdown by RNAi.[118] This capability has been attributed to its SID-1 protein, which shuttles siRNA across cellular membranes.[119-122] We propose that *C. elegans* is especially susceptible to RNAi because of diminished Coulombic repulsion between its glycocalyx and RNA, enabling RNA to diffuse more readily to the SID-1 transporter.

Most species, including mice and humans, have orthologs to SID-1.[123] Yet, systemic knockdown of gene expression by RNAi is facile only in *C. elegans*, flatworms, and a few insect species.[118,124-127] The human SID-1 homologue SIDT1 is expressed in most tissues.[45] When overproduced in pancreatic ductal adenocarcinomacells, SIDT1 delivers siRNA into cells more efficiently than do transfection reagents.[128] Additionally, SIDT1 has been demonstrated to be essential for siRNA delivery into human primary hepatocytes in vitro.[129] To access SIDT1,

siRNA must diffuse through the anionic glycocalyx. Our data suggest that a small-molecule inhibitor of sialic acid biosynthesis could enable siRNA to reach SIDT1 more efficiently.

2.5 Conslusions

We have provided a detailed analysis of the interaction of a nucleic acid with the canopy of mammalian cells—the glycocalyx. We demonstrated that the anionic charge associated with a nucleic acid correlates inversely with its affinity for the glycocalyx. Additionally, we established that reduction of the anionic charge on the cell surface (genetically with the Lec-2 and CHO-745 cell lines, or chemically upon addition of Lipofec-tamine™ 2000) enhances LO incorporation into cellular mem-branes, providing direct evidence that the anionic glycocalyx re-pels nucleic acids. We propose that an evolutionary imperative of the anionic glycocalyx is to ensure genomic stability by deterring the approach of exogenous nucleic acids while retaining endogenous ones. Finally, we encourage a search for small-molecule inhibitors of sialic acid biosynthesis, which could enhance the efficiency of the cellular delivery of nucleic acids.

2.6 Acknowledgments

We are grateful to S. Kennedy, N. Burton, B. R. Caes, and A. Choudhary for contributive discussions. M.J.P. was supported by Molecular and Cellular Pharmacology Training Grant T32 GM008688 (NIH) and predoctoral fellowship 09PRE2260125 (American Heart Association). This work was supported by Grants R01 CA073808 and R01 GM044783 (NIH).

2.7 Materials and Methods

2.7.1 General.

2 Cyanoethyl N,N-diisopropylchlorophosphoramidite, anhydrous dichloromethane (DCM), N,N diisopropylethylamine (DIEA), and octadecanol were from Sigma–Aldrich (St. Louis, MO). A 2.0 M aqueous solution of triethylammonium acetate (TEAA) was from Glen Research (Sterling, VA). "NH4OH solution" refers to a 30% v/v solution in H2O diluted as specified. All other chemicals and reagents were obtained from commercial suppliers, and used without further purification.

The removal of solvents and other volatile materials "under reduced pressure" refers to the use of a rotary evaporator at water-aspirator pressure (<20 torr) and a water bath of <40 °C.

2.7.2 Instrumentation.

NMR spectra were acquired at ambient temperature with a Bruker DMX-400 Avance spectrometer (Bruker AXS, Madison, WI, 1H, 400.1 MHz; 13C, 100.6 MHz; 31P, 162.0 MHz) at the National Magnetic Resonance Facility at Madison (NMRFAM). 13C and 31P spectra were proton-decoupled. Oligonucleotide A260 values were measured with a Varian Cary 50 ultraviolet–visible spectrometer (Agilent Technologies, Santa Clara, CA), Thermo Fisher Nano-Drop 1000 instrument (Thermo Fisher Scientific, Walham, MA), or GE NanoVue instrument (GE Healthcare, Piscataway, NJ). Confocal microscopy was performed with a Nikon Eclipse C1 laser scanning confocal microscope (Nikon, Melville, NY). Flow cytometry was done using a LSRII (BD Biosciences, San Jose, CA) at the University of Wisconsin–Madison Carbone Cancer

Center Flow Cytometry Facility. MALDI–TOF mass spectrometry was performed with a Voyager DE-Pro MALDI–TOF instrument (Applied Biosystems, Carlsbad, CA) at the University of Wisconsin–Madison Biophysics Instrumentation Facility.

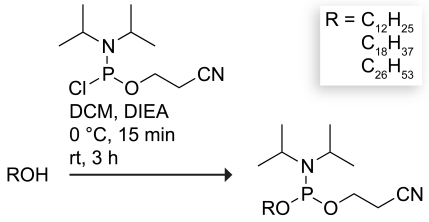

Scheme 2.1 Synthesis of Alkylphosphoramidites

2.7.3 Synthesis of Alkylphosphoramidites.

Alkylphoshoramidites were synthesized by the route in Scheme 2.1.[130,131] As an example, 2-cyanoethyl N,N diisopropyloctadecylphosphoramidite (R = C18H37) was syn-thesized as follows. Octadecanol (294 mg, 1.09 mmol) was dissolved in anhydrous DCM (13 mL) in a flask under Ar(g). DIEA (350 μL, 2 mmol) was added dropwise, and the reaction mixture was cooled to 0 °C. 2-Cyanoethyl N,N-diisopropylchlorophosphoramidite (350 μL, 1.6 mmol) was added dropwise using a glass luer-tipped syringe. After 15 min, the reac-tion mixture was allowed to warm to room temperature, and then stirred for 3 h. The organic layer was washed with saturated aqueous NaHCO3, dried over MgSO4(s), filtered, and concentrated under reduced pressure. The product was purified by flash chromatography on silica gel (mesh: 230–400 ASTM), eluting with 10% ethyl acetate/1% triethylamine/hexanes, using silica packed with triethylamine (20% v/v) in hexanes. The product was con-centrated under reduced pressure. 2-Cyanoethyl N,N diisopropyloctadecylphosphoramidite (262 mg, 0.56 mmol, 51%) was isolated as a clear oil and stored under Ar(g) at –20 °C until used. ^{1}H NMR (400 MHz, CDCl3) δ = 3.90–3.78 (m, 2H),

3.72–3.53 (m, 4H), 2.64 (t, 2H, J = 6.71 Hz), 1.60 (t, 2H, J = 6.68 Hz), 1.39–1.22 (m, 30H), 1.18 (t, 12H, J = 5.26 Hz), 0.88 (t, 3H, J = 6.45 Hz). ^{13}C NMR (100 MHz, CDCl3) δ = 117.6, 63.6, 58.2, 43.0, 31.9, 31.2, 29.6, 29.4, 25.9, 24.6, 22.7, 20.3, 14.1. ^{31}P NMR (162 MHz, CDCl3) δ = 146.3.

2.7.4 Synthesis, Purification, and Analysis of Lipid–Oligonucleotide Conjugates.

LOs and DNA oligonucleotides were synthesized with an Applied Biosystems ABI 394 DNA synthesizer at the University of Wisconsin–Madison Biotechnol-ogy Center, where an alkylphosphoramidite was the last phosphoramidite to undergo coupling. Fluorescein-conjugated oligonucleotides were synthesized by elongation on 1 dimethoxytrityloxy-3-[O-(N-carboxy-(di-O-pivaloyl-fluorescein)-3-aminopropyl)]-propyl-2-O-succinoyl-long chain alkylamino-CPG (which is 3′-(6-FAM) CPG from Glen Research, Sterling, VA). Reverse DNA synthesis was required to conjugate lipids to the 3′ end. After synthesis, the controlled pore glass was placed in a 4-mL glass vial with 1 mL of undiluted NH4OH solution and incubated at 70 °C for 2 h. The solution was then passed through a 0.45-μm filter, and dried overnight with a SpeedVac Concentrator (Thermo Scientific, Waltham, MA). The oligonucleotides were dissolved in 0.1 M TEAA in NH4OH solution (5% v/v) and sonicated briefly to break up aggregates. The solution was then passed through a 0.2 μm filter and purified by HPLC using an Ultimate 3000 instrument (Dionex Corporation, Sunnyvale, CA) equipped with a Varian PLRP-S column (100 Å, 8 μm, 300 × 75 mm) heated to 50 °C. Product was eluted at 3 mL/min with a linear gradient (40–95%) of buffer A (MeOH con-taining 0.1 M aqueous TEAA) and buffer B (H2O containing 0.1 M aqueous TEAA and 1% v/v NH4OH solution). Each fraction was analyzed by mass spectrometry to ensure that n – 1 “failure” sequences were not pooled with the intended product.

Mass spectrometry was performed using 1 μL of DNA solution, 1 μL of 113 mg/mL ammonium citrate in H2O, and 2 μL of 50 mg/mL 3-hydroxypicolinic acid in 1:1 H2O/acetonitrile. Each LO had an observed mass within 30 Da of its expected mass. LOs and oligonucleotides were stored at –20 °C as a lyophilized powder until used.

2.7.5 Cell Culture.

Cell lines were obtained from American Type Culture Collection (Rockville, MD) and were maintained according to the recommended guidelines. Cells were grown in flat-bottomed culture flasks at 37 °C under 5% v/v CO2(g). Cell medium was supplemented with FBS from Invitrogen (Carlsbad, CA) (10% v/v), penicillin (100 units/mL), and streptomycin (100 μg/mL) in the appropriate cellular medium as follows: HeLa, DMEM; K-562, RPMI; Pro-5, MEM α + ribonucleosides + deoxyribonucleosides; Lec-2, MEM α – ribonucleosides – deoxyribonucleosides; CHO-1, F-12; and CHO-745, F-12. Cells were counted by hemocytometry for dispensing into 6-well plates, 12 well plates (Corning Costar, Lowell, MA), or 8-well chambered coverglass slides (Nuc Lab-Tek II, Thermo Scientific).

2.7.6 Incorporation of LOs into the Plasma Membrane.

On the day prior to an experiment, lyophilized stocks of purified DNA were suspended in autoclaved water, and DNA concentrations were determined by absorbance at 260 nm using extinction coefficients calculated with the program SciTools OligoAnalyzer 3.1 (Integrated DNA Technologies, Coralville, IA), with the assump-tion that the lipid tails do not alter the absorbance of the conjugates. Aliquots of the DNA were put into microcentrifuge tubes and dried overnight

with a SpeedVac Concentrator. Fifteen minutes prior to incubation with cells, LO aliquots were suspended in 400 μL of cell medium giving a final concentration of 10 μM LO (unless indicated otherwise), and these solutions were warmed to 37 °C.

2.7.6.1 Non-adherent Cells.

One day prior to the experiment, 6×10^5 cells were placed into each well of a 6-well plate. On the day of the experiment, cells were washed twice with PBS, as follows. Cells were removed from the well, and collected by centrifugation in a 1.7-mL tube for 5 min at 1000 rpm. The supernatant was removed, and the cells were suspended in 1.5 mL of PBS. This process was repeated once more. Then, cells were suspended in 400 μL of cell medium containing LO at the indicated final concentration, and incubated for 10 min at 37 °C. The cells were collected by centrifugation at 1000 rpm for 5 min, washed twice with PBS as described previously, suspended in 400 μL of medium, added to flow cytometry tubes, and stored on ice until analyzed by flow cytometry.

2.7.6.2 Adherent Cells.

One day prior to the experiment, approximately 2×10^5 cells were added to the wells of 6-well plates. On the day of the experiment, the medium was removed, and the cells were rinsed twice with 1 mL of PBS. After the PBS was removed, a 400 μL suspension of LO in cell medium (unless indicated otherwise) was incubated with the cells at 37 °C for 15 min. The LO suspension was then removed, and the cells were rinsed twice with 1 mL of PBS, and incubated with 400 μL of 0.05% w/v trypsin with EDTA for 10 min at 37 °C. The cell suspension was

removed from the 6-well plate, added to flow cytometry tubes containing 80 μL of FBS, and stored on ice until analyzed by flow cytometry.

2.7.7 Lipofectamine™.

LOs were incorporated into the plasma membrane of adherent cells as described above except that after the first two PBS washings, the cells were incubated for 15 min with 400 μL of cell medium and the indicated amount of Lipofecamine 2000 (Invitrogen), washed twice with PBS, and then incu-bated with 400 μL of cell medium containing LO. The remainder of the experiment was done as described above.

2.7.8 Retention of LOs in the Plasma Membrane.

Cells were labeled as described previously except that after the 15-min incubation period, the cells were washed twice with 1 mL of PBS and incubated for the indicated time in medium containing FBS (10% v/v). After the incubation period, the cells were washed twice with 1 mL of PBS, placed directly in flow cytometry tubes, and stored on ice until analyzed by flow cytometry. If the cells were adherent, then they were washed twice with 1 mL of PBS and incubated with 400 μL of trypsin/EDTA (Invitrogen) for 10 min at 37 °C. The cell suspensions were removed and added to flow cytometry tubes containing 80 μL of FBS, and stored on ice until analyzed by flow cytometry.

2.7.9 Confocal Microscopy.

HeLa cells were plated on Nunc Lab-tek II 8-well chambered coverglass 24 h before use and grown to 80% confluency. Cells were incubated with the LO at the indicated concentrations, medium conditions, and times. Cell nuclei were stained with Hoechst 33342 (Invitrogen; 2 μg/mL) for the final 15 min of incubation. Cells were then washed twice with PBS, suspended in PBS, and examined with confocal microscopy.

2.7.10 Flow Cytometry.

Fluorescein was excited with a 488 nm solid-state laser, and the emission was collected with a 530/30 band-pass filter. To collect comparable data in each flow cytometry experiment, the sensitivity (i.e., voltage) of the photomultiplier tube was set for all data collections using mid-range Rainbow beads (Spherotech, Lake Forest, IL) to give a predetermined fluorescence target value of 2511. At least 10,000 cellular events were acquired for each sample. Additionally, at least 5,000 events of Quantum™ FITC MESF (fluorescein isothiocyanate molecules of equivalent soluble fluorochrome) high beads (Bangs Laboratories, Fishers, IN) were acquired for each experiment. Data were analyzed with FlowJo 8.1.3 software (Treestar, Ashland, OR). The relative fluorescence units (RFU) of the LO FITC fluorescence was normalized to MESF beads to calculate how many FITC molecules were affiliated with each cell. There was one FITC molecule per LO, enabling quantification of LOs/cell.

2.7.11 siRNA Transfection.

The transfection efficiency of Lec-2 and Pro-5 cells was assessed with a TransIT®-siPAK Plus Kit (Mirus Bio, Madison, WI). The day prior to the experiment, 105 cells/well were plated in a 12-well plate, which gave ~80% cell confluency on the day of the experiment. Transfection of fluorescently labeled siRNA (25 nM) was assessed by using TransIT-siQUEST concentrations 1× (that is, 1 μL) and 6× (6 μL), and TransIT-TKO concentrations 1× (2 μL) and 4× (8 μL).

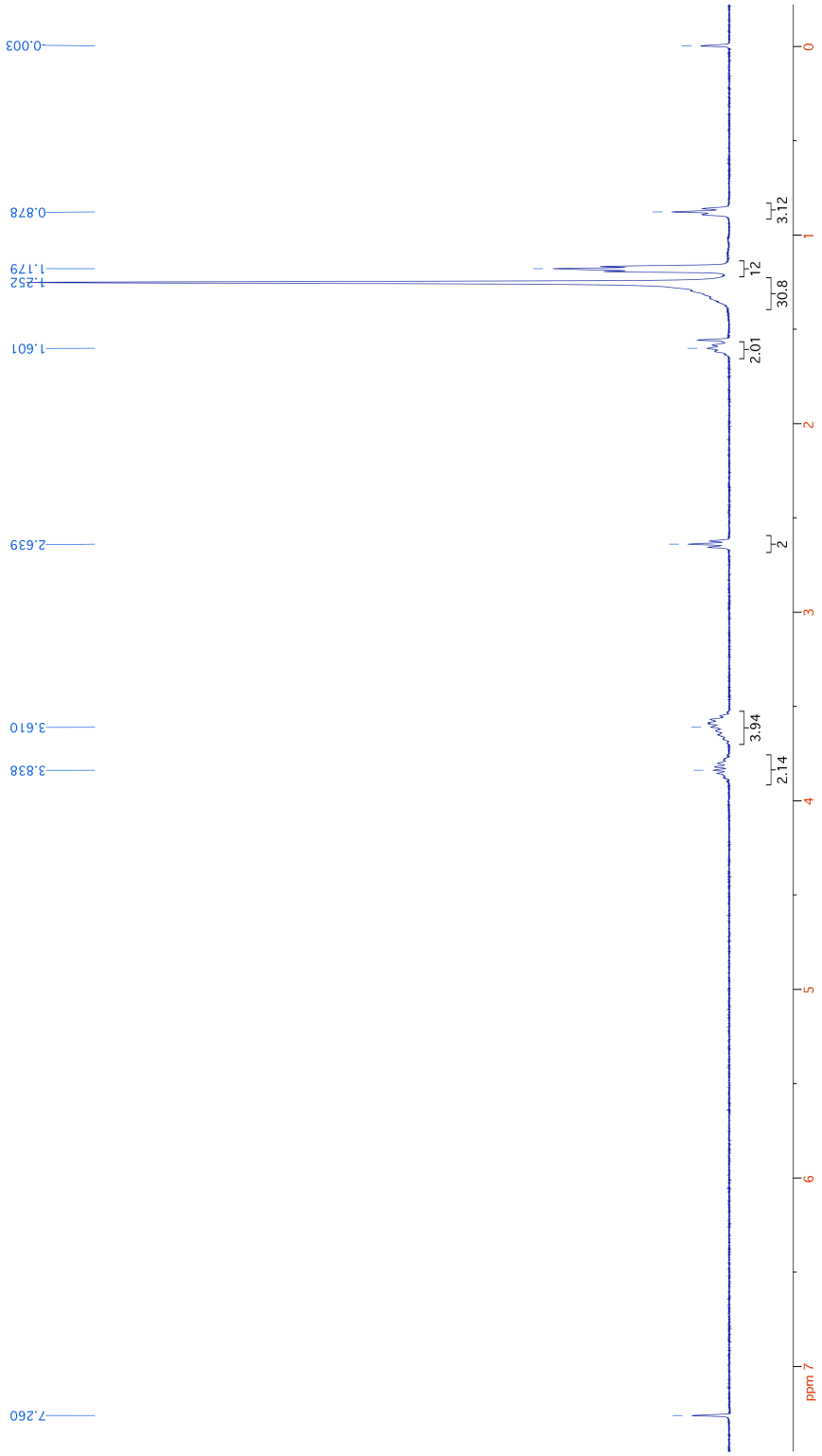
7.260
3.838
3.610
2.639
1.601
1.252
1.179
0.878
0.003
2.14
3.94
2
2.01
30.8
12
3.12
ppm 7

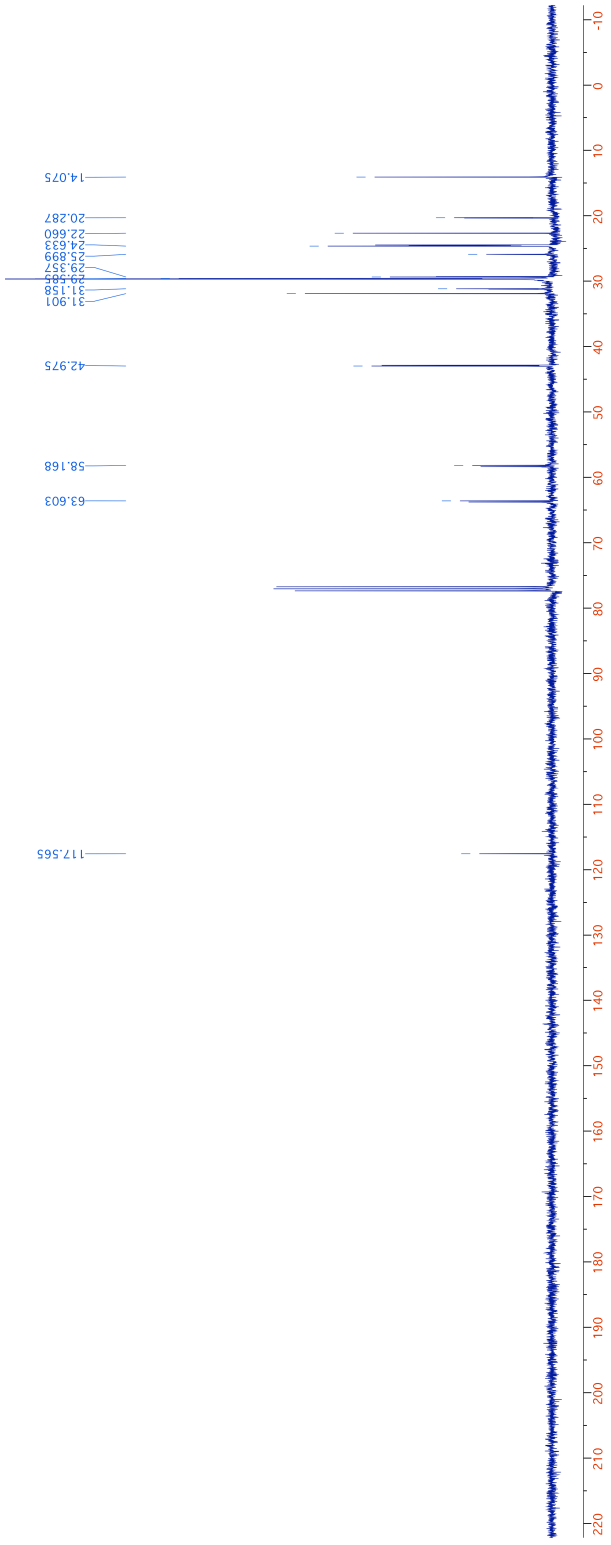
14.075
20.287
22.660
24.633
25.899
29.357
29.585
31.158
31.901
42.975
58.168
63.603
117.565
-10
0
10
20
30
40
50
60
70
80
90
100
110
120
130
140
150
160
170
180
190
200
210
220

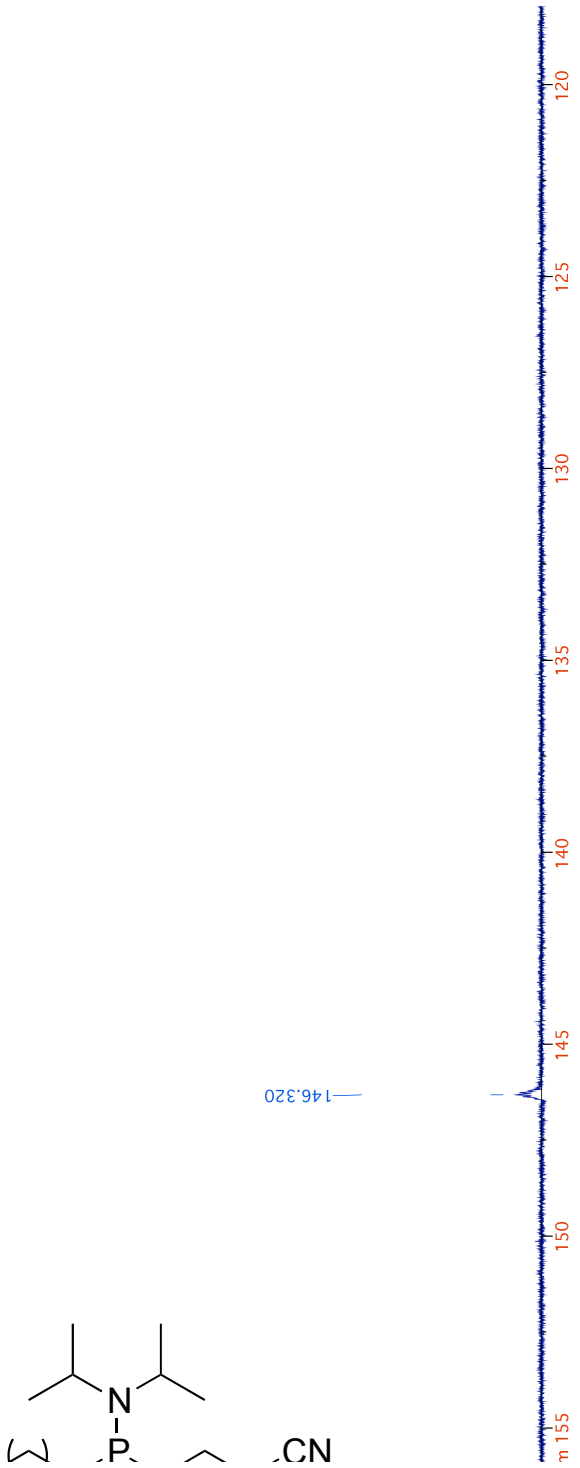
146.320
120
125
130
135
140
145
150
155
N
P
CN

Chapter Three

Ribonuclease-Activated Cancer Prodrug*

* This chapter has been published in part, under the same title. Reference: Ellis, G.A., McGrath, N.A., Palte, M.J., & Raines, R.T. Ribonuclease-activated cancer prodrug. *ACS Med. Chem. Lett.* *3*, 268–272 (2012).

3.1 Abstract

Cancer chemotherapeutic agents often have a narrow therapeutic index that challenges the maintenance of a safe and effective dose. Consistent plasma concentrations of a drug can be obtained by using a timed-release prodrug strategy. We reasoned that a ribonucleoside 3′-phosphate could serve as a pro-moiety that also increases the hydrophilicity of a cancer chemotherapeutic agent. Herein, we report an efficient route for the synthesis of the prodrug uridine 3′-(4-hydroxytamoxifen phosphate) (UpHT). UpHT demonstrates timed-released activation kinetics with a half-life of approximately 4 h at the approximate plasma concentration of human pancreatic ribonuclease (RNase 1). MCF-7 breast cancer cells treated with UpHT showed decreased proliferation upon co-incubation with RNase 1, consistent with the release of the active drug—4-hydroxytamoxifen. These data demonstrate the utility of a human plasma enzyme as a useful activator of a prodrug.

3.2 Author Contributions

Original idea for using ribonucleoside 3′-phosphate pro-moieties for timed-release was from M.J.P. Attempted syntheses of other drugs attached to uridine 3′-phosphate were first done by M.J. P. and G.A. E., then by N.A.M. and G.A.E. First attempted synthesis of UpHT was done by G.A.E.; N.A.M. optimized conditions and synthesized UpHT synthesis in good yield. Final product was HPLC purified by G.A.E. Full characterization of UpHT and intermediates were done by N.A.M. HPLC kinetics were done by G.A.E., N.A.M., and M.J.P. Protein purification and characterization, LogP and LogD calculations, and cytotoxicity experiments were done by G.A.E. G.A.E. primarily drafted the manuscript and figures with assistance from N.A.M. and M.J.P. G.A.E., N.A.M., M.J.P., and R.T.R. designed experiments, analysed data, and edited the manuscript and figures.

3.3 Introduction

Many drug candidates have demonstrable therapeutic potential *in vitro* but fail *in vivo* because of poor pharmacokinetic behavior.[132,133] The dosing of chemotherapeutic agents for cancer, in particular, is made difficult by narrow therapeutic indices.[134,135] Following parenteral administration of a drug, there is a spike in drug plasma concentration, followed by a slow decline in concentration as the drug is eliminated or metabolized, complicating maintenance of the drug at a beneficial concentration.[134,136] Timed-release prodrug technology provides one potential means to overcome this problem. A pro-moiety renders the drug inactive until liberation by an enzyme-catalyzed or non-enzymatic process. Ideally, such timed-release modulates near-toxic peaks or near-ineffective troughs in the concentration of active drug in plasma.[133,134,136-138] Although many pro-moieties exist,[132-138] few provide timed-release in plasma.

We sought a pro-moiety that would not only inactivate the parent drug, but also be released during catalysis by an endogenous plasma enzyme. Fulfilling these criteria is difficult, as few enzymes have adequate plasma concentrations and many that do have high specificity for a native substrate. Human pancreatic ribonuclease (RNase 1[44]; EC 3.1.27.5) is an exception. Contrary to its name, RNase 1 is expressed in tissues other than pancreas,[45] and circulates in human plasma at a concentration of ~0.4 mg/L.[139] Moreover, like its renowned homolog bovine pancreatic ribonuclease (RNase A[47,48]), RNase 1 catalyzes the cleavage of RNA by a transphosphorylation reaction[49-51] and has little specificity for its leaving group.[52-56] This promiscuity is the basis for the tumor-targeted activation of a phenolic nitrogen mustard from a ribonucleoside 3′-phosphate prodrug using an antibody–RNase 1 variant in an antibody-directed enzyme prodrug therapy (ADEPT) strategy.[54]

Due to the promiscuous activity of ribonucleases, we reasoned that a chemotherapeutic drug condensed with a ribonucleoside 3′-phosphate pro-moiety would be released upon catalysis by RNase 1. We were aware that the use of a ribonucleoside 3′-phosphate as a pro-moiety would be facilitated by extant, highly optimized phosphoramidite chemistry,[140,141] making the prodrug readily accessible on a laboratory or industrial scale. A pendant ribonucleoside 3′-phosphate could render inactive a small-molecule drug by hindering the interaction with its target. The hydrophilicity of a ribonucleoside 3′-phosphate could impart improved pharmacokinetics to hydrophobic drugs.[142] Additionally, small molecules with anionic groups are endowed with reduced rates of cytosolic uptake and glomerular filtration.[38-41,143-146]

For our proof-of-concept studies, we chose the model parent drug 4-hydroxytamoxifen (HT). HT is the activated form of tamoxifen (oxidized by cytochrome P450 enzymes[147]) and is significantly more potent than tamoxifen as an anti- proliferative agent against breast cancer cells.[148] Tamoxifen acts as an anti-estrogen and is one of the most commonly used hormonal drugs for the prevention and treatment of breast cancer.[149,150] Unfortunately, tamoxifen can have off-target effects and is linked to an increased risk (2–3%) of endometrial carcinoma and pulmonary embolism.[151] Presumably, these side effects could be attenuated by delivering tamoxifen at a consistent, low dose.[152-156] Tamoxifen-encapsulated liposomes have been developed for this purpose,[153] but liposomal delivery has, in general, demonstrated only modest efficacy in the clinic.[157] Hence, we elected to attach HT to uridine 3′-phosphate and analyze the activation of this model prodrug by RNase 1 (Figure 3.1).

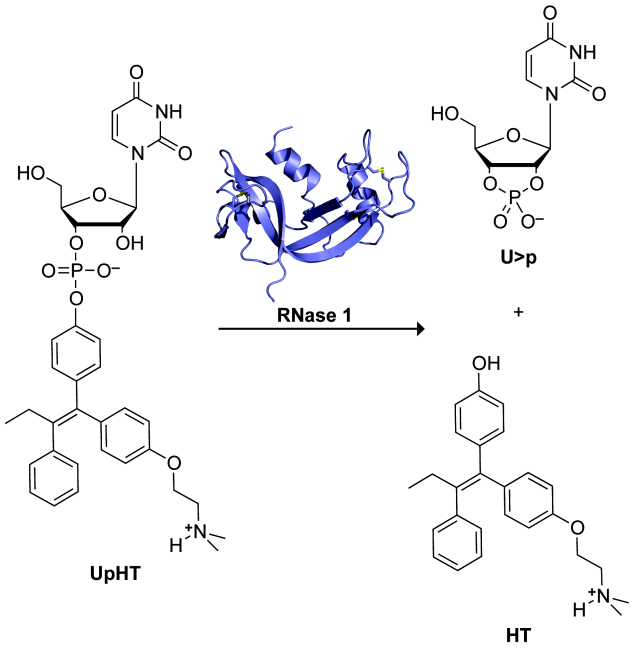

Figure 3.1 Scheme showing the cleavage of prodrug UpHT by RNase 1 to yield uridine 2′,3′-cyclic phosphate (U>p) and HT.

3.4 Results and Discussion

Uridine 3′-(4-hydroxytamoxifen phosphate) (UpHT) was synthesized in five steps from commercially available HT (≥70% *Z* isomer, which is the more active form[158,159]) and uridine phosphoramidite (Scheme 1). Briefly, HT was coupled to uridine phosphoramidite by using *N*-methylbenzimidazolium triflate as a catalyst.[160] The coupled product was oxidized with iodine and deprotected stepwise. The final product was purified by reverse-phase HPLC on C18 resin to provide UpHT in an overall yield of 58%.

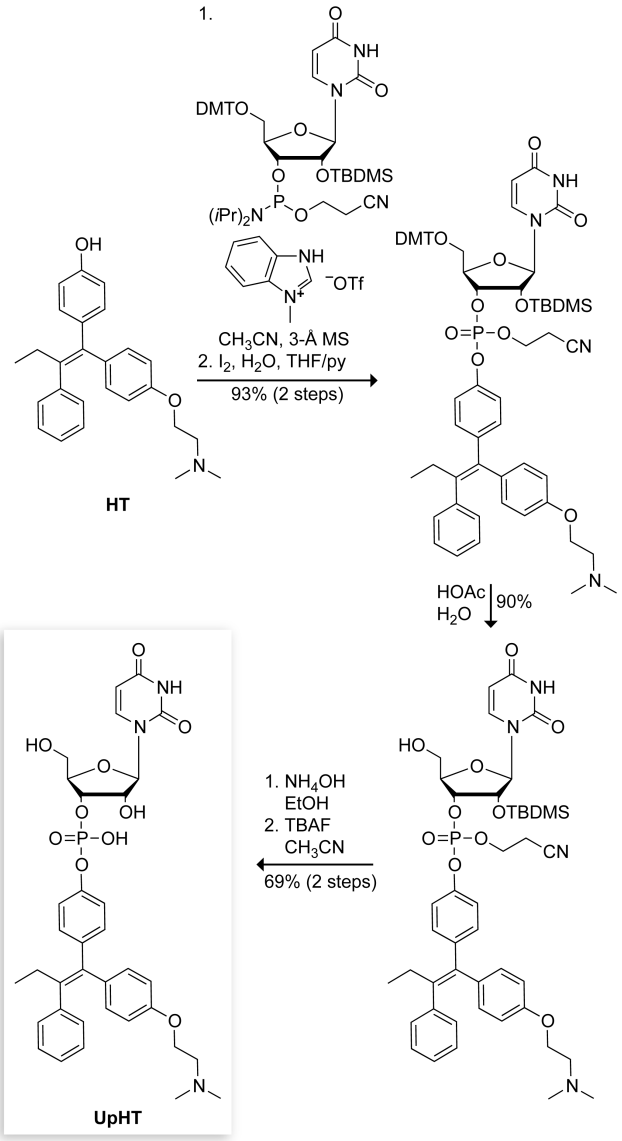

Scheme 3.1 Synthesis of UpHT

We expected the uridine 3′-phosphate moiety of UpHT to endow the prodrug with greater hydrophilicity than the parent drug, which could improve pharmacokinetic behavior. To investigate this issue, we calculated the partition (logP) and distribution (logD) coefficients of UpHT and HT.[161] The calculated logP and logD values of UpHT were indeed significantly lower than those of the parent drug HT (Table 3.1), indicative of increased hydrophilicity.

Table 3.1 Calculated partition and distribution coefficients of HT and UpHT

Coefficient	HT	UpHT
log*P* (non-ionized)	6.05	3.88
log*P* (ionized)	2.55	–2.00
log*D* (pH = 7.4)	4.66	0.12
log*D* (pH = p*I*[a])	5.69	−1.79

[a]HT, p*I* 9.01; UpHT, p*I* 5.00.

To be the basis for an effective timed-release prodrug strategy, the pro-moiety needs to be released by the activating enzyme over time. Hence, we assessed the RNase 1-catalyzed rate of HT-release from UpHT. To do so, RNase 1 (final concentration: ~0.15 μg/mL) was added to 0.10 M MES–NaOH buffer, pH 6.0, containing NaCl (0.10 M) and UpHT (0.090 mM).[162-164] The reaction mixture was incubated at 37 °C, and aliquots were withdrawn at known times and assayed for HT by HPLC. Under these conditions, which are typical for assays of ribonucleolytic activity,[48,163] HT was released with a half-life of ~4 h (Figure 3.2). Importantly, UpHT was stable in the absence of RNase 1; after 11 h at 37 °C, <6% of UpHT had degraded to HT.

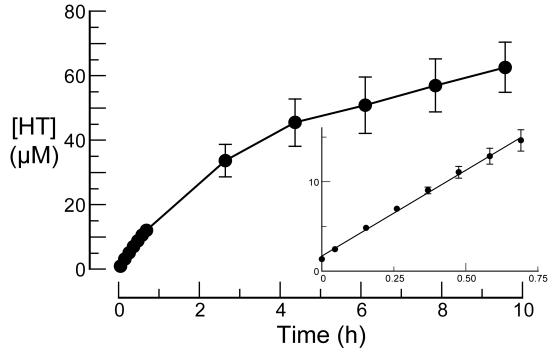

Figure 3.2 Progress curve for the release of HT from UpHT (0.090 mM) by RNase 1 (~0.15 μg/mL) in 0.10 M MES–NaOH buffer, pH 6.0, containing NaCl (0.10 M) at 37 °C. Inset: $t < 1$ h.

To assess the unmasking of UpHT under more physiological conditions, HT-release from UpHT was monitored in cell-culture medium (Figure 3.3A). In medium without added ribonucleases, HT was released with a half-life of ~9 h. To validate that UpHT is inherently unstable at pH 7.4 (as opposed to the medium containing contaminating ribonucleases), the stability of UpHT was assessed in ribonuclease-free 0.10 M sodium phosphate buffer, pH 7.4, containing NaCl (0.10 M). Again, the half-life was ~9 h. The instability of UpHT at pH 7.4 is consistent with HT being a good leaving group, as its hydroxyl group has pK_a ~9.3.[161] By comparison, the P–O$^{5'}$ bond in RNA has a half-life of 4 y.[165]

To demonstrate the efficacy of UpHT *in cellulo*, we monitored its effect on the proliferation of MCF-7 breast cancer cells, which are known to be vulnerable to HT.[148] UpHT was made more anti-proliferative by the presence of added RNase 1 (Figure 3.3B), indicating that UpHT is a ribonuclease-activatable prodrug. Thus, we have demonstrated proof-of-concept for a prodrug strategy that employs a human plasma enzyme to release a cancer chemotherapeutic agent in a timed-release manner (Figure 3.1).

3.5 Conslusions

In addition to the attributes evident in UpHT, the RNase 1/ribonucleoside 3′-phosphate prodrug system has versatile modularity. For example, the leaving group need not be an aryloxy group. Pancreatic-type ribonucleases catalyze the cleavage of P–O bonds to alkoxy groups, which could include a self-immolative linker to an amino group.[135] RNase 1 is known to cleave

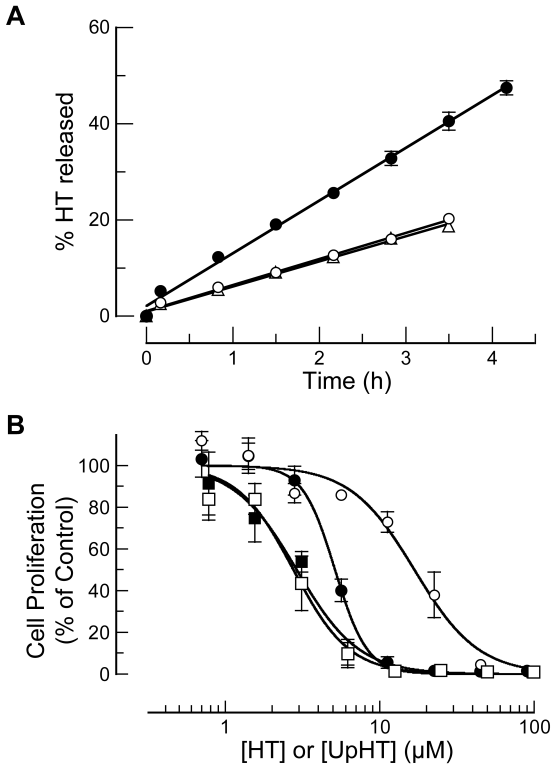

Figure 3. Stability of UpHT and effect of UpHT on the proliferation of MCF-7 cells. All data points are the mean (±SE) of separate experiments carried out in triplicate. (A) Progress curves for the release of HT from UpHT (40 μM) at 37 °C in ribonuclease-free 0.10 M sodium phosphate buffer, pH 7.4, containing NaCl (0.10 M) (△, $t_{½}$ = 9.4 h), and serum-free[166] medium in the absence (○; $t_{½}$ = 9.0 h) and presence (●; $t_{½}$ = 4.4 h) of RNase 1 (0.4 μg/mL). (B) Proliferation of MCF-7 cells in serum-free[166] medium, monitored by the incorporation of [*methyl*-^{3}H]thymidine into cellular DNA. UpHT in the absence (○; IC_{50} = 16.7 ± 0.8 μM) and presence (●; IC_{50} = 5.2 ± 0.2 μM) of RNase 1 (6.2 μg/mL). HT in the absence (□; IC_{50} = 2.7 ± 0.1 μM) and presence (■; IC_{50} = 2.7 ± 0.4 μM) of RNase 1.

RNA faster after pyrimidine than purine nucleobases.[167] Hence, cytidine- and uridine-masked drugs are likely to be activated more rapidly than adenosine- and guanosine-masked drugs. In addition, synergistic drugs could be conjugated to different ribonucleoside 3′-phosphates to achieve simultaneous release of drugs at desired concentrations. These same effects could be used to optimize simultaneous plasma concentrations of chemoprotective drugs and

chemotherapeutic drugs. The pharmacokinetics of the drug could be tuned further by modification of the ribose 5′-hydroxyl group. For instance, this hydroxyl group could be PEGylated to enhance serum half-life, extended with additional nucleoside 3′-phosphates to increase hydrophilicity, or alkylated with the intent of increasing hydrophobicity.[168]

Finally, we note that nucleoside 3′-phosphates pro-moities could impart selective activation of chemotherapeutic agents near tumor sites. Although RNase 1 was employed herein due to its abundance in plasma,[44,45,169,170] RNase 1 homologues might also activate prodrugs like UpHT *in situ*.[44] One such homologue is eosinophil-derived neurotoxin (RNase 2), which is carried and released by eosinophils.[44] These cells are known to accumulate and degranulate at tumor sites.[171-173] We anticipate that, akin to prodrug monotherapy (PMT) in which prodrugs are activated by endogenous enzymes found in abundance near tumors,[174] a prodrug strategy reliant on RNase 2 could be used to generate active drugs at adventitious sites. Studies to probe the versatility of the RNase 1/ribonucleoside 3′-phosphate prodrug system are underway in our laboratory.

3.6 Acknowledgments

The authors acknowledge M. L. Hornung for early contributions to this work. This work was supported by Grant R01 CA073808 (NIH). N.A.M. was supported by the postdoctoral fellowship F32 GM096712 (NIH). M.J.P. was supported by Molecular and Cellular Pharmacology Training Grant T32 GM008688 (NIH) and predoctoral fellowship 09PRE2260125 (American Heart Association). This study made use of the National Magnetic Resonance Facility at Madison, which is supported by NIH Grants P41RR02301 (BRTP/NCRR) and P41GM66326

(NIGMS). Additional equipment was purchased with funds from the University of Wisconsin, the NIH (RR02781, RR08438), the NSF (DMB-8415048, OIA-9977486, BIR- 9214394), and the U.S. Department of Agriculture.

3.7 Materials and Methods

3.7.1 Materials

Uridine phosphoramidite and iodine oxidizing solution were from Glen Research (Sterling, VA). Minimum 70% *Z* isomer of 4-hydroxytamoxifen (remainder, primarily *E* isomer), 3-Å molecular sieves, tetrabutylammonium fluoride (TBAF), methylbenzimidazole, and all other commercial reagents were from Sigma–Aldrich (St. Louis, MO). Methylbenzimidazole triflate was made according to literature precedent from methylbenzimidazole.[160] Spectra/Por® dialysis bags (3500 MWCO) were from Fisher Scientific (Thermo Fisher Scientific, Walham, MA). *Escherichia coli* BL21(DE3) cells were from Novagen (Madison, WI). Cell-culture medium and supplements, as well as Dulbecco's phosphate-buffered saline (DPBS) were from Invitrogen (Carlsbad, CA). [*methyl*-^{3}H]Thymidine (6.7 Ci/mmol) was from Perkin–Elmer (Boston, MA). HiTrap columns were from GE Biosciences (Piscataway, NJ). MES buffer was from Sigma–Aldrich (St. Louis, MO) and purified by anion-exchange chromatography to remove trace amounts of oligomeric vinylsulfonic acid.[164] Ribonuclease substrate 6-FAM–dArUdAdA–6-TAMRA was from Integrated DNA Technologies (Coralville, IA). Terrific Broth (TB) was from Research Products International Corp (Mt. Prospect, IL). Gels for SDS–PAGE were from Bio-Rad Laboratories (Hercules, CA). Ribonuclease-free 0.10 M sodium phosphate buffer, pH 7.4, containing NaCl (0.10 M) was prepared by making an aqueous solution of NaH_2PO_4 and NaCl

(final concentrations: 0.10 M), adjusting the pH to 7.4 with aliquots of 10 M NaOH, adding diethylpyrocarbonate to 0.1% v/v, incubating for 1 h at 37 °C, and then autoclaving the resulting solution.

3.7.2 Instrumentation and Statistical Calculations

^{1}H NMR spectra were acquired at the National Magnetic Resonance Facility at Madison (NMRFAM) at 298 K with a Bruker DMX-400 Avance spectrometer (Bruker AXS, Madison, WI, ^{1}H, 400 MHz; ^{13}C, 101 MHz; ^{31}P, 162 MHz). ^{13}C and ^{31}P spectra were proton decoupled. All ^{1}H and ^{13}C NMR spectra were referenced to TMS. All ^{31}P NMR spectra were referenced to an internal insert standard of H_3PO_4. Preparatory HPLC was performed on an instrument from Shimadzu Prominence (Kyoto, Japan) equipped with two LC-20AP pumps, a SPD-M20A photodiode array detector, and a CTO-20A column oven. Analytical HPLC was performed on an instrument from Waters (Milford, MA) equipped with two 515 pumps, a 717 plus autosampler, and a 996 photodiode array detector. Protein absorbance values were measured with a Varian Cary 50 UV–Vis Spectrometer from Agilent Technologies (Santa Clara, CA). [*methyl*-^{3}H]Thymidine incorporation into MCF-7 genomic DNA was quantified by scintillation counting using a Microbeta TriLux liquid scintillation and luminescence counter (Perkin–Elmer, Wellesley, MA). Fluorescence measurements were made with a QuantaMaster1 photon-counting cuvette fluorometer from Photon Technology International (South Brunswick, NJ). Calculations for cell proliferation assays were performed using Prism version 5.02 from GraphPad Software (La Jolla, CA).

3.7.3 Determination of Partition and Distribution Coefficients

Values of log*P*, log*D*, and p*I* were calculated with calculator plugins in the program MartinView 5.4.1.1, 2011 from ChemAxon (Budapest, Hungary). Log*P* and log*D* values were set at default: calculations used equal weights of VG, KLOP, and PHYS methods and electrolyte concentrations (Na^+,K^+) and Cl^- set to 0.1 mol/dm^3. We did not consider tautomerization in our calculations.

3.7.4 Recombinant Protein Production

Human pancreatic ribonuclease (RNase 1) was produced as described previously,[162] except that after purification by the two chromatographic steps, the protein was re-purified by both steps to ensure purity. Following purification, purity and apparent molecular mass of RNase 1 was verified with SDS–PAGE.

3.7.5 Fluorescence Assay for Ribonucleolytic Activity

The ribonucleolytic activity of RNase 1 was determined by quantitating its ability to cleave 6-FAM–dArUdAdA–6-TAMRA, as described previously.[162,163] Assays were carried out at ambient temperature in 2.0 mL of 0.10 M MES–NaOH buffer, pH 6.0, containing NaCl (0.10 M). Fluorescence data were fitted to eq 1, in which $\Delta I/\Delta t$ is the initial reaction velocity, I_0 is the fluorescence intensity before addition of ribonuclease, I_f is the fluorescence intensity after complete substrate hydrolysis, and [E] is the total ribonuclease concentration. Data were the average of three experiments. The activity of RNase 1 was $(6.0 \pm 0.7) \times 10^6$ $M^{-1}s^{-1}$. This value is similar to previous values (29% of that in ref. 3, though that enzyme lacked residue 128; 21% of

that in ref. [175], though those assays were performed in a DPBS buffer containing 0.1 mg/mL BSA).

$$k_{cat}/K_M = (\Delta I/\Delta t) / (I_f - I_0)[E] \quad (1)$$

3.7.6 HPLC Assay for Cleavage of Uridine 3'-(4-Hydroxytamoxifen phosphate) by RNase 1

Uridine 3′-(4-hydroxytamoxifen phosphate) (UpHT) was dissolved to a final concentration of 0.090 mM in 0.10 M MES–NaOH buffer, pH 6.0, containing NaCl (0.10 M NaCl). One aliquot (900 μL) of this solution was placed in HPLC vial 1, and another aliquot (300 μL) was placed in HPLC vial 2. Vials with UpHT were pre-incubated at 37 °C in an HPLC autosampler. Buffer A was 0.10 M triethylammonium acetate (TEAA) in H_2O; Buffer B was 0.10 M TEAA in acetonitrile/H_2O 95:5. RNase 1 was diluted in 0.10 M MES–NaOH buffer, pH 6.0, to a concentration of 8.5 μM (~125 mg/L). A Varian 150/4.6 Microsorb-MV 100-5 C18 reverse-phase column was equilibrated with Buffer A/Buffer B 3:7. All samples were eluted isocratically at 1 mL/min for 5 min with the same solution. First, 50 μL from vial 1 was analyzed to obtain a baseline reading. Then, an aliquot (1 μL) of the RNase 1 solution was added to the remaining 850 μL of vial 1 (final RNase 1 concentration: 10 nM, ~0.15 mg/L). Twelve assays were thus performed at known times. An aliquot (50 μL) of vial 2 was analyzed to assess the amount of UpHT activated in the absence of RNase 1. An aliquot (9 μL) of a concentrated solution of RNase 1 (144 μM) was then added to the remaining 250 μL in vial 1 to cleave >95% of the UpHT. After ~1.5 h, an aliquot (50 μL) of this solution was analyzed to quantify the total amount of attainable HT (after adjusting for dilution by RNase 1). The entire experiment was run

in triplicate (for overlaid HPLC traces from one experiment, see: Figure S1). Baseline readings were subtracted from the two HT peaks to obtain HT concentrations at each timepoint. Values are the mean ± SE for each timepoint. All data accounted for the dilution that accompanies the addition of RNase 1. These experiments were repeated to analyze the stability of UpHT (40 uM) in ribonuclease-free 0.10 M sodium phosphate buffer, pH 7.4, containing NaCl (0.10 M); cell medium in the absence of RNase 1; and cell medium in the presence of RNase 1 (0.4 mg/L).

3.7.7 Human Cell Culture

The MCF-7 cell line was a generous gift from Professor J. Wesley Pike (University of Wisconsin–Madison). Cells were grown at 37 °C in a cell-culture incubator in flat-bottomed culture flasks under CO_2 (5% v/v). "Medium A" for the growth and initial plating of cells was Dulbecco's modified Eagle's medium (DMEM) containing phenol red and supplemented with fetal bovine serum (FBS; GIBCO; 10% v/v), penicillin (100 units/mL), streptomycin (100 μg/mL), human recombinant insulin (10 μg/mL), and MEM non-essential amino acids solution (100 μM). "Medium B" for assays of UpHT stability and effect on cell-proliferation was DMEM without phenol red and without FBS, supplemented with penicillin (100 units/mL), streptomycin (100 μg/mL), human recombinant insulin (10 μg/mL), MEM non-essential amino acids solution (100 μM), and sodium pyruvate (1 mM).

3.7.8 Cell-Proliferation Assays

The effect of UpHT and HT on the proliferation of MCF-7 cells was assayed by monitoring the incorporation of [*methyl*-^{3}H]thymidine into cellular DNA, as described

previously.[176] The assay was also similar to that used in a previous study on the toxicity of tamoxifen for MCF-7 cells.[177] For assays, MCF-7 cells (100 μL of a solution of 5.0×10^4 cells/mL) in medium A were plated in each well of 96-well plates and incubated for 22 h to allow for cell adherence. Medium was removed, cells were washed with DPBS, and medium B (50 μL) was added. UpHT and HT were first dissolved in DMSO, and then diluted 1000-fold with medium B, resulting in a final DMSO concentration of 0.1% v/v. This stock solution was serial diluted with medium B containing DMSO (0.1% v/v). The highest concentration HT dilutions appeared to be cloudy, indicating that these concentrations might be reaching the solubility limit of HT in medium. Aliquots (50 μL) of these serial dilutions were added to wells (final DMSO concentration: 0.05% v/v). RNase 1 was diluted in medium B, and wells received either 1 μL of stock RNase 1 for a final concentration of 0.42 μM (~6.2 mg/L, ~15× plasma concentration of ~0.4 mg/L) or 1 μL of medium B, and the analyzed drug concentrations take into account this dilution. RNase 1 control wells received no drug, but did receive RNase 1. After a 2 h incubation, MCF-7 cells were treated with [*methyl*-^{3}H]thymidine for 4 h, and the incorporation of radioactive thymidine into cellular DNA was quantified by liquid scintillation counting. The results are shown as the percentage of [*methyl*-^{3}H]thymidine incorporated relative to control cells treated with medium B containing DMSO (final DMSO concentration 0.05% v/v). Data are the average of three measurements for each concentration, excluding those measurements that were determined to be outliers by the Grubb's test for outliers[178] with $p = 0.05$. The entire experiment was repeated in triplicate. Values for IC_{50} were calculated by fitting the curves by nonlinear regression with eq 2, in which y is the total DNA synthesis following the [*methyl*-^{3}H]thymidine pulse, and h is the slope of the curve.

$$y = 100\% / (1 + 10^{(\log(IC_{50}) - \log[\text{ribonuclease}])h}) \quad (2)$$

3.7.9 Synthesis of UpHT

3.7.9.1 Protected Uridine 3'-(4-Hydroxytamoxifen phosphate)

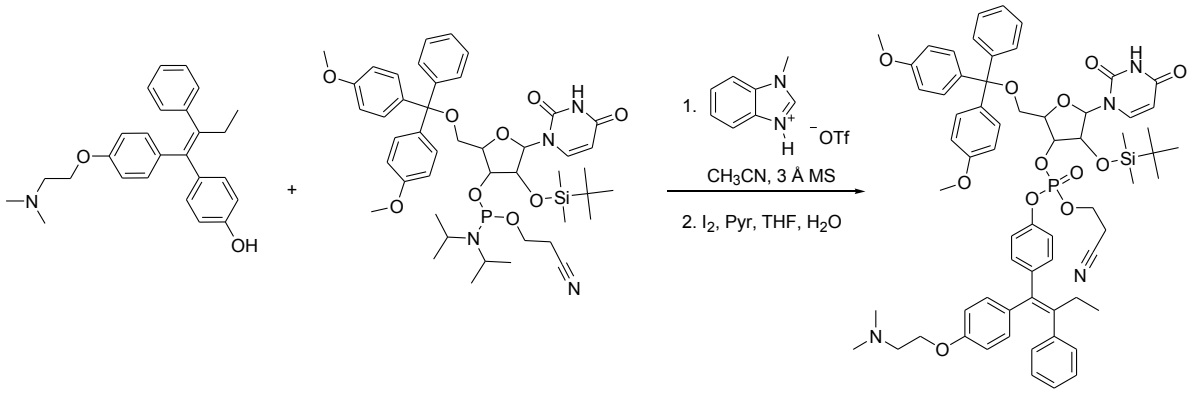

A 20-mL scintillation vial was flame-dried under vacuum. To this vial were added 3-Å molecular sieves (10 beads) followed by 4-hydroxytamoxifen (0.100 g, 0.258 mmol), phosphoramidite (0.222 g, 0.258 mmol), and anhydrous acetonitrile (2.58 mL). After stirring for 5 min, *N*-methylbenzimidazolium triflate (0.073 g, 0.258 mmol) was added and the reaction mixture was allowed to stir for an additional 2.5 h. The solution was then decanted from the sieves into a new scintillation vial, concentrated to remove acetonitrile, and treated with a 0.02 M solution of I_2 (12.6 mL, 2.52 mmol) in tetrahydrofuran, pyridine, and water (Glen Research Oxidizing Solution) for 1 h. The reaction mixture was then concentrated under vacuum and purified by flash silica gel chromatography (MeOH/DCM 1:9) to give protected uridine 3′-(4-hydroxytamoxifen phosphate) as a mixture of isomers (0.279 g, 93%).

^{1}H NMR (400 MHz, CD_3OD) (Mixture of isomers) δ = 7.91–7.83 (m, 1H), 7.43–7.35 (m, 2H), 7.34–7.20 (m, 8H), 7.19–7.01 (m, 8H), 6.91–6.82 (m, 4H), 6.80–6.73 (m, 2H), 6.65–6.56 (m, 2H), 6.00–5.85 (m, 1H), 5.43–5.31 (m, 1H), 5.08–4.96 (m, 1H), 4.64–4.50 (m, 1H), 4.48–4.36 (m, 2H), 4.34–4.21 (m, 1H), 4.15–4.01 (m, 2H), 3.76 (as, 6H), 3.65–3.45 (m, 2H), 3.40–3.10 (m, 2H), 2.95–2.85 (m, 2H), 2.74 (as, 6H), 2.51–2.30 (m, 2H), 0.95–0.82 (m, 12H), 0.20–0.06 (m, 6H).**^{13}C NMR (101 MHz, CD_3OD)** (Major Isomer) δ = 165.6, 160.3, 157.2, 152.1, 150.0, 145.8, 143.8, 143.3, 142.7, 141.7, 138.2, 137.6, 136.3, 133.2, 132.2, 131.5, 130.8, 129.3, 129.2, 129.0, 128.3, 127.4, 121.2, 118.2, 115.6, 114.7, 114.5, 103.3, 88.8, 83.4, 79.4, 75.7, 65.3, 63.7, 63.3, 57.9, 55.9, 44.3, 30.0, 26.2, 20.2, 19.0, 13.8, –4.7. **^{31}P NMR (162 MHz, CD_3OD)** (Mixture of isomers) δ = –8.57, –8.82, –9.02. **HRMS** (ESI) *m/z* 1163.4998 [calc'd for $C_{65}H_{76}N_4O_{12}PSi$ (M+H) 1163.4962].

3.7.9.2 Semi-protected Uridine 3'-(4-Hydroxytamoxifen phosphate)

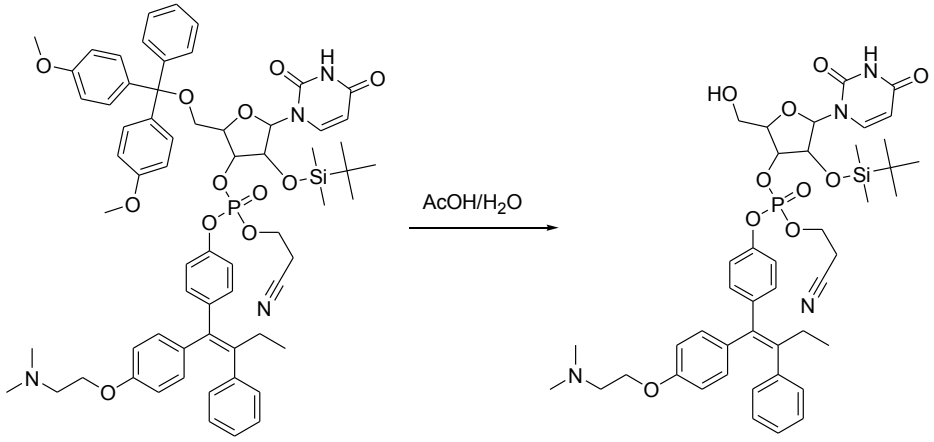

Acetic acid/H_2O 60:40 (4.6 mL) was added to a 20-mL scintillation vial containing 4-hydroxytamoxifen phosphate (0.270 g, 0.232 mmol), and the reaction mixture was allowed to stir at room temperature for 5 h until the starting material was consumed as determined by TLC

(10% MeOH, 90% DCM). The reaction was then quenched by adding saturated sodium bicarbonate (5 mL), extracted with ethyl acetate (4 × 5 mL), dried over sodium sulfate, and concentrated under vacuum. The resulting residue was purified using flash silica gel chromatography (10% MeOH, 90% DCM) to give semi-protected uridine 3′-(4-hydroxytamoxifen phosphate) (0.180 g, 90%).

^{1}H NMR (400 MHz, CD_3OD) (Mixture of isomers) δ = 8.17–7.95 (m, 1H), 7.35–7.21 (m, 3H), 7.20–6.90 (m, 6H), 6.81 (d, J = 8.6, 2H), 6.64 (d, J = 8.6, 2H), 6.09–5.89 (m, 1H), 5.82–5.66 (m, 1H), 4.63–4.25 (m, 4H), 4.20–4.07 (m, 2H), 3.87–3.53 (m, 2H), 3.43–3.26 (m, 3H), 2.97–2.90 (m, 2H), 2.87–2.74 (m, 6H), 2.50–2.40 (m, 2H), 0.97–0.79 (m, 12H), 0.15–0.01 (m, 6H)..**^{13}C NMR (101 MHz, CD_3OD)** (Major Isomer) δ = 164.4, 156.1, 151.0, 148.7, 141.9, 140.7, 137.0, 136.1, 130.8, 130.3, 129.4, 127.6, 125.9, 119.9, 118.8, 116.8, 114.1, 113.3, 102.1, 87.2, 83.7, 78.9, 74.3, 63.9, 62.3, 60.7, 56.5, 42.9, 28.5, 24.8,18.8, 17.6, 12.4, –6.02. **^{31}P NMR (162 MHz, CD_3OD)** (Mixture of Isomers) δ = –8.53, –8.64, –8.71, –8.81. **HRMS** (ESI) m/z 861.3652 [calc'd for $C_{44}H_{58}N_4O_{10}PSi$ (M+H) 861.3655].

3.7.9.3 Uridine 3'-(4-Hydroxytamoxifen phosphate)

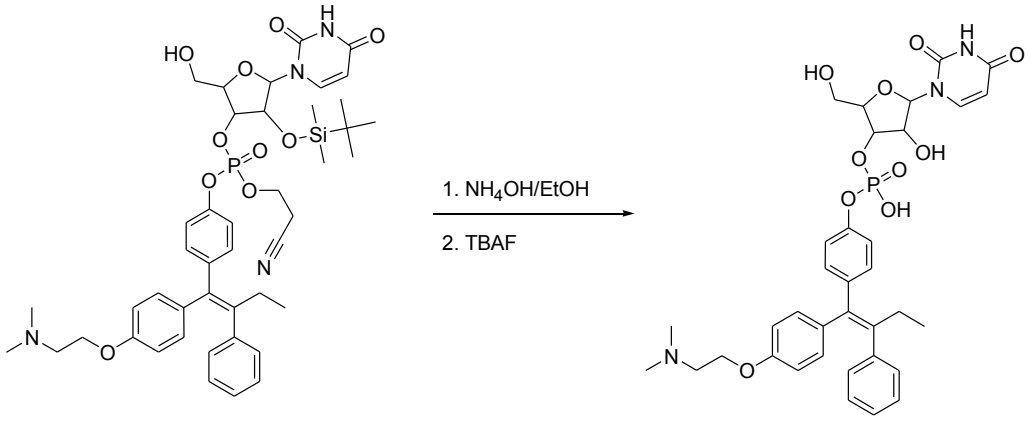

Anhydrous ethanol (1.2 mL) was added to a 20-mL scintillation vial containing semi-protected uridine 3´-(4-hydroxytamoxifen phosphate) (0.051 g, 0.059 mmol) at room temperature followed by ammonium hydroxide (0.04 mL, 1.185 mmol) and the reaction was allowed to stir for 3 h before concentrating under vacuum to give a crude residue that was used directly in the next step.

A portion of the resulting crude residue (0.030 g, 0.037 mmol) was dissolved in anhydrous acetonitrile (4.3 mL) at 0 °C, and a solution of tetrabutylammonium fluoride (0.04 mL, 0.040 mmol) was added in one portion. The reaction mixture was allowed to warm to room temperature while stirring for 5 h. The reaction mixture was then diluted with 4.3 mL of H_2O and loaded onto a column of Macherey–Nagel VP 250/21 Nucleosil 100-5 C18 reverse-phase HPLC resin that had been pre-equilibrated in a solution of acetonitrile (25% v/v) in H_2O, and maintained continually at 35 °C. Sample was washed with the same solution for 13 min. Product was eluted with a linear gradient (25–100% v/v acetonitrile in H_2O) for 68 min, providing uridine 3´-(4-hydroxytamoxifen phosphate) (0.020 g, 69%, for Bu_4N^+ salt).

^{1}H NMR (400 MHz, CD_3OD) (Both Olefin Isomers) δ = 8.03 (d, *J* = 8.1, 0.77H), 7.99 (d, *J* = 8.2, 0.23H), 7.23 (d, *J* = 8.2, 1.54H), 7.17–7.03 (m, 7.00H), 6.97 (d, *J* = 8.5, 0.46H), 6.87 (d, *J* = 8.5, 0.46H), 6.77 (at, *J* = 8.6, 2.00H), 6.61 (d, *J* = 8.6, 1.54H), 5.96 (d, *J* = 5.5, 0.77H), 5.90 (d, *J* = 5.5, 0.23H), 5.69 (at, *J* = 6.8, 1H), 4.77–4.66 (m, 0.77H), 4.64–4.56 (m, 0.23H), 4.35–4.0 (m, 4.00H), 3.80–3.66 (m, 2.00H), 3.63–3.48 (m, 0.46H), 3.31–3.17 (m, 2.00H), 2.80 (s, 1.38H), 2.74 (s, 4.62H), 2.46 (q, *J* = 7.3, 2.00H), 0.90 (t, *J* = 7.3, 3.00H). **^{13}C NMR (101 MHz, CD_3OD)** (Major Isomer Peaks + 4 Bu_4N^+ Salt Signals) δ = 164.7, 155.9, 151.4, 151.0, 142.3, 141.6, 141.1, 138.8, 137.7, 136.5, 131.7, 130.0, 129.5, 127.5, 125.8, 119.8, 113.1, 101.4, 88.5, 84.0, 74.6, 73.9, 62.4, 60.8, 58.1, 56.6, 42.9, 28.5,23.4, 19.3, 12.5, 12.4. **^{31}P NMR (162 MHz, CD_3OD)** (Both Olefin Isomers) δ = –5.90, –6.09. **HRMS** (ESI) *m/z* 716.2324 [calc'd for $C_{35}H_{40}N_3O_{10}PNa$ (M+Na) 716.2344].

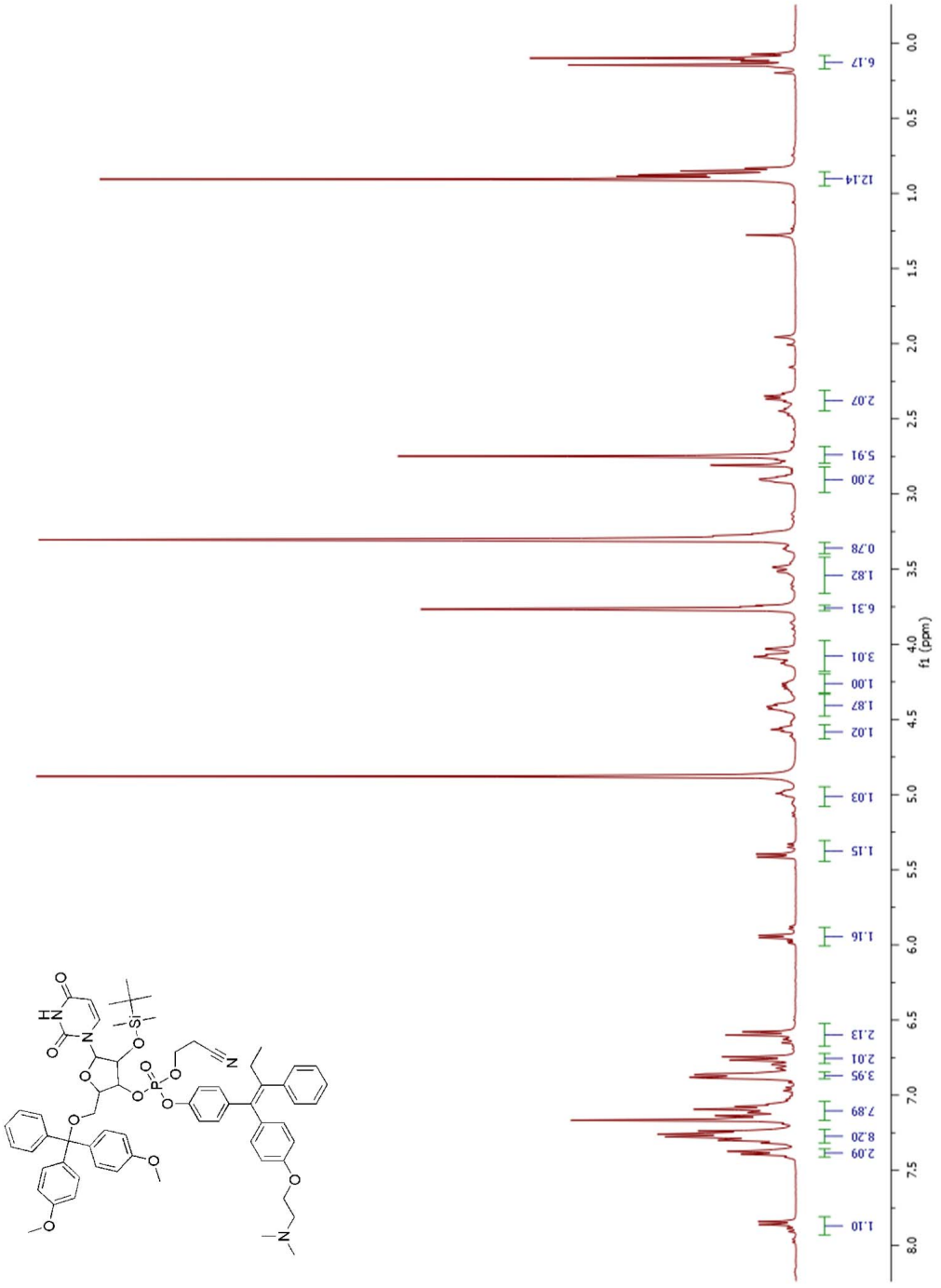
6.17
12.14
2.07
5.91
2.00
0.78
1.82
6.31
3.01
1.00
1.87
1.02
1.03
1.15
1.16
2.13
2.01
3.95
7.89
8.20
2.09
1.10
f1 (ppm)

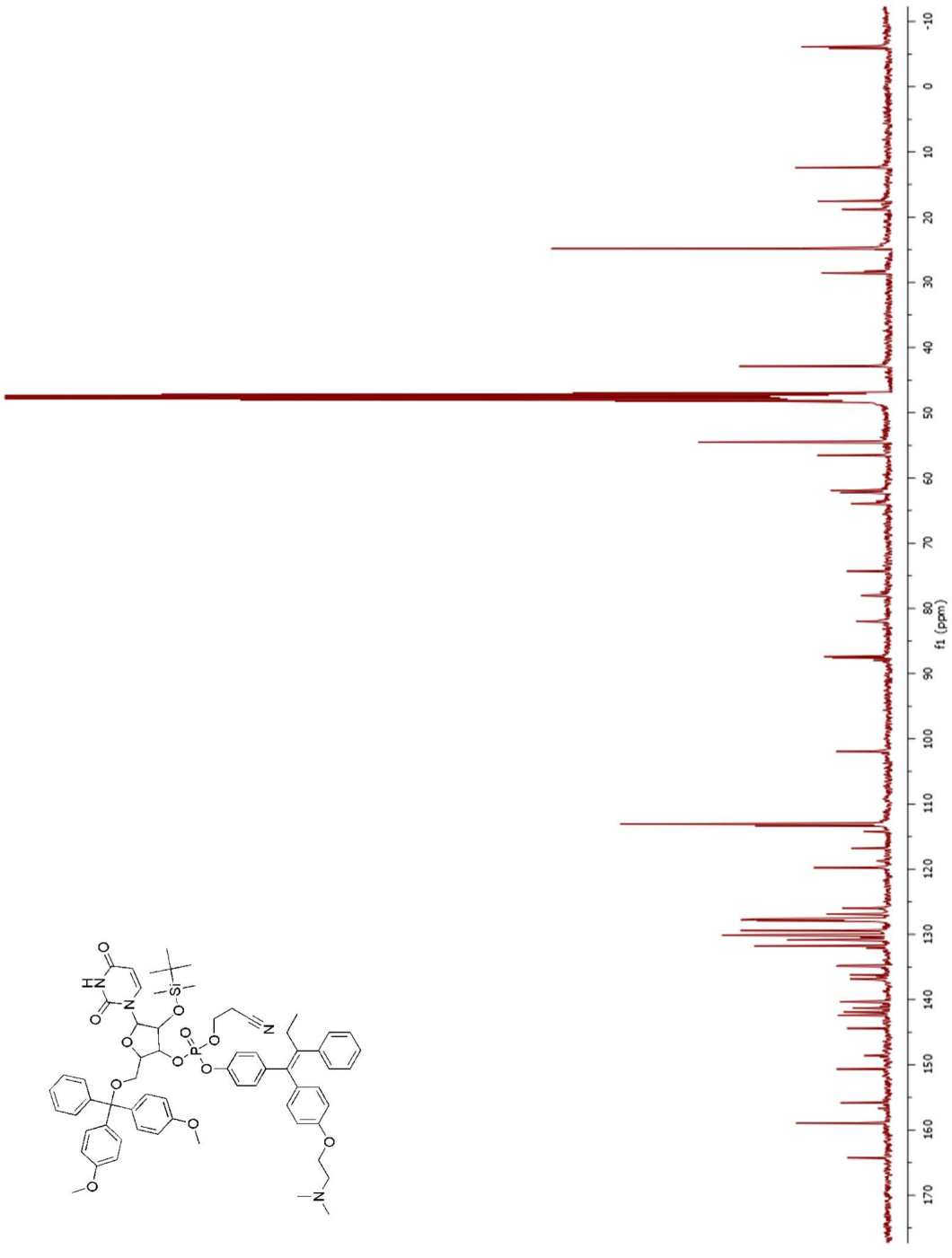
f1 (ppm)

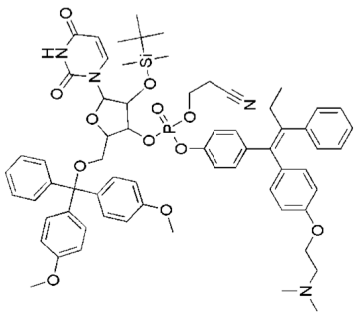

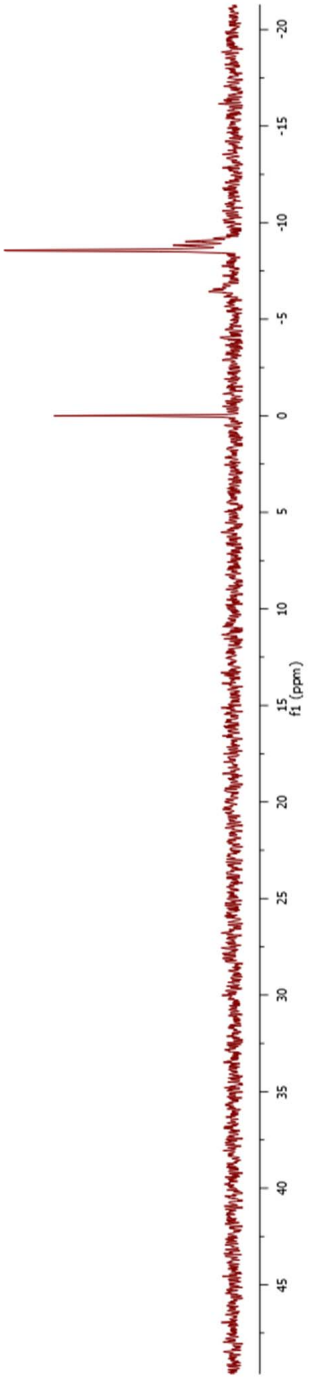
-20
-15
-10
-5
0
5
10
15
f1 (ppm)
20
25
30
35
40
45

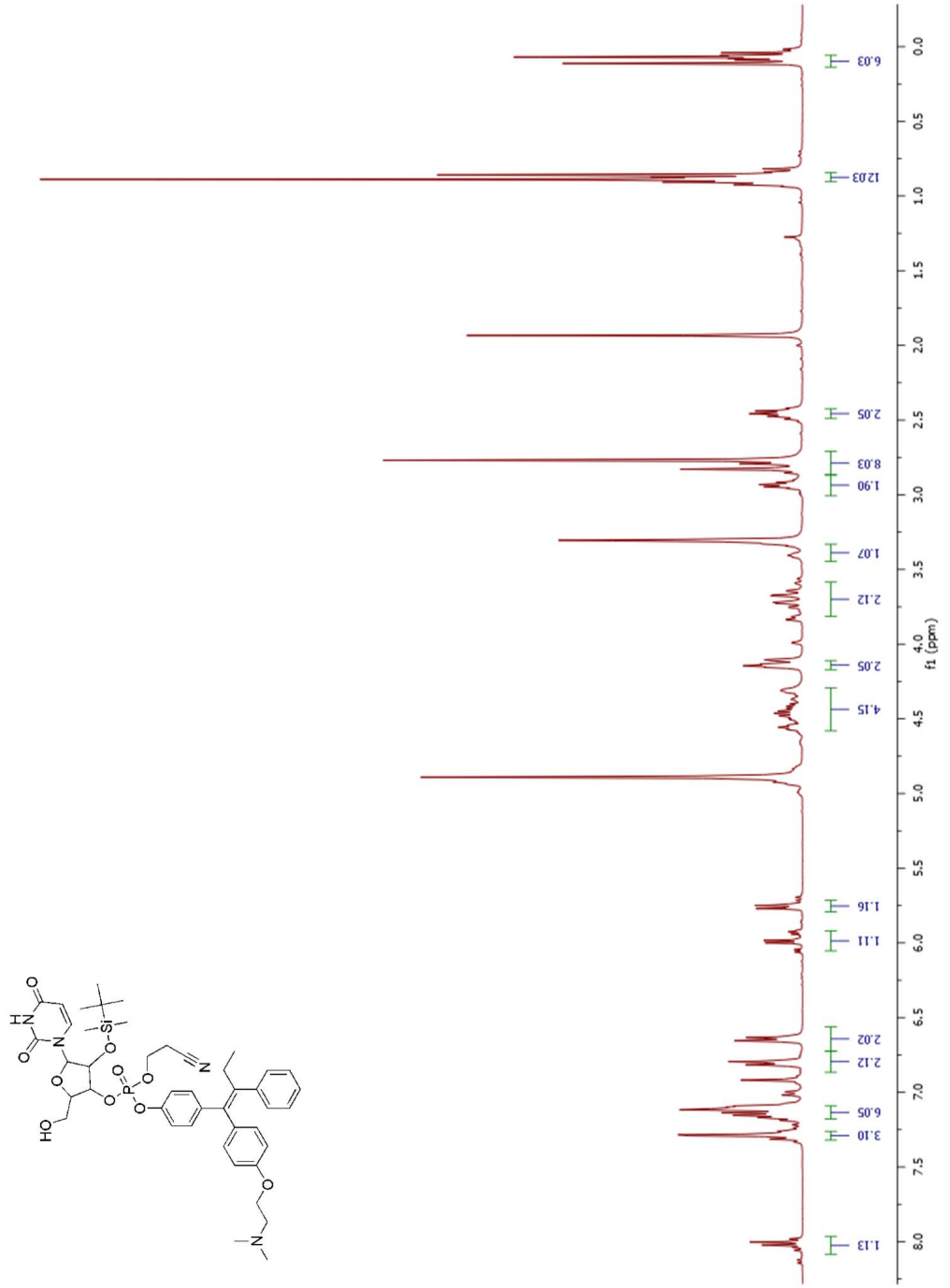
6.03
12.03
2.05
8.03
1.90
1.07
2.12
2.05
4.15
1.16
1.11
2.02
2.12
6.05
3.10
1.13
f1 (ppm)

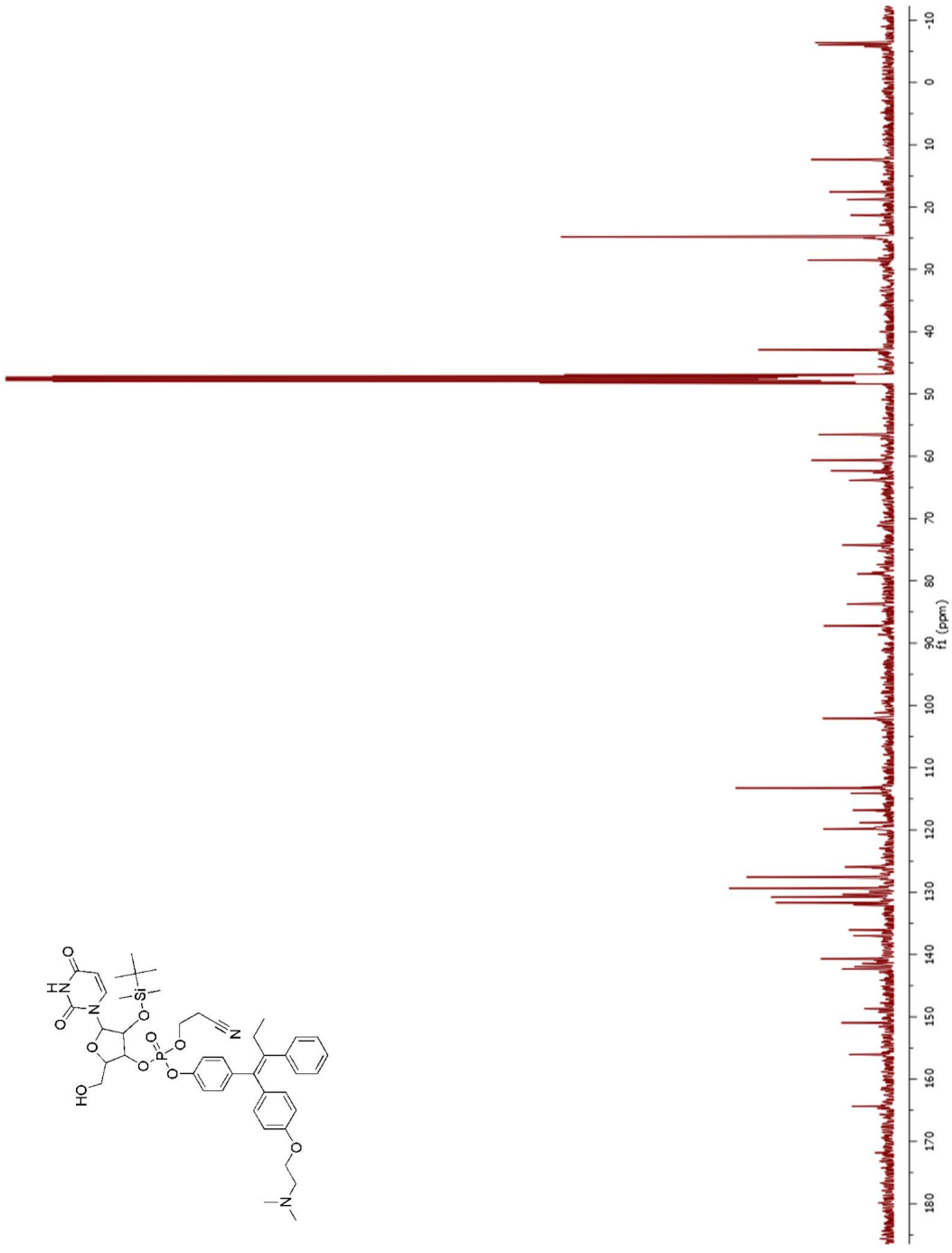
f1 (ppm)

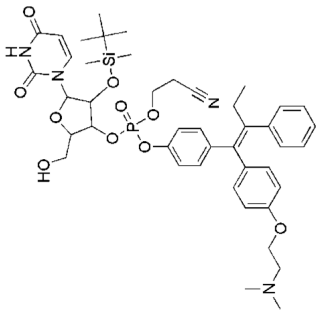

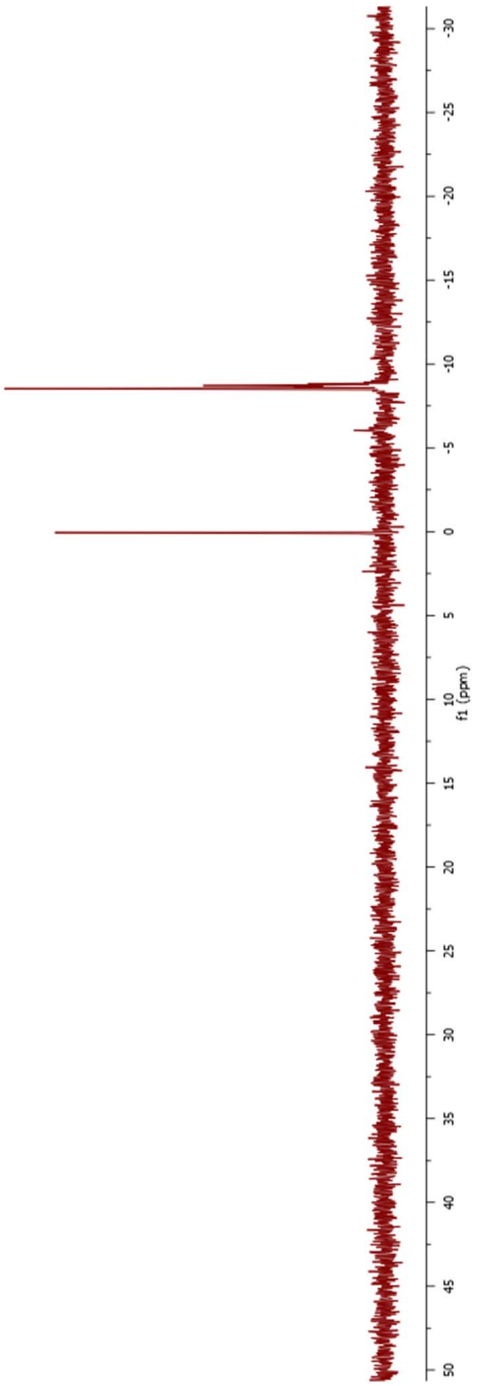
50
45
40
35
30
25
20
15
10
5
0
-5
-10
-15
-20
-25
-30
f1 (ppm)

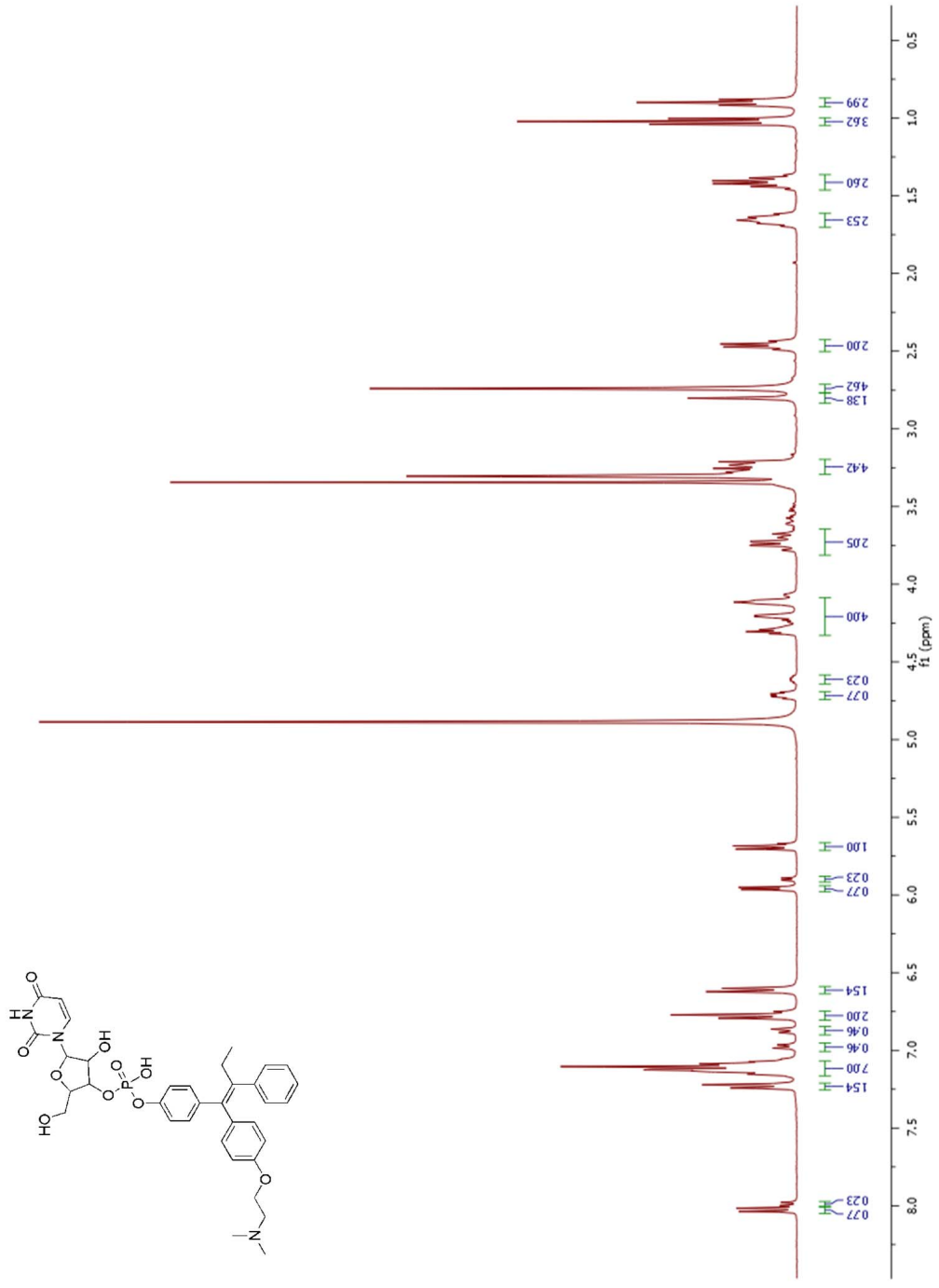
f1 (ppm)
0.5
1.0
1.5
2.0
2.5
3.0
3.5
4.0
4.5
5.0
5.5
6.0
6.5
7.0
7.5
8.0
2.99
3.62
2.60
2.53
2.00
4.62
1.38
4.42
2.05
4.00
0.77
0.23
1.00
0.77
0.23
1.54
2.00
0.46
0.46
7.00
1.54
0.77
0.23

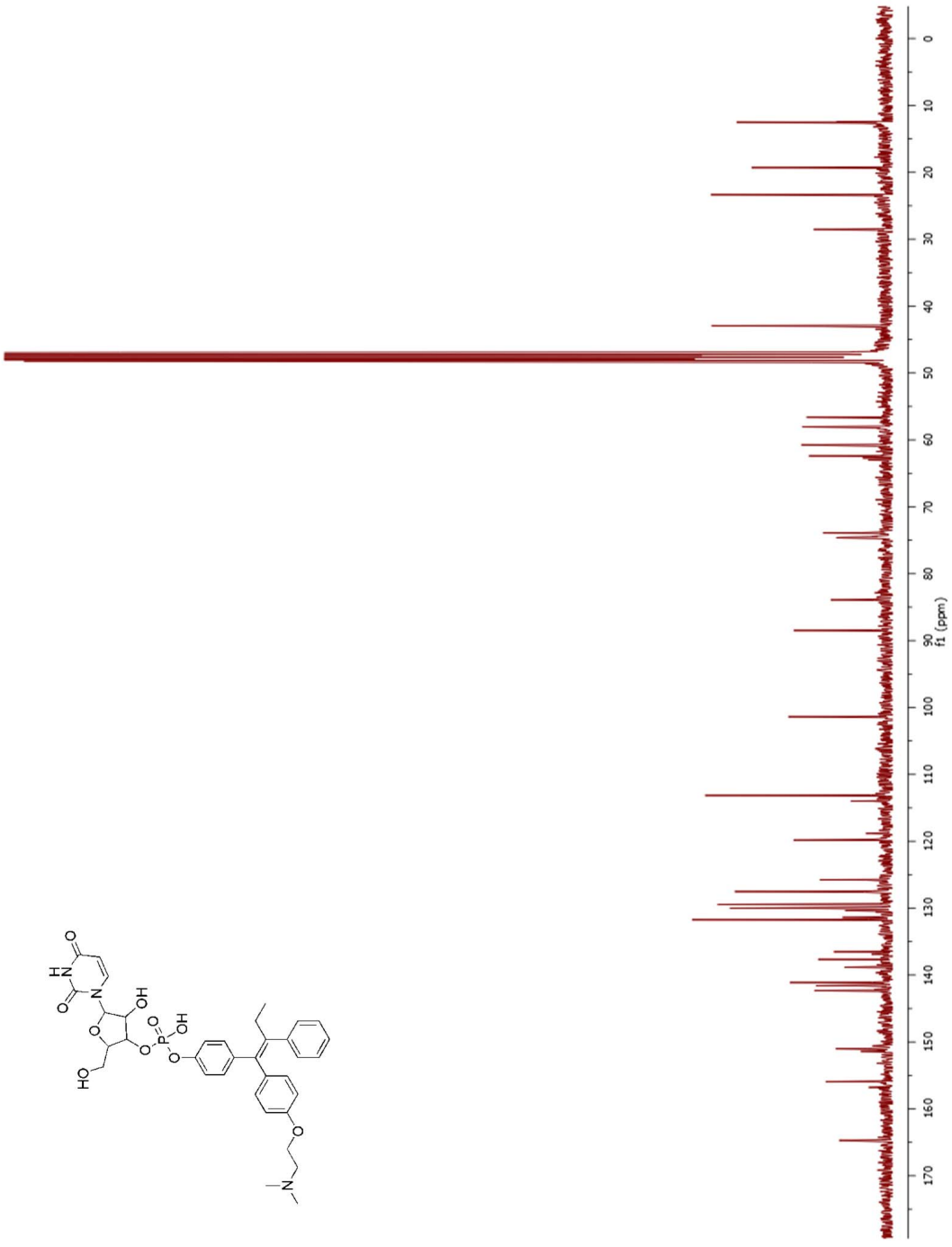
f1 (ppm)

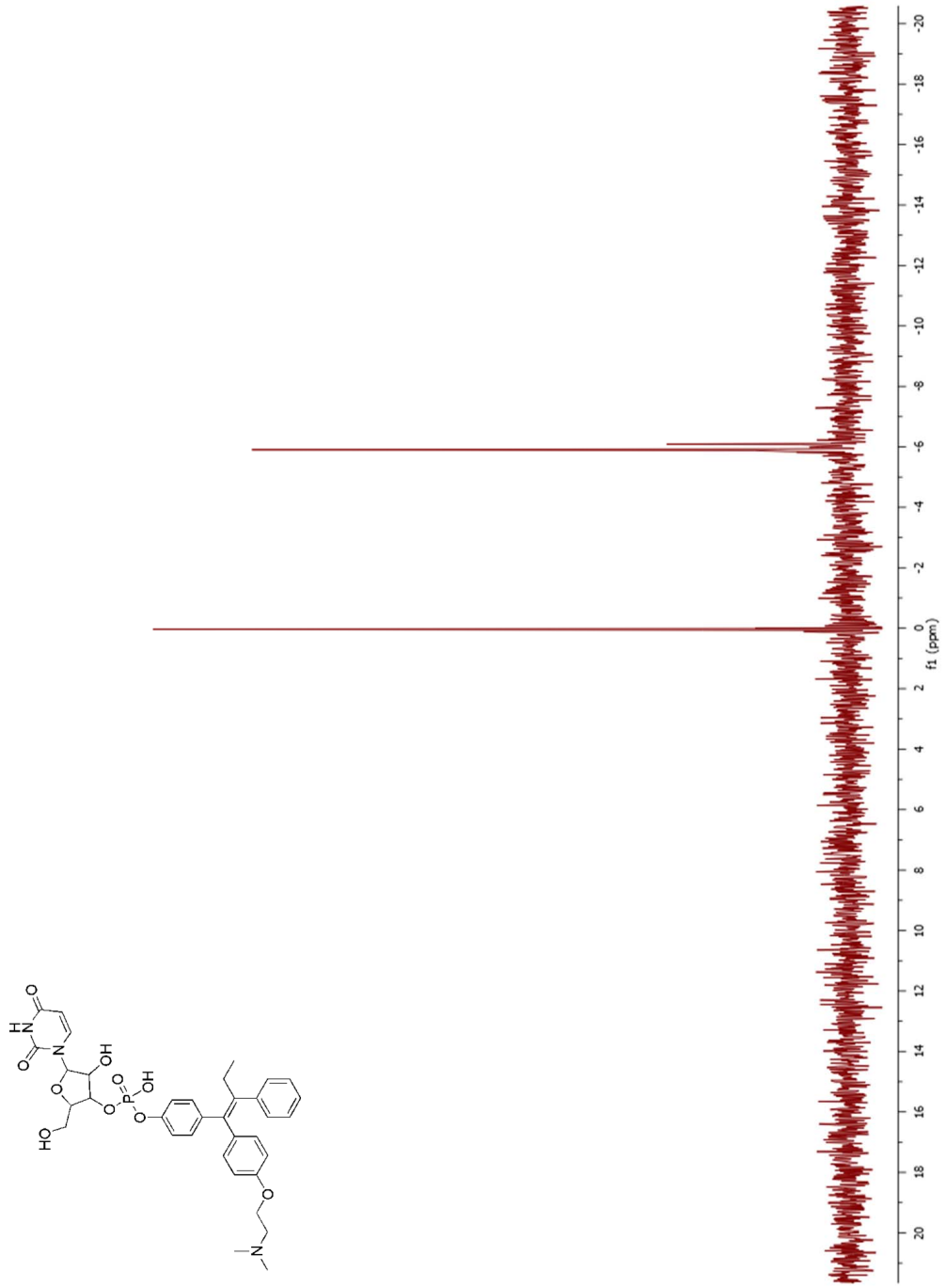
f1 (ppm)

Chapter Four

Ribonucleotide 3′-Phosphate as a Pro-Moiety for an Orally Administrable Drug

4.1 Abstract

Safe and efficient oral administration of therapeutics is crucial for modern medicine. Extended release formulations maintain therapeutic concentrations of a drug over time. Pendant phosphate esters are commonly used to overcome poor oral bioavailability of drugs due to poor aqueous solubility. We reasoned that a ribonucleoside 3′-phosphate could serve as a pro-moiety that releases a drug of interest over time, analogous to an extended release formulation, but also simultaneously enhances the hydrophilicity of a drug to enhance its oral bioavailability. Herein, we report on the efficient synthesis of ribonucleoside 3′-(metronidazol phosphate) (RpMet). RpMets demonstrate enhanced aqueous solubility compared to the parent drug as well as timed-release kinetics based upon the nucleobase. Additionally, the RpMets were inactive antimicrobials against *Bacteroides fragilis* until unmasked by human pancreatic ribonuclease. These data demonstrate the utility of a human pancreatic enzyme as a useful activator of a prodrug.

4.2 Author Contributions

Original idea for using ribonucleoside 3′-phosphate pro-moieties for timed-release was from M.J.P. A.K.F.D. and N.A.M. synthesized and characterized the prodrugs. N.A.M. ran Tris-HCl buffered kinetics. M.J.P. ran all other kinetics and analyzed the data. M.J.P., under the guidance of and in collaboration with C.A.S., established tested the MIC of the prodrugs. M.J.P.

drafted the original manuscript and figures. M.J.P., N.A.M., C.A.S., and R.T.R. planed experiments, analyzed data, and edited the manuscript and figures.

4.3 Introduction

Oral administration of therapeutics is the mainstay for the treatment of disease. Sustained release formulations have been crucial for the safe and effective dosing of orally available drugs.[179-183] They allow for the prolonged maintenance of therapeutic concentrations of a drug, reducing the required dosages per day, which enhances patient compliance. Additionally, sustained release formulations allow for tighter control over the pharmacokinetics of a drug, helping minimize side effects.[179-183] Traditional sustained release formulations have been premised on diffusion of a drug out of a matrix. The pore sizes and composition of the matrix dictates the timed-release properties of the formulation.[179,180,182,183] One major drawback to sustained release matrix formulations is that they do not allow for improved properties of the drug.

Aqueous solubility is a crucial property for any orally available drug.[36,37,184] Robust absorption across the intestinal epithelium relies upon a high concentration of the drug on the apical side of an enterocyte to drive diffusion into the cell and, eventually, into the circulatory system. On average, 35–40% of lead compounds have aqueous solubilities less than 5 mg/mL, which is defined by the U.S. Pharmacopeia as slightly soluble or worse.[185] Therefore, many compounds must be modified for improved aqueous solubility in order for them to become bioavailable and therefore efficacious.[37]

Phosphate esters have been used to improve the oral bioavailability of poorly water soluble therapeutics.[36,37,186-188] Alkaline phosphatase catalyzes the rapid hydrolysis of phosphoryl groups near the surface of enterocytes, releasing the lipophilic drug and allowing for efficient

absorption into the body. There are several U.S. Food and Drug Administration (FDA) approved drugs that use this strategy to improve oral bioavailability, including estramustine, fosamprenavir, and prednisolone phosphate.[186-188]

Recently, we reported the use of ribonucleoside 3′-phosphate as a pro-moiety for the timed-release of hydroxytamoxifen.[189] Ribonucleoside 3′-phosphates not only instill desirable release kinetics, mediated by human pancreatic ribonuclease (RNase 1[44]; EC 3.1.27.5), but also increase the aqueous-solubility of the parent drug. RNase 1 is an ideal endogenous enzyme for pro-moiety release. It is one of the main digestive enzymes excreted from the pancreas and is estimated to have a concentration of 0.9 mg/mL in human pancreatic juice.[139] Moreover, like its renowned homologue bovine pancreatic ribonuclease (RNase A[47,48]), RNase 1 catalyzes the cleavage of RNA by a transphosphorylation reaction[49-51] and has little specificity for its leaving group.[52-56] Herein, we demonstrate the use of ribonucleoside 3´-phosphates as a pro-moiety for enhanced solubility and timed-release kinetics of a model orally available drug, metronidazole.

Metronidazole is a commonly used antibiotic for a variety of protozoa and anaerobic bacterial infections, including: *Trichomonas vaginalis, Entamoeba histolytica, Bacteroides fragilis, Clostridium difficile,* and *Helicobacter pylori*.[190] In 1997, Flagyl ER, an extended release formulation of metronidazole, was approved by the FDA as a superior treatment for bacterial vaginosis.[191] Still, metronidazole has several common side effects, such as nausea, diarrhea, and metallic taste. Additionally, metronidazole therapy can occasionally cause more severe side effects, such as pancreatitis, neutropenia, neuropathies, or CNS toxicities.[192] Better control over the pharmacokinetics of metronidazole could attenuate these adverse side effects.[193] Many

prodrugs of metronidazole have been synthesized to improve water solubility, while attempting to decrease toxicity.[193] Hence, as a proof of concept study, we elected to attach metronidazole to ribonucleoside 3´-phosphates to assess the potential of this pro-moiety for orally available drugs (Figure 4.1).

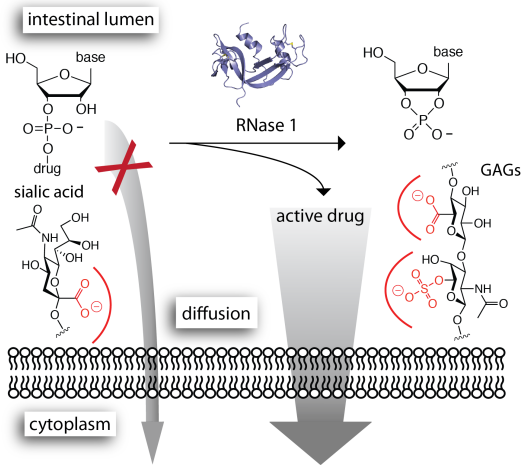

Figure 4.1 Due to the anionic charge of the ribonucleotide 3´ phosphate, diffusion of the drug into the intestinal enterocytes is prevented. Upon cleave by RNase 1, which occurs over time, the parent drug is free to diffuse into the body and becomes bioavailable.

4.4 Results and Discussion

Ribonucleoside 3´- (metronidazole phosphate) (RpMet) was synthesized in four steps from commercially available metronidazole (Met) and the ribonucleoside phosphoramidite (Scheme 1). Briefly, Met was coupled to the phosphoramidite by using *N*-methylbenzimidazolium triflate (MBIT) as a catalyst.[160] The coupled product was oxidized subsequently with iodine and deprotected stepwise. The final products were purified by silica-gel chromatography. Using this route, three RpMets were synthesized: uridine 3′-(metronidazole

phosphate) (UpMet), cytidine 3′-(metronidazole phosphate) (CpMet), and adenosine 3′-(metronidazole phosphate) (ApMet).

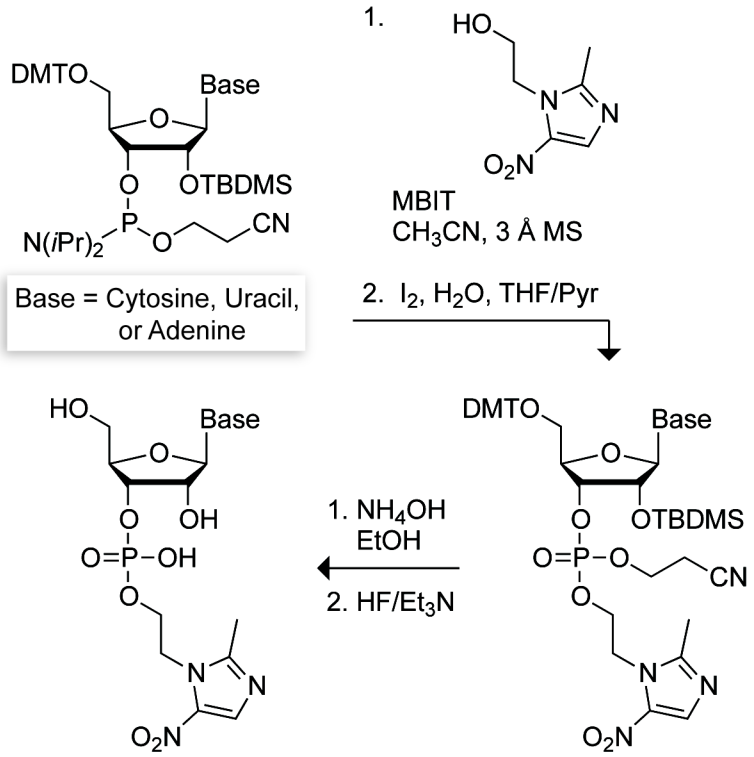

Scheme 4.1 Synthesis of RpMet

We expected the ribonucleoside 3′-phosphate moiety of a RpMet to endow the prodrug with greater hydrophilicity than the parent drug, which could improve its oral bioavailability. To investigate this issue, we calculated the partition (log *P*) and distribution (log *D*) coefficients of CpMet, UpMet, ApMet, and Met.[161] The calculated log *P* and log *D* values for the RpMets were indeed significantly lower than those of the parent drug, Met (Table 1), indicative of increased

hydrophilicity. This increase in hydrophilicity could rescue drugs that do not readily disaggregate in water and thus make them more orally bioavailable.

Table 4.1 Calculated partition and distribution coefficients of Met and RpMets

Coefficient	Met	CpMet	UpMet	ApMet
log*P*	-0.46	-2.48	-2.10	-1.78
log*D* (pH = 7.5)	-0.46	-4.86	-4.48	-4.15
log*D* (pH = 1.1)	-1.49	-3.73	-3.20	-5.57

To be the basis for an effective timed-release prodrug strategy, the pro-moiety needs to be released by the activating enzyme over time. Hence, we assessed the RNase 1-catalyzed rate of Met-release from RpMet. Wada and co-workers quantified the amount of RNase 1 from human pancreatic juice to be approximately 0.9 mg/mL.[139] We reasoned that pancreatic juice probably gets diluted by ten- to one-hundred fold in the intestine, which was the basis for using 0.1 mg/mL and 0.01 mg/mL RNase 1 for our Met-release studies. Inorganic phosphate inhibits ribonuclease A with a K_i of 2.3 mM,[194] so we initially investigated the contribution of phosphate buffer inhibition from simulated intestinal fluid (SIF) on the rates of UpMet unmasking (Figure 4.2A). Compared to a buffer with no inorganic phosphate (19.5 mM Tris-HCl, pH 7.4, 2.5% D_2O), rates of Met release were marginally slower in SIF. Next, we assessed the tunability of the rate of the RpMet hydrolysis based upon the base attached to Met. RNase A catalyzes the cleavage of RNA after cytidine residues more than after uridine residues and has significantly reduced rates of cleavage with purines as the 5' nucleotide.[195] Accordingly, we predicted that RNase 1 would unmask CpMet faster than UpMet, and unmask ApMet slowly or not at all. Gratifyingly, for both concentrations of RNase 1, we observed that the cytidine prodrug was

indeed unmasked faster than was the uridine prodrug (Figure 4.2B). The adenosine conjugate did not unmask at all, even when incubated for over 4 days at 37 ºC. Unlike our uridine hydroxytamoxifen conjugates that hydrolyzed in aqueous solutions (pH 7.4) lacking ribonucleases, our RpMet conjugates were stable in ribonuclease free SIF, which has pH 7.5, and in simulated gastric fluid (SGF), which has pH 1.1. We did not observe any appreciable degradation (< 5%) in either medium (Figure 4.4). This stability is attributable to the significantly higher pK_a of the metronidazole alkoxy group compared to the 4-hydroxytamoxiphen aryloxy group, making the alkoxy group a poorer leaving group, and therefore a more stable conjugate to a nucleotide.

Finally, we wanted to assess the antimicrobial activity of our RpMet prodrugs on *Bacteroides fragilis* (*B. fragilis*). Minimum inhibitory concentrations (MIC) of UpMet and ApMet were assessed compared to Met (Table 4.2). The MIC values are reported in μM concentrations along with the equivalent values of Met in μg/mL for literature comparative purposes. The culture medium was treated with 0.1% diethylpyrocarbonate (DEPC) in an effort to eradicate any residual ribonuclease activity in the medium, and DEPC-treatment was determined to have no effect on the MIC of Met (Figure 4.5). Both UpMet and ApMet had considerably higher MIC values than did Met, demonstrating that the prodrugs were inactive. It is unclear if residual ribonucleolytic activity in the culture medium unmasked a small portion of UpMet to make it active at 171 μM, if the UpMet stock had a small amount of contaminating Met, or if UpMet itself has a lower baseline antimicrobial activity compared to ApMet. As a control, UpMet was incubated with 0.1 mg/mL RNase 1 overnight to unmask the drug fully,

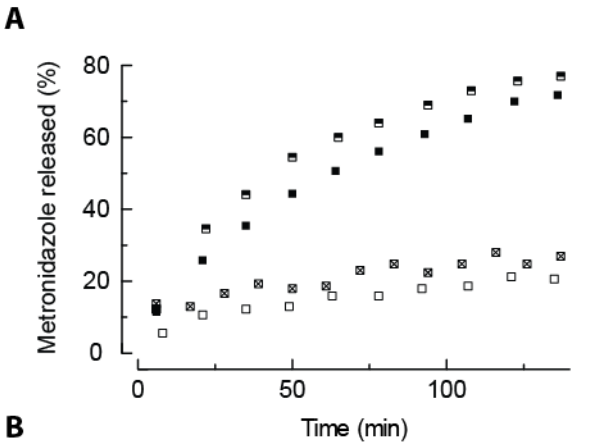

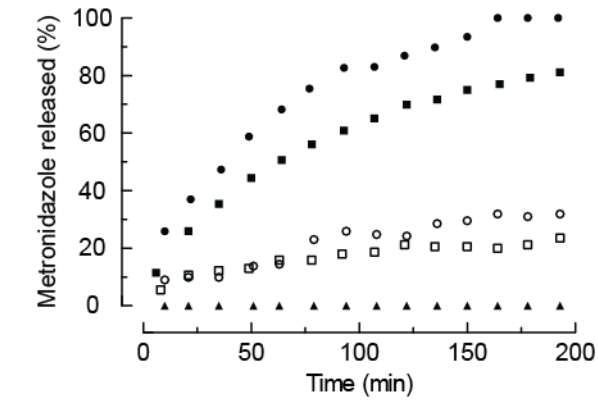

C

	nucleoside	buffer	RNase 1 (mg/mL)	$t_{1/2}$(min)
●	cytidine	SIF	0.1	39
◓	uridine	TRIS	0.1	43
■	uridine	SIF	0.1	59
○	cytidine	SIF	0.01	374
⊠	uridine	TRIS	0.01	424
□	uridine	SIF	0.01	695
▲	adenosine	SIF	0.1	ND

Figure 4.2 Progress curves for the release of Met from RpMets under various conditions. (A) Comparison of UpMet hydrolysis rates in Tris-HCl buffer vs SIF. (B) Comparison of CpMet, UpMet, and ApMet hydrolysis rates in SIF. (C) Half-life values of various RpMet conjugates. Note: Uridine SIF data is reported in both (A) and (B) for comparison.

which resulted in a MIC similar to that of Met. Additionally, to demonstrate slow release of the drug over time, UpMet was put in culture medium containing 0.01 mg/mL RNase 1. Even after the 48-h incubation time of the experiment, UpMet was not fully unmasked because it had a MIC

of 11 μM, compared to 3 μM for the fully unmasked UpMet or 171 μM for the prodrug. Thus, we have demonstrated proof-of-concept for a prodrug strategy that employs a human pancreatic enzyme to release an orally available agent in a timed- release manner (Figure 4.1).

Table 4.2. MIC values of RpMets

compound	RNase 1 (mg/mL)	MIC (μM)	MIC (equivalents of Met in μg/mL)
M	----	5–3	1–0.5
ApM	----	> 684	> 128
UpM	----	171	32
M	0.1 ON	5–3	1–0.5
UpM	0.1 ON	3	0.5
M	0.01	5–3	1–0.5
UpM	0.01	11	2

ON = incubation of RNase 1 with the compound over night prior to the MIC experiment

4.5 Conclusions

The primary advantage of this prodrug strategy is its modularity. As described here, the rate of hydrolysis of this prodrug strategy is based upon the nucleobase attached to the ribose and RNase 1 can only hydrolyze prodrugs attached to pyrimidine nucleotides. Expanding the attainable rates of hydrolysis for this system requires testing the pyrimidine nucleobase analogues. Upon development of a series of cleavable ribonucleotides, this system should allow for substantial modulation of the rate of activation of drugs.

As described previously, RNase 1 can cleave aryloxy drugs attached to the 3´-phosphate of a ribonucleotide and herein we demonstrated that it can also cleave an alkoxy group containing drug.[189] This system can be expanded even further with self-immolative linkers,

which could liberate amine-containing chemotherapeutic agents. Additionally, the 5´ hydroxyl group of the nucleotide can be modified for enhanced aqueous solubility or any other property that is desirable to impart on the prodrug. Finally, another added benefit of this system is that the product of prodrug hydrolysis, a nucleotide, is a native, non-toxic metabolite, which should not alter the toxicity profile of the parent drug.

4.6 Acknowledgments

This work was supported by Grant R01 CA073808 (NIH). M.J.P. was supported by Molecular and Cellular Pharmacology Training Grant T32 GM008688 (NIH) and predoctoral fellowship 09PRE2260125 (American Heart Association). N.A.M. was supported by the postdoctoral fellowship F32 GM096712 (NIH). This study made use of the National Magnetic Resonance Facility at Madison, which is supported by NIH Grants P41RR02301 (BRTP/NCRR) and P41GM66326 (NIGMS). Additional equipment was purchased with funds from the University of Wisconsin, the NIH (RR02781, RR08438), the NSF (DMB-8415048, OIA-9977486, BIR- 9214394), and the U.S. Department of Agriculture.

4.7 Materials and Methods

4.7.1 Materials

Uridine phosphoramidite and iodine oxidizing solution were from Glen Research (Sterling, VA). Metronidazole, 3-Å molecular sieves, tetrabutylammonium fluoride (TBAF), methylbenzimidazole, Brucella broth powder, vitamin K, Hemin, and all other commercial reagents were from Sigma–Aldrich (St. Louis, MO). Methylbenzimidazole triflate was made

according to literature precedent from methylbenzimidazole.[160] Spectra/Por® dialysis bags (3500 MWCO) and lysed horse blood were from Fisher Scientific (Thermo Fisher Scientific, Walham, MA). *Escherichia coli* BL21(DE3) cells were from Novagen (Madison, WI). Simulated intestinal fluid was from RICCA Chemical Company (Arlington, TX). HiTrap columns were from GE Biosciences (Piscataway, NJ). MES buffer was from Sigma–Aldrich (St. Louis, MO) and was purified by anion-exchange chromatography to remove trace amounts of oligomeric vinylsulfonic acid.[164] Terrific Broth (TB) was from Research Products International (Mt. Prospect, IL). Gels for SDS–PAGE were from Bio-Rad Laboratories (Hercules, CA). Quartz NMR tubes were from Wilmad-LabGlass (Vineland, NJ). *Bacteroides fragilis* was from ATCC® (strain 25285, Manassas, VA). Round, 96-well, U-bottom plates and 95-pin inoculator assemblies were from Evergreen Scientific (Los Angeles, CA).

4.7.2 Instrumentation and statistical calculations

^{1}H NMR spectra were acquired at the National Magnetic Resonance Facility at Madison (NMRFAM) at 298 K with a Bruker DMX-400 Avance spectrometer (Bruker AXS, Madison, WI, ^{1}H, 400 MHz; ^{13}C, 101 MHz; ^{31}P, 162 MHz). ^{13}C NMR spectra were also acquired on an Avance III 500 MHz spectrometer with a ^{13}C/^{15}N{^{1}H} 5-mm cryogenic probe from Bruker AXS (Madison, WI, ^{13}C, 126 MHz). ^{13}C and ^{31}P spectra were proton decoupled. All ^{1}H and ^{13}C NMR spectra were referenced to TMS. All ^{31}P NMR spectra were referenced to an internal insert standard of H_3PO_4. Protein absorbance values were measured with a Varian Cary 50 UV–Vis Spectrometer from Agilent Technologies (Santa Clara, CA). ^{1}H NMR spectra for the RpMet release kinetics were acquired at the NMRFAM at 310 K on an Avance III 500 MHz

spectrometer with a TCI 500 H-C/N-D cryogenic probe from Bruker AXS (Madison, WI, ^{1}H, 500 MHz). Photos of 96 well plates to determine the MIC values of various compounds were taken using an iPhone 4S from Apple Computer (Cupertino, CA).

4.7.3 Production and purification of RNase 1

RNase 1 was expressed and purified as reported previously.[162] RNase 1 was concentrated to 6.98 mg/mL in the elution buffer, which consisted of 65% buffer A (50 mM NaOAc and 10 mM EDTA, pH 5.0) and 35% buffer B (50 mM NaOAc, 370 mM NaCl, and 10 mM EDTA, pH 5.0). RNase 1 was diluted subsequently into the appropriate buffer for any given assay.

4.7.4 Representative procedure for kinetic analysis of prodrug hydrolysis

The degradation of RpMet by RNase 1 was assessed by ^{1}H NMR spectroscopy. Reactions consisted of 2.1 μmoles of prodrug and the indicated amount of added RNase 1. NMR experiments were conducted in simulated intestinal fluid (USP XXII formulation, without pancreatin, pH 7.5, with 2% D_2O added v/v), a 19.5 mM Tris–HCl buffer, pH 7.4, containing D_2O (2.5% v/v), or 0.1 N HCl, pH 1.1, containing D_2O (2% v/v) in a quartz NMR tube (Wilmad-Labglass). ^{1}H NMR experiments consisted of the first increment of a 2D NOESY with gradients for improved water suppression.

The NMR experiments were setup as follows. First, the spectrometer was shimmed using 3D shimming for solvent suppression to a 700 μL sample of the buffer with no added RpMet. The RpMet to be tested was dissolved in 350 μL of buffer, placed in the NMR tube, and incubated at 37 °C for five min. Simultaneously, a 2× concentrated solution of RNase 1 in the

same buffer was warmed to 37 °C for 5 min. At $t = 0$, 350 μL of the RNase 1 solution was put in the NMR tube and mixed, giving the final concentration of reaction components as described above. The NMR tube was inserted into the spectrometer, and spectra were recorded. The methyl group on the imidazole ring for the prodrug and free metronidazole were distinguishable; therefore, the degradation reaction was monitored by integrating this methyl peak throughout the course of the reaction.

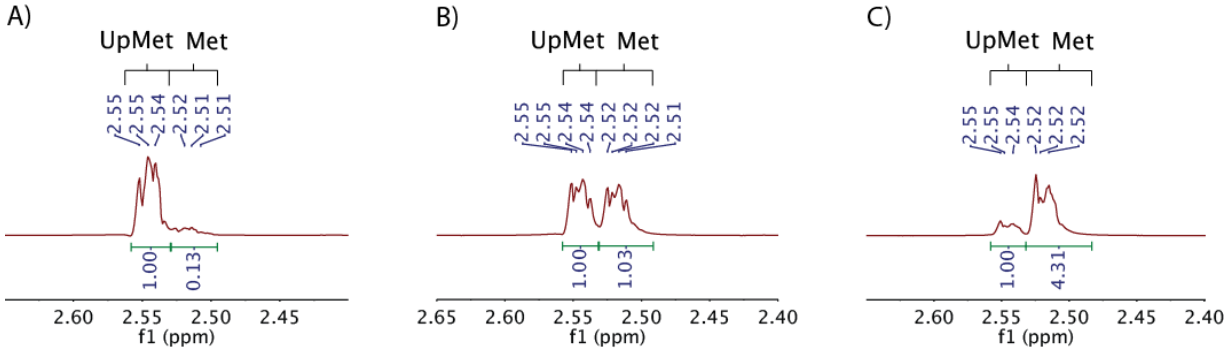

Figure 4.3 Representative ^{1}H NMR spectra for assessing the rate of prodrug hydrolysis. Degree of degradation was assessed by following the methyl imidazole peak integrations of UpMet (2.55) and Met (2.52). The assay solution contained RNase 1 (0.1 mg/mL) in simulated intestinal fluid. (**A**) 6 min, (**B**) 64 min, and (**C**) 193 min.

4.7.5 Preparation of culture medium

Guidelines for MIC determination of metronidazole with the quality control anaerobic bacterial strain *Bacteroides fragilis* (ATCC® 25285, Manassas, VA) were followed from the Clinical and Laboratory Standards Institute.[196] *B. fragilis* was cultured in supplemented Brucella broth, which consisted of Brucella broth powder (28 g), Hemin stock solution (1.0 mL), and vitamin K_1 (1.0 mL of a working solution in 900 mL of water). After the solution was sterilized at 121 °C for 15 min in an autoclave and allowed to cool to <50 °C, sterile lysed horse blood

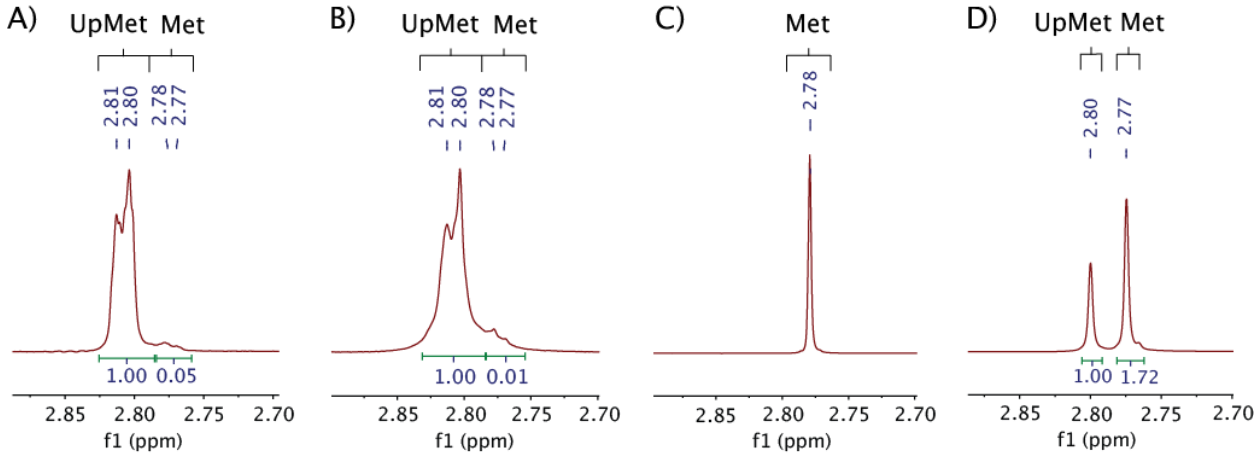

Figure 4.4 Representative ^{1}H NMR spectra for 3-h incubations in simulated gastric fluid (0.10 N HCl, 2% v/v D_2O, pH 1.1, United States Pharmacopeia) to assess the stability of these molecules in a stomach. Degree of degradation was assessed by following the methyl imidazole peak integrations of UpMet (2.80) and Met (2.78). (**A**) Spectrum of UpMet at 0 min. (**B**) Spectrum of UpMet at 3 h. (**C**) Control spectrum of Met. (**D**) Spectrum of UpMet after the 3-h incubation with added Met to confirm that the minor peak at 2.78 ppm as indeed Met. After 3 h, there was no increase in the amount of Met present; therefore UpMet is stable under these conditions. (Note: For spectra in panels C and D, the spectrometer was re-shimmed, which allowed for better resolution of the peaks compared to those in panels A and B.)

(100 mL of a 50% v/v solution) was added. Hemin stock solution was prepared by dissolving 0.1 g hemin into 2 mL of 1.0 NaOH, bringing the final volume to 20 mL with distilled water, and sterilizing at 121 °C for 15 min. Vitamin K_1 working solution was prepared by adding vitamin K_1 (0.20 mL) to 95% ethanol (20 mL). Then, 1 mL of this solution was added to 9 mL of sterile, distilled water, resulting in a 1.0 mg/mL working solution of vitamin K_1. Lysed horse blood (50% v/v) was prepared by diluting lysed horse blood (50% v/v) with sterile, distilled water. The solution was clarified by centrifugation at 12,000*g* for 20 min. The supernatant was decanted through a 40-μm, nylon cell strainer (BD, Franklin Lakes, NJ).

Diethylpyrocarbonate (DEPC) treated *B. fragilis* culture medium was prepared as described previously, except the 900-mL solution also contained DEPC (0.1% v/v) and was stirred at 37 °C for 1 h prior to sterilization by autoclave. Additionally, the 100 mL of lysed horse blood contained DEPC (0.1% v/v) and was stirred at 37 °C for 1 h prior to being added to the 900 mL solution. DEPC treatment was done to eliminate any ribonucleolytic activity in the culture medium.

4.7.6 Inoculation of 96-well plates to determine the MIC

After their preparation, test plates were equilibrated in an anaerobic chamber for 3 h prior to inoculation. *B. fragilis* was grown on Reducible Blood Agar plates from Remel (Lenexa, KS) and suspended in sterile Brucella broth to the turbidity equivalent of a 0.5 McFarland standard, which equates to ~1.5×10^8 colony forming units (CFU)/mL. This suspension of *B. fragilis* was diluted with sterile Brucella broth to a concentration of ~1.0×10^7 CFU/mL, and 10 μL/well of this *B. fragilis* suspension was used to inoculate each well using a 95-pin inoculator. The final volume of solution in each well was 100 μL, with the indicated final concentration of test compound and ~10^6 CFUs/mL of *B. fragilis*. The plates were incubated for 48 h in a 37 °C, anaerobic incubator. The anaerobic chamber was maintained under an atmosphere of 80% v/v $N_2(g)$, 10% v/v $H_2(g)$, and 10% v/v $CO_2(g)$. Any $O_2(g)$ was transformed into H_2O by Pd on alumina pellets, and the water was removed from the atmosphere using silica gel. The MIC was defined as the lowest concentration of test compound at which no bacterial growth was observed.

4.7.7 Effect of DEPC-treatment on the MIC of metronidazole for B. fragilis

Metronidazole is marginally soluble in aqueous solutions (~10 mg/mL).[197] Accordingly, for the initial dissolution of metronidazole, dimethyl sulfoxide (DMSO, 10% v/v) was added to the medium. For MIC test solutions used in the 96-well plates, <0.5% of the final volume of liquid was DMSO. For each plate, ~10 mg of metronidazole, taking note of the exact mass to make the appropriate dilutions, was added to a 4-mL glass vial, and then 1 mL of culture medium containing DMSO (10% v/v) was added. Serial dilutions (log 2) were made according to guidelines from the Clinical and Laboratory Standards Institute[196] in the indicated medium and dispensed in triplicate wells (90 μL per well) into a 96-well, U bottom plate. DEPC-treatment of the medium had no affect on the MIC of metronidazole for *B. fragilis*.

values are in µg/mL of Met

	1	2	3	4	5	6	7	8	9	10	11	12
A	256	128	64	32	16	8	4	2	1	0.5	0.25	0.13
B	256	128	64	32	16	8	4	2	1	0.5	0.25	0.13
C	256	128	64	32	16	8	4	2	1	0.5	0.25	0.13
D												
E	0.06	0.03	0									
F	0.06	0.03	0									
G	0.06	0.03	0									
H												sterile

normal medium

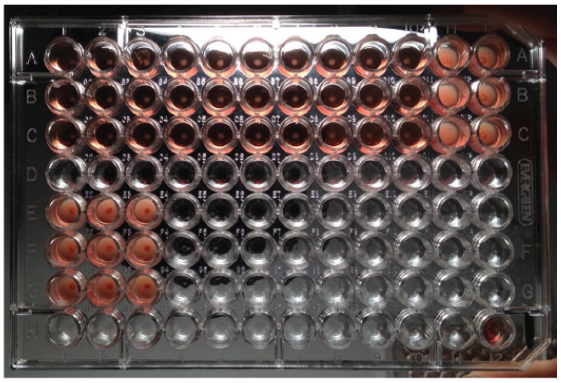

DEPC treated medium

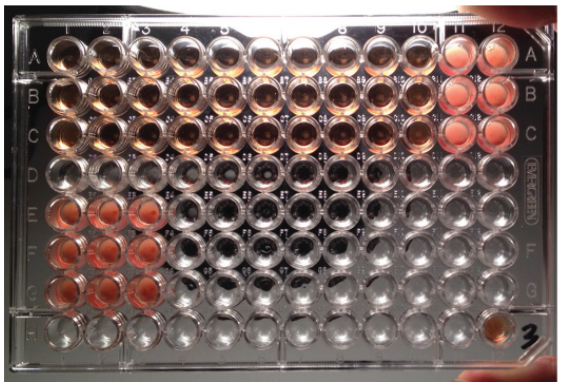

Figure 4.5 Effect of DEPC-treatment on the MIC of metronidazole for *B. fragilis*. The MIC for normal medium and DEPC-treated medium was 0.5 μg/mL, indicating that treatment with DEPC did not interfere with the proper MIC determination. For quality control purposes, the Clinical and Laboratory Standards Institute[196] defines the acceptable MIC of this strain of *B. fragilis* to be 2.00–0.25 μg/mL.

4.7.8 Determination of the MIC for RpMet prodrugs

To most accurately normalize the concentrations of metronidazole and prodrug, precise concentrations of each were measured using NMR spectroscopy. A standard solution of CD_3OD with 7.2 mM dimethylformamide (DMF) was prepared and the methyl imidazole peak (3H, 2.52

ppm) of metronidazole was integrated and compared to the DMF peaks (2.99 and 2.86 ppm) to determine the solution concentration of Met and the RpMets (Figure 4.6).

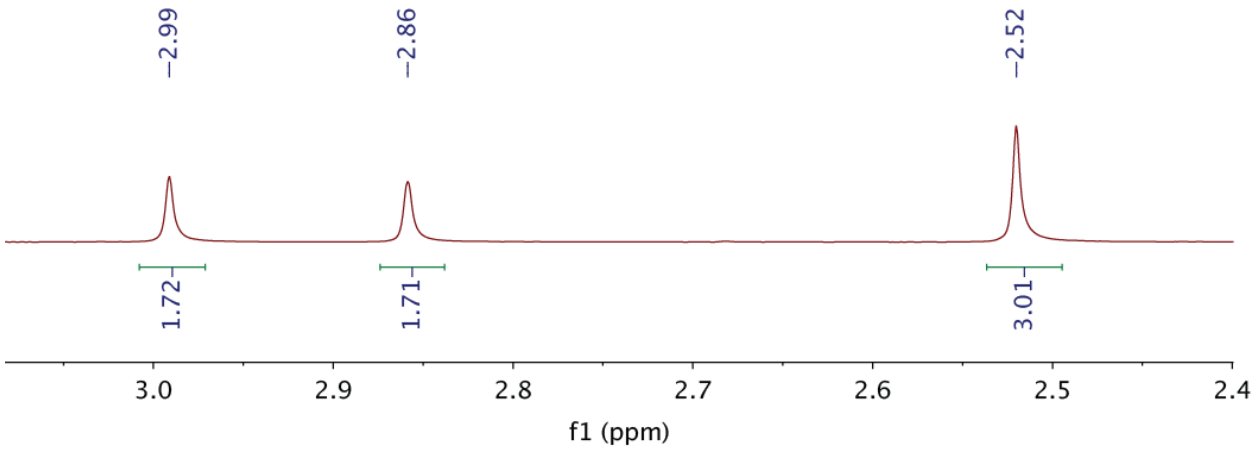

Figure 4.6 Representative NMR spectrum for determination of Met (or RpMet) concentration. DMF methyl peaks corresponded to the peaks at 2.99 and 2.86 ppm, and the methyl imidazole peak of metronidazole corresponded to the peak at 2.52 ppm.

Upon determination of the concentration of Met or the RpMet in the NMR solution, aliquots of the compounds for the initial stock solution for the serial dilution of a given plate were made into plastic 1.7-mL microcentrifuge tubes. The methanol and DMF were evaporated from the aliquots using a SpeedVac Concentrator from Thermo Scientific (Waltham, MA), and the compounds were stored at –20 °C until use. On the day of the MIC experiment, dried stock aliquots of Met or RpMets were dissolved into DEPC-treated, *B. fragilis* culture medium and diluted to create solutions with the indicated concentration of Met or an equivalent molar concentration of the RpMet. Compounds were either incubated in medium only, pre-incubated overnight with RNase 1 (0.1 mg/mL) overnight and then diluted in DEPC medium, or diluted in DEPC-treated medium containing RNase 1 (0.01 mg/mL). Upon dilution of the compounds into

a 96-well plate, the plates were incubated in the anaerobic chamber for 4 h, then inoculated as described previously. The results are depicted in Figure 4.7. (Note: These photographs were taken with a different light source than those in Figure 4.5 and were in an oxygen environment for several hours prior to taking the photograph, causing oxygenation of the media and an ensuing divergence of color.)

values are in µg/mL of Met, for RpMet plates, the equivalent molar concentration was used

	1	2	3	4	5	6	7	8	9	10	11	12
A	128	64	32	16	8	4	2	1	0.5	0.25	0.13	0.06
B	128	64	32	16	8	4	2	1	0.5	0.25	0.13	0.06
C	128	64	32	16	8	4	2	1	0.5	0.25	0.13	0.06
D												
E	0.03	0										
F	0.03	0										
G	0.03	0										
H												sterile

Met

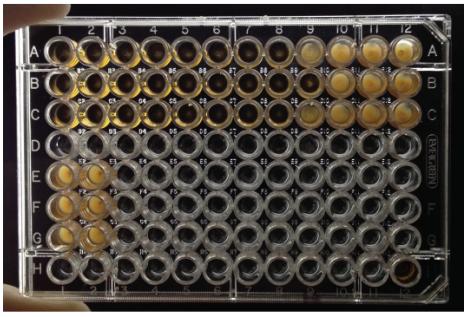

ApMet

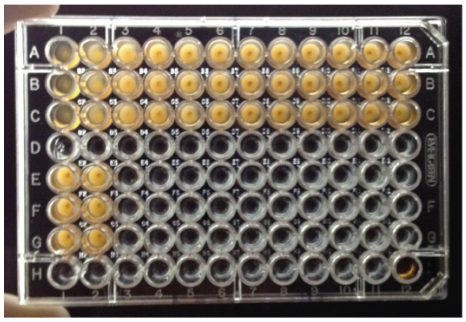

UpMet

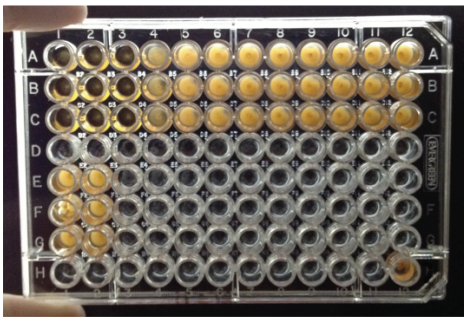

Met + 0.1 mg/mL RNase 1 over night

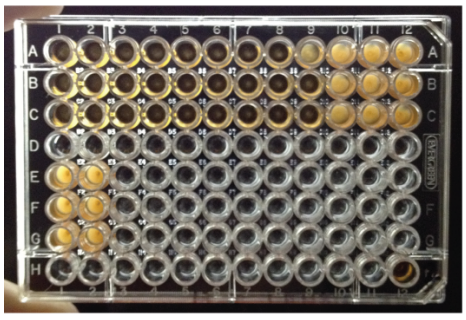

UpMet + 0.1 mg/mL RNase 1 over night

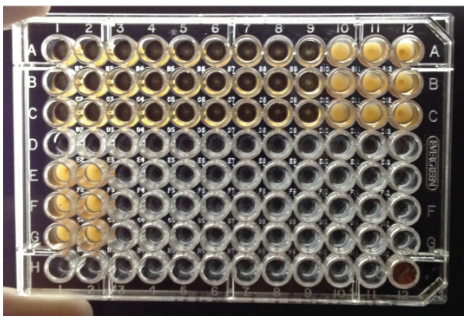

Figure 4.7 Photographs of the plates used to determine the MIC values. Assays followed the protocols of the CLSI. *Methods for Antimicrobial Susceptibility Testing of Anaerobic Bacteria; Approved Standard—Seventh Edition*. CLSI document M11-A7. Wayne, PA: Clinical and Laboratory Standards Institute; 2007.

4.7.9 Synthesis of RpMet prodrugs

4.7.9.1 Synthesis of uridine 3'-(4-metronidazole phosphate)

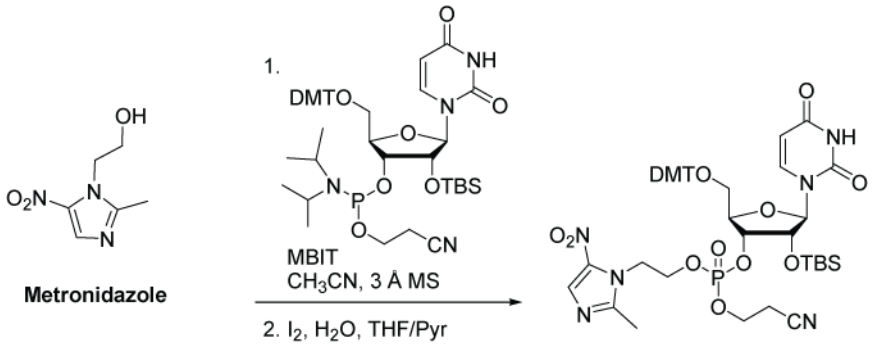

Metronidazole (0.100 g, 0.585 mmol) and phosphoramidite (0.554 g, 0.643 mmol) were added to a round-bottom flask that had been charged with 3-Å molecular sieves (approximately 20 beads) under Ar(g), and that contained 5 mL of CH_3CN. After 10 min, methylbenzimidazole triflate (MBIT) (0.165 g, 0.585 mmol) was added, and the reaction mixture was stirred for 3 h. The CH_3CN was removed by vacuum, and the reaction mixture was filtered through a plug of silica (100% ethyl acetate). Ethyl acetate was removed by vacuum, and 29.0 mL of I_2 in THF/H_2O/pyridine (0.02M) was added. The reaction mixture turned from brown to clear yellow after 1 h. The solvent was removed by vacuum and the resulting solid was purified with silica gel chromatography (ethyl acetate and then 10% methanol/90% dichloromethane) to yield pure product (0.542 g, 98% over 2 steps).

^{1}H NMR (400 MHz, CD_3OD) (Mixture of isomers) δ = 7.95 (s, 0.38H), 7.91–7.84 (m, 1.62H), 7.39 (d, J = 7.6, 2H), 7.34–7.06 (m, 7H), 6.88 (d, J = 8.8, 4H), 5.91 (t, J = 4.9, 1H), 5.33–5.27 (m, 1H), 4.68–4.56 (m, 2H), 4.53 (t, J = 4.8, 1H), 4.50–4.28 (m, 3H), 4.26–4.12 (m, 2H), 4.11–

3.99 (m, 1H), 3.76 (s, 6H), 3.61–3.52 (m, 1H), 3.49–3.40 (m, 1H), 2.80 (t, J = 5.8, 1.25H), 2.68 (dd, J = 5.8, 10.2, 0.75H), 2.50 (s, 1.1H), 2.47 (s, 1.9H), 0.88 (s, 5.6H), 0.86 (s, 3.4H), 0.12 (s, 1.9H), 0.10–0.07 (m, 4.1H); **^{13}C NMR (101 MHz, CD_3OD)** (Mixture of isomers. When the diastereomer peaks resolve, the peaks are listed in parentheses) δ = 165.7, 160.4, (153.0 & 152.9), 152.0, 145.7, 141.7, 140.1, (136.2 & 136.2), (133.1 & 133.0), 131.5, 129.4, 129.1, 128.3, 118.3, 114.4, 103.1, (89.3 & 89.2), 88.8, (83.4 & 83.2), 78.4, 75.7, (68.2 & 68.0), (64.6 & 64.4), 63.4, 55.8, (47.1 & 47.0), 26.2, 20.1, 19.0, 14.4, (–4.6 & –4.7); **^{31}P NMR (162 MHz, CD_3OD)** (Mixture of isomers) δ = –3.32, –3.73; **HRMS** (ESI) m/z 969.3218 [calc'd for $C_{45}H_{55}N_6O_{13}PSiNa$ (M+Na) 969.3227].

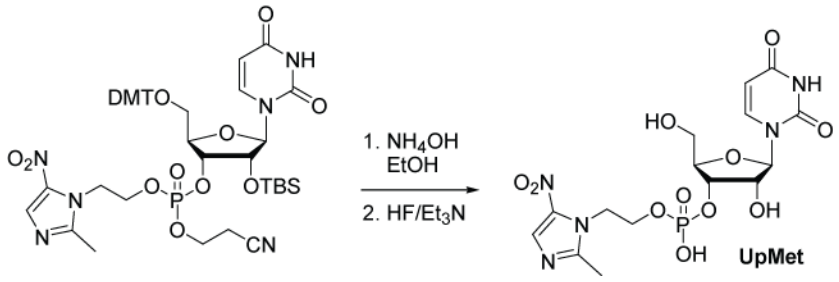

The oxidized metronidazole adduct (0.180 g, 0.190 mmol) was added to NH_4OH (0.13 mL, 3.800 mmol) in ethanol (3.8 mL). The resulting reaction mixture was stirred at room temperature for 3h. The solvent was removed by vacuum. $Et_3N{\cdot}HF$ (0.310 mL, 1.900 mmol) was added in CH_3CN (3.8 mL), and the reaction mixture was stirred at 65 °C for an additional 8 h. The reaction mixture was then cooled to room temperature and quenched with aqueous bicarbonate solution, and the solvent was removed by vacuum. The resulting solid was purified by flash chromatography (10% methanol/90% dichloromethane to 100% methanol) to yield product (0.075 g, 82% over 2 steps).

^{1}H NMR (400 MHz, CD_3OD) δ = 8.02 (d, J = 8.1, 1H), 7.93 (s, 1H), 5.90 (d, J = 5.4, 1H), 5.69 (d, J = 8.1, 1H), 4.62 (t, J = 4.7, 2H), 4.45–4.37 (m, 1H), 4.24 (dt, J = 4.3, 8.4, 2H), 4.20 (t, J = 5.2, 1H), 4.12 (dd, J = 2.5, 3.6, 1H), 3.81–3.67 (m, 2H), 2.57 (s, 3H); **^{13}C NMR (126 MHz, CD_3OD)** δ 152.0, 141.0, 138.6, 131.3, 129.1, 127.8, 127.2, 112.4, 101.5, 88.6, 84.1, 74.0, 64.1, 60.7, 13.1; **^{31}P NMR (162 MHz, CD_3OD)** δ = –1.14; **HRMS** (ESI) m/z 476.0845 [calc'd for $C_{15}H_{19}N_5O_{11}P$ (M–H) 476.0824].

4.7.9.2 Synthesis of adenosine 3'-(4-metronidazole phosphate)

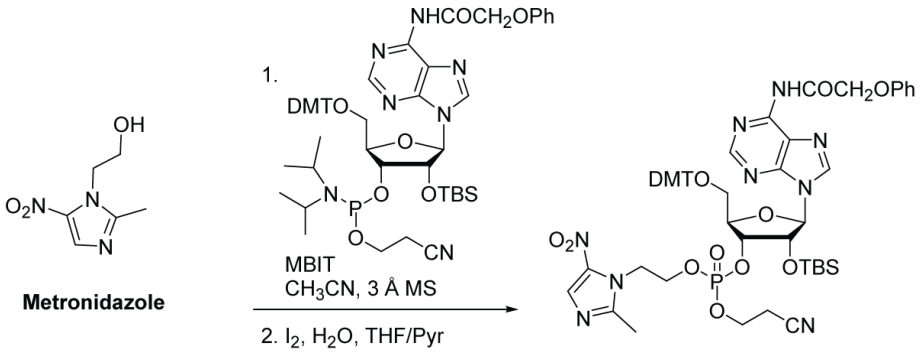

Metronidazole (0.076 g, 0.447 mmol) and phosphoramidite (0.500 g, 0.491 mmol) were added to a round-bottom flask that had been charged with 3-Å molecular sieves (approximately 20 beads) under Ar(g), and that contained 5 mL of CH_3CN. After 10 min, methylbenzimidazole triflate (MBIT) (0.126 g, 0.447 mmol) was added, and the reaction mixture was stirred for 3 h. The CH_3CN was removed by vacuum, and the reaction mixture was filtered through a plug of

silica (100% v/v ethyl acetate). Ethyl acetate was removed by vacuum, and 22.4 mL of I_2 (0.02 M) in THF/H_2O/pyridine was added. The reaction mixture turned from brown to clear yellow after 1 h. The solvent was removed by vacuum and the resulting solid was purified with silica gel chromatography (ethyl acetate) to yield pure product (0.407 g, 75% over 2 steps).

^{1}H NMR (400 MHz, CD_3OD) (Mixture of isomers) δ 8.57–8.51 (m, 2H), 7.99 (s, 0.39H), 7.88 (s, 0.61H), 7.46 (d, J = 6.3, 2H), 7.36–7.20 (m, 9H), 7.07 (d, J = 8.3, 2H), 7.00 (t, J = 7.4, 1H), 6.85 (d, J = 6.7, 4H), 6.07 (d, J = 6.2, 0.61H), 6.02 (d, J = 6.2, 0.39H), 5.21 (t, J = 4.9, 1H), 4.99 (s, 2H), 4.73–4.66 (m, 1H), 4.63 (t, J = 5.2, 0.78H), 4.58 (t, J = 5.2, 1.22H), 4.33–4.15 (m, 3H), 4.03–3.80 (m, 2H), 3.77 (s, 6H), 3.62–3.55 (m, 1H), 3.42 (td, J = 10.0, 3.8, 1H), 2.70 (t, J = 5.9, 1.22H), 2.60 (t, J = 5.8, 0.78H), 2.54 (s, 1.17H), 2.48 (s, 1.83H), 0.75 (s, 5.49H), 0.72 (s, 3.51H), –0.06 to –0.10 (m, 3H), –0.25 (s, 1.83H), –0.30 (s, 1.17H); **^{13}C NMR (101 MHz, CD_3OD)** (Mixture of isomers. When the diastereomer peaks resolve, the peaks are listed in parentheses) δ 170.1, 160.4, 159.3, (153.4 & 153.2), (150.4 & 150.2), 146.3, (145.5 & 145.3), 140.3, 138.6, (137.0 & 136.9), 133.2, (131.6 & 131.5), 130.8, 129.5, 129.1, 128.2, 125.7, 124.7, 123.1, 118.5, 116.1, 114.4, 89.8, 88.3, 84.6, 79.7, 74.3, 69.2, 68.4, (64.8 & 64.6), 61.7, 55.9, 47.3, 21.0, 20.3, 18.9, 14.6, (–4.4 & –5.0); **^{31}P NMR (162 MHz, CD_3OD)** (Mixture of isomers) δ = –3.42, –3.58; **HRMS** (ESI) *m/z* 1126.3859 [calc'd for $C_{54}H_{62}N_9O_{13}PSiNa$ (M+Na) 1126.3867].

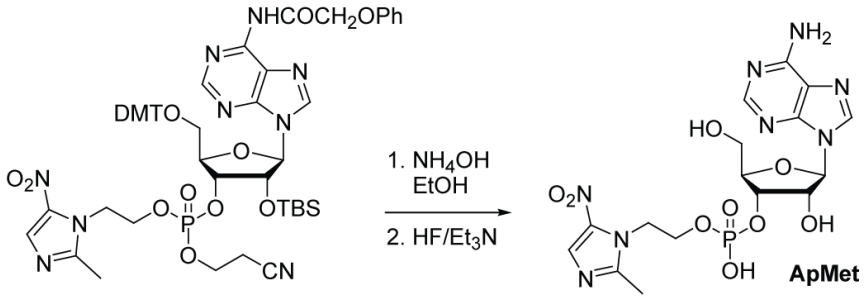

The oxidized metronidazole adduct (0.468 g, 0.424 mmol) was added to NH_4OH (29.72 μL, 0.848 mmol) in ethanol (8.5 mL). The resulting reaction mixture was stirred at room temperature for 3 h. The solvent was removed by vacuum and $Et_3N{\cdot}HF$ (1.38 mL, 8.480 mmol) was added in CH_3CN (7.36 mL) and the reaction mixture was stirred at 65 °C for an additional 8 h. The reaction mixture was then cooled to room temperature and quenched with aqueous bicarbonate solution, and the solvent was removed by vacuum. The resulting solid was purified by flash chromatography (10% methanol/90% dichloromethane to 100% methanol) to yield product (0.180 g, 85% over 2 steps).

^{1}H NMR (400 MHz, CD_3OD) δ 8.31 (s, 1H), 8.18 (s, 1H), 7.93 (s, 1H), 5.93 (d, *J* = 6.9, 1H), 4.79–4.75 (m, 1H), 4.66–4.61 (m, 3H), 4.32–4.24 (m, 3H), 3.83 (d, *J* = 12.7, 1H), 3.75 (d, *J* = 12.7, 1H), 2.60 (s, 3H); **^{13}C NMR (126 MHz, CD_3OD)** *δ* 156.2, 152.1, 152.0, 148.6, 140.7, 138.6, 131.3, 119.7, 89.6, 85.9, 75.4, 73.5, 64.1, 61.8, 21.6, 13.1; **^{31}P NMR (162 MHz, CD_3OD)** *δ* = –1.08; **HRMS** (ESI) *m/z* 501.1259 [calc'd for $C_{16}H_{22}N_8O_9P$ (M+H) 501.1242].

4.7.9.3 Synthesis of cytidine 3'-(4-metronidazole phosphate)

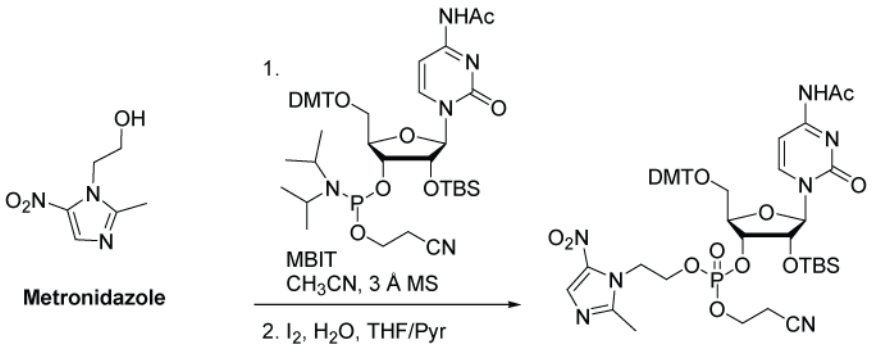

Metronidazole (0.173 g, 1.010 mmol) and phosphoramidite (1.000 g, 1.110 mmol) were added to a round-bottom flask that had been charged with 3-Å molecular sieves (approximately 20 beads) under Ar(g), and that contained 11 mL of CH_3CN. After 10 min, methylbenzimidazole triflate (MBIT) (0.285 g, 1.010 mmol) was added, and the reaction mixture was stir for 3 h. The CH_3CN was removed by vacuum, and the reaction mixture was filtered through a plug of silica (100% v/v ethyl acetate). Ethyl acetate was removed by vacuum, and 55.0 mL of I_2 (0.02 M) in THF/H_2O/pyridine was added. The reaction mixture turned from brown to clear yellow after 1 h. The solvent was removed by vacuum, and the resulting solid was purified with silica gel chromatography (ethyl acetate and then 10% methanol/90% dichloromethane) to yield pure product (1.026 g, 93% over 2 steps).

^{1}H NMR (400 MHz, CD_3OD) δ (Mixture of isomers) 8.46–8.39 (m, 1H), 7.95 (s, 0.39H), 7.90 (s, 0.61H), 7.42 (d, J = 7.6, 2H), 7.38–7.25 (m, 7H), 7.05 (d, J = 7.6, 0.39H), 7.00 (d, J = 7.5, 0.61H), 6.90 (d, J = 8.7, 4H), 5.91–5.86 (m, 1H), 4.95–4.90 (m, 1H), 4.69–4.52 (m, 3H), 4.45–4.26 (m, 3H), 4.2–4.05 (m, 2H), 3.81 (s, 6H), 3.71 (t, J = 11.2, 1H), 3.51 (t, J = 10.4, 1H), 2.79

(t, *J* = 5.8, 1.22H), 2.66 (s, 0.78H), 2.49 (s, 1.17H), 2.46 (s, 1.83H), 2.16 (s, 3H), 0.92–0.87 (m, 9H), 0.18–0.07 (m, 6H); **^{13}C NMR (126 MHz, CD_3OD)** (Mixture of isomers. When the diastereomer peaks resolve, the peaks are listed in parentheses) δ 173.0, 164.5, (160.6 & 160.6), (158.1 & 158.0), (153.1 & 153.0), (146.0 & 145.9), (145.7 & 145.7), 140.3, (136.5 & 136.4), (133.1 & 133.1), 131.7, (129.8 & 129.7), 129.3, 128.6, (118.5 & 118.5), 114.5, 98.5, (92.2 & 92.0), (89.0 & 88.9), (82.8 & 82.6), (76.7 & 76.4), (68.5 & 68.4), (68.2 & 68.2), (64.8 & 64.7), 62.4, 55.9, (47.2 & 47.1), 26.4, 24.7, (20.3 & 20.3), 19.2, (14.5 & 14.5), (-4.3 & -4.7); **^{31}P NMR (162 MHz, CD_3OD)** (Mixture of isomers) δ = –3.10, –3.76; **HRMS** (ESI) *m/z* 988.3672 [calc'd for $C_{47}H_{59}N_7O_{13}PSi$ (M+H) 988.3673].

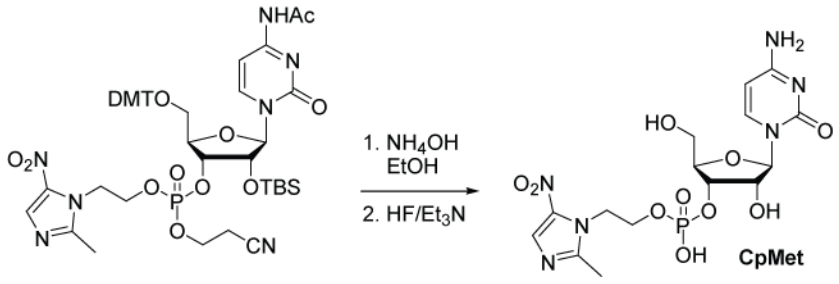

The oxidized metronidazole adduct (1.026 g, 1.035 mmol) was added to NH_4OH (72.5 μL, 2.071 mmol) in ethanol (20.7 mL). The reaction mixture was stirred ture for 3 h. Solvent was removed by vacuum, $Et_3N{\cdot}HF$ (3.37 mL, 20.7 mmol) was added in CH_3CN (20.7 mL), and the reaction mixture was stirred at 65 °C for an additional 8 h. The reaction mixture was then cooled to room temperature and quenched with aqueous sodium bicarbonate solution, and the solvent was removed by vacuum. The resulting solid was purified by flash chromatography (10% methanol/90% dichloromethane to 100% methanol) to yield product (0.083 g, 17% over 2 steps).

^{1}H NMR (400 MHz, CD_3OD) δ 8.04 (d, J = 7.5, 1H), 7.92 (s, 1H), 5.90–5.85 (m, 2H), 4.61 (t, J = 4.7, 2H), 4.45–4.38 (m, 1H), 4.27–4.18 (m, 3H), 4.14–4.10 (m, 1H), 3.82 (dd, J = 10.4, 2.5, 1H), 3.74 (dd, J = 10.4, 2.5, 1H), 2.56 (s, 3H); **^{13}C NMR (126 MHz, CD_3OD)** δ 166.3, 157.0, 152.0, 141.5, 138.6, 131.2, 94.5, 90.2, 83.3, 74.2, 73.0, 64.1, 60.2, 29.4, 13.1; **^{31}P NMR (162 MHz, CD_3OD)** δ = –1.10; **HRMS** (ESI) m/z 475.0968 [calc'd for $C_{15}H_{20}N_6O_{10}P$ (M–H) 475.0984].

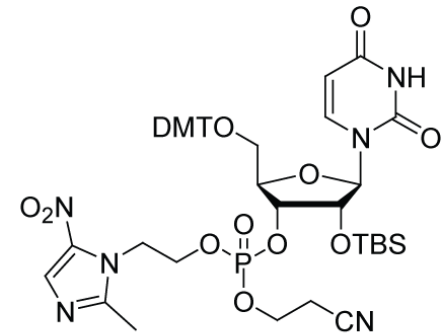
O
NH
DMTO
N
O
O
O_2N
O
O
P
O
OTBS
N
O
N
CN

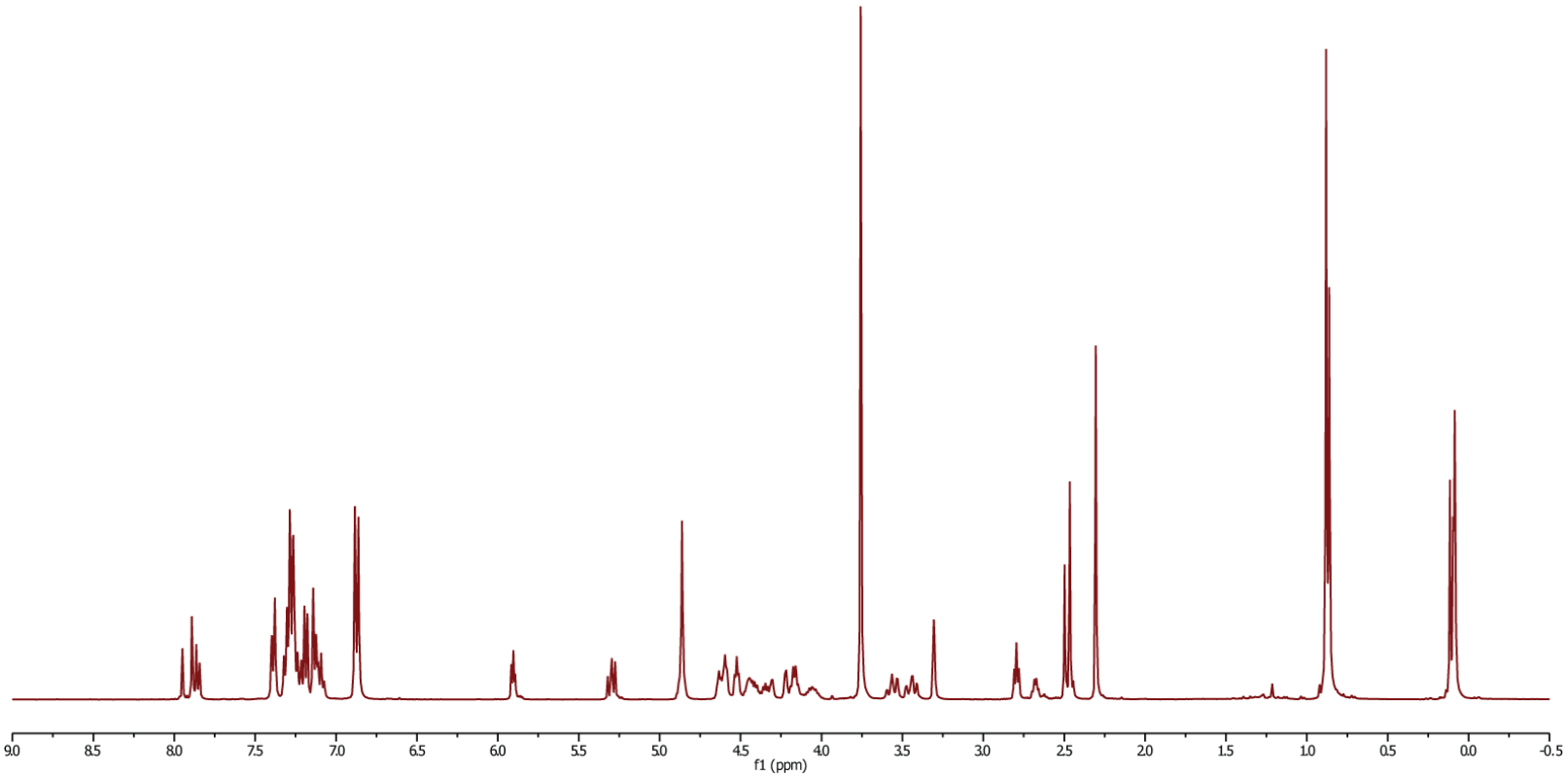
9.0
8.5
8.0
7.5
7.0
6.5
6.0
5.5
5.0
4.5
4.0
3.5
3.0
2.5
2.0
1.5
1.0
0.5
0.0
-0.5
f1 (ppm)

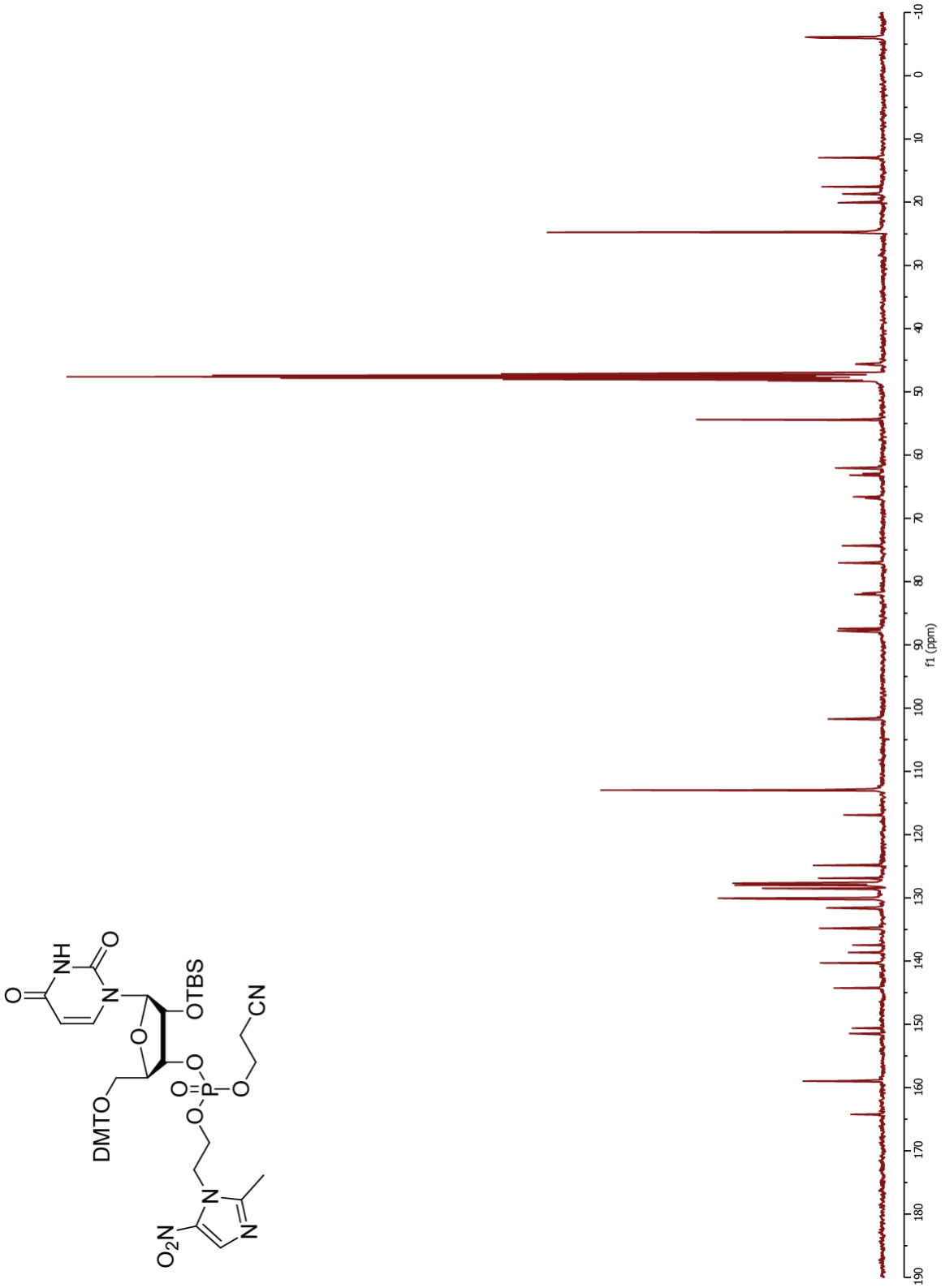
NH
O
O
N
O
OTBS
DMTO
O
O
P
O
O
CN
N
N
O_2N
f1 (ppm)

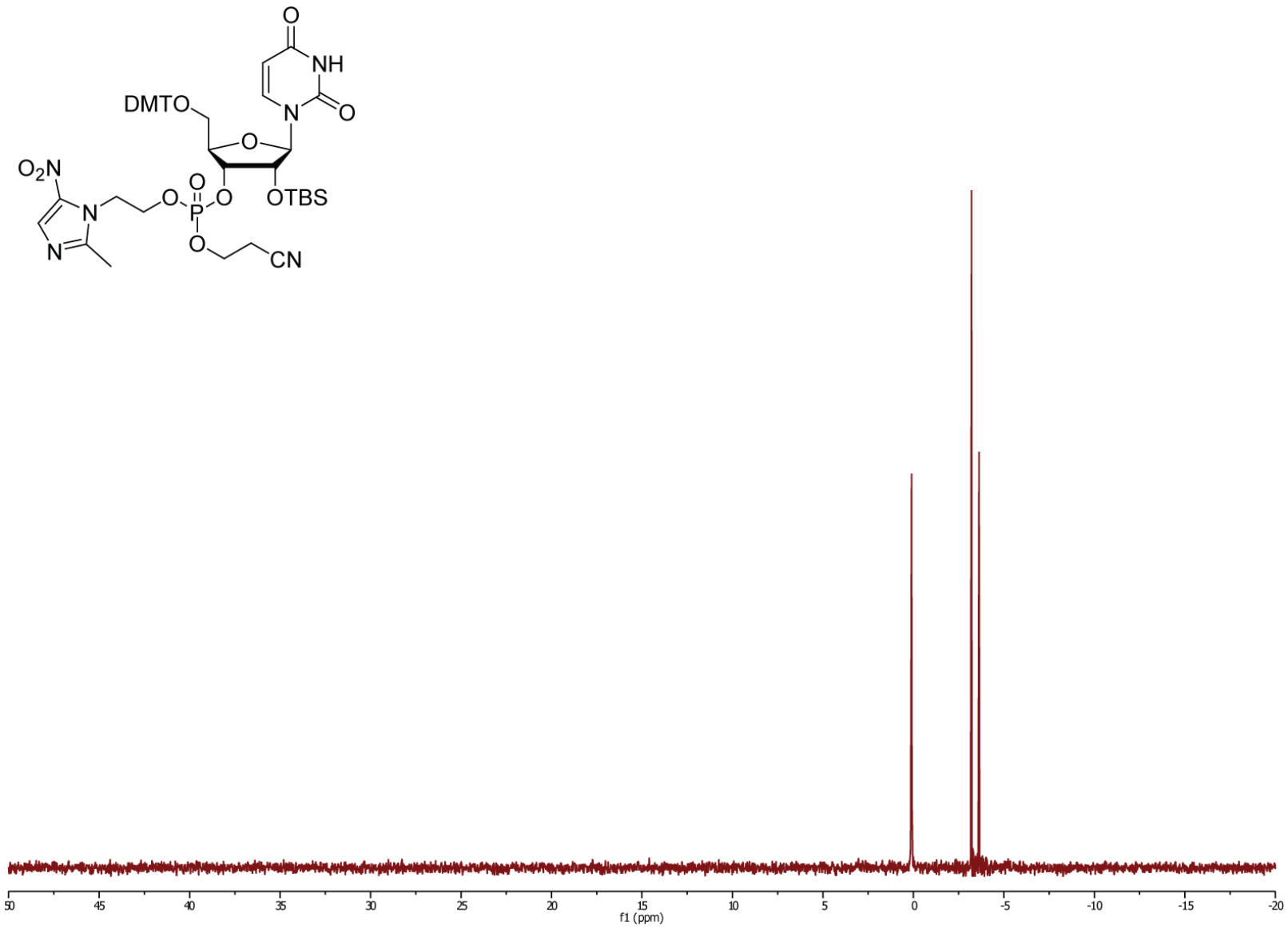
O
NH
DMTO
N
O
O
O_2N
O
O
P
O
OTBS
N
O
N
O
CN
50
45
40
35
30
25
20
15
10
5
0
-5
-10
-15
-20
f1 (ppm)

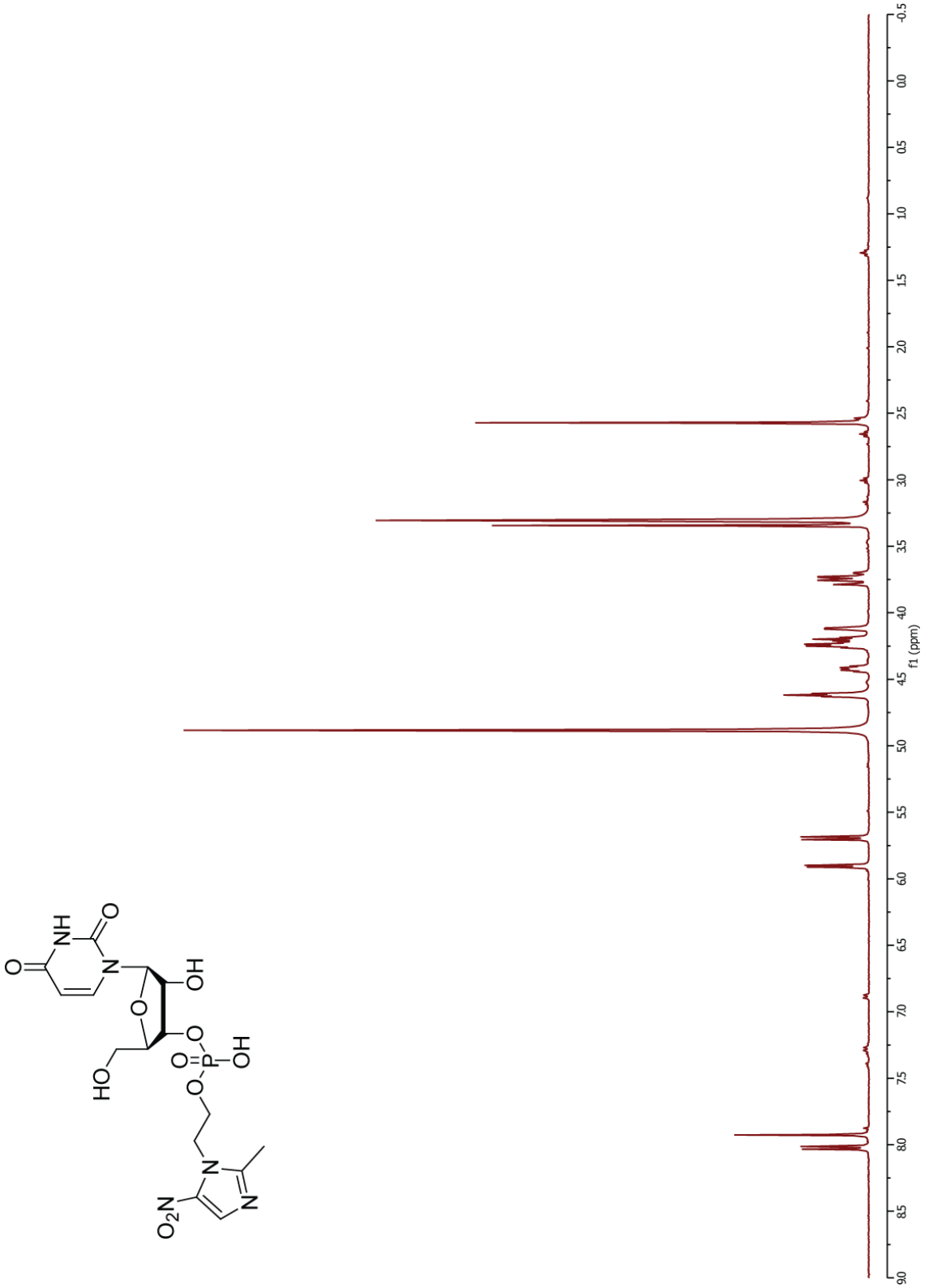
NH
O
O
N
O
OH
HO
O
O
P
OH
O
N
N
O_2N
f1 (ppm)

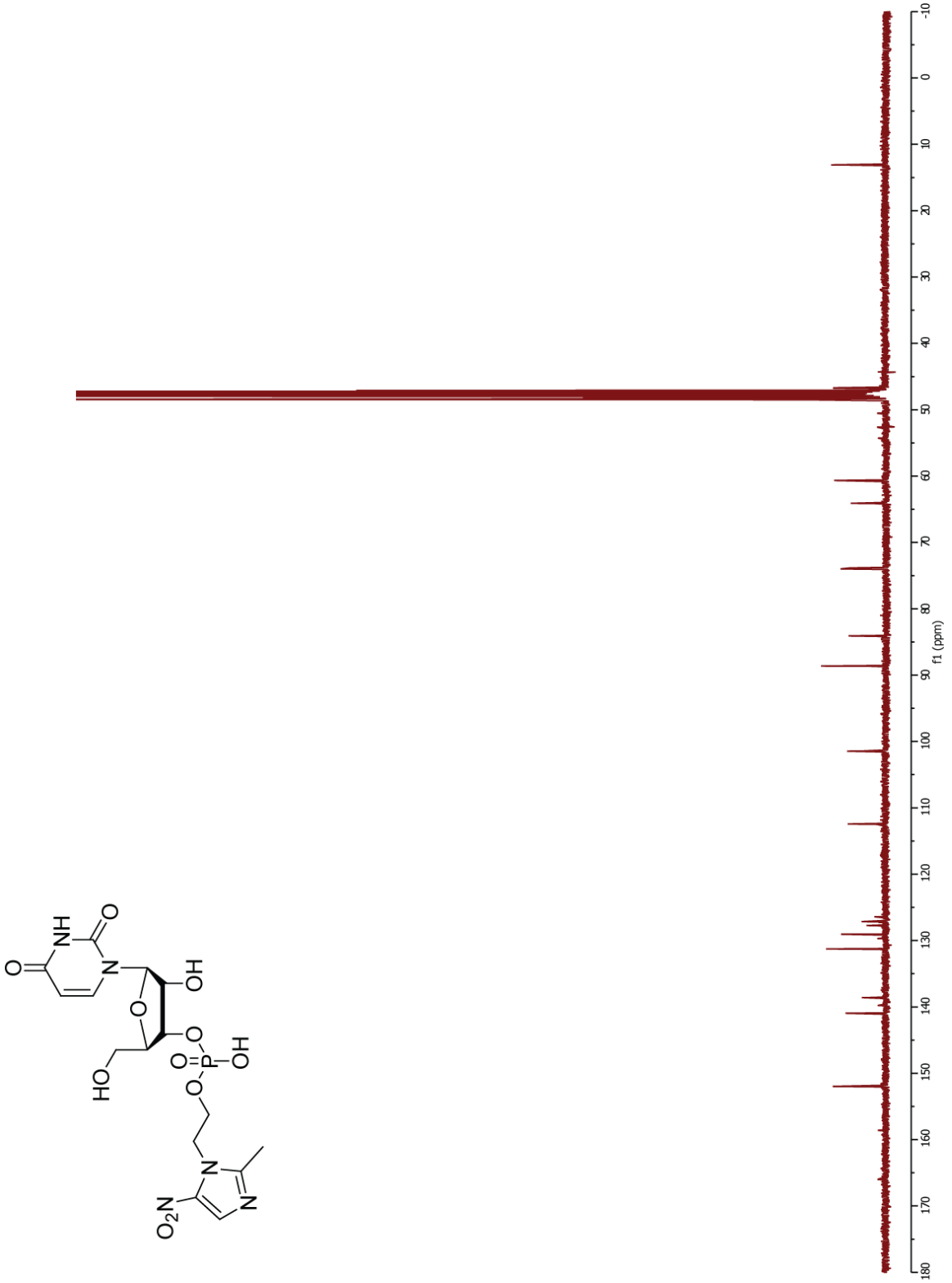
f1 (ppm)

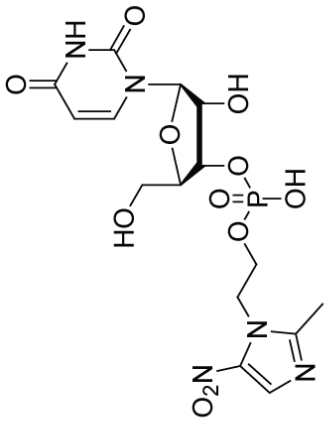

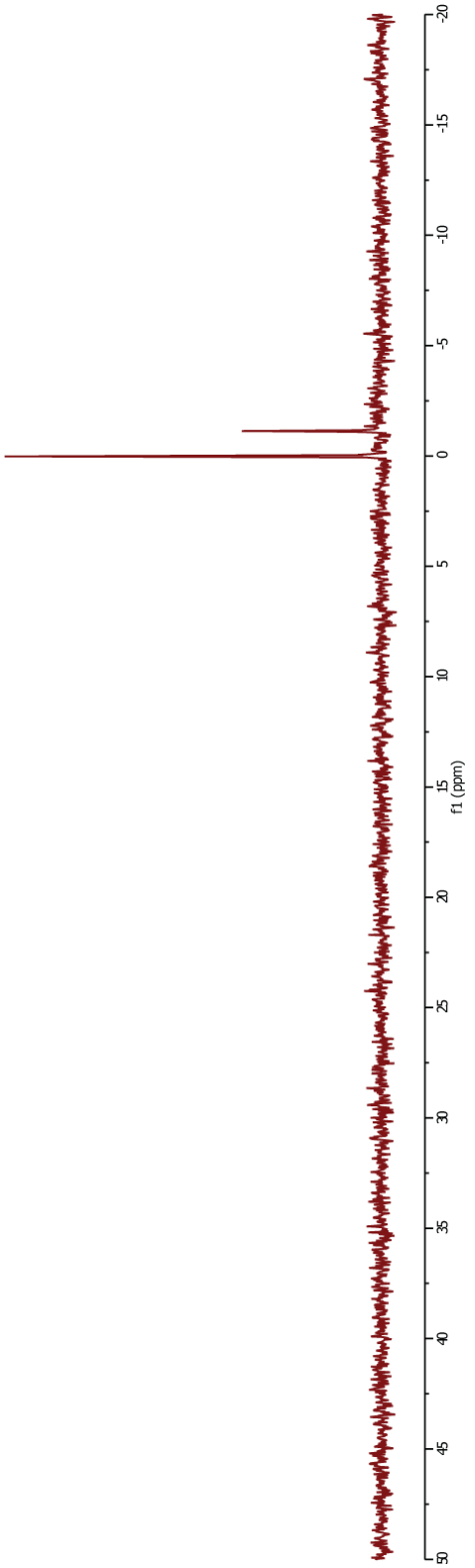
f1 (ppm)

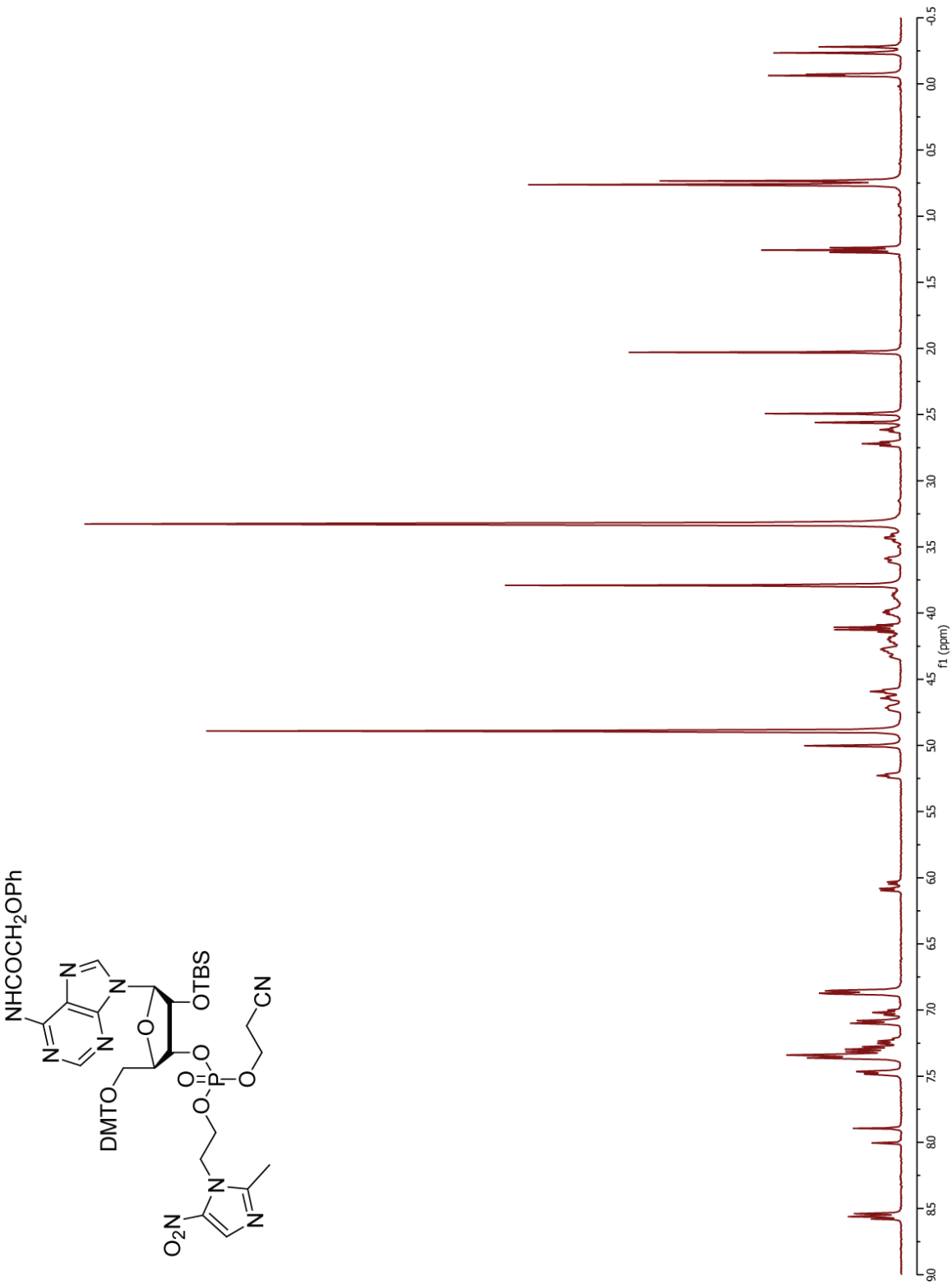
NHCOCH2OPh
N
N
N
N
O
OTBS
DMTO
O
P
O
O
O
CN
N
N
O2N
f1 (ppm)
90
85
80
75
70
65
60
55
50
45
40
35
30
25
20
15
10
05
00
-0.5

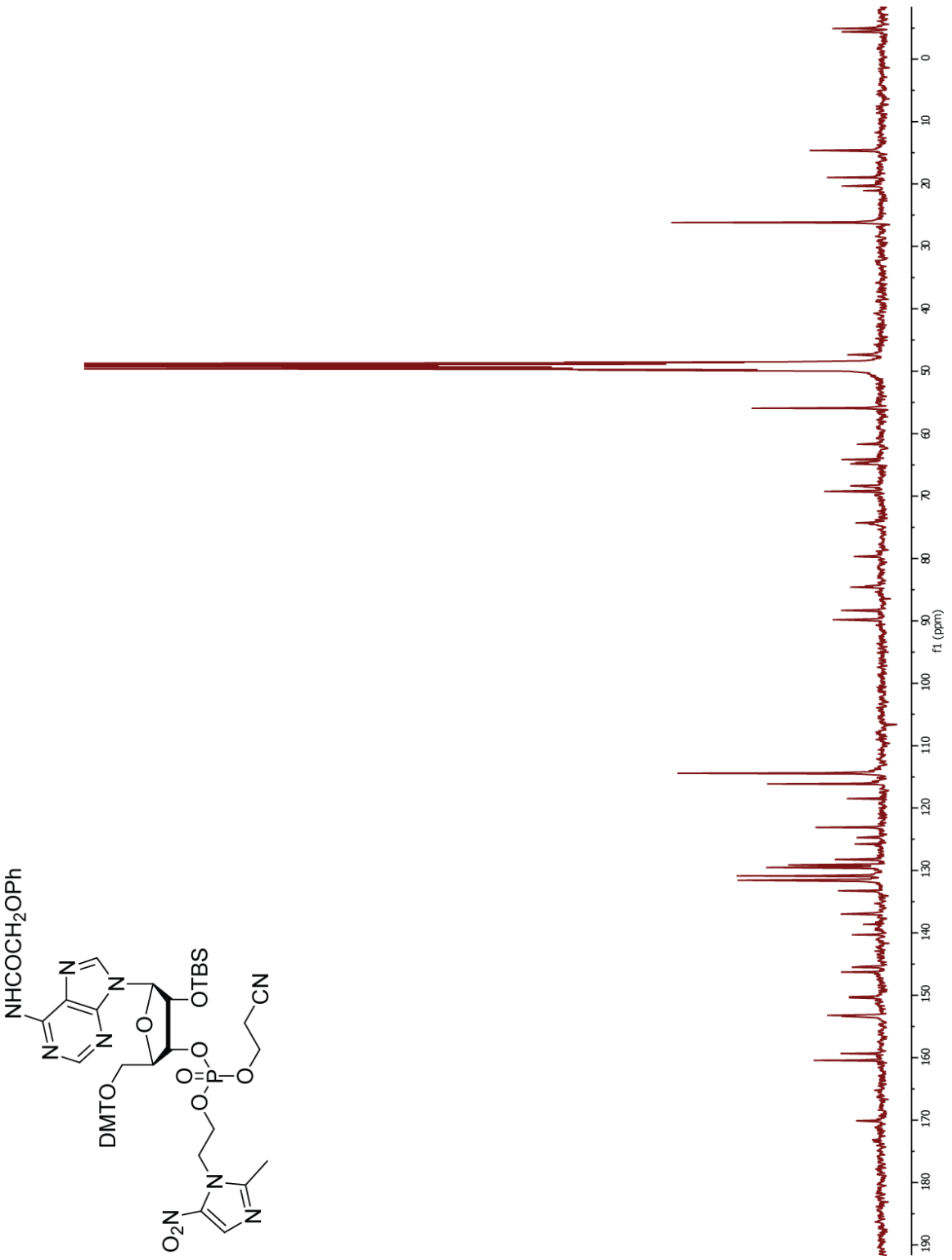
NHCOCH2OPh
DMTO
OTBS
CN
O2N
f1 (ppm)

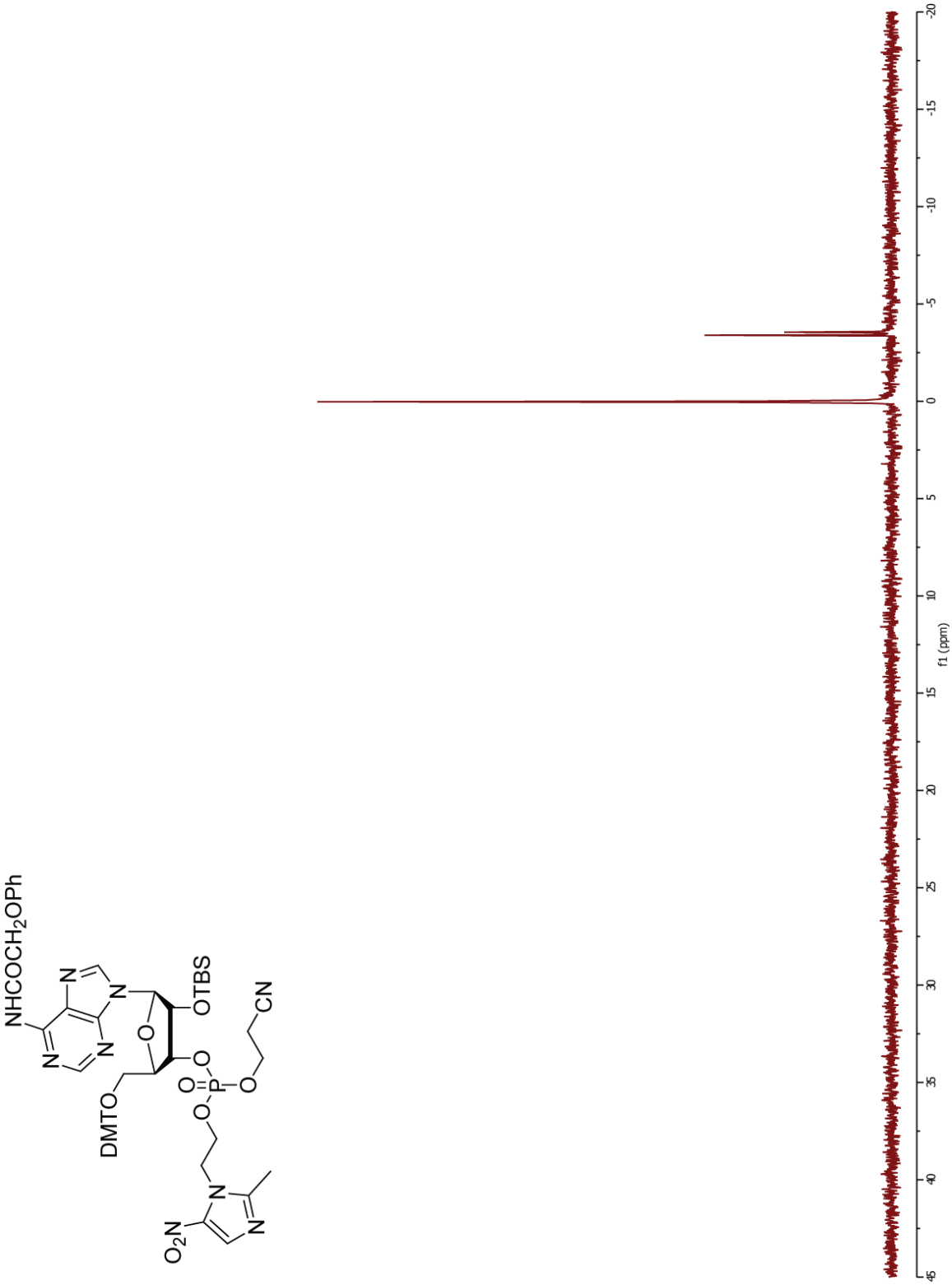
NHCOCH2OPh
DMTO
OTBS
CN
O2N
f1 (ppm)

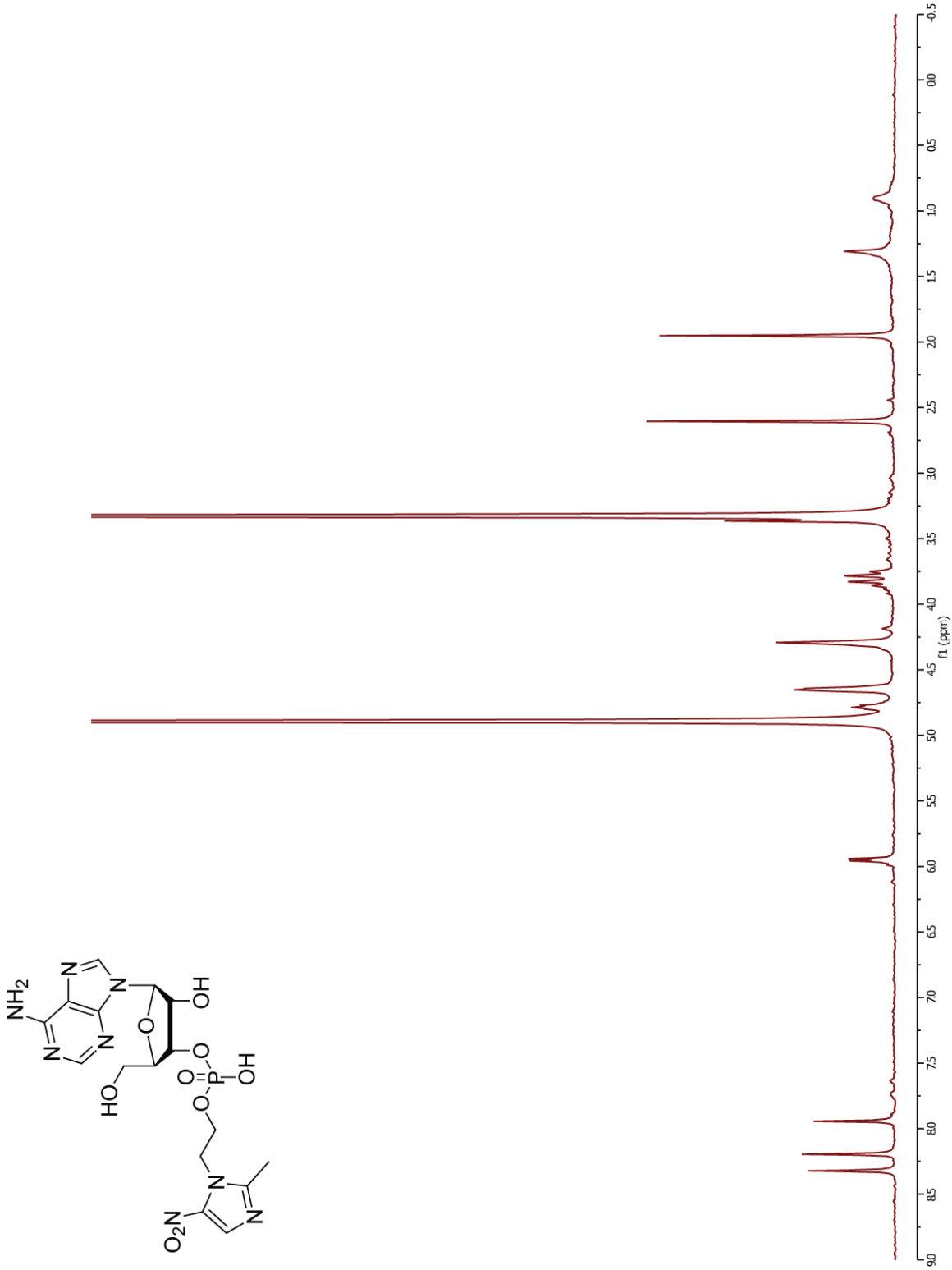
NH2
N
N
N
N
O
OH
HO
O
P
O
OH
O
N
N
O2N
f1 (ppm)
90
85
80
75
70
65
60
55
50
45
40
35
30
25
20
15
10
5
0
-0.5

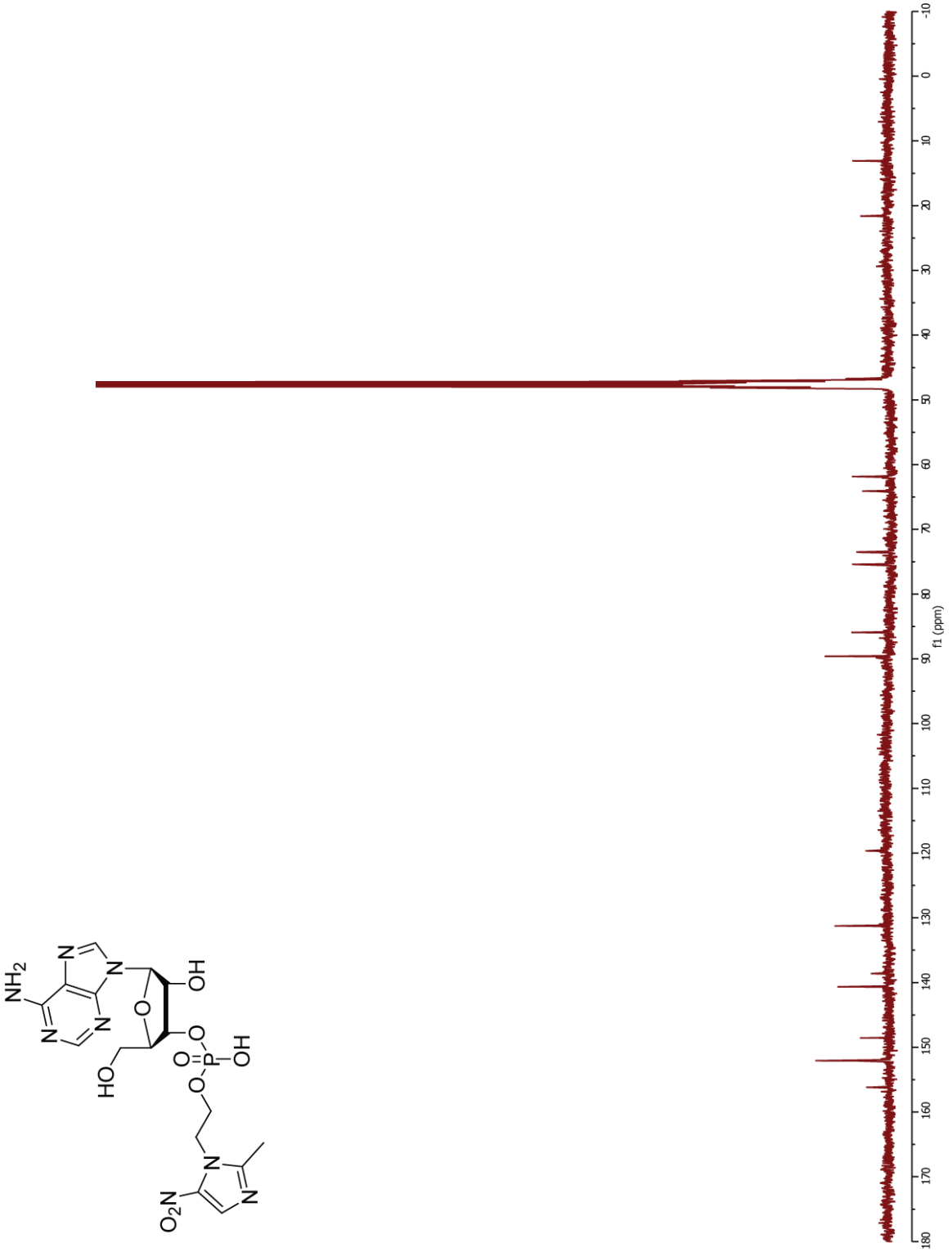
NH2
N
N
N
N
O
OH
HO
O
O
P
O
OH
O
N
N
O2N
f1 (ppm)
-10
0
10
20
30
40
50
60
70
80
90
100
110
120
130
140
150
160
170
180

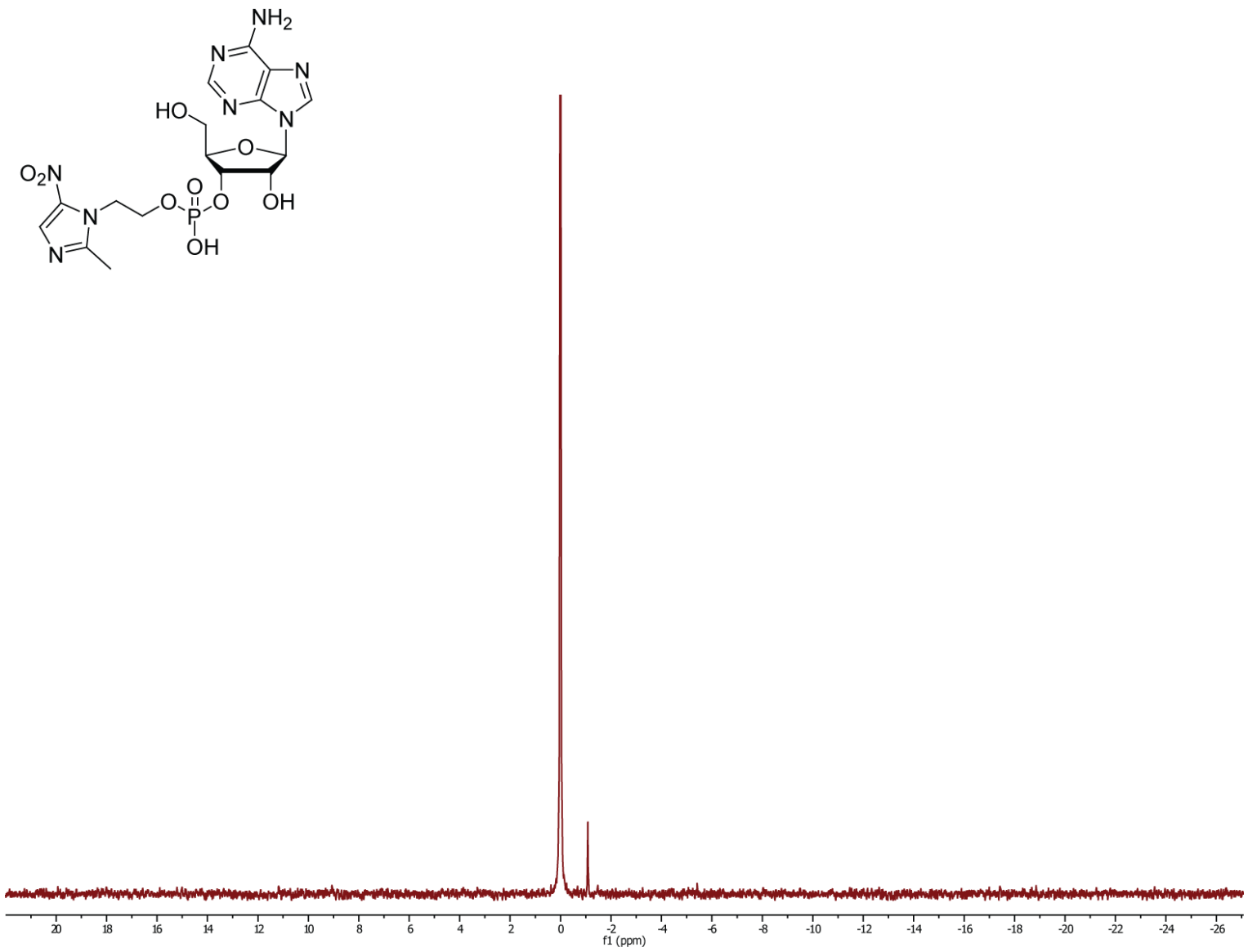
NH2
N
N
N
N
HO
O
O2N
N
O
O
P
O
OH
OH
N
20
18
16
14
12
10
8
6
4
2
0
-2
-4
-6
-8
-10
-12
-14
-16
-18
-20
-22
-24
-26
f1 (ppm)

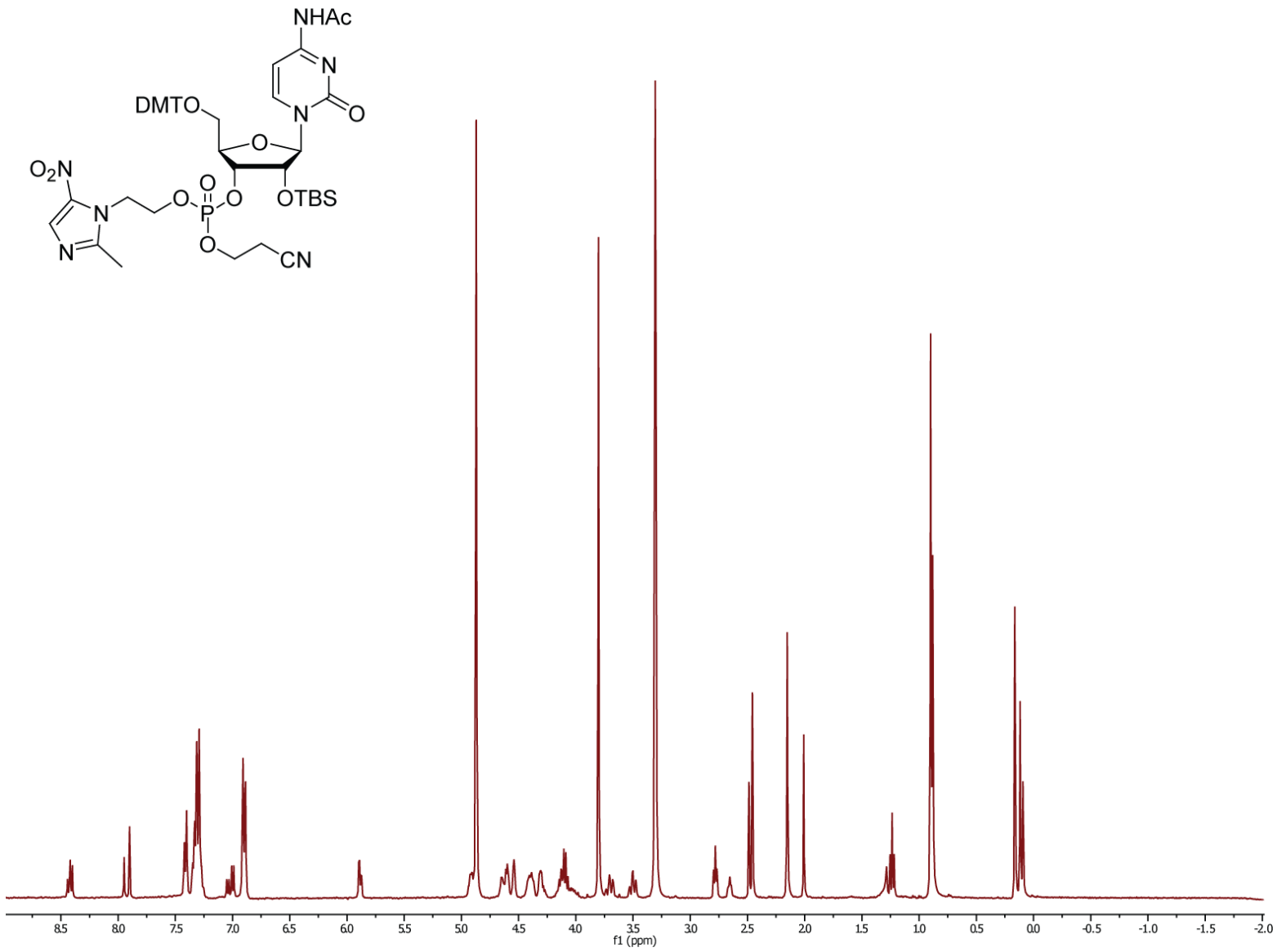
NHAc
N
O
N
DMTO
O
OTBS
O_2N
O
O
O
P
N
N
O
CN
8.5
8.0
7.5
7.0
6.5
6.0
5.5
5.0
4.5
4.0
3.5
3.0
2.5
2.0
1.5
1.0
0.5
0.0
-0.5
-1.0
-1.5
-2.0
f1 (ppm)

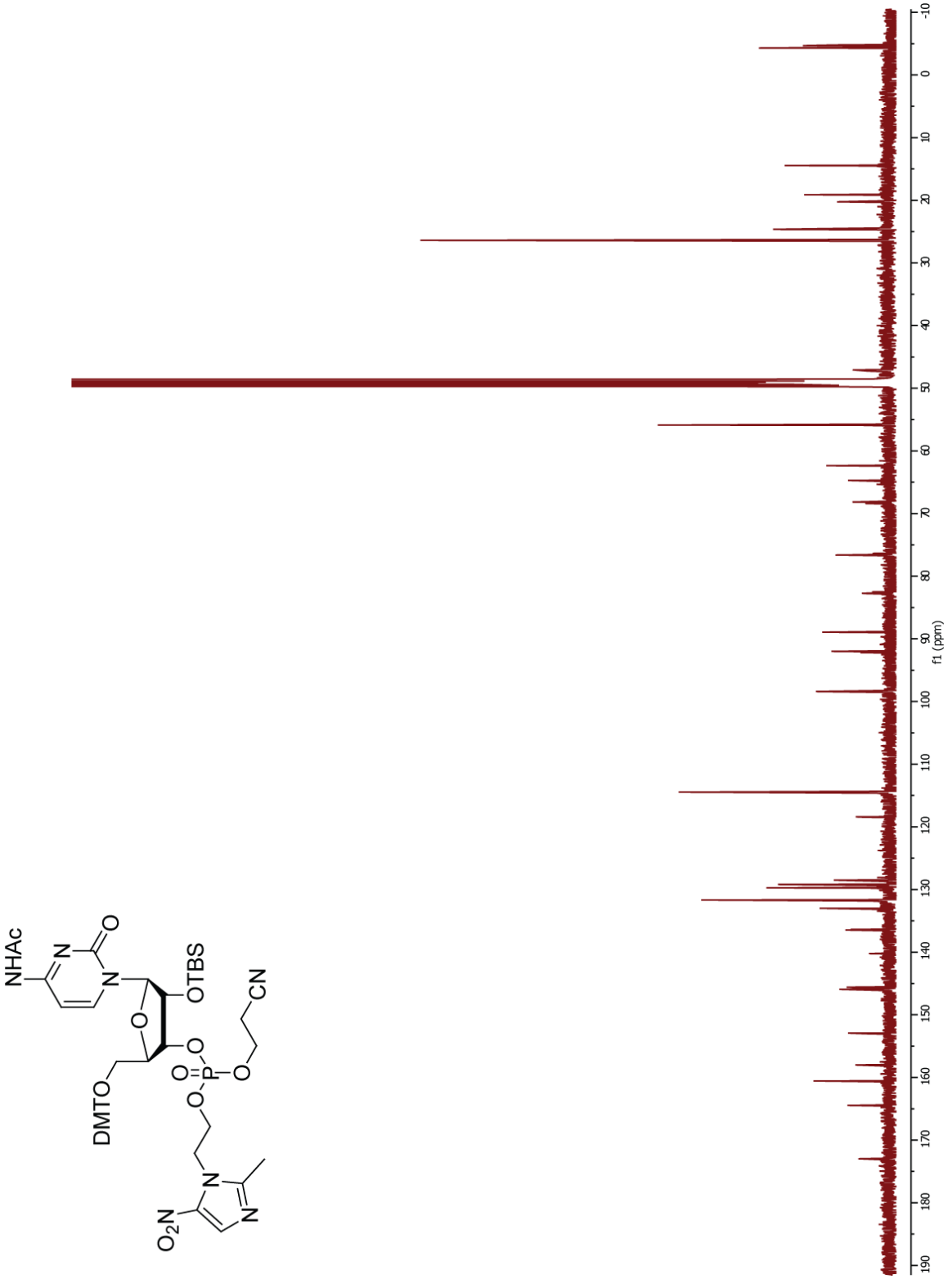
NHAc
N
O
N
O
OTBS
DMTO
O
O
O
P
O
O
CN
O
N
N
O_2N
f1 (ppm)

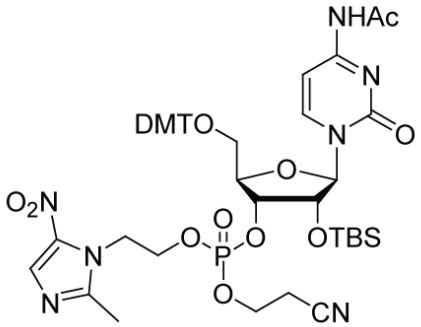
NHAc
N
N
O
DMTO
O
O2N
O
P
O
O
OTBS
N
N
O
CN

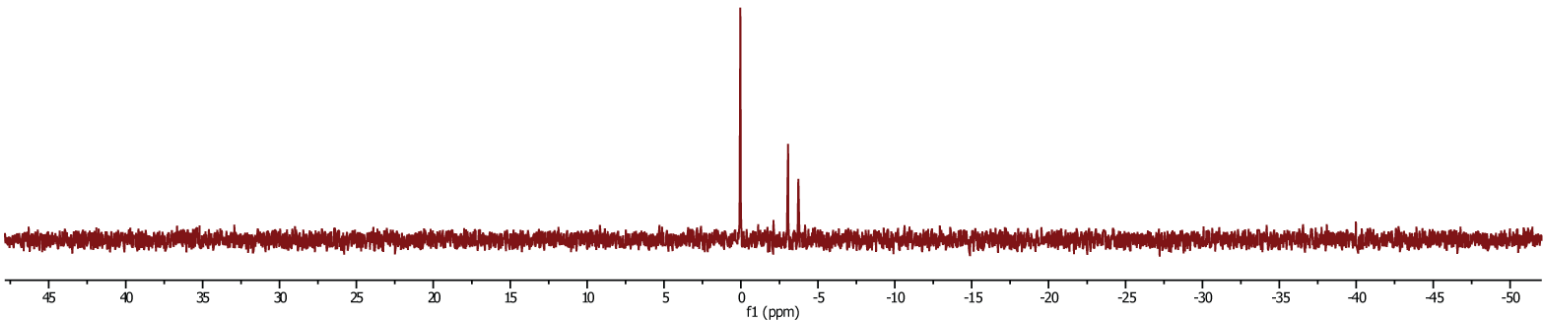
45
40
35
30
25
20
15
10
5
0
-5
-10
-15
-20
-25
-30
-35
-40
-45
-50
f1 (ppm)

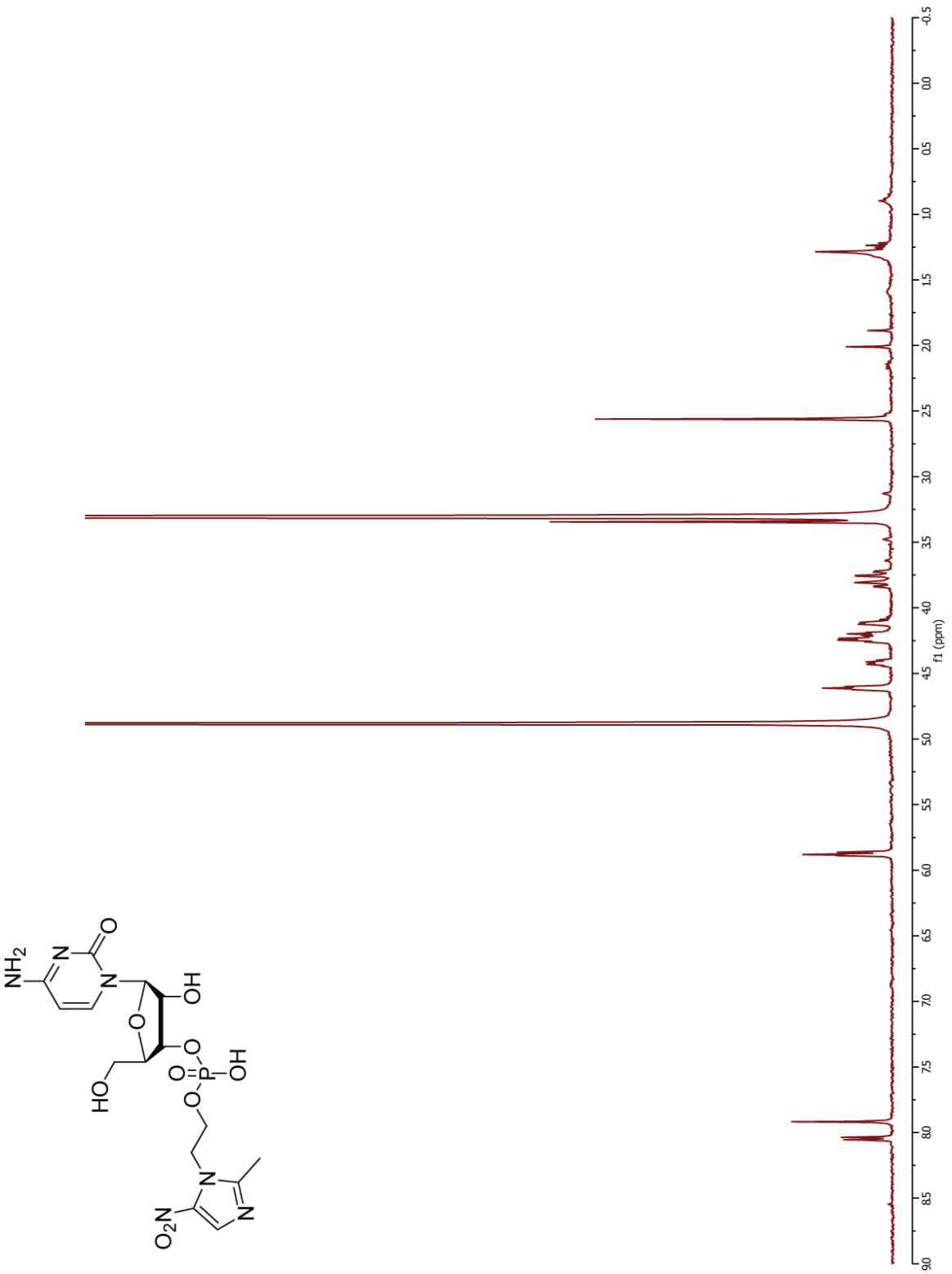
NH2
N
O
N
O
OH
HO
O
O
O=P
OH
O
N
N
O2N
f1 (ppm)
90
85
80
75
70
65
60
55
50
45
40
35
30
25
20
15
10
5
0
-0.5

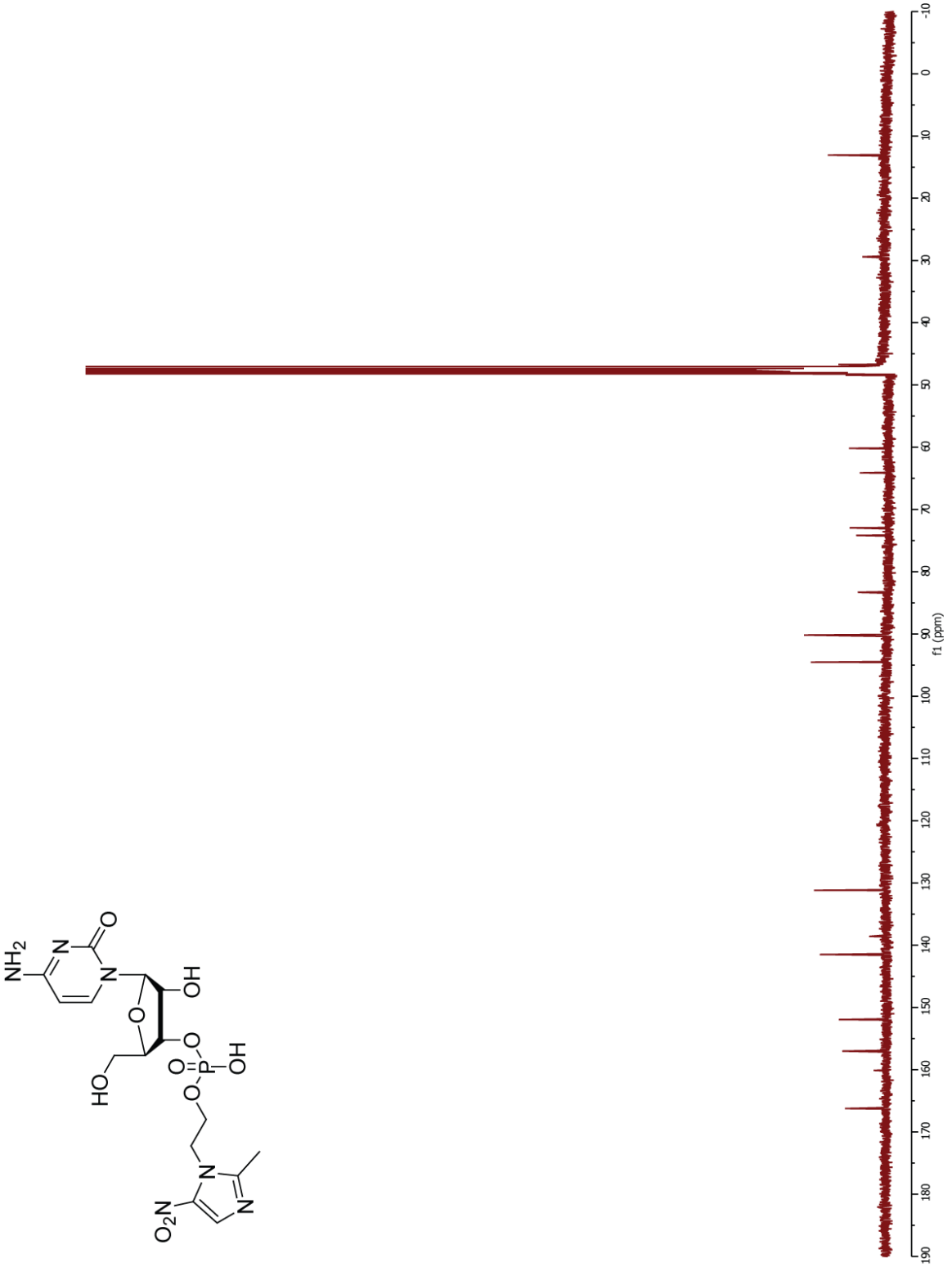
NH2
N
O
N
O
OH
HO
O
O
O=P
OH
O
N
N
O2N
f1 (ppm)
-10
0
10
20
30
40
50
60
70
80
90
100
110
120
130
140
150
160
170
180
190

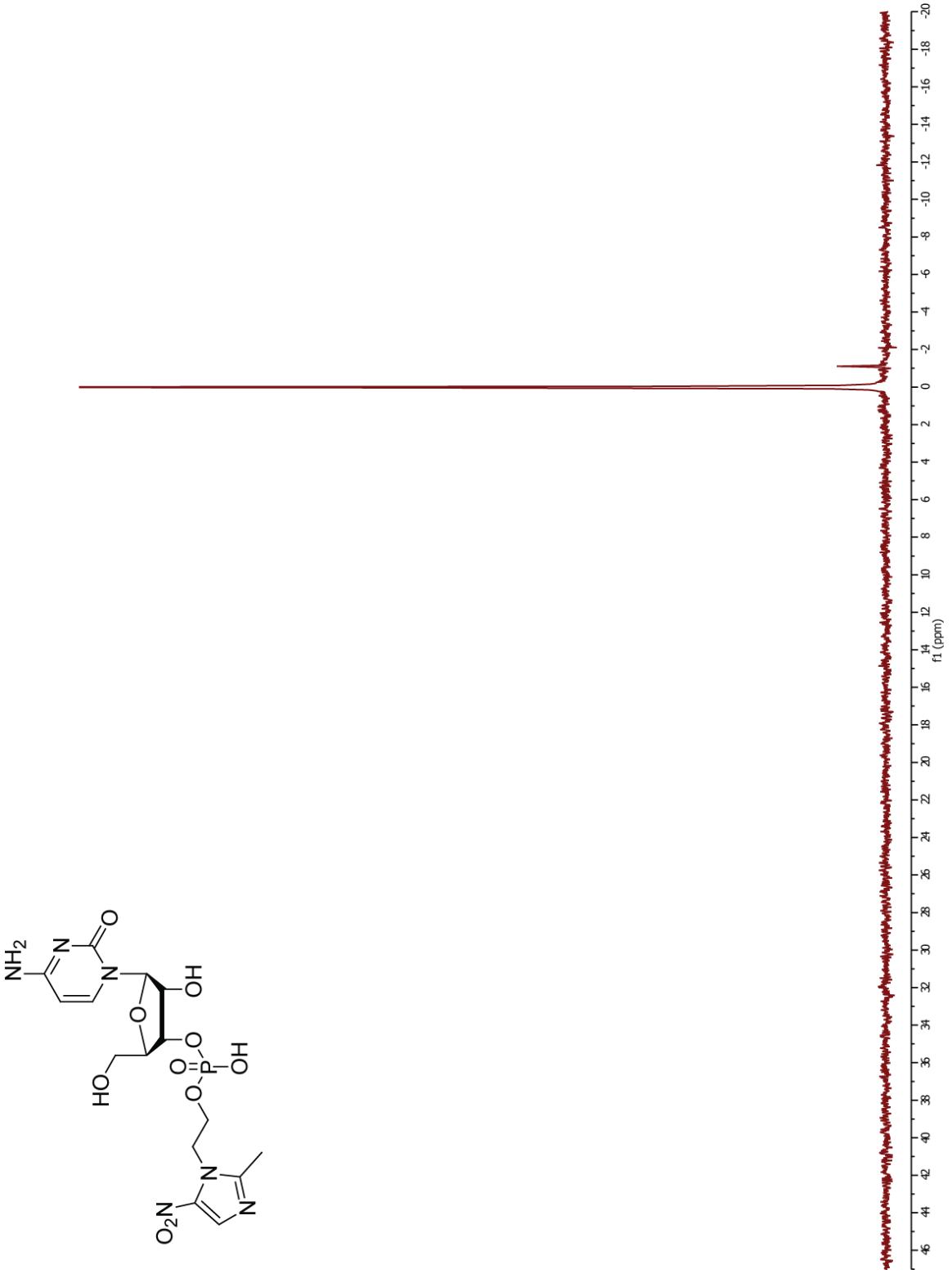
NH2
N
O
N
OH
O
HO
O
O
P
OH
N
N
O2N
f1 (ppm)

Chapter Five

Boronate-Mediated Biologic Delivery*

* This chapter has been published in part, under the same title. Reference: Ellis, G.A.[†], Palte, M.J.[†], & Raines, R.T. Boronate-mediated biologic delivery. *J. Am. Chem. Soc.* 134, 3631-3634 (2012). ([†] denotes equal contribution)

Additionally, of note was that this work was featured in Chemical & Engineering News: Drug Delivery Hooked On Sugar. 2012 Feb 15 and in *Nature*, 484, 9 (2012): Community Choice Highlight, Proteins' ticket into the cell.

5.1 Abstract

Inefficient cellular delivery limits the landscape of macromolecular drugs. Boronic acids readily form boronate esters with the 1,2- and 1,3-diols of saccharides, such as those that coat the surface of mammalian cells. Here pendant boronic acids are shown to enhance the cytosolic delivery of a protein toxin. Thus, boronates are a non-cationic carrier that can deliver a polar macromolecule into mammalian cells.

5.2 Author Contributions

Original idea for using boronic acids for drug delivery was from M.J.P. Original idea to couple boronic acids to RNase A to demonstrate delivery was from G.A.E. ^{1}H Determination of K_a values between boronates and glycans was performed by M.J.P. Flow cytometry assays and confocal microscopy were performed by M.J.P. Coupling conditions were determined jointly by G.A.E. and M.J.P. Protein purification and characterization was done by G.A.E. Heparin affinity assays, fluorescence polarization assays, ribonucleolytic activity assays, RI-evasion assays, and

cytotoxicity assays were performed by G.A.E. Preliminary cytotoxicity assays were done by M.L.H. The original manuscript and figures were jointly drafted by M.J.P. and G.A.E. M.J.P., G.A.E., and R.T.R. planed experiments, analyzed data, and edited the manuscript and figures.

5.3 Introduction

The utility of many biologic drugs is limited by inefficient cellular delivery.[58,59,61] Previous efforts to overcome this limitation have focused largely on the use of cationic domains—peptidic (*e.g.*, HIV–TAT, penetratin, and nonaarginine) or non-peptidic (*e.g.*, PAMAM dendrimers and polyethylenimine)—to enhance the attraction between a chemotherapeutic agent and the anionic cell surface.[60,62-64] Natural ligands (*e.g.*, folic acid, substance P, and the RGD tripeptide) have also been used to facilitate cellular delivery by targeting agents to specific cell-surface receptors.[65-67] Although these methods have achieved some success, additional delivery strategies are desirable.

The cell surface is coated with a dense forest of polysaccharides known as the glycocalyx.[198] We anticipated that targeting therapeutic agents to the glycocalyx would enhance their cellular delivery, as has been demonstrated with lectin conjugates.[199] Boronic acids readily form boronate esters with the 1,2- and 1,3-diols of saccharides,[68] including those in the glycocalyx.[73,74,78-81] In addition, boronate groups are compatible with human physiology, appearing in chemotherapeutic agents and other remedies.[70,72,76,77,200] Further, pendant boronic acids conjugated to polyethylenimine have been shown to enhance DNA transfection.[75] Here we demonstrate the use of pendant boronic acids to mediate the delivery of a protein into the cytosol of mammalian cells.

Bovine pancreatic ribonuclease (RNase A) is a small, well-characterized enzyme that has been the object of much seminal work in protein chemistry.[48,201-203] If this ribonuclease can gain access to the RNA that resides in the cytosol, then its prodigious catalytic activity can lead to cell death.[204-209] Hence, RNase A can serve as an ideal model for assessing the delivery of a protein

into the cytosol (rather than an endosome) because success can be discerned with assays of cytotoxic activity.

5.4 Results and Discussion

Initially, we quantified the affinity of simple boronic acids to relevant saccharides. Sialic acid is of particular interest because of its abundance in the glycocalyx of cancer cells.[210] Phenylboronic acid (PBA) binds with higher affinity to sialic acid than to other pyranose saccharides,[211-213] suggesting that simple boronic acids could target chemotherapeutic agents selectively to tumors. 2-Hydroxymethylphenylboronic acid (benzoxaborole[214-216]) has the highest reported affinity for pyranose saccharides,[211-213,217,218] which are abundant in the glycocalyx; hence, we reasoned that benzoxaborole could be an ideal boronate for drug delivery. We used ^{1}H NMR spectroscopy to evaluate directly the affinity of PBA and benzoxaborole for fructose, glucose, and *N*-acetylneuraminic acid (Neu5Ac), which contains a sialic acid moiety, under physiological conditions. Our K_a values (Table 5.1) are in accord with values determined by other workers using competition and other assays (Table 2).[211,213,217,218] We found that benzoxaborole has greater affinity than PBA for each saccharide in our panel, and that benzoxaborole like PBA has a greater affinity for Neu5Ac than for glucose. Accordingly, we chose benzoxaborole for our boronate-mediated delivery studies.

Table 5.1 Values of K_a (M^{-1}) for boronic acids and saccharides.[a]

	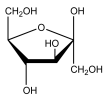 D-fructose	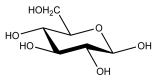 D-glucose	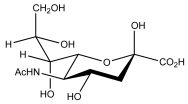 Neu5Ac
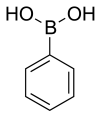	128 ± 20	5 ± 1	13 ± 1
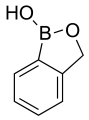	336 ± 43	28 ± 4	43 ± 5

Table 5.2 Literature values of K_a (M^{-1}) for boronic acids and saccharides.

	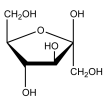 D-fructose	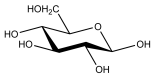 D-glucose	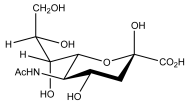 Neu5Ac	Method	Reference
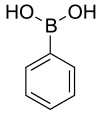	128 ± 20	5 ± 1	13 ± 1	^{1}H NMR in H_2O containing D_2O (2% v/v) [a]	This work
	160	4.6	21	Competition with alizarin red S [a]	213
	—	—	11.6 ± 1.9	^{11}B NMR in H_2O/D_2O/MeOH mixture	211
	79	0	—		218
	160	6	21	^{1}H NMR in D_2O (100% v/v) [a]	219
				Competition with alizarin red S [a]	
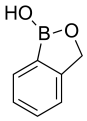	336 ± 43	28 ± 4	43 ± 5	^{1}H NMR in H_2O containing D_2O (2% v/v) [a]	This work
	606	17	—	^{1}H NMR in D_2O (100% v/v) [a]	218
	—	31	—	Competition with alizarin red S [a]	217
	664	21	160	Competition with alizarin red S [a]	219

[a] Values were determined in 0.10 M sodium phosphate buffer, pH 7.4.

To display benzoxaborole moieties on RNase A, we conjugated 5-amino-2-hydroxymethylphenylboronic acid (**1**) to protein carboxyl groups by condensation using a carbodiimide (Figure 5.1). Of the 11 carboxyl groups of RNase A, 7.5 ± 2.0 were condensed with boronate **1**, as determined by mass spectrometry.

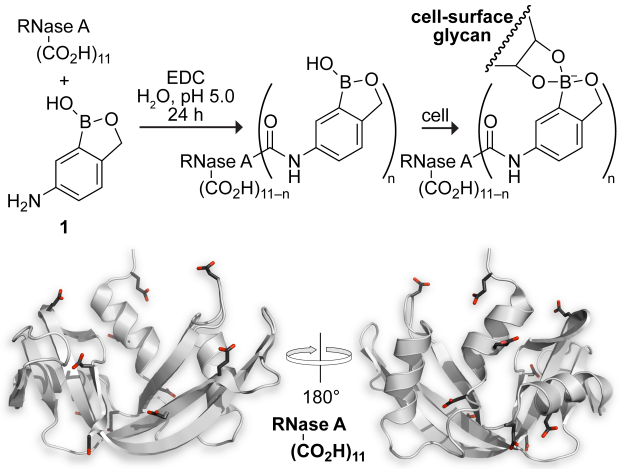

Figure 5.1 Boronation of RNase A. The location of each carboxyl group of RNase A is depicted in the ribbon diagram (PDB entry 7rsa[220]).

Boronation should increase the affinity of a protein for oligosaccharides. To test this hypothesis qualitatively, we measured the retention of boronated and unmodified RNase A on a column of heparin, a common physiological polysaccharide. Boronated RNase A was indeed retained longer on the column (Figure 5.2). If the prolonged retention were due to boron–saccharide complexation, then fructose in the buffer should compete with immobilized heparin for boron complexation. When these conditions were employed, the retention of boronated RNase A was indeed diminished (Figure 5.2).

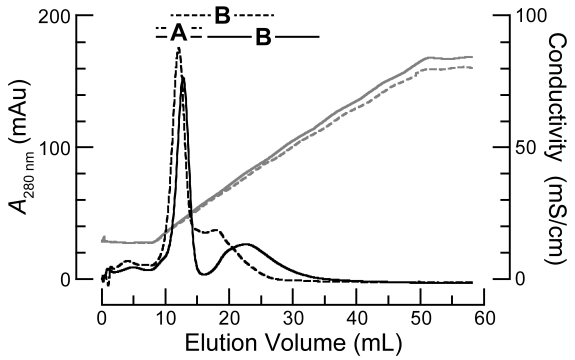

Figure 5.2 Elution profile of a mixture of unmodified RNase A (eluting in region "A") and boronated RNase A (eluting in region "B") from a column of immobilized heparin in the absence (solid line) or presence (dashed line) of fructose (0.10 M). Black lines, $A_{280\ nm}$; gray lines, conductivity.

To evaluate the enhanced affinity of boronated RNase A for oligosaccharides, we measured its affinity for ganglioside GD3 within a 1,2-dioleoyl-*sn*-glycero-3-phosphocholine liposome. This ganglioside has two sialic acid residues and is overexpressed on the surface of cancer cells.[221] By using fluorescence polarization to analyze binding, we found that boronation increased the affinity of the protein for the ganglioside, an effect that was abrogated by fructose (Figure 5.3). The K_d value of boronated protein for GD3 ganglioside liposomes was (53 ± 11) μM. This affinity is ~440-fold greater than that for the binding of a single benzoxaborole to Neu5Ac (Table 5.1), consistent with a multivalent interaction between the boronated protein and the ganglioside.

Encouraged by the enhanced affinity of the boronated protein for oligosaccharides *in vitro*, we sought to test our hypothesis that boronate conjugation increases cellular uptake. To quantify cellular internalization, we used fluorophore-labeled protein and flow cytometry. To

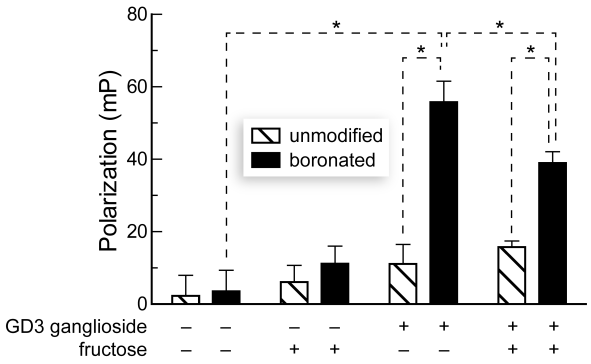

Figure 5.3 Fluorescence polarization assay of ribonucleases binding ganglioside-labeled liposomes in the presence or absence of 10 mM fructose. Data was normalized to polarization of each ribonuclease incubated with non-extruded DOPC lipids. Data points represent the mean (±SD) of triplicate experiments. Asterisks indicate values with $p < 0.05$.

determine concurrently if the pendant boronates elicited selectivity for cells with higher quantities of cell-surface sialic acid, we employed a line of Chinese hamster ovary cells (Lec-2) that have lower levels of sialic acid in their glycocalyx than their progenitor line (Pro-5).[222] We found that boronation of RNase A increased its cellular uptake by 4- to 5-fold (Figure 5.4). This enhancement was eliminated by fructose. Cell-surface sialic acid-content did not affect uptake significantly, consistent with the modest (1.5-fold) increase in the K_a value for benzoxaborole with sialic acid versus glucose (Table 5.1). Confocal microscopy of boronated protein revealed punctate staining (Figure 5.4, insert), which is consistent with uptake by endocytosis following complexation with cell-surface saccharides.

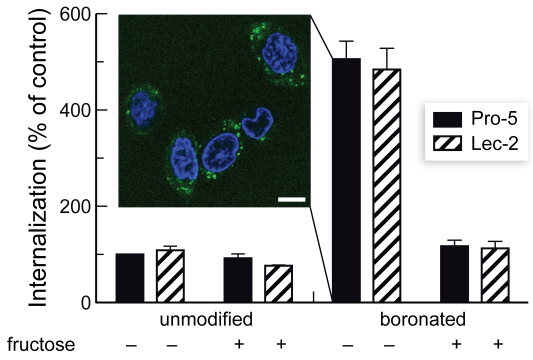

Figure 5.4 Internalization of unmodified and boronated RNase A into Pro-5 and Lec-2 cells in the absence or presence of fructose (0.25 M). Flow cytometry data were normalized to the internalization of unmodified RNase A into Pro-5 cells. Error bars represent the SD. Insert: Confocal microscopy image of live Pro-5 cells incubated for 4 h with boronated RNase A (5 μM) that had been labeled covalently with a green fluorophore. Nuclei were stained blue with Hoechst 33322 (2 μg/mL). Scale bar: 10 μm.

Although flow cytometry can quantify protein internalization into a cell, it does not differentiate between proteins in endosomes versus those in the cytosol. Delivery into the cytosol is essential for the efficacy of numerous putative chemotherapeutic agents. Boronated RNase A retained 17% of its ribonucleolytic activity.[223] Accordingly, boronated RNase A has the potential to be cytotoxic if it can gain entry to the cytosol. We found that boronated RNase A inhibited the proliferation of human erythroleukemia cells (Figure 5.5). The addition of fructose diminished cytotoxic activity, presumably by decreasing overall internalization. Chemically inactivated, boronated RNase A was much less cytotoxic, indicating that ribonucleolytic activity induced toxicity, not the pendant boronates. We conclude that boronation not only facilitates cellular uptake of a protein, but also enhances its delivery to the cytosol.

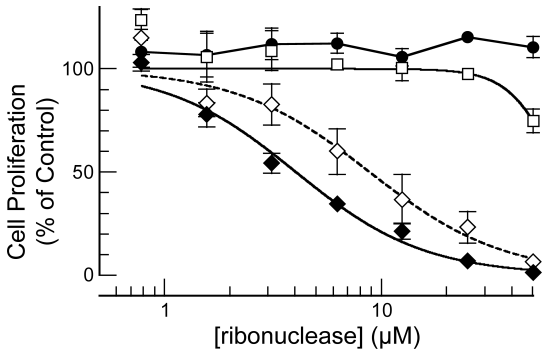

Figure 5.5 Inhibition of K-562 cell proliferation by unmodified and boronated RNase A. (●) Unmodified RNase A (IC_{50} >50 μM); (◆) boronated RNase A (IC_{50} 4.1 ± 0.4 μM); (◇) boronated RNase A in the presence of fructose (50 mM) (IC_{50} 9 ± 1 μM); (□) boronated RNase A alkylated with 2-bromoacetate (IC_{50} >50 μM). The proliferation of K-562 cells was measured by the incorporation of [*methyl*-^{3}H]thymidine. Data points represent the mean (±SEM) of three separate experiments performed in triplicate.

5.5 Conclusions

Boronates have attributes that make them attractive as mediators of drug delivery. First, endosomes become more acidic as they mature. In synergy, the affinity of boronates for saccharides decreases with decreasing pH.[213] Moreover, the ensuing loss of complexation causes boronates to become more hydrophobic.[69] These attributes could facilitate translocation to the cytosol. Second, boronates are not cationic,[224] averting the non-specific Coulombic interactions elicited by cationic domains,[60,62-64] which can lead to high rates of glomerular filtration and opsonization *in vivo*.[225,226] Finally, we note that numerous diseases are associated with changes in cell-surface glycosylation,[210,227] and we anticipate that boronic acids with specificity for particular glycans could serve as the basis for targeted delivery strategies.[228]

5.6 Acknowledgments

M.J.P. was supported by Molecular and Cellular Pharmacology Training Grant T32 GM008600 (NIH) and predoctoral fellowship 09PRE2260125 (American Heart Association). This work was supported by Grants R01 GM044783 and R01 CA073808 (NIH).

5.7 Materials and Methods

5.7.1 Materials

N-Acetylneuraminic acid was from Carbosynth (Berkshire, UK). Phenylboronic acid, 2-hydroxymethylphenylboronic acid, and 5-amino-2-hydroxymethylphenylboronic acid were from Combi-Blocks (San Diego, CA). BODIPY® FL, STP ester was from Molecular Probes (Eugene, OR). *N*-(3-Dimethylaminopropyl)-*N′*-ethylcarbodiimide hydrochloride (EDC) and wild-type RNase A (Type III-A) were from Sigma–Aldrich (St. Louis, MO) and used without further purification. MES buffer was from Sigma–Aldrich and purified by anion-exchange chromatography to remove trace amounts of oligomeric vinylsulfonic acid.[229] Spectra/Por® dialysis bags (3500 MWCO) were from Fisher Scientific (Thermo Fisher Scientific, Walham, MA). *Escherichia coli* BL21(DE3) cells were from Novagen (Madison, WI). [*methyl*-^{3}H]Thymidine (6.7 Ci/mmol) was from Perkin–Elmer (Boston, MA). Columns of HiTrap Heparin HP resin for protein purification and analytical resins were from GE Biosciences (Piscataway, NJ). Ribonuclease substrate 6-FAM–dArUdAdA–6-TAMRA was from Integrated DNA Technologies (Coralville, IA). Non-binding surface (NBS) 96-well plates were from Corning (Corning, NY). Terrific Broth (TB) was from Research Products International Corp (Mt. Prospect, IL). Bovine Serum Albumin (BSA) was from Thermo Scientific (Rockfield, IL). SDS–

PAGE gels were from Bio-Rad Laboratories (Hercules, CA). GD3 Ganglioside (bovine milk; ammonium salt), 1,2-dioleoyl-*sn*-glycero-3-phosphocholine (DOPC), and an extruder were from Avanti Polar Lipids (Alabaster, Alabama). Cell culture medium and supplements were from Invitrogen (Carlsbad, CA). Phosphate-buffered saline was either Dulbecco's PBS (DPBS) from Invitrogen or the same solution made in the laboratory (PBS), containing (in 1.0 L): 0.2 g KCl, 0.2 g KH_2PO_4, 8 g NaCl, and 2.16 g $Na_2HPO_4 \cdot 7H_2O$ at pH 7.4. All other chemicals used were of commercial reagent grade or better, and were used without further purification.

5.7.2 Instrumentation and Statistics

^{1}H NMR spectra were acquired at the National Magnetic Resonance Facility at Madison at 298 K on an Avance III 500 MHz spectrometer with a TCI 500 H-C/N-D cryogenic probe from Bruker AXS (Madison, WI, ^{1}H, 500 MHz). Protein absorbance values were measured on a Varian Cary 50 UV–Vis Spectrometer (Agilent Technologies, Santa Clara, CA) and/or a NanoVue spectrometer (GE Healthcare, Piscataway, NJ). Confocal microscopy was carried out using an Eclipse C1 laser scanning confocal microscope from Nikon (Melville, NY). Flow cytometry was done using a LSRII (BD Biosciences, San Jose, CA) at the University of Wisconsin–Madison Carbone Cancer Center Flow Cytometry Facility. The mass of RNase A and boronated RNase A conjugates were confirmed at the University of Wisconsin–Madison Biophysics Instrumentation Facility by matrix-assisted laser desorption/ionization time-of-flight (MALDI–TOF) mass spectrometry with a Voyager-DE-PRO Biospectrometry Workstation from Applied Biosystems (Foster City, CA). [*methyl*-^{3}H]Thymidine incorporation into K-562 genomic DNA was quantified by scintillation counting using a Microbeta TriLux liquid scintillation and

luminescence counter from Perkin–Elmer. Fluorescence measurements were made with an infinite M1000 plate reader from Tecan (Männedorf, Switzerland). Calculations for statistical significance were performed with GraphPad Prism version 5.02 software from GraphPad Software (La Jolla, CA), and a value of $p < 0.05$ was considered to be significant.

5.7.3 Determination of K_a Values by ^{1}H NMR Spectroscopy

Methodology to determine the values of K_a for boronic acids and saccharides was adapted from work by Hall and coworkers.[217,218] A boronic acid (B) and a saccharide (S) were assumed to bind in one modality, B·S:

(1) $B + S \rightleftharpoons BS$

(2) $K_a = \dfrac{[BS]}{[S][B]}$

The [B·S]/[B] ratio was determined by the integration of aryl protons of the boronic acid·saccharide complex and the free boronic acid. The individual [B], [B·S], and [S] can be calculated from eq 1–5.

$$[BS] + [B] = [B_T]$$

$$\frac{[BS]}{[B]} + 1 = \frac{[B_T]}{[B]}$$

(3) $$[B] = \frac{[B_T]}{\frac{[BS]}{[B]} + 1}$$

(4) $$[BS] = \frac{[BS]}{[B]}[B]$$ where [B] is calculated from eq 3.

$$[BS] + [S] = [S_T]$$

(5) $[S] = [S_T] - [BS]$ where [BS] is calculated from eq 4.

Each value of K_a arose from at least two independent experiments with freshly prepared solutions, and each experiment consisted of a titration with 6–9 different concentrations. All NMR spectra were analyzed with Topspin 3.0 software from Bruker AXS. NMR experiments were done in a 0.10 M NaH_2PO_4 buffer, pH 7.4, containing D_2O (2% v/v). ^1H NMR experiments consisted of the first increment of a 2D NOESY with gradients for improved water suppression.

5.7.3.1 Representative Procedure for Making a Boronic Acid Solution

NaH_2PO_4 (3.0 g, 25 mmol) and PBA (458 mg, 3.75 mmol) were dissolved in distilled, deionized water in a volumetric flask (~200 mL H_2O, 5 mL D_2O). The pH was adjusted carefully to 7.4 using 10 M NaOH, and additional water was added for a final volume of 250 mL. Final solutions were 15 mM boronic acid (PBA = solution 1; benzoxaborole = solution 2) in 0.10 M sodium phosphate monobasic buffer, pH 7.4, containing D_2O (2% v/v).

5.7.3.2 Determination of the Value of K_a for PBA and Fructose

To a 25-mL volumetric flask, D-fructose (674 mg, 3.75 mmol) and ~20 mL of solution 1 was added. The solution was adjusted carefully to pH 7.4 by the addition of 10 M NaOH. (The volume of added NaOH was used in the calculation of the boronic acid concentration.) The volume was then increased to 25 mL by adding solution 1. This procedure resulted in a pH 7.4 solution of PBA (15 mM), D-fructose (150 mM), NaH_2PO_4 (0.10 M), and D_2O (2% v/v) (solution A). Mixing various volumes of solution 1 and solution A generated D-fructose concentrations in the range of 4–14 mM. The [B·S]/[B] ratio was determined for every concentration as follows.

5.7.3.3 Representative Procedure for Determining the Chemical Shifts of Aryl Protons in Bound and Free Boronic Acids

A ^1H NMR spectra of solution 1 (Figure 5.6A) and solution A (Figure 5.6B) were acquired. The two spectra were overlaid to determine which peaks belonged to the bound boronic acid and free boronic acid (Figure 5.6C). This analysis was used to interpret the spectra from the titrations with sugars (Figure 5.6D).

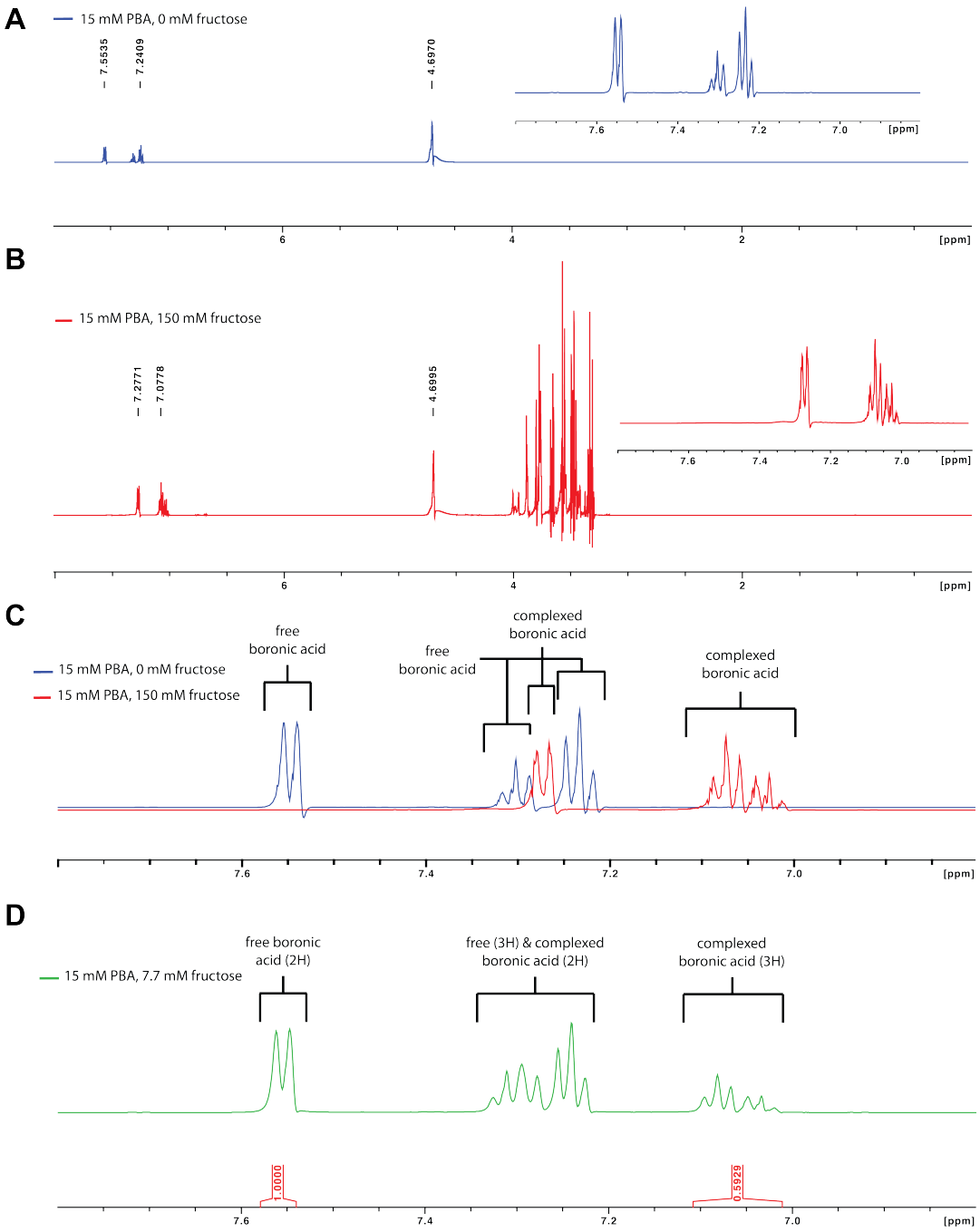

Figure 5.6 Determination of the peaks corresponding to the aryl protons in bound and free boronic acid. (A) ^{1}H NMR spectrum of solution 1. (B) ^{1}H NMR spectrum of solution A. (C) Overlay of aromatic region of spectra from panels A and B. (D) Example of a spectrum that was interpreted using the overlay from panel C, and used to determine the value of K_a for fructose with PBA. The [B·S]/[B] ratio was calculated from the isolated peaks for the complex (3H, 7.01–7.11 ppm) and the isolated peaks for the free boronic acid (2H, 7.54–7.58 ppm).

5.7.3.4 Determination of the Value of K_a for Benzoxaborole and Fructose

To a 25-mL volumetric flask, D-fructose (674 mg, 3.75 mmol) and ~20 mL of solution 2 was added. The solution was adjusted carefully to pH 7.4 by the addition of 10 M NaOH. (The volume of added NaOH was used in the calculation of the boronic acid concentration.) The volume was then increased to 25 mL by adding solution 2. This procedure resulted in a pH 7.4 solution of benzoxaborole (15 mM), D-fructose (150 mM), NaH_2PO_4 (0.10 M), and D_2O (2% v/v) (solution B). Mixing various volumes of solution 2 and solution B generated fructose concentrations in the range of 4–14 mM. The [B·S]/[B] ratio was determined as depicted in Figure 5.7. A value for K_a was calculated for every concentration as described above.

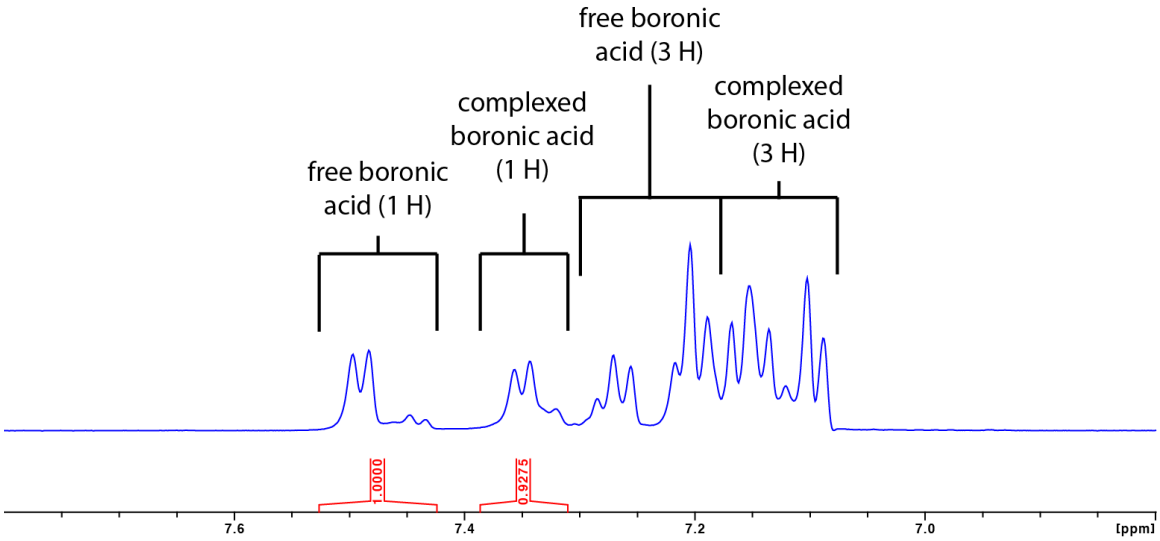

Figure 5.7 Example of a ^{1}H NMR spectrum that was used to determine the K_a value for benzoxaborole and D-fructose (10.3 mM). Peaks corresponding to the aryl protons in bound and free boronic acid were determined a described above. The [B·S]/[B] ratio was calculated from the isolated peaks for the complex (1H, 7.31–7.38 ppm, a mixture of isomeric species) and the isolated peaks for the free boronic acid (1H, 7.43–7.53 ppm, a mixture of isomeric species). Additional saccharide decreased the integration of the small peak at 7.44 ppm equally with that at 7.49 ppm, which arise from free boronic acid; and the shoulder peak at 7.31 ppm increased equally with that at 7.35 ppm, which arises from the complex.

5.7.3.5 Determination of the Value of K_a for PBA and Glucose

To a 25-mL volumetric flask, D-glucose (2.25 g, 12.5 mmol) and ~20 mL of solution 1 was added. The solution was adjusted carefully to pH 7.4 by the addition of 10 M NaOH. (The volume of added NaOH was used in the calculation of the boronic acid concentration.) The volume was then increased to 25 mL by adding solution 1. This procedure resulted in pH 7.4 solution of PBA (15 mM), D-glucose (500 mM), 0.1 M NaH_2PO_4 (0.10 M), and D_2O (2% v/v) (solution C). Mixing various volumes of solution 1 and solution C generated D-glucose concentrations in the range of 20–70 mM. The [B·S]/[B] ratio was determined as depicted in Figure 5.8. A value for K_a was calculated for every concentration as described above.

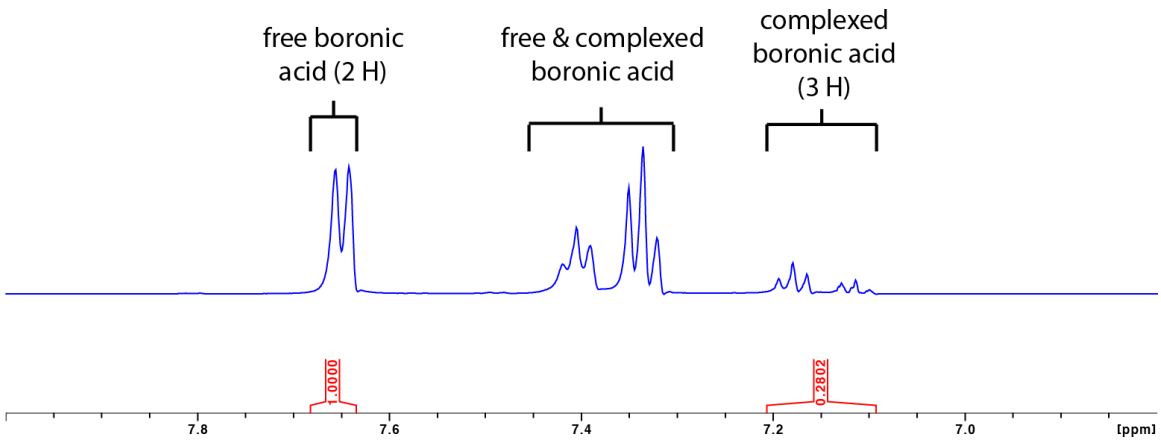

Figure 5.8 Example of a ^{1}H NMR spectrum that was used to determine the K_a value for PBA and D-glucose (44.9 mM). Peaks corresponding to the aryl protons in bound and free boronic acid were determined a described above. The [B·S]/[B] ratio was calculated from the isolated peaks for the complex (3H, 7.09–7.21 ppm) and the peaks for the free boronic acid (2H, 7.64–7.68 ppm).

5.7.3.6 Determination of the Value of K_a for Benzoxaborole and Glucose

To a 25-mL volumetric flask, D-glucose (2.25 g, 12.5 mmol) and ~20 mL of solution 2 was added. The solution was adjusted carefully to pH 7.4 by the addition of 10 M NaOH. (The volume of added NaOH was used in the calculation of the boronic acid concentration.) The volume was then increased to 25 mL by adding solution 2. This procedure resulted in a pH 7.4 solution of benzoxaborole (15 mM), D-glucose (500 mM), NaH_2PO_4 (0.10 M), and D_2O (2% v/v) (solution D). Mixing various volumes of solution 2 and solution D generated D-glucose concentrations in the range of 20–70 mM. The [B·S]/[B] ratio was determined as depicted in Figure 5.9. A value for K_a was calculated for every concentration as described above.

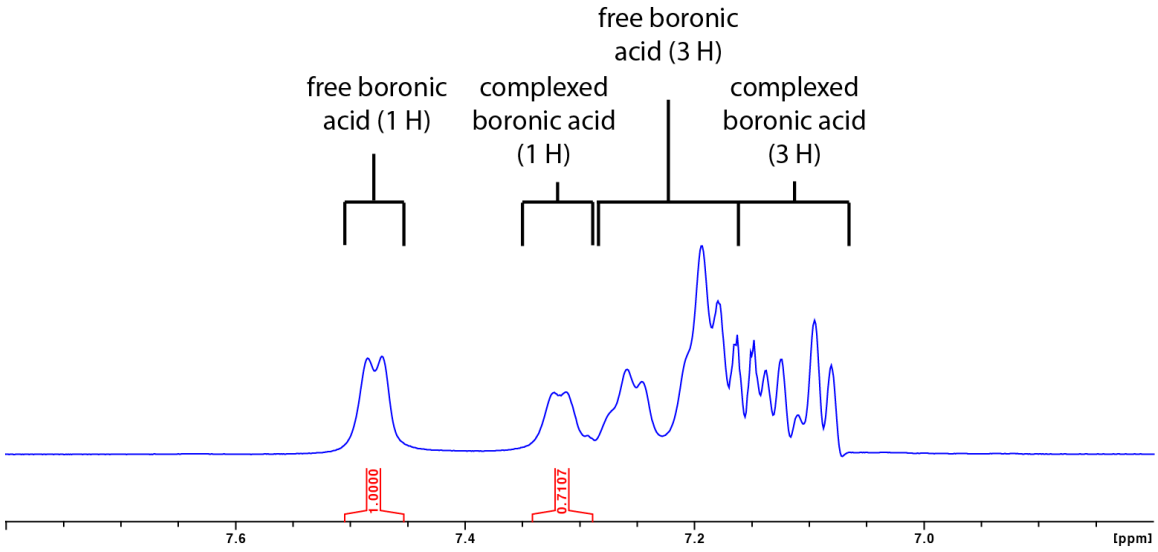

Figure 5.9 Example of a ^{1}H NMR spectrum that was used to determine the K_a value for benzoxaborole and D-glucose (32.9 mM). Peaks corresponding to the aryl protons in bound and free boronic acid were determined a described above. The [B·S]/[B] ratio was calculated from the isolated peaks for the complex (^{1}H, 7.29–7.34 ppm) and the isolated peaks for the free boronic acid (^{1}H, 7.45–7.51 ppm). Note the broadening of the aryl protons, which had been reported for NMR spectra of boronic acids in the presence of pyranose sugars.[217]

5.7.3.7 Determination of the Value of K_a for PBA and Neu5Ac

To a 10-mL volumetric flask, Neu5Ac (1.53 g, 5.0 mmol) and ~20 mL of solution 1 was added. The solution was adjusted carefully to pH 7.4 by the addition of 10 M NaOH. (The volume of added NaOH was used in the calculation of the boronic acid concentration.) The volume was then increased to 25 mL by adding solution 1. This procedure resulted in a pH 7.4 solution of PBA (14.2 mM), Neu5Ac (500 mM), NaH_2PO_4 (0.10 M), and D_2O (2% v/v) (solution E). Mixing various volumes of solution 1 and solution E, generated Neu5Ac concentrations in the range of 7–65 mM. The [B·S]/[B] ratio was determined as depicted in Figure 5.10. A value for K_a was calculated for every concentration as described above.

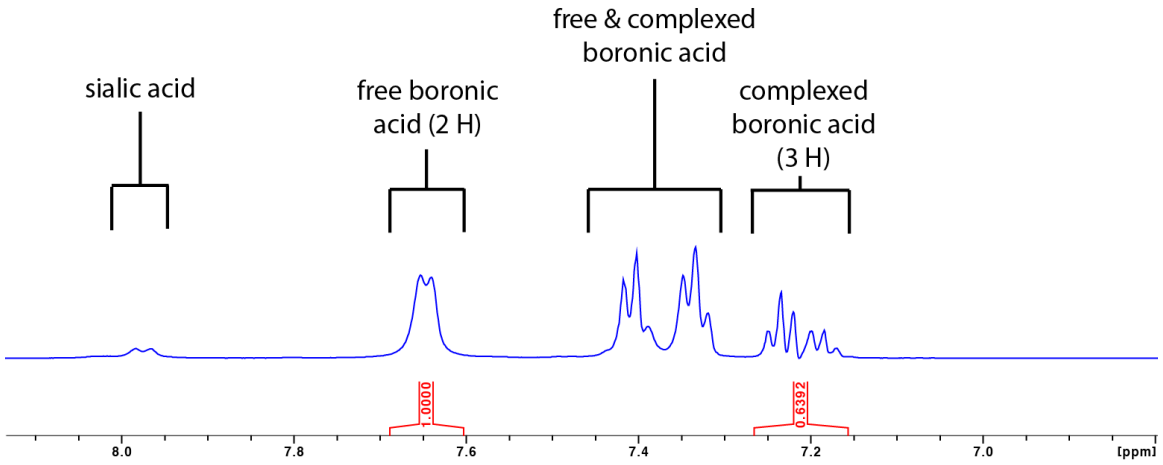

Figure 5.10 Example of a ^{1}H spectrum that was used to determine the K_a value for PBA with Neu5Ac (35.4 mM). Peaks corresponding to the aryl protons in bound and free boronic acid were determined a described above. The [B·S]/[B] ratio was calculated from the isolated peaks for the complex (3H, 7.15–7.26 ppm) and the isolated peaks for the free boronic acid (2H, 7.6–7.69 ppm). Note that the aryl peaks have been broadened by the addition of the saccharide.

5.7.3.8 Determination of the Value of K_a for Benzoxaborole and Neu5Ac

To a 10-mL volumetric flask, Neu5Ac (1.56 g, 5.0 mM) and ~20 mL of solution 2 was added. The solution was adjusted carefully to pH 7.4 by the addition of 10 M NaOH. (The

volume of added NaOH was used in the calculation of the boronic acid concentration.) The volume was then increased to 25 mL by adding solution 2. This procedure resulted in a pH 7.4 solution of benzoxaborole (14.2 mM), Neu5Ac (500 mM), NaH_2PO_4 (0.10 M), and D_2O (2% v/v) (solution F). Mixing various volumes of solution 2 and solution F generated Neu5Ac concentrations in the range of 7–65 mM. The K_a value was calculated for every concentration as previously described. F The [B·S]/[B] ratio was determined as depicted in Figures 5.11 and 5.12. A value for K_a was calculated for every concentration as described above.

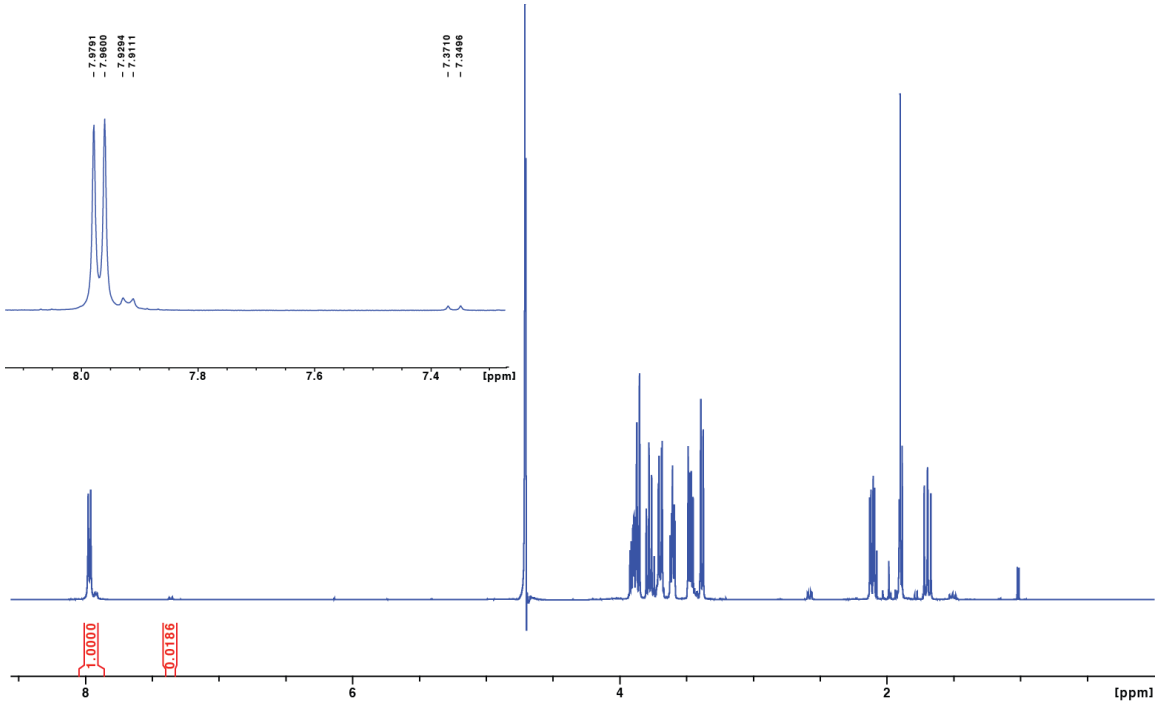

Figure 5.11 Apparent in the ^{1}H NMR spectrum of Neu5Ac is a small peak that overlapped with the aromatic regions of the boronic acids. This peak was subtracted out of all NMR spectra used to evaluate the interaction of benzoxaborole and Neu5Ac.

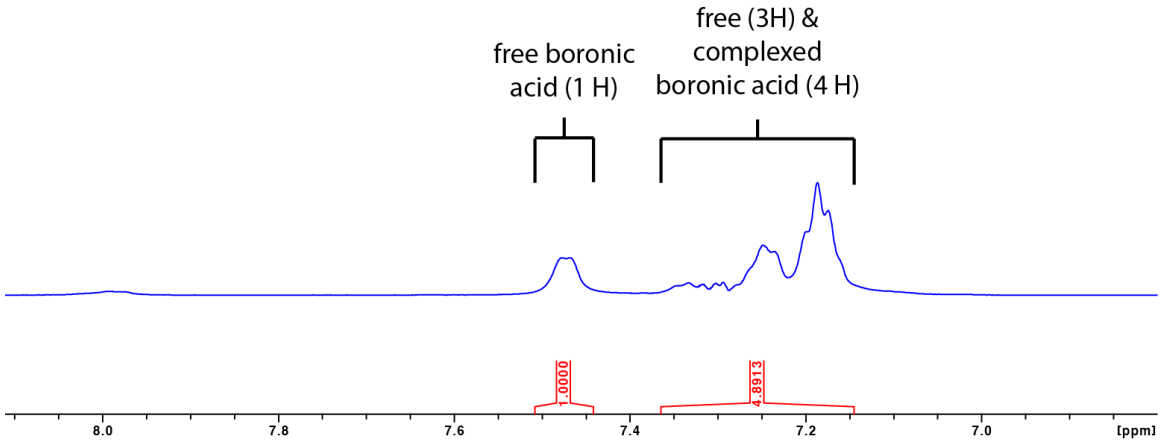

Figure 5.12 Example of a ^{1}H spectrum that was used to determine the K_a value for benzoxaborole with Neu5Ac (14.4 mM). Peaks corresponding to the aryl protons in bound and free boronic acid were determined a described above. The [B·S]/[B] ratio was determined from the isolated peaks for the free boronic acid (1H, 7.44–7.51 ppm) and the remainder of the aromatic region (7.15–7.36 ppm), which represented 3H from the free boronic acid and all 4 aromatic protons from the complex. Unlike D-fructose and D-glucose, the single isolated proton of the complexed species (7.33 ppm) was too broad to integrate accurately, and the entire region was used instead.

5.7.4 Preparation of Boronated RNase A

5-Amino-2-hydroxymethylphenylboronic acid (320 mg, 1.70 mmol) was added to 30 mL of distilled, deionized H_2O, and the resulting solution was adjusted to pH 5.0 with NaOH. To this solution was added RNase A (200 mg, 15 μmol), followed by EDC (640 mg, 3.30 mmol), and the pH was adjusted again to 5.0 with NaOH. The reaction mixture was incubated at ambient temperature overnight on a nutating mixer by BD (Franklin Lakes, NJ). Additional EDC (360 mg, 1.9 mmol) was added, and the solution was incubated at the same conditions for 3.5 h (24 h total). The solution was then subjected to centrifugation (5 min at 1000 rpm, and 5 min at 5000 rpm) to remove insoluble boronic acid, and dialyzed (3500 molecular weight cutoff) against distilled, deionized H_2O for 3 d at 4 °C, with daily water exchanges. The solution was then passed through a 0.45-μm filter and loaded onto a 5-mL column of HiTrap Heparin HP

resin. To prepare a high-salt buffer, NaCl (58.4 g, 1.00 mol) was added to 100 mL of a 10× stock solution of PBS. This solution was diluted with distilled, deionized H_2O to a final volume of 1 L, and adjusted to pH 7.4, making a buffer of PBS plus an additional 1 M NaCl. The resin was washed with 75 mL of PBS buffer, and protein was eluted with a linear gradient of 225 mL of additional NaCl (0.0–1.0 M) in PBS buffer. Fractions were collected, pooled, concentrated, stored at 4 °C, and analyzed by MALDI–TOF mass spectrometry. The mass spectrum between 13–16 kDa was fitted to a Gaussian curve with GraphPad Prism version 5.02 software to determine the average mass. Conjugation to 5-amino-2-hydroxymethylboronic acid was confirmed by trypsin-digest mass spectrometry, which revealed the additional mass (113 Da, corresponding to dehydrated 5-amino-2-hydroxymethylboronic acid) of carboxylic acid containing peptide fragments. The ribonucleolytic activity of boronated RNase A ($k_{cat}/K_M = 1.6 \pm 0.2 \times 10^7$ $M^{-1}\cdot s^{-1}$) was 17% that of unmodified RNase A ($k_{cat}/K_M = 9.6 \pm 0.7 \times 10^7$ $M^{-1}\cdot s^{-1}$).

5.7.5 Preparation of Inactivated, Boronated RNase A

RNase A (38 mg, 2.8 μmol) was dissolved in 575.5 μL of 0.10 M sodium acetate buffer, pH 4.9. In a separate solution, 2-bromoacetic acid (123 mg, 883 μmol) was dissolved in 9.2 mL of 0.10 M sodium acetate buffer and the resulting solution was adjusted to pH 5.2. An aliquot (288 μL) of the 2-bromoacetic acid solution was added to the RNase A solution to generate a final concentration of 32 mM 2-bromoacetic acid and 3.2 mM RNase A. The reaction mixture was incubated at ambient temperature for 24 h on a nutating mixer, after which the reaction was dialyzed overnight against distilled, deionized H_2O. The inactivated RNase A was then loaded onto a column of Mono S HR 16/10 cation-exchange resin from Pharmacia. The resin was

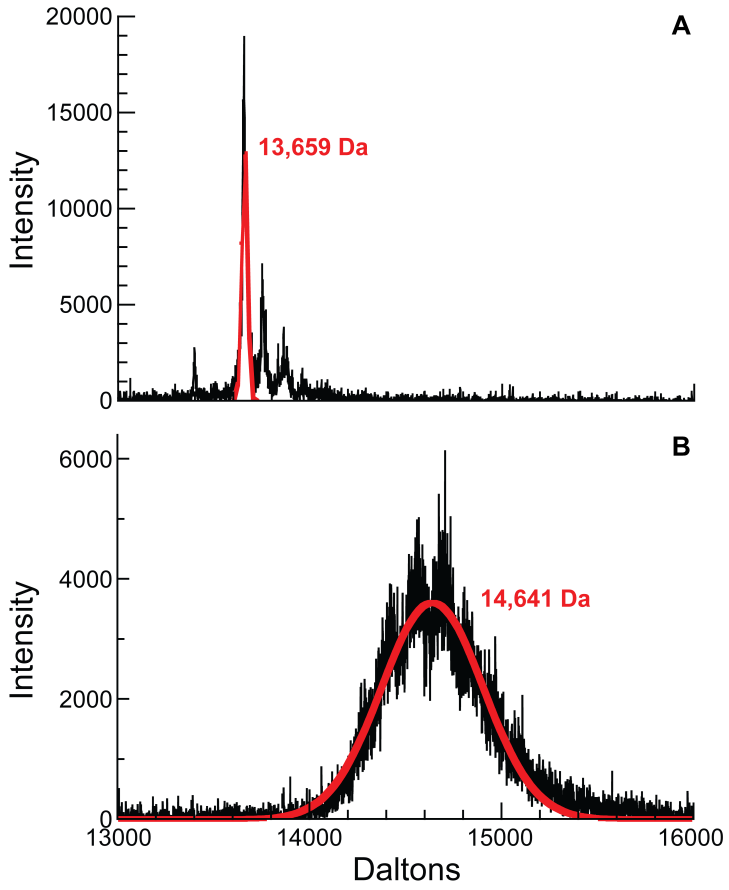

Figure 5.13 MALDI–TOF spectra of (A) unmodified RNase A and (B) boronated RNase A. Data were fitted to a Gaussian curve (red line). The observed molecular mass of unmodified RNase A (13,659 Da) was subtracted from the observed molecular mass of boronated RNase A (14,641 Da) to give 982 Da. This value was divided by the molecular mass of 5-amino-2-hydroxymethylphenylboronic acid after correcting for the water lost during conjugation (148.95 Da – 18.02 Da = 130.93 Da) to give 7.5 ± 2.0 boronic acids conjugated to RNase A, where SD = 2.0 arises from the SD of the Gaussian fit, 265.2 Da, divided by 130.93 Da.

washed with a 40-mL linear gradient of NaCl (0.00–0.05 M) in 10 mM sodium phosphate buffer, pH 6.0, and eluted with a 603-mL linear gradient of NaCl (0.05–0.40 M) in 10 mM sodium phosphate buffer, pH 6.0. Fractions were collected, pooled, and dialyzed overnight at 4 °C against 50 mM sodium acetate buffer, pH 5. Inactivated RNase A was then loaded onto a 5-mL

column of HiTrap Heparin HP resin. The resin was washed with 10 mL of 50 mM sodium acetate buffer, pH 5.0, and eluted with a 200-mL linear gradient of NaCl (0.0–0.4 M) in 50 mM sodium acetate buffer, pH 5.0. Fractions were collected, and analyzed by MALDI–TOF mass spectrometry. Fractions with a molecular mass greater than that of wild-type RNase A were pooled and dialyzed extensively with distilled, deionized H_2O at 4 °C. 5-Amino-2-hydroxymethylphenylboronic acid was then conjugated as described above. Briefly, to 0.5 mL of chemically inactivated RNase A (6 mg, 400 nmol) was added 5-amino-2-hydroxymethylphenylboronic acid (10 mg, 50 μmol), and adjusted to pH 5. EDC was then added (19 mg, 100 μmol), and the resulting solution was adjusted to pH 5. The reaction mixture was incubated at ambient temperature for 20.5 h on a nutating mixer before adding additional EDC (11 mg, 56 μmol), and then incubated for an additional 3.5 h. Inactivated, boronated RNase A was dialyzed against distilled, deionized H_2O and purified on a 1-mL column of HiTrap Heparin HP resin as described for boronated RNase A, but scaled for the 1-mL column. The ribonucleolytic activity of inactivated, boronated RNase A ($k_{cat}/K_M = 3.0 \pm 0.2 \times 10^5$ $M^{-1}{\cdot}s^{-1}$) was 2% that of boronated RNase A ($k_{cat}/K_M = 1.6 \pm 0.2 \times 10^7$ $M^{-1}{\cdot}s^{-1}$).

5.7.6 Preparation of BODIPY FL-Labeled Ribonucleases

Both unmodified and boronated RNase A were labeled with BODIPY FL. An aliquot (3.83 mL) of a solution of ribonuclease (120 μM) was adjusted to pH 8.3. BODIPY FL STP ester (5 mg; 9 μmol) was dissolved in 0.5 mL of DMF. To the solution of ribonuclease was added 125 μL of the BODIPY FL STP ester solution. The reaction mixture was incubated at ambient temperature on a nutating mixer for 4–6 h, and then incubated at 4 °C on a nutating mixer

overnight. Labeled ribonuclease was loaded onto a 1-mL column of HiTrap Heparin HP resin. The resin was washed with 30 mL of 10 mM sodium phosphate buffer, pH 6.0. The protein was eluted with a 60-mL linear gradient of NaCl (0.0–1.5 M) and pH (6.0–7.4) in 10 mM sodium phosphate buffer, pH 7.4. Fractions were collected, pooled, concentrated, and analyzed by SDS–PAGE and MALDI–TOF mass spectrometry.

Labeled ribonucleases were dissolved in at least a 10× volume of DPBS, passed through a 0.45-μm syringe filter from Whatman (Piscataway, NJ), and re-concentrated before being used in assays. In this manner, the proteins were dissolved in solution that was largely DPBS. Concentrations of proteins were determined by UV spectroscopy using the extinction coefficient of RNase A at 280 nm (ε = 0.72 (mg·mL^{-1})$^{-1}$·cm^{-1})[230] but on a molar basis (ε = 9.9 mM^{-1}·cm^{-1}). The absorbance of benzoxaborole was found to be negligible, contributing <6% to the $A_{280\ nm}$ of the boronated ribonuclease. The concentration of labeled ribonucleases was corrected for fluorophore absorbance by using the manufacturer's protocol (http://tools.invitrogen.com/content/sfs/manuals/mp00143.pdf). Percent labeling was determined by UV spectroscopy at 504 nm using the extinction coefficient of BODIPY FL (ε = 68,000 M^{-1}·cm^{-1}) as per the manufacturer's protocol.

5.7.7 Heparin-Affinity Assays

The affinity of unmodified and boronated RNase A for heparin was assessed by retention on a 1.0-mL column of HiTrap Heparin HP resin (GE Healthcare, Piscataway, NJ). Unmodified and boronated RNase A were mixed in a 1:1 ratio (~146 nmol each) in DPBS, and the resulting solution was loaded onto the resin. The resin was washed with 5 mL of PBS, followed by elution

with 45 mL of a linear gradient of NaCl (0.0–1.0 M) in PBS. Elution was monitored by absorbance at 280 nm, and eluted proteins were identified by mass spectrometry. A small amount of unmodified RNase A was apparent in peak B (Figure 5.2). We hypothesize that boronated RNase A was able to complex to a small amount of unmodified RNase A and extend its elution time. The same assay was then repeated with 100 mM D-fructose in both buffers. To make D-fructose–supplemented buffers, fructose (18 g, 100 mmol) was added to 100 mL of a 10× stock solution of PBS, either no additional NaCl or NaCl (58.4 g, 1.00 mol) was added, and both buffers were diluted to a final volume of 1 L and adjusted to pH 7.4.

5.7.8 Fluorescence Polarization Assays

Liposomes were formed by transferring DOPC (dissolved in chloroform solution) and GD3 gangliosides (dissolved in 63:35:5 chloroform/methanol/water) to glass tubes and drying them under Ar(g) and then under vacuum. Lipids were re-suspended in 25 mM HEPES buffer, pH 7.0, containing NaCl (75 mM). The solution of lipids was mixed by vortexing for 2 min, and incubated at 37 °C for 1 h. For DOPC liposomes, DOPC was resuspended at a concentration of 5 mM. For GD3 ganglioside-labeled liposomes, DOPC and GD3 gangliosides were mixed at 3 and 2 mM concentrations, respectively. Large unilammelar vesicles were formed by extrusion through a 0.1-μm polycarbonate filter from Whatman (GE Healthcare, Piscataway, NJ). This process produces a population of vesicles of near uniform size (~100–150 nm diameter as measured by dynamic light scattering). A portion of the DOPC lipids before extrusion were aliquoted as a control.

Fluorescence polarization assays were performed using 50 nM BODIPY FL-labeled unmodified and boronated RNase A in black NBS 96-well plates (Corning Costar, Lowell, MA). Ribonucleases were incubated with DOPC liposomes (625 μM total lipid) or GD3 ganglioside-labeled liposomes (375 μM DOPC, 250 μM GD3 ganglioside = 625 μM total lipid) in 25 mM HEPES buffer, pH 7.0, containing NaCl (75 mM) in the absence or presence of D-fructose (10 mM). In control wells, ribonucleases were incubated with non-extruded DOPC lipids. Fluorescence polarization at 470/535 nm with a *G*-factor of 1.257 was recorded after shaking the plate briefly and incubating at ambient temperature for 1 h. Control well polarization was subtracted from experimental well polarization for each ribonuclease. The assay was performed in triplicate.

The affinity of boronated RNase A for GD3 ganglioside-labeled liposomes was assessed by using serially diluted liposomes. GD3 ganglioside-labeled liposomes were serially diluted in 25 mM HEPES, pH 7.0, containing NaCl (75 mM) with dilutions of 62.5 nM–1250 μM total lipid. Because the composition of these liposomes was 3:2 DOPC/GD3 ganglioside, this dilution resulted in solutions containing GD3 ganglioside at 25 nM–500 μM. Control DOPC liposomes (with no GD3 ganglioside) were likewise diluted in the same buffer, producing solutions of 62.5 nM–1250 μM total lipid. Liposomes were then incubated with 50 nM BODIPY FL-labeled boronated RNase A in the same buffer in a black NBS 96-well plate. Fluorescence polarization was recorded after shaking the plate briefly and incubating at ambient temperature for 35 min. Fluorescence polarization from GD3 ganglioside-labeled liposomes was subtracted from that of DOPC-only liposomes, thereby correcting for binding to DOPC and for changes in solution viscosity. The assay was performed in duplicate. The fraction of labeled ribonuclease bound for

each sample well was calculated by dividing its polarization from the polarization of ribonucleases incubated with the highest concentration of GD3 ganglioside (set at 100% bound). The value of K_d was calculated by plotting the fraction bound against the concentration of GD3 ganglioside and fitting the data to a binding isotherm.[231]

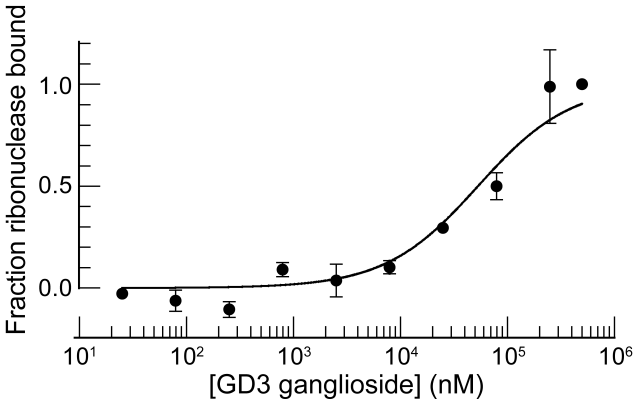

Figure 5.14 Fluorescence polarization data for the binding of boronated RNase A to GD3 ganglioside in liposomes. BODIPY FL-labeled boronated RNase A was incubated with liposomes containing GD3 ganglioside in 25 mM HEPES buffer, pH 7.0, containing NaCl (75 mM). Data points represent the mean (± SE) of duplicate experiments. Data were fitted to a binding isotherm[231] to give K_d = (53 ± 11) μM.

5.7.9 Cell Culture

Cell lines were obtained from American Type Culture Collection (Manassas, VA) and were maintained according to the recommended procedures. Cells were grown in a cell culture incubator at 37 °C under CO_2 (5% v/v) in flat-bottomed culture flasks. Cell medium was supplemented with GIBCO fetal bovine serum (FBS) (10% v/v), penicillin (100 units/mL), and

streptomycin (100 μg/mL) in the appropriate cellular medium as follows: Pro-5, MEM α + ribonucleosides + deoxyribonucleosides; Lec-2, MEM α – ribonucleosides – deoxyribonucleosides; and K562, RPMI 1640. Cells were counted by hemocytometry for dispensing into 12-well plates (Corning Costar, Lowell, MA) or 8-well chambered coverglass slides (Nuc Lab-Tek II, Thermo Scientific).

5.7.10 Flow Cytometry Assays

BODIPY-FL was excited with a 488 nm solid-state laser and the emission was collected with a 530/30 bandpass filter. To collect the most reproducible data, for every flow cytometry experiment, the sensitivity (voltage) of the photomultiplier tube was set for all data collections using mid-range Rainbow beads from Spherotech (Lake Forest, IL) to a predetermined fluorescence target value. At least 10,000 cellular events were acquired for each sample. Data were analyzed using FlowJo 8.1.3 (Treestar, Ashland, Oregon).

The day prior to an experiment, Pro-5 and Lec-2 cells were plated in 12-well plates at 1×10^5 cells/well. The day of the experiment, the appropriate amount of D-fructose was dissolved into the cellular medium to obtain a final D-fructose concentration of 250 mM, and the medium was passed through a 0.45-μm syringe filter from Whatman. Non–fructose-containing medium was filtered likewise. Stock solutions of fluorescently labeled ribonucleases were diluted into the cell culture to a final concentration of 5 μM. Ribonucleases were incubated with cells for 4 h. Then, the cells were rinsed with PBS (2×400 μL), removed from the cell culture plate with trypsin (400 μL, 0.05% (1×) with EDTA; Invitrogen, Carlsbad, California), placed in flow cytometry tubes containing 80 μL of FBS, and incubated on ice until analyzed by flow

cytometry. Final fluorescence values were divided by the percent fluorophore labeling of the ribonuclease to determine the corrected value of fluorescence. Experiments were run twice in triplicate.

5.7.11 Confocal Microscopy

Pro-5 cells were plated on Nunc Lab-tek II 8-well chambered coverglass 24 h before use and grown to 80% confluency. Cells were incubated with 5 μM BODIPY FL-labeled ribonucleases for 4 h. Cell nuclei were stained with Hoechst 33342 (Invitrogen, 2 μg/mL) for the final 15 min of incubation. Cells were then washed twice with PBS, suspended in PBS, and examined using a Nikon Eclipse C1 laser scanning confocal microscope.

5.7.12 Ribonucleolytic Activity Assays

The ribonucleolytic activities of RNase A, boronated RNase A, and inactivated, boronated RNase A were determined by quantifying their ability to cleave 6-FAM–dArUdAdA–6-TAMRA, as described previously.[232] Assays were carried out at ambient temperature in 2 mL of 0.10 M MES–NaOH buffer, pH 6.0, containing NaCl (0.10 M). Fluorescence data were fitted to the equation: $k_{cat}/K_M = (\Delta I/\Delta t) / (I_f - I_0)[E]$, in which $\Delta I/\Delta t$ is the initial reaction velocity, I_0 is the fluorescence intensity before addition of ribonuclease, I_f is the fluorescence intensity after complete substrate hydrolysis, and [E] is the total ribonuclease concentration. The assay was performed in triplicate.

5.7.13 Cell-Proliferation Assays

The effect of unmodified and boronated RNase A on the proliferation of K-562 cells was assayed as described previously.[233] For assays, 5 μL of a solution of ribonuclease or PBS (control) was added to 95 μL of cells (5.0×10^4 cells/mL). For co-treatment assays with D-fructose, ribonucleases were first serially diluted at 2× concentration, followed by addition of an equal volume of 2 M D-fructose in PBS to each ribonuclease dilution, resulting in a 1× ribonuclease dilution as before but now containing 1 M D-fructose. Then, 5 μL of each dilution was added to cells as above, including a control of PBS containing 1 M D-fructose. Because 5 μL of samples were added to 95 μL of cells, the final concentration of D-fructose in each well was 50 mM. After a 44-h incubation, K-562 cells were treated with [*methyl*-^{3}H]thymidine for 4 h, and the incorporation of radioactive thymidine into cellular DNA was quantitated by liquid scintillation counting. The results are shown as the percentage of [*methyl*-^{3}H]thymidine incorporated relative to control cells treated with PBS. Data are the average of three measurements for each concentration, and the entire experiment was repeated in triplicate. Values for IC_{50} were calculated by fitting the curves by nonlinear regression to the equation: $y = 100\% / (1 + 10^{(\log(IC_{50}) - \log[\text{ribonuclease}])h})$, in which y is the total DNA synthesis following the [*methyl*-^{3}H]thymidine pulse and h is the slope of the curve.

Chapter Six

Future Directions

6.1 Developing Sialic Acid Inhibitors for the Delivery of siRNAs

As described in Chapter Two, the anionic glycocalyx is a substantial barrier to the cellular uptake of oligonucleotides, including siRNAs. We postulated that inhibitors of the expression of GAGs or sialic acid should enhance siRNA delivery into mammalian cells. Methodologies for the development of O-linked glycosylation inhibitors and for inhibitors of sulfotransferases have already been developed.[234-237] Bertozzi and co-workers have developed several azide containing glycans that can be naturally incorporated into the cell surface of a mammalian cell. *N*-Azidoacetylmannosamine (ManAz) can be metabolized and incorporated into glycans where sialic acid normally resides.[238-240] This results in an azide-containing analogue of sialic acid being expressed on the cell surface, which can react with a strained alkyne to attach a fluorophore onto the cell surface.[238-240] This system can quantitate the level of sialic acid expression on a cell. Therefore, in a high throughput screen, one should be able to determine if a compound of interest is inhibiting ManAz incorporation. Any positive hits in the screen that truly are inhibitors of sialic acid expression should then be tested as enhancers of siRNA uptake as described in Chapter Two.

6.2 Expanding the Use of Ribonucleoside 3´ Phosphate Pro-moieties

The primary advantage of this prodrug strategy is its immense modularity. As described in Chapter Four, the rate of hydrolysis of this prodrug strategy is based upon the nucleobase attached to the ribose and RNase 1 can only hydrolyze prodrugs attached to pyrimidine

nucleotides. To expand upon the obtainable rates of hydrolysis for this system, pyrimidine nucleobase analogues will need to be tested. Upon development of a series of cleavable ribonucleotides, this system should allow for substantial modulation of the rate of activation of drugs.

As described in Chapter Three, RNase 1 can cleave aryloxy groups attached to the 3´ phosphate of a ribonucleotide and in Chapter Four we demonstrated that it can also cleave an alkoxy group. This system can be expanded even further with self-immolative linkers, which could liberate amine-containing therapeutics. Additionally, the 5´ hydroxyl group of the nucleotide can be modified for enhanced aqueous solubility or any other property one would want to impart on the prodrug.

Ultimately, an *in vivo* experiment is needed to assess the true viability of this pro-drug strategy. The ideal drug for an initial study would have substantial side effects and contain hydroxyl or amine functional groups to conjugate to a ribonucleotide 3´ phosphate. To date, doxorubicin is the best-known example of how a drug delivery system can significantly improve the therapeutic index of a drug. Doxorubicin is one of the most commonly used anticancer agents for hematological and solid tumors. Cardiomyopathy is the dose-limiting toxicity associated with doxorubicin use and approximately 2% of patients who receive a lifetime dose of 450-500mg/m^2 will experience this condition, which can lead to congestive heart failure and death.[241] However, by formulating doxorubicin in a polyethylene glycosylated liposome (Doxil), clinicians are now able to dose doxorubicin at significantly higher doses, simultaneously increasing the efficacy of doxorubicin while reducing cardiotoxicity.[242] Additionally,

doxorubicin contains both phenolic and alkoxy hydroxy groups and contains one free amine. Using protecting groups, synthesis of a ribonucleotide 3´-(doxorubicin phosphate) conjugate should be attainable. By comparing doxorubicin and Doxil to the ribonucleotide 3´-(doxorubicin phosphate) for treatment of a xenograft tumor in a mouse, the efficacy of ribonucleotide 3´ phosphates as a prodrug strategy can be determined.

6.3 Expanding the Use of Boronate-Mediated Biologic Delivery

We tested boronates for the delivery of two other proteins, lysozyme and albumin. The lysozyme-boronate conjugates had enhanced delivery compared to wild-type protein (data not shown), however, the albumin conjugate crashed out of solution (data not shown). We think the albumin conjugate self-oligomerized because the protein is covered in glycans. Therefore, there will be certain proteins that are amendable to boronate-mediated delivery and others that are not. Future studies should determine what types of proteins are amendable to this strategy.

Boronates with specificity to cancer specific glycans have been developed.[228] These types of moieties would make intriguing tumor targeting agents, but would have to be tested in a xenograft tumor mouse model to assess their efficacy. Additionally, by moving into an *in vivo* model, the efficacy as a general drug delivery reagent could be assessed. More specifically, the pharmacokinetics of boronated proteins would be very interesting to determine. From a charge perspective, benzoxaborole, which is anionic at pH 7.4, should either hinder the rate of clearance or not affect the parent protein's clearance rate.[225,226,243]

Appendix One

DNA-Mediated, Liposome–Cell Fusion

A1.1 Abstract

Adverse drug reactions are a leading cause of death in the United States. Consequently, there is significant interest in drug carrier systems designed to specifically deliver drugs to their site of action to reduce adverse side effects. Many drug delivery strategies have been proposed over the past 40 years, but to date, liposomes have been the most extensively studied.

Liposomes were once considered to be the most promising drug delivery vehicle due to their non-immunogenic properties, ability to easily encapsulate chemotherapeutic agents, and perceived capacity to directly fuse with cellular membranes. It was soon discovered that liposomes have two major shortcomings as a drug delivery vehicle: (i) they rely on the endocytic pathway to deliver their therapeutic contents to the cytoplasm and (ii) they confer only a small degree of specificity for particular cell types. Researchers have been trying to overcome these obstacles for over thirty years. To date, only two liposomal drug formulations, doxorubicin and amphotericin B, have gained widespread clinical use.

To overcome both of these limitations, we proposed a strategy inspired by SNARE (soluble *N*-ethylmaleimide-sensitive factor attachment protein receptor) protein-mediated vesicular fusion. Similar to the helical, coiled-coil SNARE complex, lipid-anchored, complementary oligonucleotides displayed on the surface of vesicles have been shown to form helices that mediate vesicle-to-vesicle fusion. By labeling cells with oligonucleotides, I attempted to adapt this technology to drive liposome–cell fusion, creating the first liposomal

system to directly deliver liposomal contents to the cytoplasm of a cell independent of the endocytic pathway.

A1.2 Author Contributions

R.T.R. proposed using DNA to fuse liposomes to cells. M.J.P. performed the research and drafted this chapter and figures. M.J.P. and R.T.R. designed experiments and analyzed data.

A1.3 Introduction

According to a recent meta-analysis, adverse drug reactions are estimated to be between the 4th and 6th leading cause of death in the United States.[244] More specifically, the cardiovascular system is most commonly affected. For the past decade, the most frequent cause for withdrawal of a drug off the market or severe restriction of use has been development of cardiotoxicity.[245] To date, doxorubicin is the best known example of how a drug delivery system can significantly improve the therapeutic index of a drug.[241,242] To significantly reduce adverse drug effects, it is paramount that specific and efficient drug delivery systems are developed. Many drug delivery strategies have been proposed over the past 40 years, but to date, liposomes have been the most extensively studied.

Early studies on cell–liposome interactions incorrectly concluded that vesicles passively fuse with the plasma membrane.[246] Further research elucidated that liposomes depend upon endocytosis for cytoplasmic delivery.[27,247-254] Therefore, encapsulated contents have three possible fates (Figure A1.1). Small molecules that exist as a neutral species along the endosomal pathway (pH 7.4–4.0) will reach the cytoplasm by passively diffusing out of the endocytic pathway (Figure A1.1-1).[255] Some liposome formulations destabilize lipid-bilayers in a mildly acidic environment, allowing for the escape of polar molecules (Figure A1.1-2).[256-264] Otherwise, liposomes and their contents are shuttled to the lysosome for degradation (Figure A1.1-3). All current liposomal technology relies on escape from the endocytic pathway in order to deliver encapsulated contents into cells. This project sought to develop novel liposomal technology that will drive vesicle-plasma membrane fusion and efficiently deliver liposomal contents directly to the interior of cells (Figure A1.1).

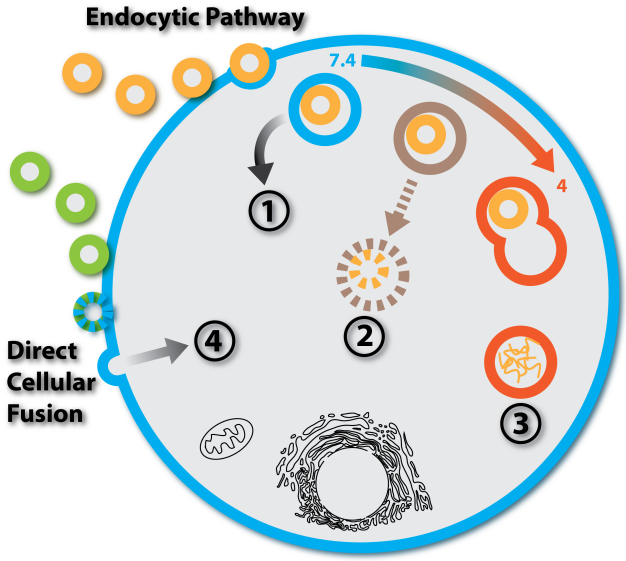

Figure A1.1 Mechanisms of Liposomal Delivery: Current liposomal technology relies on endocytosis. Therefore, encapsulated contents reach the cytoplasm by: **(1)** passive diffusion across the lipid bilayers or **(2)** destabilization of the liposome–endosome complex to allow content leakage. The third fate is **(3)** lysosomal degradation of the liposome and its contents. This proposal aims to develop liposomes that **(4)** directly fuse to the plasma membrane to deliver therapeutics, circumventing entirely the endocytic pathway.

We sought to premise our delivery strategy after SNARE (soluble N-ethylmaleimide-sensitive factor attachment protein receptor) proteins, which provide the driving force for fusion between secretory vesicles and the plasma membrane in eukaryotic cells. The coiling and transformation of the *trans*-SNARE complex to the *cis*-SNARE helix induces membrane fusion (Figure A1.2).[1] SNARE-mediated membrane fusion is the most tightly regulated, spatially accurate, and fastest (less than 1 ms) membrane fusion event occurring in mammalian cells.[265-267] SNAREs consist of three regions: the N terminal helical forming domain, linker domain, and the C terminal transmembrane domain.[1] The dynamic coiling of the helical region is believed to

drive membrane fusion since anchoring two membranes within close approximation is not sufficient for fusion.[1,268] Lengthening the linker domain abolishes fusion, and the structure of the linker domain is not significant.[269-271] Any anchor, lipid or protein, that spans both leaflets of the vesicle is sufficient for membrane fusion, whereas the target membrane anchor only needs to be hydrophobic enough to anchor a SNARE to the membrane.[268,272]

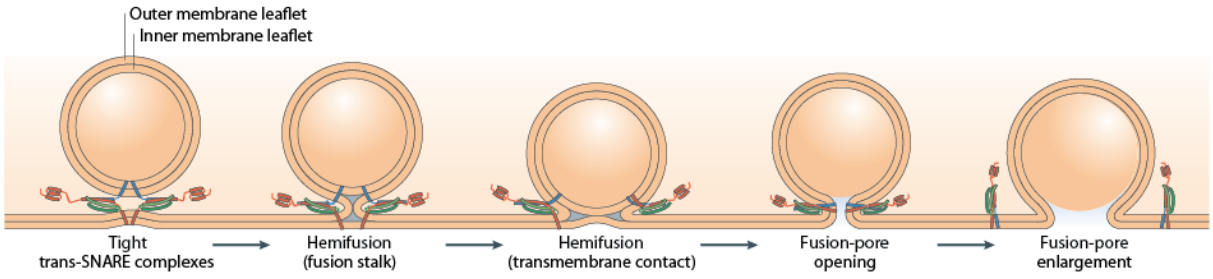

Figure A1.2 Proposed Transition States of SNARE-Mediated Membrane Fusion: The tight *trans*-SNARE complex perturbs the lipid bilayers, forcing the outer membrane leaflets to fuse (hemifusion). Then the inner membrane leaflets contact and fuse, initially creating a pore, which enlarges and allows full content mixing. The energetically favorable transformation from a *trans*-

Recently, oligonucleotide[2,273] and leucine zipper[274] helical formation was shown to induce SNARE-like membrane fusion *in vitro*. Of these systems, Boxer and coworkers achieved the greatest percentage of content mixing between liposomes using lipid–oligonucleotide conjugates to incorporate oligonucleotides into vesicular lipid bilayers. The poly-deoxyadenosine (dA)/deoxythymine (dT) complementary lipid–oligonucleotide pair induced significantly greater content mixing than any other pair tested, achieving ~15% liposomal content mixing after an

hour compared to ~0% for control liposomes (Figure A1.3).[2] These results demonstrate clearly the dramatic increase in membrane fusion events the poly-dA/dT lipid-oligonucleotide system can achieve relative to control liposomes. Based upon these *in vitro* studies, we hypothesized that oligonucleotide-labeled liposomes would efficiently and specifically fuse with cells bearing the complementary oligonucleotide.

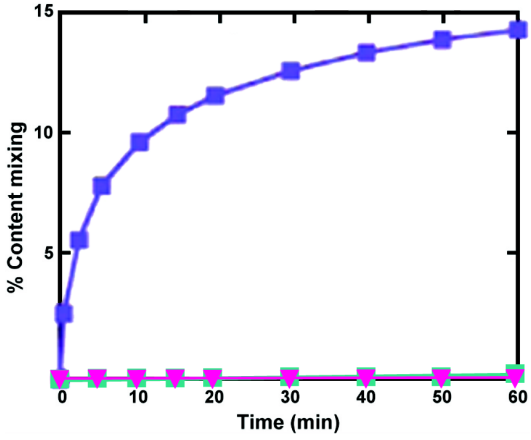

Figure A1.3 Content mixing of lipid-oligonucleotide driven vesicle–vesicle fusion: Content mixing between liposomes was measured by formation of the fluorescent $Tb^{+3}(DPA)^{-3}$ complex. Experiments consisted of liposomes labeled with: complementary 5′– and 3′–poly-dA/dT coupled DNA **(purple)**, complementary 5′–coupled DNA **(cyan)**, and noncomplementary 5′– and 3′–coupled DNA **(magenta)**. The no DNA liposome trial plot is obscured by the noncomplementary 5′– and 3′–coupled DNA plot. Figure was adapted from Chan *et al.*[2]

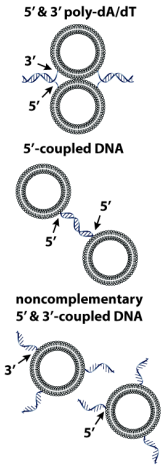

For the past 30 years, many developments in liposomal cancer chemotherapies have been aimed at specifically targeting liposomes to tumors. The antineoplastic drug doxorubicin was one of the first drugs formulated in a liposome.[275] Not only did this formulation reduce toxic cardiac side effects compared to doxorubicin alone, the liposomal formulation also passively enhanced tumor specificity.[242] Further study determined that liposomes, which are typically 50–100 nm in size, have increased biodistribution to tumors compared to normal tissues as tumors possess highly permeable vasculature (100–780 nm pores)[276] and no lymphatic drainage system.[277-279] Further tumor specificity has been achieved through labeling liposomes with

tumor-specific antibodies or ligands for receptors that are up-regulated in tumors.[280-289] However, the aforementioned liposomal strategies rely on endocytosis for drug delivery. Our system relied on anchoring to the lipid-bilayer of a cell with a lipid, therefore we sought lipid anchors that had a propensity to accumulate into a tissue of interest (tumors). We hypothesized that by using tumor targeting lipids, we could specifically label cancer cells with oligonucleotides and therefore our liposomal drug delivery system would have the potential to efficiently and specifically deliver therapeutics into these cells. Consequently, this would significantly increase the therapeutic index of current cancer chemotherapies.

We proposed to achieve tumor specificity by anchoring oligonucleotides to cancer-targeting lipids. In the 1960's, it was observed that tumors have a higher concentration of ether lipids than normal tissues.[290,291] Although the specific mechanism of accumulation is still unknown, antineoplastic C_{16}, C_{18}, and C_{22} alkylphosphocholine (APC) analogues have been shown to accumulate in tumor cell membranes.[292-294] More recently, structure-activity relationship studies on radioiodinated phosphoether lipids have revealed a novel lipid, NM-404, that upon intravenous injection specifically accumulates in the plasma membranes of tumors.[295] Preclinical trials in non-small-cell lung cancer patients revealed tumor uptake and prolonged retention.[295] NM-404 has been proven to accumulate in 47 different solid tumor types and is currently in clinical trials for adjunctive and/or curative treatment of non-small-cell lung cancer, pancreatic cancer, and primary or metastatic brain cancer.[296] NM-404 structurally consists of two components: the radio-iodide that allows for detection of NM-404's location in the body and an alkylphosphocholine that dictates specificity to neoplasms. The phenyl ring of NM-404 prevents S_N2 reactions that would displace the radio-iodide, but it is unclear if the phenyl ring or

phenyliodide also functions as a necessary component for tumor specificity. Additionally, it is unclear how important the phosphatidylcholine head group is for tumor specificity, therefore we proposed investigating the use of octadecanol as the lipid anchor in our primary studies for DNA-mediated, liposomal–cell fusion (Figure A1.4 for an overview of the proposed delivery system).

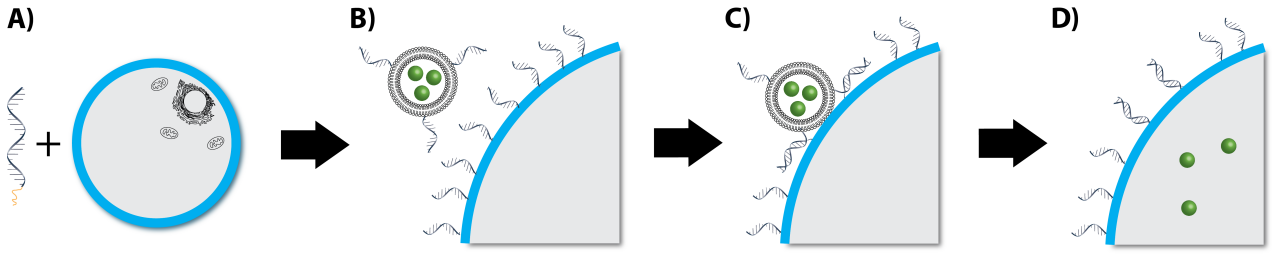

Figure A1.4 Overview of Proposed Delivery System: **A)** First, cells are labeled by incubating the cells with media containing the lipid–oligonucleotide conjugates (LOs) **B)** Then liposomes labeled with complementary DNA are added to the media **C)** Complementary DNA strands anneal, causing a SNARE-like liposome–cell fusion event **D)** And finally, liposomal contents are delivered directly to the cytoplasm of the cell

A1.4 Results and Discussion

Regardless of the conditions tried, delivery of calcein encapsulated liposomes only demonstrated punctate staining (Figure A1.5A). If robust cytoplasmic delivery were occurring, diffuse cytoplasmic staining should occur as seen with Calcein AM (Figure A1.5B). Unfortunately, there are several things that could be going wrong with this system.

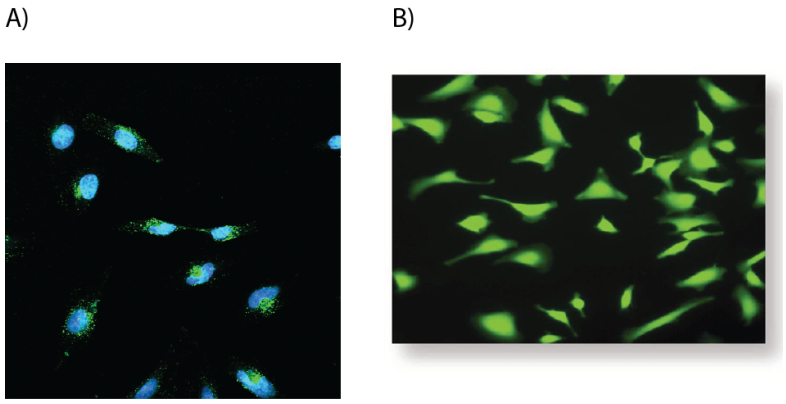

Figure A1.5 (A) Representative image of calcein delivery using this liposomal system. As seen, there is significant punctate staining (green) indicating the calcein is entrapped in endosomes. The nucleus is stained blue with Hoechst 33342 (Invitrogen; 2 μg/mL). (B) Hela cells treated with Calcein AM demonstrating robust cytoplasmic delivery of calcein into a cell. Image is from the Anaspec website.

As described in Chapter Two, LOs are substantially repelled from the cell surface and are in constant equilibrium with the cellular medium. Consequently, during these experiments, the LOs most likely came into equilibrium between being localized on the liposomes or on the cell surface and were able to hybridize with their complementary LO without driving a fusion event. Therefore, the first issue to troubleshoot is engineering a more stable LO by using more hydrophobic lipids and a LO that is not repelled from the cell surface. I found that even a LO with a 1,2-O- dioctadecyl-rac-glycerol lipid was not stably incorporated into the glycocalyx (Chapter Two), therefore elimination of the charge-charge repulsions of a LO with the glycocalyx is essential. This could be accomplished by synthesizing an oligonucleotide out of peptide nucleic acid monomers, which results in an oligonucleotide containing a peptide backbone as opposed to a phosphodiester ribonucleotide backbone.[297]

Upon resolving the LO stability on the cell surface issue, there are still several hurtles that need to be overcome in order for this system to function properly. In order for two membranes to fuse, the membranes need to be strained into a fusogenic orientation by the fusion machinery, where the only route for energy release is bilayer fusion (Figure A1.6).[298]

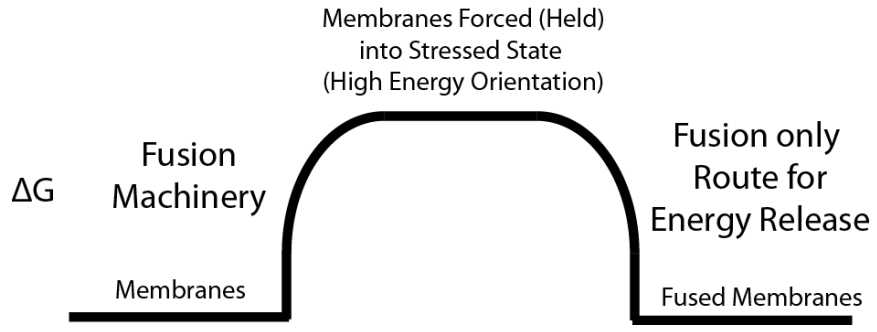

Figure A1.6 Example reaction coordinate of the membrane fusion process.

Due to the cellular glycocalyx, the system where one lipid-bilayer is the plasma membrane and the other lipid-bilayer is a liposome significantly complicates membrane fusion (Figure A1.7). Initially, the liposome must dock with the oligonucleotide that is anchored to the cell surface. It is unclear how far out from the cell surface the average glycocalyx reaches, therefore it is unclear how long the oligonucleotide needs to be to permit efficient docking. After the liposome anchored oligonucleotide initiates hybridization with the cell-anchored oligonucleotide, there are several requirements that need to be met for a successful fusion event to occur. In order of energy strength/forces, the force anchoring the oligonucleotide into the cell membrane has to be the largest/strongest force in the system. Otherwise the easiest route to

reducing strain in the system would be for the anchor of one oligonucleotide to flip out of the lipid-bilayer of one membrane and into the lipid-bilayer of the other membrane as depicted in Figure A1.7. The next strongest force required in the system would be the strength of hybridization. If the force required to "move" any glycans in the cell surface away from the interface of the liposome and plasma membrane is greater than the driving force of hybridization, then the system will get stuck in a hemi-hybridized state as depicted in Figure A1.7. So long as these forces are greater than the forces required to drag a liposome through the glycocalyx while not rupturing the liposome and move the glycans out of the way, the force required to dehydrate the space between membranes, and the force required to pucker the membranes, then successful fusion will occur.[298]

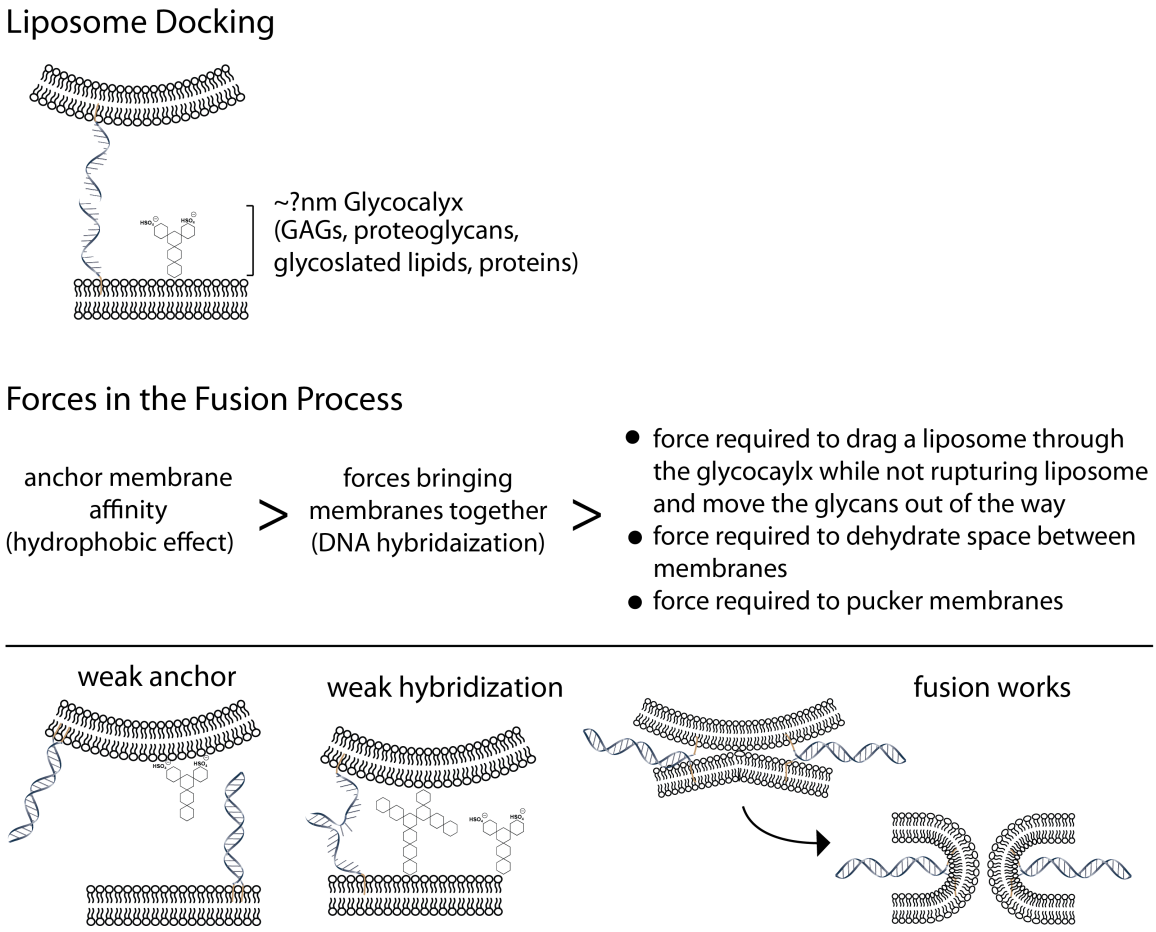

Figure A1.7 Steps of the liposomal fusion process using oligonucleotides. The first step is liposome docking, however it is unclear as to how long an oligonucleotide would have to be in order to span the glycocalyx and hybridize with its complementary oligonucleotide. Upon initiation of hybridization, in order for the fusion process to occur, there are several force requirements. Mainly, the anchor membrane affinity has to be greater than the force applied to the system by hybridization and the forces required for fusion of two lipid bilayers to occur.

A1.5 Conclusions

Rothman and co-workers demonstrated that two cells can be fused together by expressing SNAREs on the cell surface.[299] Therefore, the additional barriers to fusion that the glycocalyx imposes on this system can be surmounted, however, a great deal of engineering will be required to get this system to function fully.

A1.6 Materials and Methods

In order to have the most fusogenic liposomes possible that were also relatively stable, liposomes were made from 55% 1,2-dioleoyl-*sn*-glycero-3-phosphoethanolamine (DOPE), 30% 1,2-dioleoyl-sn-glycero-3-phosphocholine (DOPC), and 15% cholesterol. Lipids (Avanti Polar Lipids, Alabaster, Alabama) dissolved in chloroform were dispensed into a glass vial, dried with argon gas, and put under high vaccuum for one hour. Buffered solutions to be captured inside of liposomes contained solutions that were isotonic to mammalian physiological buffers (250-300 mOsM) to prevent rupture in cellular medium. Calcein containing liposomes were made in the following buffer: 80 mM NaCl, 20 mM Tris, 50 mM calcein, at pH 7.4. 1 mL of this buffer was added to the dried lipids, making a 4 mM total lipid solution, and mixed by vortex for 2 min. Then the lipid solution was freeze/thawed five times by switching the glass tube between a solution of ethanol in dry ice and a 30º C water bath. This process enhances encapsulation of calcein into liposomes. Then the solution was incubated for 30 min in the water bath. Finally, the solution was extruded through an Avanti Mini Extruder with 0.1 μm polycarbonate filter a total of 19 times. Then a LO was added to the solution to achieve approximately a 100:1 LO:vesicle ratio. This solution was incubated overnight at 4º C. Liposome size were confirmed by dynamic

light scattering in the bioinformatics instrumentation facility. Then the liposomes were purified over a 10 mL CL-4B column. The calcein encapsulated, LO labeled liposomes came off the column as an amber solution. The first few 0.5 mL fractions off the column were collected as the most pure fractions of liposomes. Concentrations of lipids in the final solutions were determined by the phosphorous assay. Liposomes were kept at 4º C in an aluminum foil covered vial until use.

Hela cells were plated (6×10^4 cells/well) into 8 chamber glass slides as described in Chapter Two. These cells were labeled with the complementary LO as described in Chapter Two and incubated with various concentrations (1x, 10x, and 100x) of LO labeled, calcein-encapsulated liposomes for either 15 min, 1 h, or 3 h. Cells were assessed for cytoplasmic calcein delivery by confocal microscopy.

Appendix Two

A Potent, Versatile Disulfide-Reducing Agent from Aspartic Acid*

* This chapter has been published in part, under the same title. Reference: Lukesh, J.C., Palte, M.J., & Raines, R.T. A potent, versatile disulfide-reducing agent from aspartic acid. *J. Am. Chem. Soc.*134, 4057-4059 (2012).

Additionally, of note was that this work was featured in Chemical & Engineering News: A Better Disulfide Reducing Agent. 2012 Feb 29.

A2.1 Abstract

Dithiothreitol (DTT) is the standard reagent for reducing disulfide bonds between and within biological molecules. At neutral pH, however, >99% of DTT thiol groups are protonated and thus unreactive. Herein, we report on (2*S*)-2-amino-1,4-dimercaptobutane (dithiobutylamine or DTBA), a dithiol that can be synthesized from L-aspartic acid in a few high-yielding steps that are amenable to a large-scale process. DTBA has thiol pK_a values that are ~1 unit lower than those of DTT and forms a disulfide with a similar $E°'$ value. DTBA reduces disulfide bonds in both small molecules and proteins faster than does DTT. The amino group of DTBA enables its isolation by cation-exchange and facilitates its conjugation. These attributes indicate that DTBA is a superior reagent for reducing disulfide bonds in aqueous solution.

A2.2 Author Contributions

M.J.P. established protocols for enzyme assays and taught J.C.L. how to do and analyze enzyme kinetics. M.J.P. assisted with the separation of DTBA using an ion-exchange resin.

J.C.L. performed all other research and drafted the original manuscript and figures. J.C.L., M.J.P., and R.T.R. planed experiments, analyzed data, and edited the manuscript and figures.

A2.3 Introduction

Approximately 20% of human proteins are predicted to contain disulfide bonds between cysteine residues. Small-molecule thiols can reduce these (and other) disulfide bonds, thereby modulating biomolecular function.[300-311] The reaction mechanism involves thiol–disulfide interchange initiated by a thiolate.[312-319] The ensuing mixed disulfide can become trapped if the reagent is a monothiol, such as β-mercaptoethanol (βME).[139] To overcome this problem, Cleland developed racemic (2*S*,3*S*)-1,4-dimercaptobutane-2,3-diol (dithiothreitol or DTT; Table A2.1), a dithiol that resolves a mixed disulfide by forming a six-membered ring.[2a,] DTT is a potent reducing agent ($E°'$ –0.327 V),[306] and has been the preferred reagent for the quantitative reduction of disulfide bonds for decades, despite its high cost.[168,320]

At physiological pH, DTT is a sluggish reducing agent. The reactivity of a dithiol is governed by the lower of its two thiol pK_a values.[2,3] With its lower thiol pK_a value being 9.2 (Table A2.1), <1% of DTT resides in a reactive thiolate form at pH 7.0.[161]

A2.4 Results and Discussion

We sought to develop a non-racemic dithiol with low thiol pK_a and disulfide $E°'$. Moreover, we sought a reagent that could be accessed in high yield from an inexpensive source. We envisioned that (2*S*)-2-amino-1,4-dimercaptobutane (dithiobutylamine or DTBA; Table A2.1) could fulfill our physicochemical criteria, and be synthesized from L-aspartic acid, which is an abundant amino acid.[321] We accessed DTBA *via* the two routes depicted in Scheme A2.1. A five-step route commenced with the esterification of the amino acid and protection of its amino group. Reduction with lithium aluminum hydride yielded a diol, which

was subjected to Mitsunobu conditions to install the requisite sulfur functionality.[322] Deprotection gave DTBA as its HCl salt in 99% purity and an overall yield of 60%. A six-step route that avoids generation of triphenylphosphine oxide, a recalcitrant byproduct of the Mitsunobu reaction,[322] provided DTBA·HCl in an overall yield of 56%. In both routes, the product of every step is a white solid.

Table A2.1 Physical properties of disulfide-reducing agents.

	Thiol pK_a	Disulfide Reduction Potential ($E°'$)
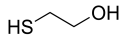 **βME**	9.61 [a]	–0.196 V [b]
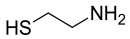 **cysteamine**	8.37 [c]	–0.203 V [b]
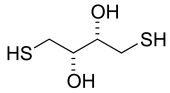 **DTT** (racemate)	9.2 (10.1) [d]	–0.327 V [e]
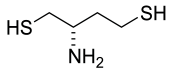 **DTBA**	8.2 ± 0.2 (9.3 ± 0.1) [f]	(–0.317 ± 0.002) V [f]

[a] Value is from ref. [323]. [b] Values are from ref. [314]. [c] Value is from ref. [324]. [d] Values are from ref. [312]. [e] Value is from ref. [325]. [f] Values are the mean ± SE from this work.

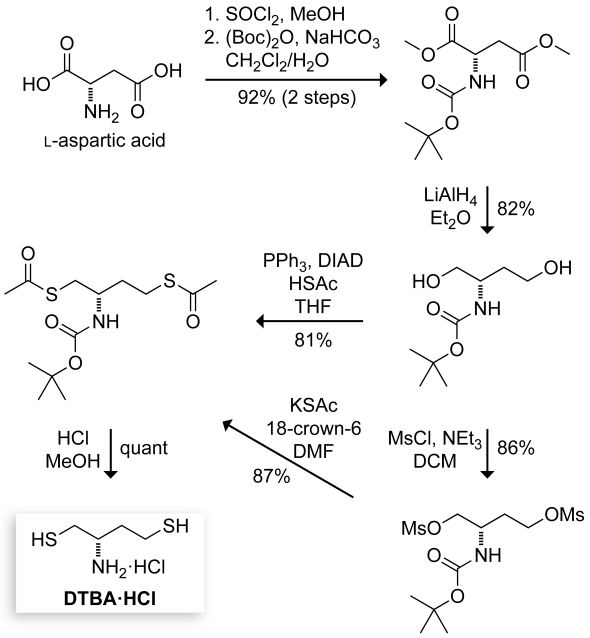

Scheme A2.1 Synthesis of DTBA

DTBA has desirable physicochemical attributes. Its HCl salt is a nearly odorless white solid with high solubility in water. Using a pH-titration monitored by ultraviolet spectroscopy,[326,327] we determined the thiol pK_a values of DTBA be 8.2 ± 0.2 and 9.3 ± 0.1 (Figure S1; Table 1).[166] These values are ~1 unit lower than those of DTT. This difference is comparable to that between cysteamine and βME, and likely results from the strong Coulombic and inductive effects of the protonated amino group. By equilibrating reduced DTBA with oxidized DTT and using HPLC to quantify reduced and oxidized species, we found the reduction potential of oxidized DTBA to be $E^{\circ\prime}$ = (–0.317 ± 0.002) V (Figure S2; Table 1). This $E^{\circ\prime}$ value is slightly less than that of DTT, consistent with more acidic thiols forming less stable disulfide bonds and with the preorganization of DTT for disulfide-bond formation by its hydroxyl groups, which can form an intramolecular hydrogen bone and manifest a *gauche* effect.

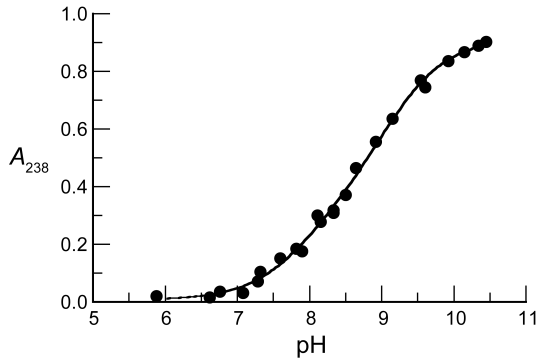

Figure A2.1 Effect of pH on absorbance at 238 nm of DTBA (0.10 mM) in 0.10 M potassium phosphate buffer. Fitting the data to eq 1 yielded pK_a values of 8.2 ± 0.2 and 9.3 ± 0.1, and extinction coefficients of $\varepsilon^{S^-}_{S^-}$ = 83.17 $M^{-1}cm^{-1}$, $\varepsilon^{S^-}_{SH}$ = 3436 $M^{-1}cm^{-1}$, and $\varepsilon^{S^-}_{S^-}$ = $M^{-1}cm^{-1}$ with r^2 > 0.99.

DTBA is an efficacious reducing agent for disulfide bonds in small molecules. We found that DTBA reduces the disulfide bond in oxidized βME 3.5-fold faster than does DTT at pH 7.0, and 4.4-fold faster at pH 5.5 (Figure A2.1A). These rate accelerations are commensurate with the lower thiol pK_a of DTBA. At pH 7.0, DTBA reduces oxidized L-glutathione 5.2-fold more rapidly than does DTT (Figure A1.1B). As oxidized L-glutathione has a net charge of –2 near neutral pH, a favorable Coulombic interaction could contribute to this higher rate acceleration.

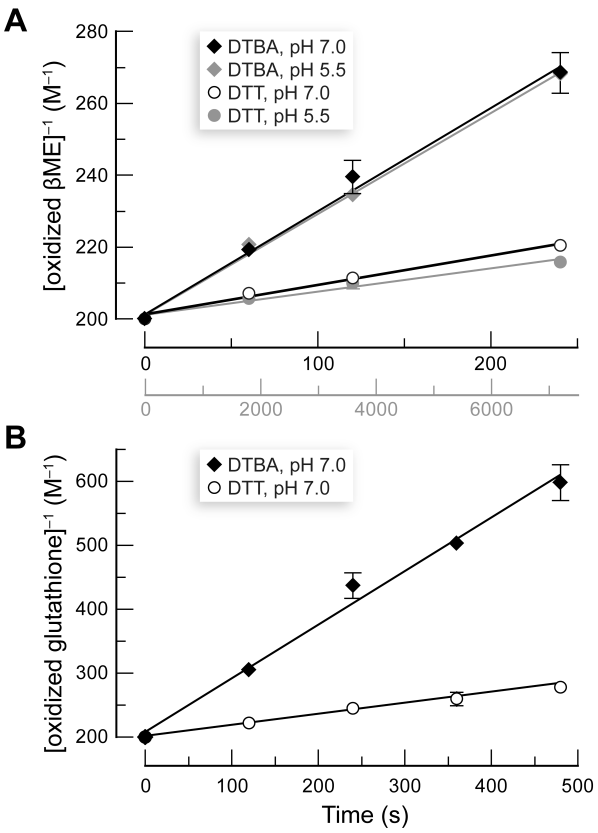

Figure A2.2 Time-course for the reduction of a mixed disulfide in small molecules by DTBA and DTT in 50 mM potassium phosphate buffer. **A.** Reduction of oxidized βME; $k_{obs}^{DTBA}/k_{obs}^{DTT} = 3.5$ at pH 7.0; $k_{obs}^{DTBA}/k_{obs}^{DTT} = 4.4$ at pH 5.5. **B.** Reduction of oxidized L-glutathione; $k_{obs}^{DTBA}/k_{obs}^{DTT} = 5.2$ at pH 7.0.

DTBA is also an efficacious reducing agent for disulfide bonds in proteins. A cysteine residue resides within the active site of papain (Cys25) and near that of creatine kinase (Cys283). Forming a mixed disulfide with that cysteine residue is known to eliminate their enzymatic activities.[311,328,329] These two enzymes differ, however, in the electrostatic environment of their active sites. The active site of papain is hydrophobic like its substrates, though there is an anionic region nearby (Figure 2.3A).[330,331] In contrast, the active site of creatine kinase is cationic,

complementary to its anionic substrates (Figure 2.3B).[332-335] We found that DTBA reduces a disulfide bond in the hydrophobic/anionic active site of papain 14-fold faster than does DTT (Figure 2.3A). In contrast, the two reagents reduce a disulfide bond near the cationic active site of creatine kinase at a similar rate.

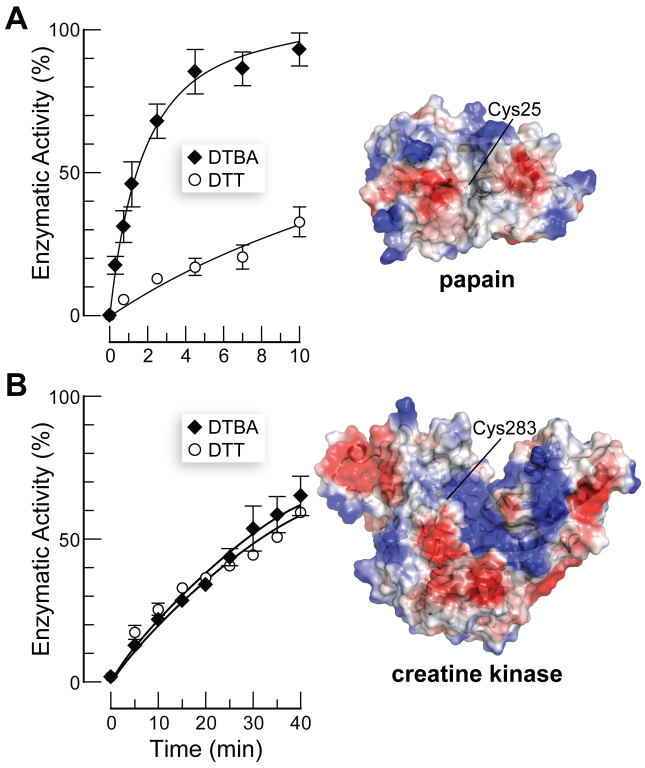

Figure A2.3 Time-course for the reduction of a mixed disulfide in enzymic active sites by DTBA and DTT in 0.10 M imidazole–HCl buffer, pH 7.0, containing EDTA (2 mM). **A.** Reduction of papain-Cys35–S–S–CH_3; $k_{obs}^{DTBA}/k_{obs}^{DTT}$ = 14. **B.** Reduction of creatine kinase-Cys283–S–S–L-glutathione; $k_{obs}^{DTBA}/k_{obs}^{DTT}$ = 1.1. Insets: Electrostatic potential maps with red = anionic and blue = cationic, as generated by the program PyMOL (Schrödinger, Portland, OR) using PDB entries 1ppn[331] and 2crk.[335]

A2.5 Conclusions

The amino group of DTBA confers additional benefits. For example, a disulfide-reducing agent that can be readily isolated, regenerated, and reused incurs less cost and generates less waste.[336-338] Moreover, extraneous disulfide bonds absorb light at 280 nm, which can confound standard measurements of protein concentration. We reasoned that DTBA could be isolated by its adsorption to a cation-exchange resin. Indeed, >99% of DTBA (but <1% of DTT) was removed from sodium phosphate buffer, pH 8.0, upon addition of Dowex® 50 resin (see: Supporting Information). We also note that the amino group of DTBA enables its covalent attachment to a soluble molecule, resin, or surface by simple reactions, such as reductive amination (which preserves the cationic charge) or *N*-acylation. We conclude that the attributes of DTBA could enable it to supplant DTT as the preferred reagent for reducing disulfide bonds in biomolecules.

A2.6 Acknowledgements

We are grateful to Professor W. W. Cleland and S. B. Johnston for enabling advice, and to N. McElfresh for preliminary work on this project. M.J.P. was supported by Molecular and Cellular Pharmacology Training Grant T32 GM008600 (NIH) and predoctoral fellowship 09PRE2260125 (American Heart Association). This work was supported by Grant R01 GM044783 (NIH).

A2.7 Materials and Methods

A2.7.1 General.

Commercial reagents were used without further purification. Dithiothreitol (DTT) was from Research Products International (Mt. Prospect, IL). Bis(2-mercaptoethyl)sulfone (BMS) was from Santa Cruz Biotechnology (Santa Cruz, CA). Papain (lyophilized powder from papaya latex), creatine kinase (lyophilized powder from rabbit muscle), hexokinase (lyophilized powder from *Saccharomyces cerevisiae*), glucose-6-phosphate dehydrogenase (ammonium sulfate suspension from baker's yeast), N_{α}-benzoyl-L-arginine-4-nitroanilide hydrochloride, (*S*)-methyl methanethiosulfonate (Kenyon's reagent), *trans*-4,5-dihydroxy-1,2-dithiane (oxidized DTT), oxidized L-glutathione, oxidized 2-mercaptoethanol, and DOWEX 50WX4-400 ion-exchange resin were from Sigma Chemical (St. Louis, MO). Bis(2-mercaptoethyl) sulfone disulfide (oxidized BMS) was synthesized as reported previously.[306]

All glassware was oven or flame-dried, and reactions were performed under N_2(g) unless stated otherwise. Dichloromethane, diethyl ether, and tetrahydrofuran were dried over a column of alumina. Dimethylformamide and triethylamine were dried over a column of alumina and purified further by passage through an isocyanate scrubbing column. Flash chromatography was performed with columns of 40–63 Å silica, 230–400 mesh (Silicycle, Québec City, Canada). Thin-layer chromatography (TLC) was performed on plates of EMD 250-μm silica 60-F_{254}. The term "concentrated under reduced pressure" refers to the removal of solvents and other volatile materials using a rotary evaporator at water aspirator pressure (<20 torr) while maintaining the water-bath temperature below 40 °C. Residual solvent was removed from samples at high vacuum (<0.1 torr). The term "high vacuum" refers to vacuum achieved by a mechanical belt-

drive oil pump. ^{1}H NMR spectra were acquired at ambient temperature with a Bruker DMX-400 Avance spectrometer at the National Magnetic Resonance Facility at Madison (NMRFAM) and referenced to TMS or residual protic solvent. ^{13}C NMR spectra were acquired with a Varian MercuryPlus 300 and referenced to residual protic solvent. Electrospray ionization (ESI) mass spectrometry was performed with a Micromass LCT at the Mass Spectrometry Facility in the Department of Chemistry at the University of Wisconsin–Madison. Ellman's assay for sulfhydryl groups was performed with a Varian Cary 50 Bio UV–Vis spectrophotometer. UV absorbance spectra of oxidized DTBA and oxidized DTT were acquired with a Varian Cary 300 Bio UV–Vis spectrophotometer. Thiol pK_a values were determined by using a Varian Cary 50 Bio UV–Vis spectrophotometer. Equilibrium, reduction potential, and kinetic studies on peptides and small molecules were performed on an analytical HPLC (Waters system equipped with a Waters 996 photodiode array detector, Empower 2 software and a Varian C18 reverse phase column). Kinetic studies on proteins were carried out using a Varian Cary 300 Bio UV–Vis spectrometer with a Cary temperature controller.

A2.7.2 Chemical Syntheses.

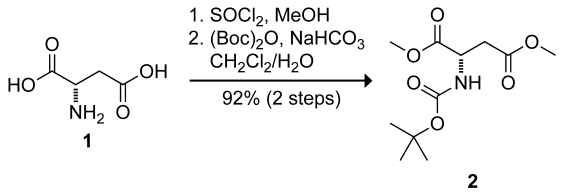

1 **2**

L-Aspartic acid (**1**; 5.002 g, 37.58 mmol) was added to an oven-dried round-bottom flask and placed under an atmosphere of dry N_2(g). The starting material was then dissolved partially with 60 mL of anhydrous methanol, and the mixture was cooled to 0 °C. Once the desired temperature was reached, thionyl chloride (8.2 mL, 110 mmol) was added drop-wise. After the

addition was complete, the reaction mixture became homogenous, and was warmed slowly to room temperature and left to stir for 14 h. The reaction mixture was then concentrated under reduced pressure, and the resulting diester was dissolved in 150 mL of DCM and 100 mL of water. To this biphasic solution was added sodium bicarbonate (4.212 g, 50.14 mmol) and di-*t*-butyl dicarbonate (9.841 g, 45.09 mmol), and the reaction mixture was heated at reflux for 4 h. After the reaction was confirmed to be complete by TLC, the reaction mixture was allowed to cool to room temperature. The organic layer was separated, and the aqueous layer was extracted three times with 150 mL of DCM. The organic extracts were combined, washed with 250 mL of saturated NaCl(aq), dried over $MgSO_4$(s), and concentrated under reduced pressure. Flash chromatography (35% v/v ethyl acetate in hexanes) was used to isolate **2** as a white solid (9.080 g, 92%, 2 steps).

^{1}H NMR (400 MHz, $CDCl_3$) δ = 5.49 (d, J = 8.3 Hz, 1H), 4.60–4.57 (m, 1H), 3.76 (s, 3H), 3.70 (s, 3H), 3.01 (dd, J = 17, 4.4 Hz, 1H), 2.83 (dd, J = 17.0, 4.7), 1.45 (s, 9H); **^{13}C NMR (75 MHz, $CDCl_3$)** δ = 171.6, 171.5, 155.5, 80.3, 52.8, 52.1, 50.0, 36.8, 28.4; **HRMS** (ESI) calculated for $[C_{11}H_{19}NO_6Na]^+$ (M+Na^+) requires m/z = 284.1105, found 284.1113.

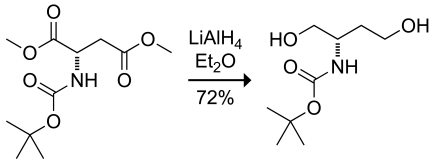

2 **3**

An oven-dried round-bottom flask was charged with lithium aluminum hydride (0.870 g, 22.9 mmol) and placed under an atmosphere of dry N_2(g). The flask was cooled to 0 °C in an ice

bath, and 100 mL of anhydrous diethyl ether was added. In a separate dry round-bottom flask, compound **2** (2.021 g, 7.735 mmol) was dissolved in 50 mL of anhydrous diethyl ether. Sonication was required to make the solution completely homogenous. The ester was then added drop-wise to the reaction mixture. Once the addition was complete, the reaction mixture was stirred at 0 °C for an additional 30 min, warmed to room temperature, and allowed to react for an additional 2 h. Subsequently, the reaction mixture was quenched at 0 °C by the slow, sequential addition of 0.87 mL of water, 0.87 mL of 15% w/w NaOH, and 2.6 mL of water. The mixture was left to stir at room temperature for 1 h. The aluminum salts were collected by vacuum filtration, and subjected to continuous solid–liquid extractions with dichloromethane using a Soxhlet apparatus. The organic extracts and the original organic filtrate were combined and concentrated under reduced pressure. Flash chromatography (ethyl acetate) was used to isolate **3** as a white solid (1.310 g, 82%). Compound **3** had been prepared from L-aspartic acid by a different route.[339]

^{1}H NMR (400 MHz, DMSO-d_6) δ = 6.46 (d, J = 8.8 Hz, 1H), 4.56 (t, J = 5.7 Hz, 1H), 4.34 (t, J = 5.1 Hz, 1H), 3.46–3.37 (m, 3H), 3.32 (dt, J = 10.6, 5.4 Hz, 1H), 3.23 (dt, J = 10.6, 5.9 Hz, 1H), 1.69–1.61 (m, 1H), 1.45–1.37 (m, 1H), 1.37 (s, 9H); **^{13}C NMR (75 MHz, $CDCl_3$)** δ = 157.2, 80.1, 65.4, 58.9, 49.5, 35.0, 28.5; **HRMS** (ESI) calculated for $[C_9H_{19}NO_4Na]^+$ ($M+Na^+$) requires m/z = 228.1207, found 228.1201.

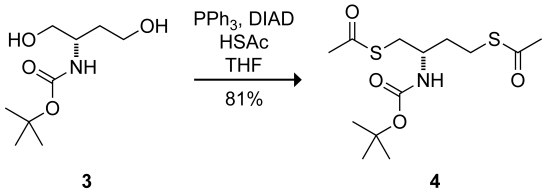

3 **4**

A dry round-bottom flask was charged with triphenylphosphine (1.711 g, 6.523 mmol) and placed under an atmosphere of dry N_2(g). Anhydrous THF (27 mL) was then added, and the solution was placed in an ice bath and cooled to 0 °C. Diisopropyl azodicarboxylate (1.3 mL, 6.6 mmol) was added drop-wise to the flask. Once the addition was complete, the reaction mixture was allowed to stir for an additional 20 min. Compound **3** (0.559 g, 2.72 mmol) in 10 mL of dry THF and thioacetic acid (0.47 mL, 6.6 mmol) was then added with stirring. The reaction mixture was stirred at 0 °C for 1 h, and then at room temperature for 16 h. (Longer reaction times resulted in lower yields.) The mixture was concentrated under reduced pressure. Flash chromatography (30% v/v ethyl acetate in hexanes) was used to isolate **4** as a white solid (0.711 g, 81%). Compound **4** had been prepared from L-aspartic acid by a different route.[339]

^{1}H NMR (400 MHz, $CDCl_3$) δ = 4.59 (d, J = 7.9 Hz, 1H), 3.85–3.76 (m, 1H), 3.12–2.95 (m, 3H), 2.82 (ddd, J = 13.7, 8.5, 7.1 Hz, 1H), 2.36 (s, 3H), 2.33 (s, 3H), 1.84–1.75 (m, 1H), 1.74–1.64 (m, 1H), 1.44 (s, 9H); **^{13}C NMR (75 MHz, $CDCl_3$)** δ = 195.9, 195.6, 155.6, 79.7, 50.1, 34.5, 33.8, 30.73, 30.71, 28.5, 25.9; **HRMS** (ESI) calculated for $[C_{13}H_{23}NO_4S_2Na]^+$ (M+Na^+) requires m/z = 344.0961, found 344.0962.

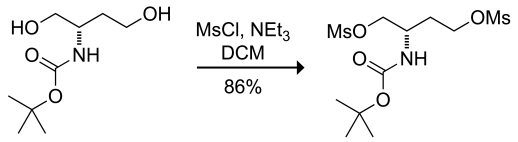

3 6

A dry round-bottom flask was charged with **3** (1.178 g, 5.739 mmol) and placed under dry N_2(g), Anhydrous DCM (125 mL) was then added, and the solution was cooled to 0 °C. Triethylamine (4.0 mL, 29 mmol) was added, followed by slow drop-wise addition of methanesulfonyl chloride (MsCl) (1.0 mL, 13 mmol). After stirring at 0 °C for 30 min, the reaction mixture was allowed to warm slowly to room temperature and left to react for an additional 30 min. The reaction mixture was quenched by the addition 100 mL of water, and extracted with DCM. The combined organic extracts were washed with brine, dried over $MgSO_4$(s), and concentrated under reduced pressure. Flash chromatography (60% v/v ethyl acetate in hexanes) was used to isolate **6** as a white solid (1.782 g, 86%).

^{1}H NMR (400 MHz, $CDCl_3$) δ = 4.81 (d, J = 9.7 Hz, 1H), 4.39–4.26 (m, 4H), 4.10–4.05 (m, 1H), 3.06 (s, 3H), 3.05 (s, 3H), 2.13–1.96 (m, 2H), 1.48 (s, 9H); **^{13}C NMR (75 MHz, $CDCl_3$)** δ = 155.4, 80.6, 71.0, 66.3, 47.0, 37.7, 37.6, 31.2, 28.5; **HRMS** (ESI) calculated for $[C_{11}H_{23}NO_8S_2Na]^+$ (M+Na^+) requires m/z = 384.0758, found 384.0775.

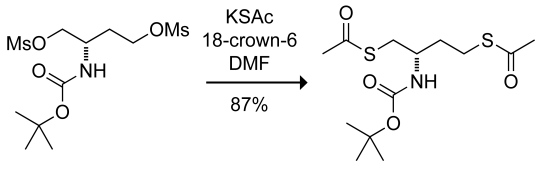

6 4

Compound **6** (0.610 g, 1.688 mmol), potassium thioacetate (0.482 g, 4.22 mmol), and 18-crown-6 (1.351 g, 5.111 mmol) were added to a dry round-bottom flask and dissolved with 150 mL of anhydrous DMF. The reaction mixture was stirred under under dry N_2(g) for 24 h. The DMF was removed under reduced pressure. Flash chromatography (30% v/v ethyl acetate in hexanes) was used to isolate **4** as a white solid (0.475 g, 87%). Compound **4** had been prepared from L-aspartic acid by a different route.[339]

^{1}H NMR (400 MHz, $CDCl_3$) δ = 4.59 (d, J = 7.9 Hz, 1H), 3.85–3.76 (m, 1H), 3.12–2.95 (m, 3H), 2.82 (ddd, J = 13.7, 8.5, 7.1 Hz, 1H), 2.36 (s, 3H), 2.33 (s, 3H), 1.84–1.75 (m, 1H), 1.74–1.64 (m, 1H), 1.44 (s, 9H); **^{13}C NMR (75 MHz, $CDCl_3$)** δ = 195.9, 195.6, 155.6, 79.7, 50.1, 34.5, 33.8, 30.73, 30.71, 28.5, 25.9; **HRMS** (ESI) calculated for $[C_{13}H_{23}NO_4S_2Na]^+$ ($M+Na^+$) requires m/z = 344.0961, found 344.0962.

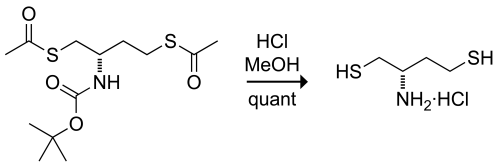

4 **5** (DTBA·HCl)

Compound **4** (0.601 g, 1.87 mmol) was added to a flame-dried round-bottom flask under dry N_2(g). Anhydrous methanol (20 mL) was added, followed by 10 mL of 3 N HCl in methanol. The reaction mixture was heated at reflux for 4 h, concentrated under reduced pressure, and stored *in vacuo* with P_2O_5 and KOH for 48 h.[301] (Scratching the bottom of the flask facilitated crystal formation.) Compound **5** (DTBA·HCl) was rinsed with cold toluene, and isolated by

vacuum filtration as a white solid (0.320 g, quant). DTBA made in this manner was determined to be 99% pure according to Ellman's assay for sulfhydryl groups (*vide infra*).[340-342]

^{1}H NMR (400 MHz, DMSO-d_6) δ = 8.29 (s, 3H), 3.34–3.32 (m, 1 H), 2.96 (t, J = 8.7 Hz, 1H), 2.81–2.75 (m, 2H), 2.60–2.56 (m, 3H), 1.95–1.86 (m, 2H); **^{13}C NMR (75 MHz, DMSO-d_6)** δ = 51.2, 35.0, 26.0, 19.6; **HRMS** (ESI) calculated for $[C_4H_{12}NS_2]^+$ (M^+) requires m/z = 138.0406, found 138.0405.

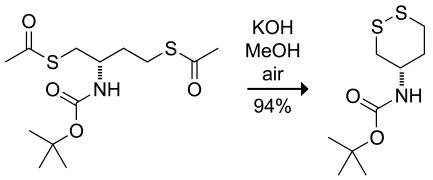

4 **7**

Compound **4** (0.482 g, 1.50 mmol) and potassium hydroxide (0.340 g, 6.06 mmol) were dissolved in 50 mL of methanol, and the resulting solution was stirred for 16 h while bubbling a light stream of air through the solution. The methanol was removed under reduced pressure, and the mixture was extracted with DCM, washed with brine, and dried over $MgSO_4$(s). Flash chromatography (20% v/v ethyl acetate in hexanes) was used to isolate **7** as a white solid (0.331 g, 94%).

^{1}H NMR (400 MHz, DMSO-d_6) δ = 7.08 (d, J = 7.9 Hz, 1H), 3.53–3.41 (m, 1H), 3.07–3.01 (m, 1H), 2.91–2.85 (m, 2H), 2.60 (dd, J = 13.0, 10.5 Hz, 1 H), 2.08–2.03 (m, 1H), 1.67–1.57 (m,

1H), 1.38 (s, 9H); **^{13}C NMR (75 MHz, DMSO-d_6)** δ = 155.2, 78.7, 49.3, 37.9, 34.9, 34.5, 28.9; **HRMS** (ESI) calculated for $[C_9H_{17}NO_2S_2]^+$ (M^+) requires m/z = 258.0593, found 258.0602.

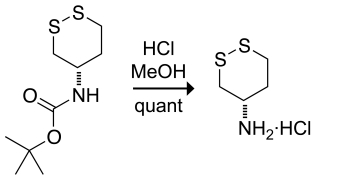

7 **8** (oxidized DTBA·HCl)

Compound **7** (0.402 g, 1.71 mmol) was added to a round-bottom flask. Anhydrous methanol (20 mL) was added, followed by 10 mL of 3 N HCl in methanol. The reaction mixture was heated at reflux for 4 h under N_2(g), concentrated under reduced pressure, and stored *in vacuo* with P_2O_5 and KOH for 24 h. (Scratching the bottom of the flask facilitated crystal formation.) Compound **8**, oxidized DTBA·HCl, was isolated as a white solid (0.289 g, quant).

^{1}H NMR (400 MHz, DMSO-d_6) δ = 8.29 (s, 3H), 3.43–3.37 (m, 1H), 3.15–3.08 (m, 2H), 3.02–2.96 (m, 1H), 2.88 (dd, J = 13.1, 10.6 Hz, 1H), 2.32–2.28 (m, 1H), 1.85–1.77 (m, 1H); **^{13}C NMR (75 MHz, DMSO-d_6)** δ = 48.7, 34.6, 32.8, 31.5; **HRMS** (ESI) calculated for $[C_4H_{10}NS_2]^+$ (M^+) requires m/z = 136.0250, found 136.0249.

A2.7.3 Purity of DTBA assessed by Ellman's assay for sulfhydryl groups.

A reaction buffer (0.10 M sodium phosphate buffer, pH 8.0, containing 1 mM EDTA) was prepared by the Pierce protocol. Ellman's reagent solution was primed by adding Ellman's reagent (4 mg) to 1 mL of the reaction buffer. A 2.50×10^{-4} M solution of DTBA was then prepared using the reaction buffer. Ellman's reagent solution (50 μL) was added to each of two

vials containing 2.5 mL of reaction buffer. Reaction buffer (250 μL) was added to one of these vials, and its absorbance at 412 nm was used as a blank. DTBA solution (250 μL) was added to the other vial. After 10 min, its absorbance at 412 nm was recorded. Using Beer's law ($c = A/(\varepsilon \cdot l)$ with $A = 0.623$, $l = 1$ cm, and $\varepsilon = 14{,}150\ M^{-1}cm^{-1}$) gave a thiol concentration of 4.40×10^{-5} M. Because DTBA contains two thiol groups, the assay solution had a DTBA concentration of 2.20×10^{-5} M. Accounting for dilution and using the equation $M_1 \cdot V_1 = M_2 \cdot V_2$, where $V_1 = 2.50 \times 10^{-4}$ L, $M_2 = 2.20 \times 10^{-5}$ M, and $V_2 = 2.8 \times 10^{-3}$ L, yielded $M_1 = 2.46 \times 10^{-4}$ M and thus a DTBA purity of $(2.46 \times 10^{-4}\ M)/(2.50 \times 10^{-4}\ M) \times 100\% = 98.4\%$. Three repetitions of this assay gave (99 ± 1)% purity. This assay revealed that commercial DTT and BMS had >98% purity.

A2.7.4 Determination of thiol pK_a values

The thiol pK_a values of DTBA were determined by measuring its absorbance at 238 nm in solutions of various pH. The deprotonated thiolate absorbs much more strongly at 238 nm than does its protonated counterpart.[327] This attribute was exploited for determining thiol pK_a values as described previously.[326] Buffered stock solutions of K_3PO_4, K_2HPO_4, and KH_2PO_4 (100 mM) were degassed and flushed with N_2(g) for 1 h immediately prior to use. A stock solution of DTBA (1.5 mM) in KH_2PO_4 was then prepared. Various combinations of the buffered stock solutions were combined in duplicate to give two identical sets of 1-mL solutions of pH 5.5–11. KH_2PO_4 stock solution (70 μL) was added to each replicate pair of solutions and used to set the A_{238} to zero. Dithiol solution (70 μL) was then added to its complementary 1-mL vial, and its absorbance at 238 nm was recorded. The pH of the solution was then immediately measured

using a Beckman pH meter, which had been calibrated prior to use with pH 7 and pH 10 standard solutions from Fisher Scientific. This process was repeated multiple times to obtain a plot of A_{238} *vs* pH (Figure A2.1).

pK_a values were determined by fitting the data in Figure A2.1 to eq 1,[326] which is derived from Beer's law and the definition of the acid dissociation constant.[326] In eq 1, C_T is total thiol concentration, ε_{SH}^{SH} is the extinction coefficient of the doubly protonated form, $\varepsilon_{SH}^{S^-}$ is the extinction coefficient of the singly protonated form, and $\varepsilon_{S^-}^{S^-}$ is the extinction coefficient of the unprotonated form. Both pK_a values and extinction coefficients were determined from the curve fit with the program Prism 5.0 (GraphPad Software, La Jolla, CA).

$$A_{238} = C_T \left(\frac{\varepsilon_{S^-}^{S^-} 10^{pH-pK_{a2}} + \varepsilon_{SH}^{S^-} + \varepsilon_{SH}^{SH} 10^{pK_{a1}-pH}}{10^{pH-pK_{a2}} + 1 + 10^{pK_{a1}-pH}} \right) \quad (1)$$

A2.7.5 Reduction potential of DTBA

The reduction potential ($E°'$) of DTBA was determined by using HPLC to determine the equilibrium constant for its reaction with oxidized DTT (eq 2), and then inserting this value into a variation of the Nernst equation (eq 3).[306] Data were obtained by a procedure similar to that described previously.[306,326] DTBA (10.5 mg, 0.06 mmol) and oxidized DTT (9.2 mg, 0.06 mmol) were added to a 25-mL round-bottom flask. The flask was then flushed with N_2(g) for 30 min.

$$K_{eq} = \frac{[\text{DTT}][\text{oxidized DTBA}]}{[\text{DTBA}][\text{oxidized DTT}]} = \frac{[\text{DTT}]^2}{[\text{oxidized DTT}]^2} \quad (2)$$

$$E_{\text{DTBA}}{}^{\circ\prime} = E_{\text{DTT}}{}^{\circ\prime} - \frac{RT}{nF} \ln \frac{[\text{DTT}]^2}{[\text{oxidized DTT}]^2} \quad (3)$$

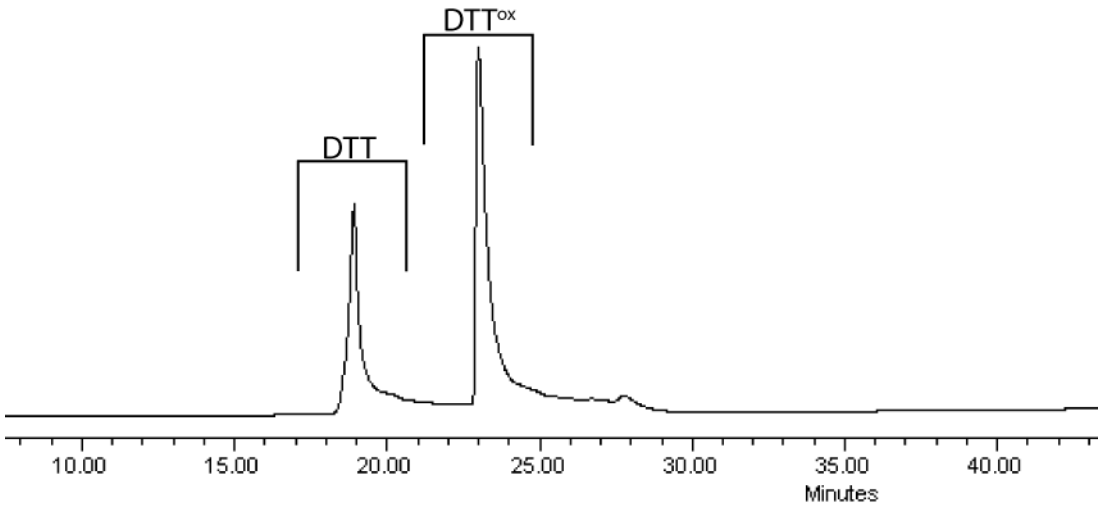

Figure A2.4 Representative HPLC chromatogram of the redox equilibrium between DTBA and DTT. Compounds were detected by their absorbance at 205 nm.

A 50 mM stock solution of potassium phosphate buffer (pH 7) was degassed and purged with N_2(g) for 30 min immediately prior to use. Buffer (15 mL) was added, and the reaction mixture was stirred under N_2(g) for 24 h at room temperature. The reaction mixture was then quenched by the addition of 3 N HCl (1:100 dilution). The reaction mixture was passed through a 4.5-μm filter, and 100 μL of the reaction mixture was analyzed immediately by HPLC using a Waters system equipped with a Waters 996 photodiode array detector, Empower 2 software, and a Varian C18 reverse-phase column. The column was eluted at 1.0 mL/min with water (5.0 mL),

followed by a linear gradient (0–40% v/v) of acetonitrile/water over 40 min. Compounds were detected by their absorbance at 205 nm. Reduced and oxidized DTBA are highly polar and elute from the column immediately (as confirmed by LC–MS). Two peaks, however, were clearly visible in the chromatogram (Figure A2.4). HPLC analysis of standards revealed that the two peaks were reduced DTT (retention time: 19 min) and oxidized DTT (retention time: 23 min). Calibration curves were generated and found to be linear over the used concentration range. From these curves, the equilibrium concentrations of reduced and oxidized DTT were determined, and a $K_{eq} = 0.469 \pm 0.131$ for the reaction was found. Assuming that DTT has $E°' =$ –0.327 V,[301] eq 3 (which is a variation of the Nernst equation) was used to calculate that DTBA has $E°' = -(0.317 \pm 0.002)$ V. This value is the mean ± SE from seven experiments. The reverse reaction between oxidized DTBA and reduced DTT revealed that equilibrium had been established under the experimental conditions.

A2.7.6 Reduction potential of BMS

The procedure described in Section V was also performed with BMS. With $K_{eq} = 0.0517 \pm 0.0194$ and assuming $E°' = -0.327$ V for DTT,[301] BMS was found to have $E°' = (-0.291 \pm 0.002)$ V, which was again the mean ± SE from seven experiments. The reduction potential for BMS was reported previously to be $E°' = -0.31$ V.[306]

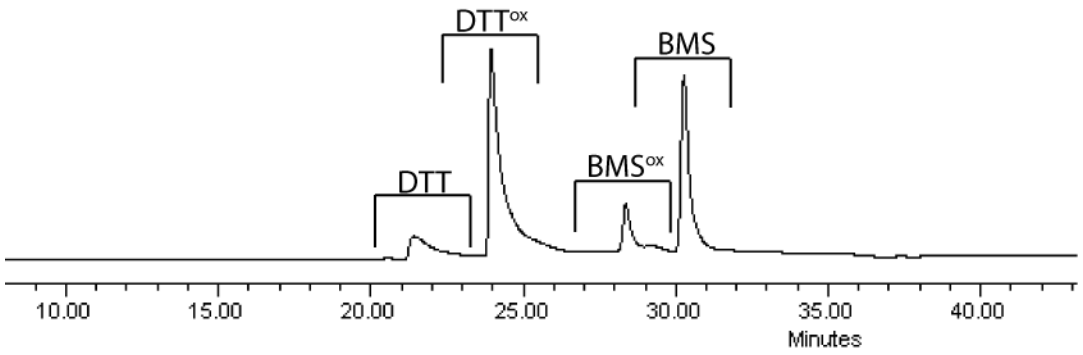

Figure A2.5 Representative HPLC chromatogram of the redox equilibrium between BMS and DTT. Compounds were detected by their absorbance at 205 nm.

A2.7.7 Kinetic studies on the reduction of oxidized βME

$$-\frac{\partial[\text{disulfide}]_{\text{total}}}{\partial t} = k_{\text{obs}}[\text{disulfide}]_{\text{total}}[\text{thiol}]_{\text{total}}$$

The observed second-order rate constant (k_{obs}) for a thiol–disulfide interchange reaction was determined by adapting a procedure describe previously.[300] For disulfide = oxidized βME, a 50 mM stock solution of potassium phosphate buffer was degassed and purged with N_2(g) for 30 min immediately prior to use. A stock solution of oxidized βME (10 mM) in 50 mM potassium phosphate buffer, pH 7.0, was purged with N_2(g) for 30 min immediately prior to use. A 25-mL round-bottom flask was charged with DTBA (4.3 mg, 0.025 mmol) or DTT (3.9 mg, 0.025 mmol), and placed under N_2(g). Phosphate buffer (2.5 mL) was added to the round-bottom flask containing the dithiol. Oxidized βME stock solution (2.5 mL) was then added, and the reaction mixture was stirred at room temperature under N_2(g) for 1 min. The reaction mixture

was quenched by the addition of 0.10 mL of 3 N HCl. The reaction mixture was passed through a 4.5-μm filter, and 100 μL of the reaction mixture was analyzed immediately by HPLC using a Varian C18 reverse-phase column. The column was eluted at 1.0 mL/min with water (5.0 mL), followed by a linear gradient (0–40% v/v) of acetonitrile/water over 40 min. The extent of reduction was determined by integrating the newly formed peak corresponding to βME at 205 nm (retention time: 8 min). This process was repeated for reaction times of 2 and 4 min. Calibration curves were generated and found to be linear over the used concentration range. The amount of residual oxidized βME was calculated, and second-order rate constants were calculated from a linear fit of the data in Figure A2.2A (that is, $k_{obs} = [(1/c_{final}) - (1/c_{initial})]/t$). The initial values of concentration in the reaction mixture were [DTBA or DTT] = [oxidized βME] = $c_{initial}$ = 5 mM. Rate constants were the mean ± SE from three experiments. DTBA: k_{obs} = (0.29 ± 0.02) $M^{-1}s^{-1}$ and DTT: k_{obs} = (0.084 ± 0.004) $M^{-1}s^{-1}$. The same procedure was performed for reactions at pH 5.5, giving DTBA: k_{obs} = (0.0093 ± 0.0003) $M^{-1}s^{-1}$ and DTT: k_{obs} = (0.0021 ± 0.0002) $M^{-1}s^{-1}$ (Figure A2.1A).

A2.7.8 Kinetic studies on the reduction of oxidized L-glutathione

An experiment similar to that in Section VII was conducted with disulfide = oxidized L-glutathione. Reactions were quenched at various time points (2, 4, 6, and 8 min) and 100 μL was analyzed by HPLC (1.0 mL/min with water (5.0 mL) in 0.1% v/v TFA, followed by a linear gradient (0–40% v/v) of acetonitrile in 0.1% v/v TFA over 40 min). The extent of reduction was determined by integrating the newly formed L-glutathione reduced peak at 220 nm (retention time of 7 min). Second-order rate constants were calculated from a linear fit of the data in

Figure A2.2B (that is, $k_{obs} = [(1/c_{final}) - (1/c_{initial})]/t$). Rate constants were the mean ± SE from three experiments. DTBA: $k_{obs} = (0.83 \pm 0.04)\ M^{-1}s^{-1}$ and DTT: $k_{obs} = (0.16 \pm 0.02)\ M^{-1}s^{-1}$.

A2.7.9 Kinetic studies on the reactivation of papain

papain-Cys25–SH + $CH_3S(O_2)SCH_3$ ⟶ papain-Cys25–S–S–CH_3 + CH_3SO_2H

k_{obs}

papain-Cys25–S–S–CH_3 + DTBA (or DTT) ⟶ papain-Cys25–SH + oxidized DTBA (or oxidized DTT)

papain-Cys25–SH

$C_6H_5C(O)$–Arg–NH-C_6H_4-p-NO_2 + H_2O ⟶ $C_6H_5C(O)$–ArgOH + **H_2N-C_6H_4-*p*-NO_2**

Cys25 near the active site of papaya latex papain was oxidized as a mixed disulfide by a procedure described previously.[307] Briefly, a stock solution of methyl methanethiosulfonate (3.5 mM) was prepared by dilution of 5 μL of methyl methanethiosulfonate with 15 mL of 0.10 M potassium phosphate buffer, pH 7.0, containing EDTA (2 mM). KCl (0.011 g, 0.15 mmol) was added to 1.5 mL of this stock solution. The solution was deoxygenated by bubbling N_2(g) through it for 15 min. Next, papain (5 mg, 150 units) was added, and the resulting solution was incubated at room temperature under N_2(g) for 12 h. Excess methyl methanethiosulfonate was removed by size-exclusion chromatography using a Sephadex G-25 column. The final concentration of papain was determined by A_{280} using $\varepsilon_{280} = 5.60 \times 10^4\ M^{-1}cm^{-}$

[1].[343] A solution (0.26 mL) of the chromatographed protein was diluted with 4.94 mL of deoxygenated aqueous buffer (0.10 M imidazole–HCl buffer, pH 7.0, containing 2 mM EDTA). Enzyme solution (1.25 mL) was then added to four separate vials. DTBA or DTT (10 μL of a 1 mM solution) was added to one of the vials, and a timer was started. The initial concentrations in the reaction mixture were dithiol reducing agent: 7.9×10^{-6} M and inactive protein: 4.9×10^{-6} M. At various times, an 0.20-mL aliquot was removed from the reaction mixture and added to a cuvette of 0.8 mL of substrate solution (1.25 mM *N*-benzoyl-L-arginyl-*p*-nitroanilide in 0.10 M imidazole–HCl buffer, pH 6.0, containing 2 mM EDTA). The rate of change in absorbance at 410 nm was recorded at 25 °C. A unit of protein is defined by the amount of enzyme required to produce 1 μmol/min of 4-nitroaniline. Using an extinction coefficient for 4-nitroaniline of ε = 8,800 $M^{-1}cm^{-1}$ at 410 nm, the number of units of active papain in solution at each time point was calculated. To determine the possible number of units of active papain in the reaction mixture, a large excess of DTT (~10^3-fold) was added to one vial and the activity was assessed. As a control, it was determined that the concentrations of DTT used had no bearing on the assay data other than activating the protein. y = enzymatic activity (%) at particular times was calculated by dividing the number of active units of enzyme by the possible number of units in the solution, and was plotted in Figure A2.3A. To determine the value of the second-order rate constant k_{obs} for the reducing agents, the second-order rate equation (eq 4) was transformed into eq 5, which was fitted to the data with the program Prism 5.0. In eq 4 and 5, A_o = [inactive protein]$_{t=0}$, A = [inactive protein]$_t$ = $A_o - A_o y$, B_o = [reducing agent]$_{t=0}$, and B = [reducing agent]$_t$ = $B_o - A_o y$. Values of k_{obs} were the mean ± SE from three experiments. DTBA: k_{obs} = (1275 ± 69) $M^{-1}s^{-1}$ and DTT: k_{obs} = (90.4 ± 5.2) $M^{-1}s^{-1}$.

$$\frac{1}{B_o - A_o} \ln \frac{A_o B}{A B_o} = k_{obs} t \tag{4}$$

$$y = \frac{B_o - B_o e^{k_{obs} t (A_o - B_o)}}{B_o - A_o e^{k_{obs} t (A_o - B_o)}} \times 100\% \tag{5}$$

A2.7.10 Kinetic studies on the reactivation of creatine kinase

creatine kinase-Cys283–SH + GSSG $\longrightarrow$ creatine kinase-Cys283–S–SG + GSH

$$\xrightarrow{k_{obs}}$$

creatine kinase-Cys283–S–SG + DTBA (or DTT) $\longrightarrow$ creatine kinase-Cys283–SH + oxidized DTBA (or DTT)

$$\xrightarrow[\text{creatine kinase-Cys283–SH}]{}$$

creatine phosphate + ADP $\longrightarrow$ creatine + ATP

$$\xrightarrow[\text{hexokinase}]{}$$

ATP + D-glucose $\longrightarrow$ ADP + D-glucose-6-phosphate

$$\xrightarrow[\text{glucose-6-phosphate dehydrogenase}]{}$$

D-glucose-6-phosphate + $NADP^+$ $\longrightarrow$ D-gluconate-6-phosphate + H^+ + **NADPH**

Cys283 in the active site of rabbit muscle creatine kinase was oxidized as a mixed disulfide by a procedure described previously,[344] but with a slight modification in the measurement of active enzyme. A unit of enzyme was defined as the amount required to produce 1 μmol/min of NADPH. Using an extinction coefficient for NADPH of ε = 6.22 $mM^{-1}cm^{-1}$ at 340 nm, the units of active creatine kinase in solution at a particular time were calculated. To determine the

possible number of units of active creatine kinase in the reaction mixture, a large excess of DTT (~10^3-fold) was added to one vial and the activity was assessed. As a control, it was determined that the concentrations of DTT used had no bearing on the assay data other than activating the protein. Enzymatic activity (%) at particular times was calculated by dividing the number of active units of enzyme by the possible number of units in the solution, and was plotted in Figure A2.3B. Values of the second-order rate constant k_{obs} were determined by using eq 5 as described in Section IX, and were the mean ± SE from three experiments. DTBA: k_{obs} = (16.2 ± 0.7) $M^{-1}s^{-1}$ and DTT: k_{obs} = (14.7 ± 0.4) $M^{-1}s^{-1}$.

A2.7.11 Separation of DTBA using an ion-exchange resin

A reaction buffer (0.10 M sodium phosphate, pH 8.0, 1 mM EDTA) was prepared. Ellman's reagent solution was prepared by adding Ellman's reagent (4 mg) to 1 mL of the reaction buffer. Next, to 25 mL of reaction buffer (0.10 M sodium phosphate, pH 8.0, 1 mM EDTA) was added DTBA (2.2 mg, 1.27 × 10^{-5} mol) and 1.7 g of DOWEX 50WX4-400 ion-exchange resin. The mixture was swirled for several minutes and filtered through a fritted syringe. Ellman's reagent solution (50 μL) was added to two separate vials containing 2.5 mL of reaction buffer. As a blank, 250 μL of reaction buffer was added to one of the vials, and the absorbance at 412 nm was set to zero. Filtrate (250 μL) was then added to the other vial and its absorbance was recorded. With A_{412} = 0.012 and using an extinction coefficient of ε = 14,150 $M^{-1}cm^{-1}$,[341,342] it was calculated that >99% of DTBA was retained by the resin and thus removed from solution. The same assay was repeated with DTT, resulting in <1% being removed from

solution. See section A2.7.3 for a more detailed explanation of similar calculations using Ellman's assay.

A2.7.12 Ultraviolet spectra of oxidized DTBA and oxidized DTT

Solutions of oxidized DTBA and DTT (1.0 mM) were prepared in Dulbecco's phosphate buffered saline (DPBS), and their ultraviolet spectra were recorded (Figure S4).

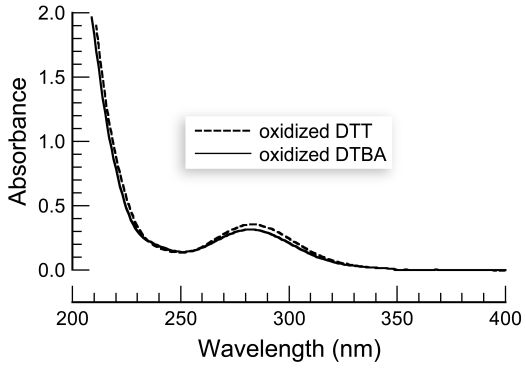

Figure A2.6 Ultraviolet spectrum of oxidized DTBA and oxidized DTT in DPBS.

^{1}H NMR($CDCl_3$) and ^{13}C NMR($CDCl_3$) of **2**

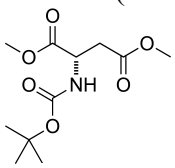

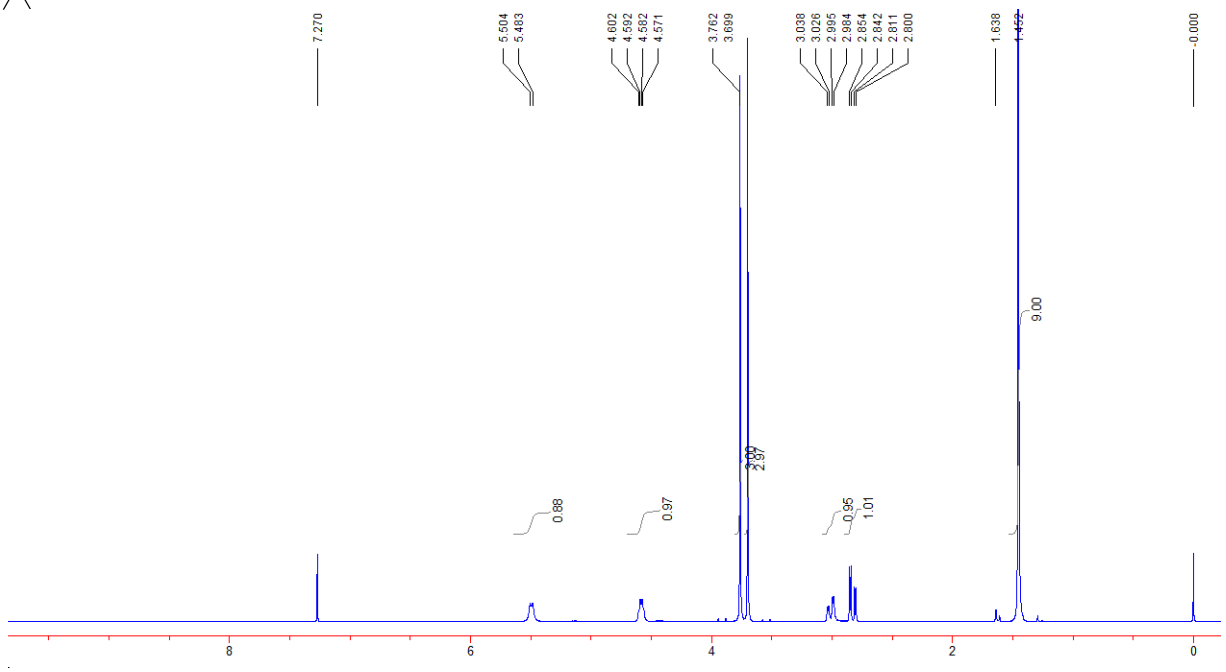

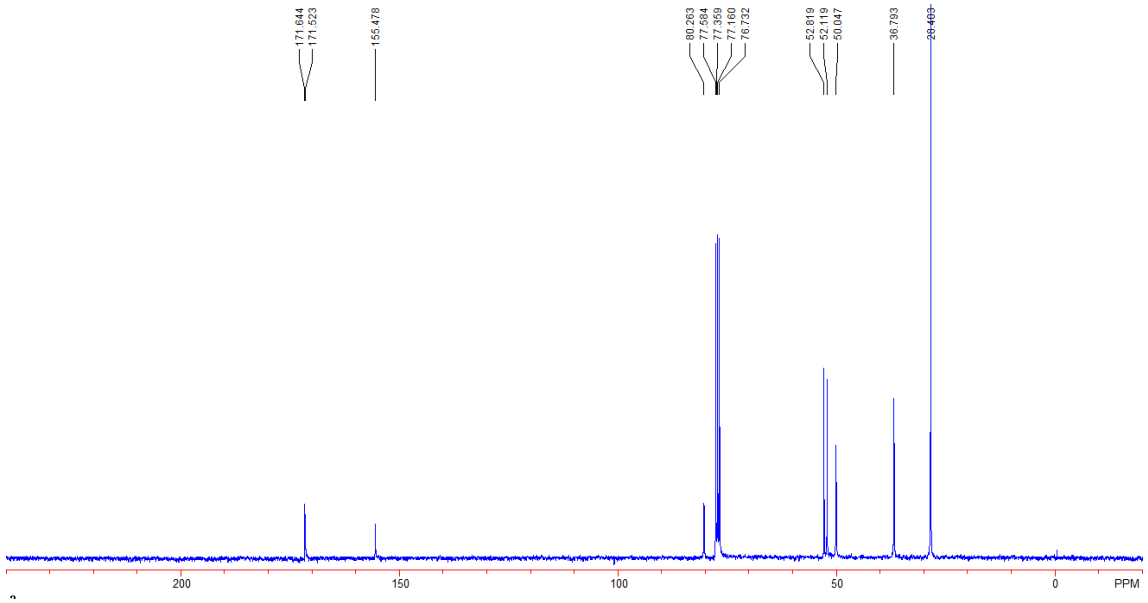

^{1}H NMR(DMSO-***d***$_6$) and ^{13}C NMR($CDCl_3$) of **3**

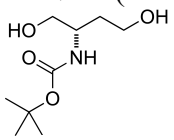

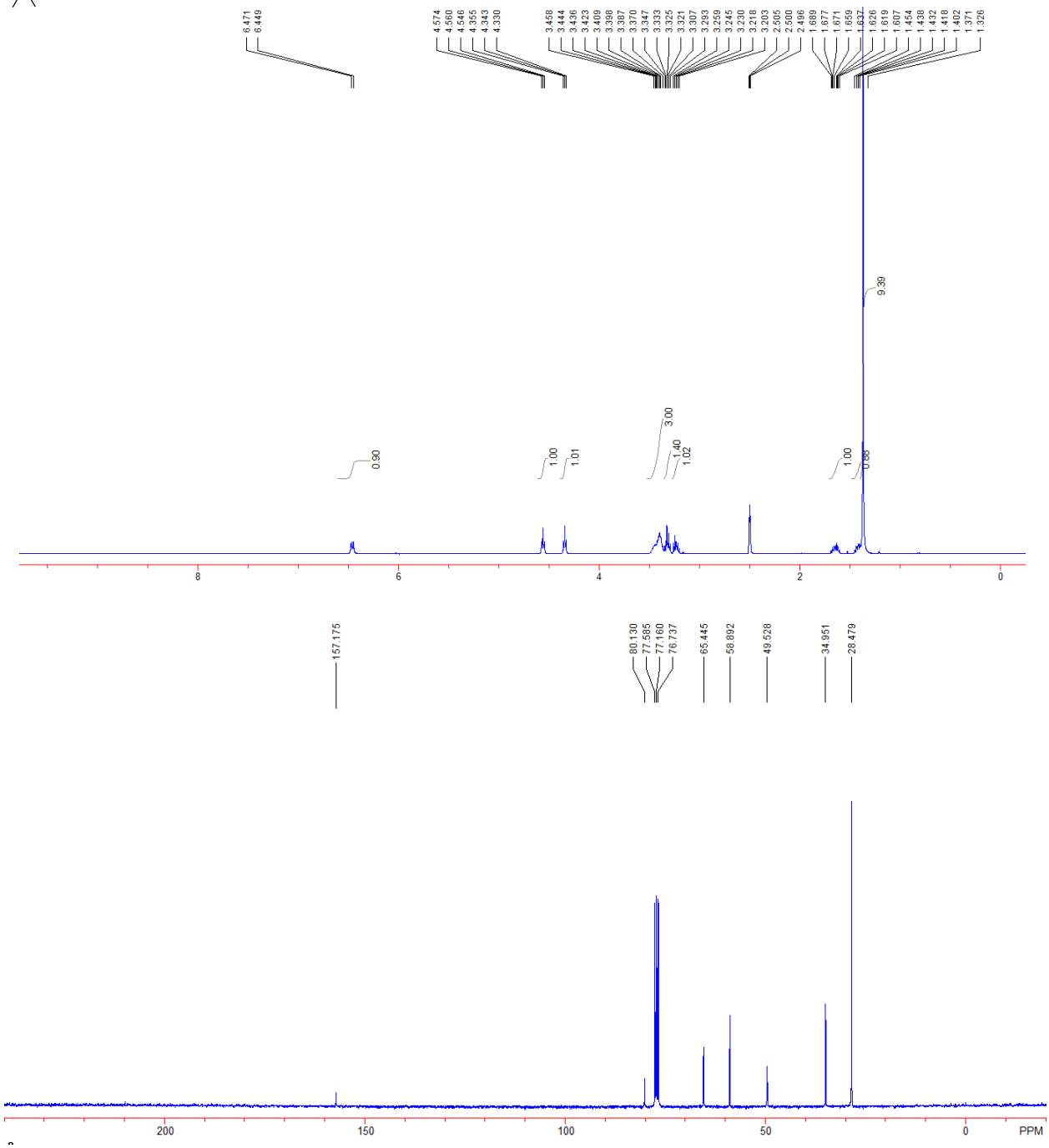

^{1}H NMR($CDCl_3$) and ^{13}C NMR($CDCl_3$) of **4**

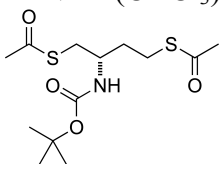

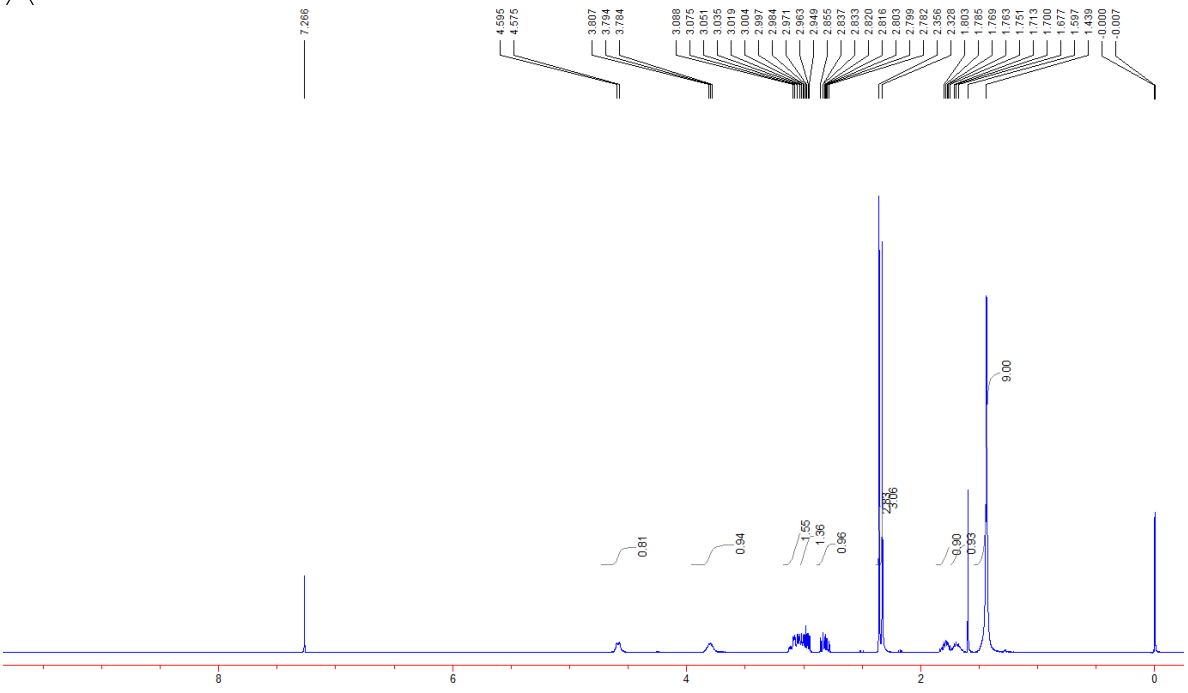

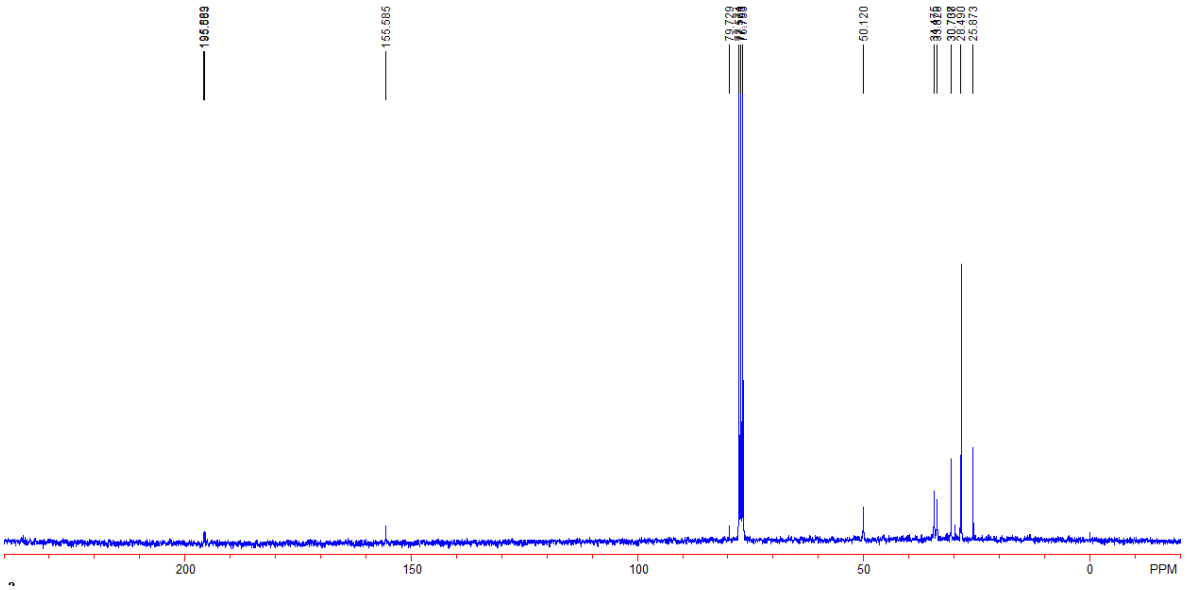

^{1}H NMR(DMSO-d_6) and ^{13}C NMR(DMSO-d_6) of **5**

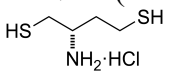

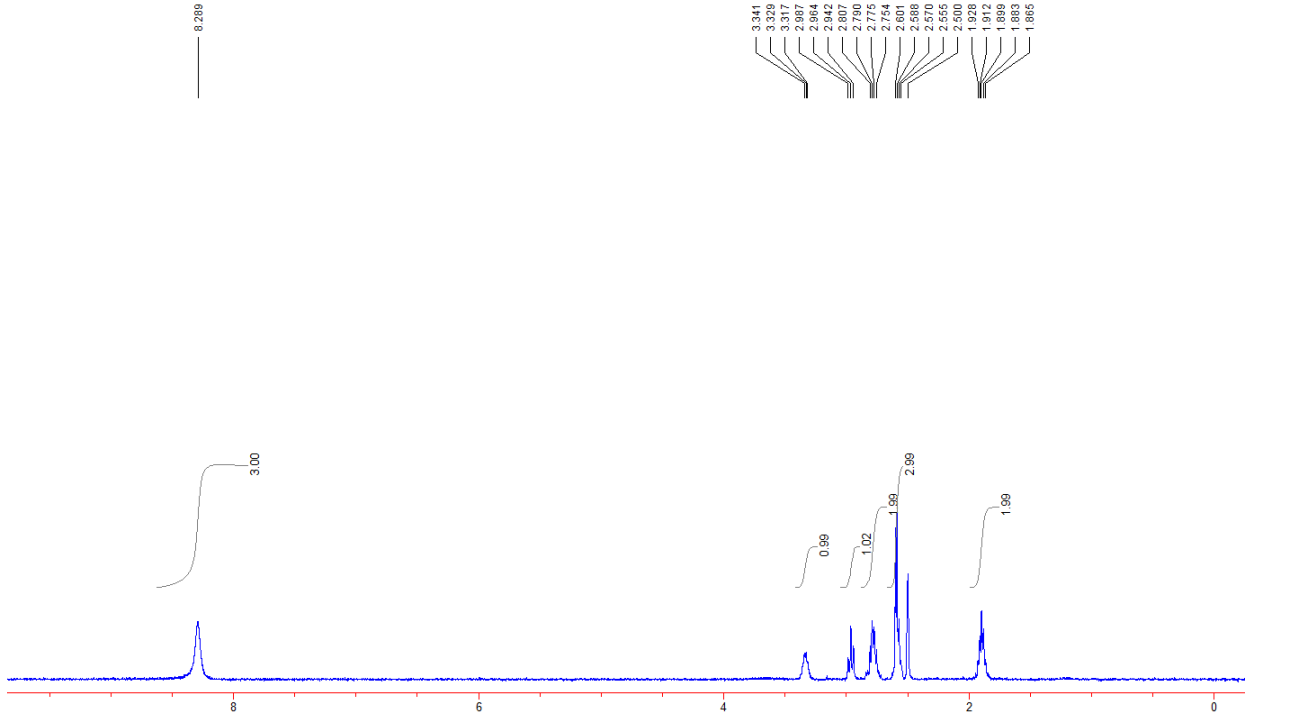

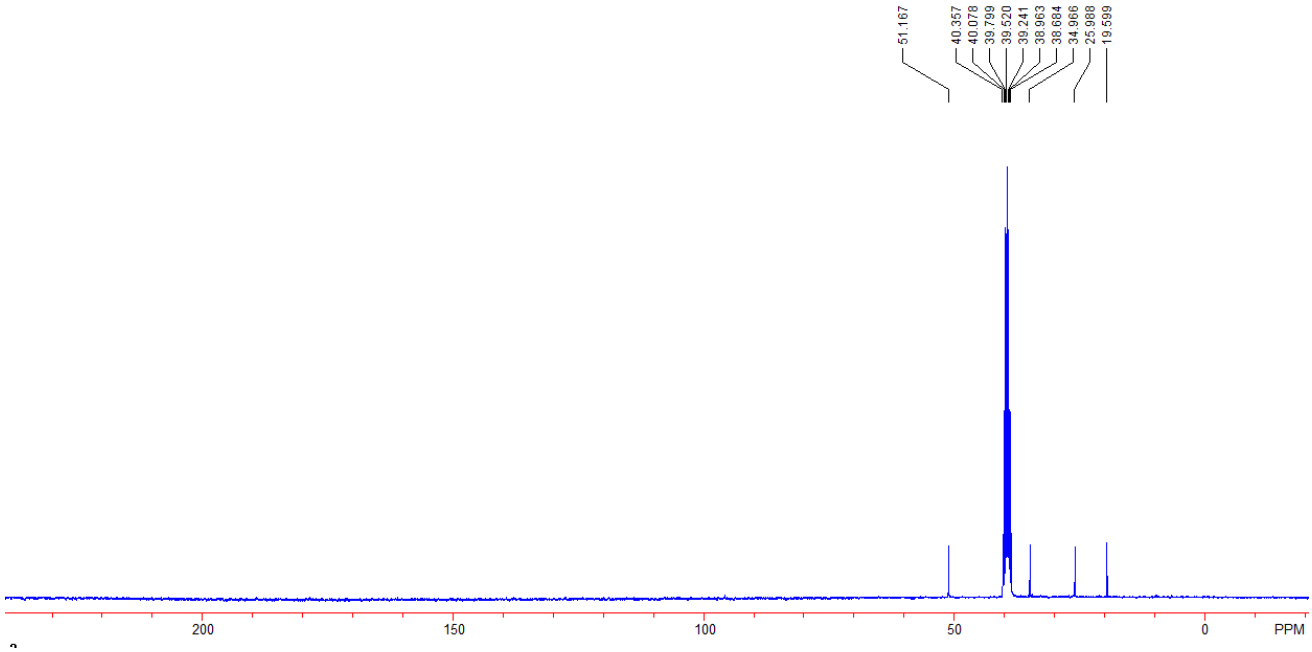

^{1}H NMR($CDCl_3$) and ^{13}C NMR($CDCl_3$) of **6**

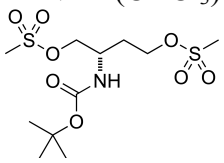

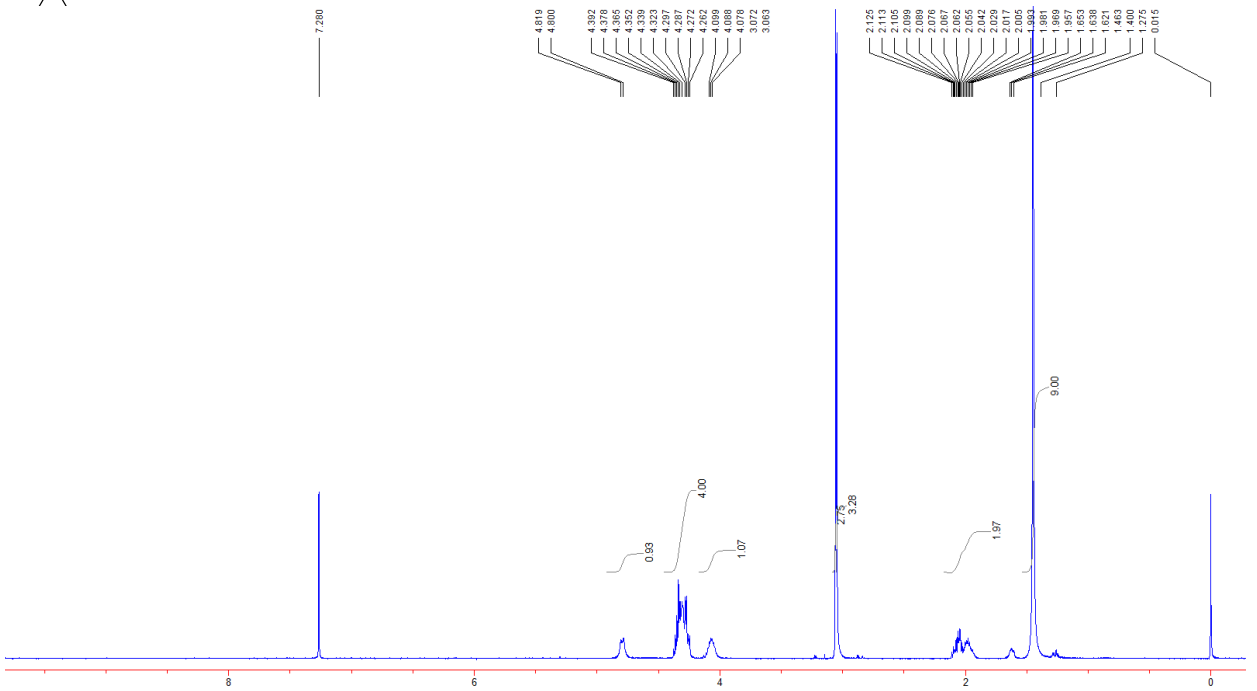

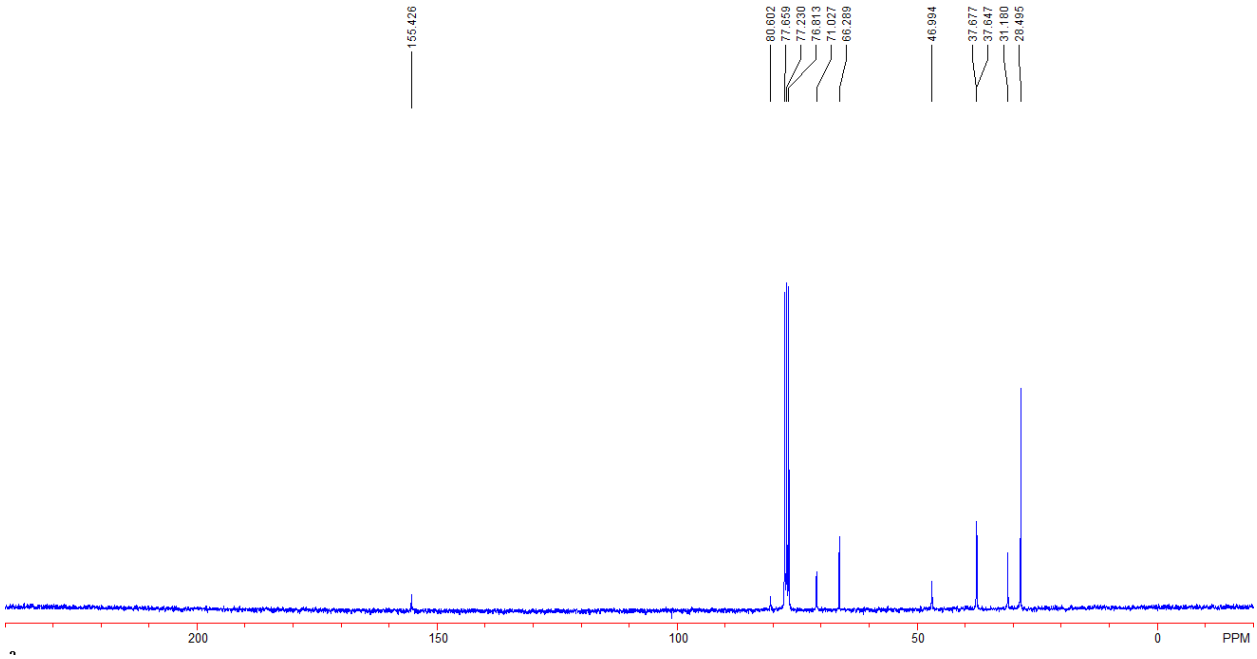

^{1}H NMR(DMSO-d_6) and ^{13}C NMR(DMSO-d_6) of **7**

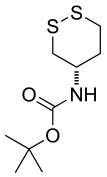

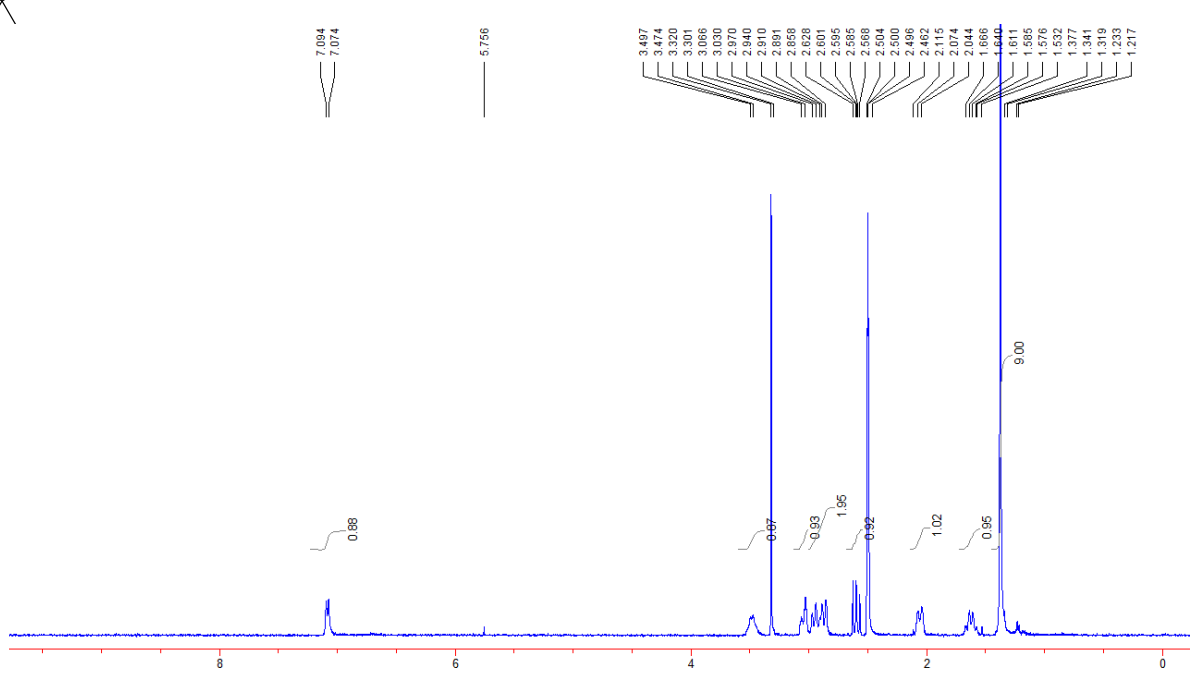

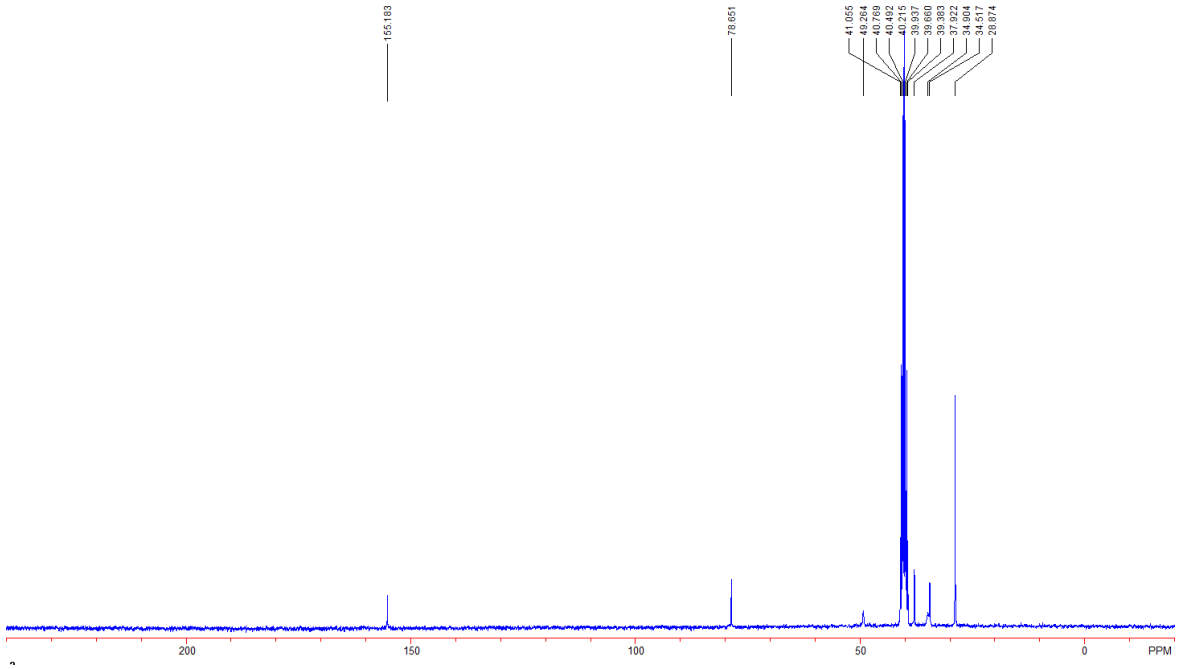

^{1}H NMR(DMSO-d_6) and ^{13}C NMR(DMSO-d_6) of **8**

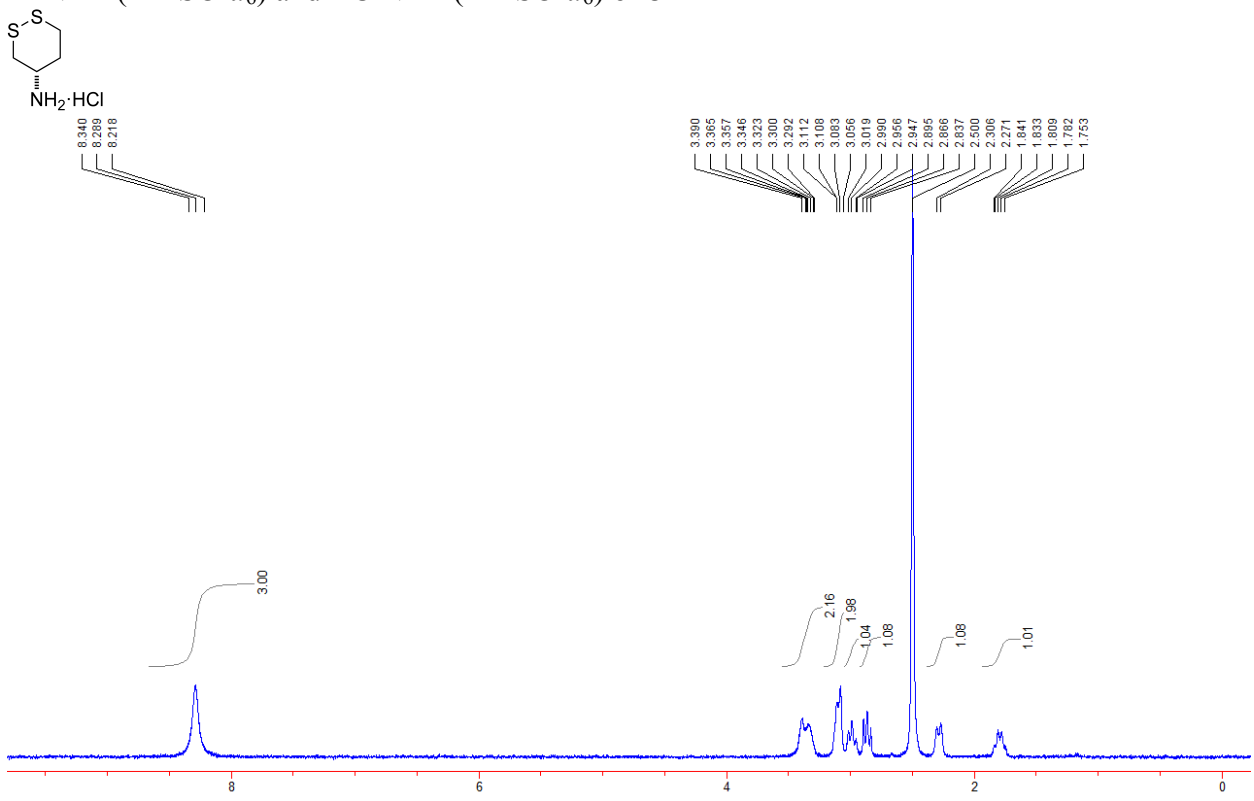

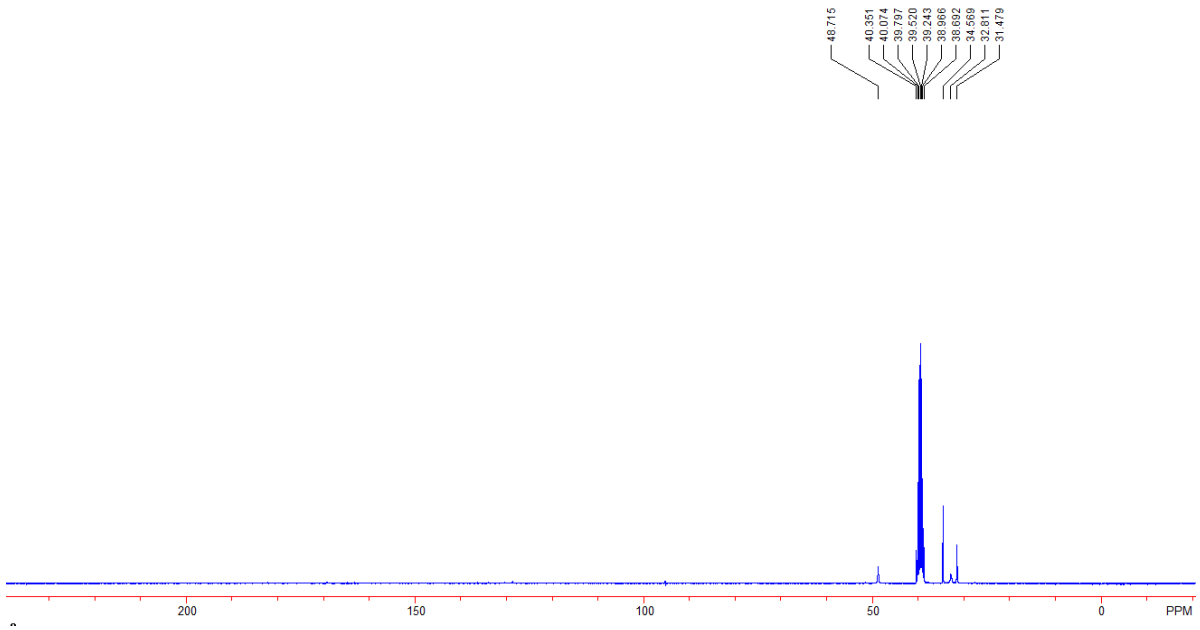

References

1 Jahn, R. & Scheller, R.H., SNAREs—engines for membrane fusion. *Nat. Rev. Mol. Cell Biol.* 7 631-643 (2006).

2 Chan, Y., van Lengerich, B., & Boxer, S., Lipid-anchored DNA mediates vesicle fusion as observed by lipid and content mixing. *Biointerphases* 3 FA17-FA21 (2008).

3 Hopkins, A.L. & Groom, C.R., The druggable genome. *Nat. Rev. Drug Discov.* 1 727-730 (2002).

4 Russ, A.P. & Lampel, S., The druggable genome: an update. *Drug Discov. Today* 10 1607-1610 (2005).

5 Wolff, J.A., The "grand" problem of synthetic delivery. *Nat. Biotechnol.* 20 768-769 (2002).

6 Both, G. *et al.*, Gene therapy: Therapeutic applications and relevance to pathology. *Pathology (Phila.)* 43 642-656 (2011).

7 Aagaard, L. & Rossi, J.J., RNAi therapeutics: Principles, prospects and challenges. *Adv. Drug Deliv. Rev.* 59 75-86 (2007).

8 Noble, I. 'Secret of life' discovery turns 50 (BBC News, 2003).

9 Watson, J.D. & Crick, F.H., Molecular structure of nucleic acids; a structure for deoxyribose nucleic acid. *Nature* 171 737-738 (1953).

10 Hershey, A.D. & Chase, M., Independent functions of viral protein and nucleic acid in growth of bacteriophage. *J. Gen. Physiol.* 36 39-56 (1952).

11 Ingram, V.M., A specific chemical difference between the globins of normal human and sickle-cell anaemia haemoglobin. *Nature* 178 792-794 (1956).

12 Khorana, H.G. *et al*., Studies on polynucleotides. 103. Total synthesis of the structural gene for an alanine transfer ribonucleic acid from yeast. *J. Mol. Biol*. 72 209-217 (1972).

13 Friedmann, T., A brief history of gene therapy. *Nat. Genet*. 2 93-98 (1992).

14 Sakmar, T.P., Har Gobind Khorana (1922-2011): Chemical biology pioneer. *ACS Chem. Biol*. 7 250-251 (2012).

15 Cline, M.J. *et al*., Gene transfer in intact animals. *Nature* 284 422-425 (1980).

16 Mercola, K.E., Stang, H.D., Browne, J., Salser, W., & Cline, M.J., Insertion of a new gene of viral origin into bone marrow cells of mice. *Science* 208 1033-1035 (1980).

17 Wade, N., Gene therapy pioneer draws Mikadoesque rap. *Science* 212 1253 (1981).

18 Scollay, R., Gene therapy: A brief overview of the past, present, and future. *Ann. N. Y. Acad. Sci*. 953 26-30 (2001).

19 Hacein-Bey-Abina, S. *et al*., LMO2-associated clonal T cell proliferation in two patients after gene therapy for SCID-X1. *Science* 302 415-419 (2003).

20 Porter, D.L., Levine, B.L., Kalos, M., Bagg, A., & June, C.H., Chimeric antigen receptor-modified T cells in chronic lymphoid leukemia. *N. Engl. J. Med*. 365 725-733 (2011).

21 Wigler, M., Pellicer, A., Silverstein, S., & Axel, R., Biochemical transfer of single-copy eucaryotic genes using total cellular DNA as donor. *Cell* 14 725-731 (1978).

22 Graham, F.L. & van der Eb, A.J., A new technique for the assay of infectivity of human adenovirus 5 DNA. *Virology* 52 456-467 (1973).

23 Felgner, P.L. *et al*., Lipofection: A highly efficient, lipid-mediated DNA-transfection procedure. *Proc. Natl. Acad. Sci. USA* 84 7413-7417 (1987).

24 Wu, G.Y. & Wu, C.H., Receptor-mediated in vitro gene transformation by a soluble DNA carrier system. *J. Biol. Chem.* 262 4429-4432 (1987).

25 Tros de Ilarduya, C., Sun, Y., & Duzgunes, N., Gene delivery by lipoplexes and polyplexes. *Eur. J. Pharm. Sci.* 40 159–170.

26 Duzgunes, N. & Felgner, P.L., Intracellular delivery of nucleic acids and transcription factors by cationic liposomes. *Methods Enzymol.* 221 303-306 (1993).

27 Pires, P. *et al.*, Interaction of cationic liposomes and their DNA complexes with monocytic leukemia cells. *Biochim. Biophys. Acta* 1418 71-84 (1999).

28 Xu, Y., Hui, S.W., Frederik, P., & Szoka, F.C., Jr., Physicochemical characterization and purification of cationic lipoplexes. *Biophys. J.* 77 341-353 (1999).

29 Luo, D. & Saltzman, W.M., Synthetic DNA delivery systems. *Nat. Biotechnol.* 18 33-37 (2000).

30 Rambourg, A. & Leblond, C.P., Electron microscope observations on the carbohydrate-rich cell coat present at the surface of cells in the rat. *J. Cell Biol.* 32 27–53 (1967).

31 Angata, T. & Varki, A., Chemical diversity in the sialic acids and related alpha-keto acids: an evolutionary perspective. *Chem. Rev.* 102 439–469 (2002).

32 Gandhi, N.S. & Mancera, R.L., The structure of glycosaminoglycans and their interactions with proteins. *Chem. Biol. Drug Des.* 72 455–482 (2008).

33 Coulomb, C.A., *Collection de Mémoires Relatifs a la Physique*. (Gauthier–Villars, Paris, 1884).

34 Gillmor, C.S., *Coulomb and the Evolution of Physics and Engineering in Eighteenth-Century France*. (Princeton University Press, Princeton, NJ, 1971).

35 Palte, M.J. & Raines, R.T., Interaction of nucleic acids with the glycocalyx. *J. Am. Chem. Soc.* (2012).

36 Rautio, J. *et al*., Prodrugs: design and clinical applications. *Nat. Rev. Drug Discov*. 7 255-270 (2008).

37 Jana, S., Mandlekar, S., & Marathe, P., Prodrug design to improve pharmacokinetic and drug delivery properties: Challenges to the discovery scientists. *Curr. Med. Chem*. 17 3874-3908 (2010).

38 Anastasi, C. *et al*., New antiviral nucleoside prodrugs await application. *Curr. Med. Chem*. 10 1825-1843 (2003).

39 Micklefield, J., Backbone modification of nucleic acids: Synthesis, structure and therapeutic applications. *Curr. Med. Chem*. 8 1157-1179 (2001).

40 Schultz, C., Prodrugs of biologically active phosphate esters. *Bioorg. Med. Chem*. 11 885-898 (2003).

41 Wagner, C.R., Iyer, V.V., & McIntee, E.J., Pronucleotides: Toward the in vivo delivery of antiviral and anticancer nucleotides. *Med. Res. Rev*. 20 417-451 (2000).

42 Hanahan, D. & Weinberg, R.A., Hallmarks of cancer: The next generation. *Cell* 144 646-674 (2011).

43 Alnaim, L., Therapeutic drug monitoring of cancer chemotherapy. *J. Oncol. Pharm. Pract*. 13 207-221 (2007).

44 Sorrentino, S., The eight human "canonical" ribonucleases: Molecular diversity, catalytic properties, and special biological actions of the enzyme proteins. *FEBS Lett*. 584 2194-2200 (2010).

45 Su, A.I. *et al*., A gene atlas of the mouse and human protein-encoding transcriptomes. *Proc. Natl. Acad. Sci. USA* 101 6062-6067 (2004).

46 Weickmann, J.L., Olson, E.M., & Glitz, D.G., Immunological assay of pancreatic ribonuclease in serum as an indicator of pancreatic cancer. *Cancer Res*. 44 1682-1687 (1984).

47 Cuchillo, C.M., Nogués, M.V., & Raines, R.T., Bovine pancreatic ribonuclease: Fifty years of the first enzymatic reaction mechanism. *Biochemistry* 50 7835-7841 (2011).

48 Raines, R.T., Ribonuclease A. *Chem. Rev.* 98 1045-1065 (1998).

49 Cuchillo, C.M. *et al.*, The role of 2′,3′-cyclic phosphodiesters in the bovine pancreatic ribonuclease A catalysed cleavage of RNA: Intermediates or products? *FEBS Lett.* 333 207-210 (1993).

50 Markham, R. & Smith, J.D., The structure of ribonucleic acids. 1. Cyclic nucleotides produced by ribonuclease and by alkaline hydrolysis. *Biochem. J.* 52 552-557 (1952).

51 Thompson, J.E., Venegas, F.D., & Raines, R.T., Energetics of catalysis by ribonucleases: Fate of the 2′,3′-cyclic phosphodiester intermediate. *Biochemistry* 33 7408-7414 (1994).

52 Davis, A.M., Regan, A.C., & Williams, A., Experimental charge measurement at leaving oxygen in the bovine ribonuclease A catalyzed cyclization of uridine 3′-phosphate aryl esters. *Biochemistry* 27 9042-9047 (1988).

53 Stowell, J.K., Widlanski, T.S., Kutateladze, T.G., & Raines, R.T., Mechanism-based inactivation of ribonuclease A. *J. Org. Chem.* 60 6930-6936 (1995).

54 Taylorson, C.J. *et al.*, US Patent No. 5985281 (Nov. 16, 1999 1999).

55 Thompson, J.E. & Raines, R.T., Value of general acid–base catalysis to ribonuclease A. *J. Am. Chem. Soc.* 116 5467-5468 (1994).

56 Witmer, M.R. *et al.*, U-3′-BCIP: A chromogenic substrate for the detection of RNase A in recombinant DNA expression systems. *Nucleic Acids Res.* 19 1-4 (1991).

57 Chao, T.Y., Lavis, L.D., & Raines, R.T., Cellular uptake of ribonuclease A relies on anionic glycans. *Biochemistry* 49 10666-10673 (2010).

58 Malik, D.K., Baboota, S., Ahuja, A., Hasan, S., & Ali, J., Recent advances in protein and peptide drug delivery systems. *Curr. Drug Deliv.* 4 141-151 (2007).

59 Patil, S.D., Rhodes, D.G., & Burgess, D.J., DNA-based therapeutics and DNA delivery systems: a comprehensive review. *AAPS J*. 7 E61-77 (2005).

60 Rapoport, M. & Lorberboum-Galski, H., TAT-based drug delivery system--new directions in protein delivery for new hopes? *Expert Opin. Drug Deliv*. 6 453-463 (2009).

61 Shim, M.S. & Kwon, Y.J., Efficient and targeted delivery of siRNA in vivo. *FEBS J*. 277 4814-4827 (2010).

62 Sun, X. & Zhang, N., Cationic polymer optimization for efficient gene delivery. *Mini Rev. Med. Chem*. 10 108-125 (2010).

63 Gao, Y., Gao, G., He, Y., Liu, T., & Qi, R., Recent advances of dendrimers in delivery of genes and drugs. *Mini Rev. Med. Chem*. 8 889-900 (2008).

64 Schmidt, N., Mishra, A., Lai, G.H., & Wong, G.C., Arginine-rich cell-penetrating peptides. *FEBS Lett*. 584 1806-1813 (2010).

65 Mohanty, C., Das, M., Kanwar, J.R., & Sahoo, S.K., Receptor mediated tumor targeting: an emerging approach for cancer therapy. *Curr. Drug Deliv*. 8 45-58 (2011).

66 Rizk, S.S. *et al*., An engineered substance P variant for receptor-mediated delivery of synthetic antibodies into tumor cells. *Proc. Natl. Acad. Sci. USA* 106 11011-11015 (2009).

67 Zhao, X., Li, H., & Lee, R.J., Targeted drug delivery via folate receptors. *Expert Opin. Drug Deliv*. 5 309-319 (2008).

68 James, T.D., Phillips, M.D., & Shinkai, S., *Boronic Acids in Saccharide Recognition*. (Royal Society of Chemistry, Cambridge, UK, 2006).

69 Mothana, S., Grassot, J.M., & Hall, D.G., Multistep phase-switch synthesis by using liquid–liquid partitioning of boronic acids: Productive tags with an expanded repertoire of compatible reactions. *Angew. Chem. Int. Ed*. 49 2883-2887 (2010).

70 Barth, R.F., Boron neutron capture therapy at the crossroads: challenges and opportunities. *Appl. Radiat. Isot.* 67 S3-6 (2009).

71 Barth, R.F., Coderre, J.A., Vicente, M.G., & Blue, T.E., Boron neutron capture therapy of cancer: current status and future prospects. *Clin. Cancer Res.* 11 3987-4002 (2005).

72 Westmark, P.R. & Smith, B.D., Boronic acids facilitate the transport of ribonucleosides through lipid bilayers. *J. Pharm. Sci.* 85 266-269 (1996).

73 Vandenburg, Y.R., Zhang, Z.Y., Fishkind, D.J., & Smith, B.D., Enhanced cell binding using liposomes containing an artificial carbohydrate-binding receptor. *Chem. Commun.* 149-150 (2000).

74 Yang, W. *et al.*, The first fluorescent diboronic acid sensor specific for hepatocellular carcinoma cells expressing sialyl Lewis X. *Chem. Biol.* 11 439-448 (2004).

75 Peng, Q., Chen, F., Zhong, Z., & Zhuo, R., Enhanced gene transfection capability of polyethylenimine by incorporating boronic acid groups. *Chem. Commun.* 46 5888-5890 (2010).

76 Wu, W., Mitra, N., Yan, E.C., & Zhou, S., Multifunctional hybrid nanogel for integration of optical glucose sensing and self-regulated insulin release at physiological pH. *ACS Nano* 4 4831-4839 (2010).

77 Jay, J.I. *et al.*, Multivalent benzoboroxole functionalized polymers as gp120 glycan targeted microbicide entry inhibitors. *Mol. Pharm.* 7 116-129 (2009).

78 Matsumoto, A., Cabral, H., Sato, N., Kataoka, K., & Miyahara, Y., Assessment of tumor metastasis by the direct determination of cell-membrane sialic acid expression. *Angew. Chem. Int. Ed.* 49 5494-5497 (2010).

79 Matsumoto, A., Sato, N., Kataoka, K., & Miyahara, Y., Noninvasive sialic acid Detection at cell membrane by using phenylboronic acid modified self-assembled monolayer gold electrode. *J. Am. Chem. Soc.* 131 12022-12023 (2009).

80 Polsky, R., Harper, J.C., Wheeler, D.R., Arango, D.C., & Brozik, S.M., Electrically addressable cell immobilization using phenylboronic acid diazonium salts. *Angew. Chem. Int. Ed.* 120 2671-2674 (2008).

81 Zhong, X., Bai, H.J., Xu, J.J., Chen, H.Y., & Zhu, Y.H., A reusable interface constructed by 3 aminophenylboronic acid functionalized multiwalled carbon nanotubes for cell capture, release, and cytosensing. *Adv. Funct. Mater.* 20 992-999 (2010).

82 Patil, S.D., Rhodes, D.G., & Burgess, D.J., DNA-based therapeutics and DNA delivery systems: A comprehensive review. *AAPS J.* 7 E61-E77 (2005).

83 Mello, C.C., Return to the RNAi world: Rethinking gene expression and evolution (Nobel lecture). *Angew. Chem. Int. Ed.* 46 6985-6994 (2007).

84 Fire, A.Z., Gene silencing by double-stranded RNA (Nobel lecture). *Angew. Chem. Int. Ed.* 46 6966-6984 (2007).

85 Shim, M.S. & Kwon, Y.J., Efficient and targeted delivery of siRNA in vivo. *FEBS J.* 277 4814-4827 (2010).

86 Lares, M.R., Rossi, J.J., & Ouellet, D.L., RNAi and small interfering RNAs in human disease therapeutic applications. *Trends Biotechnol.* 28 570-579 (2010).

87 Pecot, C.V., Calin, G.A., Coleman, R.L., Lopez-Berestein, G., & Sood, A.K., RNA interference in the clinic: Challenges and future directions. *Nat. Rev. Cancer* 11 59-67 (2011).

88 Beck, G.F., Irwin, W.J., Nicklin, P.L., & Akhtar, S., Interactions of phosphodiester and phosphorothioate oligonucleotides with intestinal epithelial Caco-2 cells. *Pharm. Res.* 13 1028-1037 (1996).

89 Hawley, P. & Gibson, I., Interaction of oligodeoxynucleotides with mammalian cells. *Antisense Nucleic Acid Drug Dev.* 6 185-195 (1996).

90 Loke, S.L. *et al.*, Characterization of oligonucleotide transport into living cells. *Proc. Natl. Acad. Sci. USA* 86 3474-3478 (1989).

91 McCoy, S.L. *et al*., Quantification of DNA binding to cell-surfaces by flow cytometry. *J. Immunol. Methods* 241 141-146 (2000).

92 Stein, C.A., Controversies in the cellular pharmacology of oligodeoxynucleotides. *Antisense Nucleic Acid Drug Dev*. 7 207-209 (1997).

93 Takagi, T. *et al*., Involvement of specific mechanism in plasmid DNA uptake by mouse peritoneal macrophages. *Biochem. Biophys. Res. Commun*. 245 729-733 (1998).

94 Varki, A. *et al*., Symbol nomenclature for glycan representation. *Proteomics* 9 5398-5399 (2009).

95 Fuchs, S.M. & Raines, R.T., Arginine grafting to endow cell permeability. *ACS Chem. Biol*. 2 167-170 (2007).

96 Fuchs, S.M., Rutkoski, T.J., Kung, V.M., Groeschl, R.T., & Raines, R.T., Increasing the potency of a cytotoxin with an arginine graft. *Protein Eng. Des. Select*. 20 505-509 (2007).

97 Johnson, R.J., Chao, T.-Y., Lavis, L.D., & Raines, R.T., Cytotoxic ribonucleases: The dichotomy of Coulombic forces. *Biochemistry* 46 10308-10316 (2007).

98 Wolff, J.A. & Rozema, D.B., Breaking the bonds: Non-viral vectors become chemically dynamic. *Mol. Ther*. 16 8-15 (2007).

99 Eguchi, A. & Dowdy, S.F., siRNA delivery using peptide transduction domains. *Trends Pharmacol. Sci*. 30 341-345 (2009).

100 Cronican, J.J. *et al*., Potent delivery of functional proteins into mammalian cells in vitro and in vivo using a supercharged protein. *ACS Chem. Biol*. 5 747-752 (2010).

101 McNaughton, B.R., Cronican, J.J., Thompson, D.B., & Liu, D.R., Mammalian cell penetration, siRNA transfection, and DNA transfection by supercharged proteins. *Proc. Natl. Acad. Sci. USA* 106 6111-6116 (2009).

102 Felgner, P.L. *et al*., Lipofection: A highly efficient, lipid-mediated DNA-transfection procedure. *Proc. Natl. Acad. Sci. USA* 84 7413-7417 (1987).

103 Borisenko, G.G., Zaitseva, M.A., Chuvilin, A.N., & Pozmogova, G.E., DNA modification of live cell surface. *Nucleic Acids Res*. 37 e28 (2009).

104 Liu, H.P. *et al*., DNA-Based micelles: Synthesis, micellar properties and size-dependent cell permeability. *Chem.—Eur. J*. 16 3791-3797 (2010).

105 Selden, N.S. *et al*., Chemically programmed cell adhesion with membrane-anchored oligonucleotides. *J. Am. Chem. Soc*. 134 765-768 (2012).

106 Patwa, A., Gissot, A., Bestel, I., & Barthélémy, P., Hybrid lipid oligonucleotide conjugates: synthesis, self-assemblies and biomedical applications. *Chem. Soc. Rev*. 40 5844-5854 (2011).

107 Chandra, R.A., Douglas, E.S., Mathies, R.A., Bertozzi, C.R., & Francis, M.B., Programmable cell adhesion encoded by DNA hybridization. *Angew. Chem. Int. Ed*. 45 896-901 (2006).

108 Hsiao, S.C. *et al*., DNA-coated AFM cantilevers for the investigation of cell adhesion and the patterning of live cells. *Angew. Chem. Int. Ed*. 47 8473-8477 (2008).

109 Kauzmann, W., Some factors in the interpretation of protein denaturation. *Adv. Protein Chem*. 14 1-63 (1959).

110 Tanford, C., *The Hydrophobic Effect: Formation of Micelles and Biological Membranes*. (John Wiley & Sons, New York, 1973).

111 Deutscher, S.L., Nuwayhid, N., Stanley, P., Briles, E.I., & Hirschberg, C.B., Translocation across Golgi vesicle membranes: A CHO glycosylation mutant deficient in CMP-sialic acid transport. *Cell* 39 295-299 (1984).

112 A significant change was observed, even though these experiments were conducted in cell-culture medium that has a high ionic strength.

113 Chao, T.-Y., Lavis, L.D., & Raines, R.T., Cellular uptake of ribonuclease A relies on anionic glycans. *Biochemistry* 49 10666-10673 (2010).

114 Esko, J.D., Stewart, T.E., & Taylor, W.H., Animal cell mutants defective in glycosaminoglycan biosynthesis. *Proc. Natl. Acad. Sci. USA* 82 3197-3201 (1985).

115 Esko, J.D. *et al*., Inhibition of chondroitin and heparan sulfate biosynthesis in Chinese hamster ovary cell mutants defective in galactosyltransferase I. *J. Biol. Chem*. 262 12189-12195 (1987).

116 Ruponen, M., Honkakoski, P., Tammi, M., & Urtti, A., Cell-surface glycosaminoglycans inhibit cation-mediated gene transfer. *J. Gene Med*. 6 405-414 (2004).

117 Westheimer, F.H., Why nature chose phosphates. *Science* 235 1173-1178 (1987).

118 Timmons, L. & Fire, A., Specific interference by ingested dsRNA. *Nature* 395 854 (1998).

119 Grishok, A., RNAi mechanisms in *Caenorhabditis elegans*. *FEBS Lett*. 579 5932-5939 (2005).

120 May, R.C. & Plasterk, R.H., RNA interference spreading in *C. elegans*. *Methods Enzymol*. 392 308-315 (2005).

121 Winston, W.M., Molodowitch, C., & Hunter, C.P., Systemic RNAi in *C. elegans* requires the putative transmembrane protein SID-1. *Science* 295 2456-2459 (2002).

122 Shih, J.D., Fitzgerald, M.C., Sutherlin, M., & Hunter, C.P., The SID-1 double-stranded RNA transporter is not selective for dsRNA length. *RNA* 15 384-390 (2009).

123 Li, H. *et al*., TreeFam: A curated database of phylogenetic trees of animal gene families. *Nucleic Acids Res*. 34 D572-D580 (2006).

124 Amdam, G.V., Simoes, Z.L., Guidugli, K.R., Norberg, K., & Omholt, S.W., Disruption of vitellogenin gene function in adult honeybees by intra-abdominal injection of double-stranded RNA. *BMC Biotechnol*. 3 1 (2003).

125 Bucher, G., Scholten, J., & Klingler, M., Parental RNAi in *Tribolium* (Coleoptera). *Curr. Biol.* 12 R85-R86 (2002).

126 Dong, Y. & Friedrich, M., Nymphal RNAi: Systemic RNAi mediated gene knockdown in juvenile grasshopper. *BMC Biotechnol.* 5 25 (2005).

127 Sanchez Alvarado, A. & Newmark, P.A., Double-stranded RNA specifically disrupts gene expression during planarian regeneration. *Proc. Natl. Acad. Sci. USA* 96 5049-5054 (1999).

128 Duxbury, M.S., Ashley, S.W., & Whang, E.E., RNA interference: A mammalian SID-1 homologue enhances siRNA uptake and gene silencing efficacy in human cells. *Biochem. Biophys. Res. Commun.* 331 459-463 (2005).

129 Wolfrum, C. *et al.*, Mechanisms and optimization of in vivo delivery of lipophilic siRNAs. *Nat. Biotechnol.* 25 1149-1157 (2007).

130 Chan, Y.H., van Lengerich, B., & Boxer, S.G., Lipid-anchored DNA mediates vesicle fusion as observed by lipid and content mixing. *Biointerphases* 3 FA17 (2008).

131 Chan, Y.H., van Lengerich, B., & Boxer, S.G., Effects of linker sequences on vesicle fusion mediated by lipid-anchored DNA oligonucleotides. *Proc. Natl. Acad. Sci. USA* 106 979-984 (2009).

132 Rautio, J. *et al.*, Prodrugs: Design and clinical applications. *Nat. Rev. Drug Discov.* 7 255-270 (2008).

133 Wang, B., Siahaan, T., & Soltero, R., *Drug Delivery: Principles and Applications*. (John Wiley & Sons, 2005).

134 Gennaro, A.R., *Remington: The Science and Practice of Pharmacy, 21st ed.* (Lippincott Williams & Wilkins, Baltimore, MD, 2005).

135 Kratz, F., Muller, I.A., Ryppa, C., & Warnecke, A., Prodrug strategies in anticancer chemotherapy. *ChemMedChem* 3 20-53 (2008).

136 Langer, R., New methods of drug delivery. *Science* 249 1527-1533 (1990).

137 Brown, D.M., *Drug Delivery Systems in Cancer Therapy*. (Humana Press, Totowa, N.J., 2004).

138 Testa, B. & Mayer, J.M., *Hydrolysis in Drug and Prodrug Metabolism: Chemistry, Biochemistry, and Enzymology*. (Wiley–VCH, Zürich, Switzerland, 2003).

139 The ribonucleolytic activity in serum is attributable to RNase 1. Its concentration there is 156 units/mL with 1 unit of activity arising from 2.6 ng of enzyme. Weickmann, J. L.; Olson, E. M.; Glitz, D. G. Immunological assay of pancreatic ribonuclease in serum as an indicator of pancreatic cancer. *Cancer Res*. **1984**, *44*, 1682-1687. Also see: Landré, J. B. P.; Hewett, P. W.; Olivot, J.-M.; Friedl, P.; Sachinidis, A.; Moenner, M. Human endothelial cells selectively express large amounts of pancreatic-type ribonuclease (RNase 1). *J. Cell. Biochem*. **2002**, *86*, 540-552.

140 Beaucage, S.L. & Caruthers, M.H., Deoxynucleoside phosphoramidites—a new class of key intermediates for deoxypolynucleotide synthesis. *Tetrahedron Lett*. 22 1859-1862 (1981).

141 Caruthers, M.H., A brief review of DNA and RNA chemical synthesis. *Biochem. Soc. Trans*. 39 575-580 (2011).

142 Stella, V.J. & Nti-Addae, K.W., Prodrug strategies to overcome poor water solubility. *Adv. Drug Deliv. Rev*. 59 677-694 (2007).

143 Hecker, S.J. & Erion, M.D., Prodrugs of phosphates and phosphonates. *J. Med. Chem*. 51 2328-2345 (2008).

144 Khandazhinskaya, A., Matyugina, E., & Shirokova, E., Anti-HIV therapy with AZT prodrugs: AZT phosphonate derivatives, current state and prospects. *Expert Opin. Drug Met*. 6 701-714 (2011).

145 Owens, D.E., 3rd & Peppas, N.A., Opsonization, biodistribution, and pharmacokinetics of polymeric nanoparticles. *Int. J. Pharm*. 307 93-102 (2006).

146 Venturoli, D. & Rippe, B., Ficoll and dextran vs. globular proteins as probes for testing glomerular permselectivity: Effects of molecular size, shape, charge, and deformability. *Am. J. Physiol–Renal* 288 F605-613 (2005).

147 Desta, Z., Ward, B.A., Soukhova, N.V., & Flockhart, D.A., Comprehensive evaluation of tamoxifen sequential biotransformation by the human cytochrome P450 system in vitro: Prominent roles for CYP3A and CYP2D6. *J. Pharmacol. Exp. Ther.* 310 1062-1075 (2004).

148 Coezy, E., Borgna, J.L., & Rochefort, H., Tamoxifen and metabolites in MCF7 cells: Correlation between binding to estrogen receptor and inhibition of cell growth. *Cancer Res.* 42 317-323 (1982).

149 O'Regan, R.M. & Jordan, V.C., The evolution of tamoxifen therapy in breast cancer: Selective oestrogen-receptor modulators and downregulators. *Lancet Oncol.* 3 207-214 (2002).

150 Powles, T.J., Anti-oestrogenic chemoprevention of breast cancer-the need to progress. *Eur. J. Cancer* 39 572-579 (2003).

151 Fisher, B. *et al.*, Tamoxifen for the prevention of breast cancer: Current status of the National Surgical Adjuvant Breast and Bowel Project P-1 study. *J. Natl. Cancer Inst.* 97 1652-1662 (2005).

152 Decensi, A. *et al.*, A randomized trial of low-dose tamoxifen on breast cancer proliferation and blood estrogenic biomarkers. *J. Natl. Cancer Inst.* 95 779-790 (2003).

153 Layek, B. & Mukherjee, B., Tamoxifen citrate encapsulated sustained release liposomes: Preparation and evaluation of physicochemical properties. *Sci. Pharm.* 78 507-515 (2010).

154 Bergman, L. *et al.*, Risk and prognosis of endometrial cancer after tamoxifen for breast cancer. Comprehensive cancer centres' ALERT group. Assessment of liver and endometrial cancer risk following tamoxifen. *Lancet* 356 881-887 (2000).

155 Veronesi, U., Maisonneuve, P., & Decensi, A., Tamoxifen: An enduring star. *J. Natl. Cancer Inst.* 99 258-260 (2007).

156 Vitseva, O., Flockhart, D.A., Jin, Y., Varghese, S., & Freedman, J.E., The effects of tamoxifen and its metabolites on platelet function and release of reactive oxygen intermediates. *J. Pharmacol. Exp. Ther.* 312 1144-1150 (2005).

157 Andresen, T.L., Jensen, S.S., & Jorgensen, K., Advanced strategies in liposomal cancer therapy: Problems and prospects of active and tumor specific drug release. *Prog. Lipid Res.* 44 68-97 (2005).

158 Katzenellenbogen, J.A., Carlson, K.E., & Katzenellenbogen, B.S., Facile geometric isomerization of phenolic non-steroidal estrogens and antiestrogens: Limitations to the interpretation of experiments characterizing the activity of individual isomers. *J. Steroid Biochem.* 22 589-596 (1985).

159 Murphy, C.S., Langan-Fahey, S.M., McCague, R., & Jordan, V.C., Structure–function relationships of hydroxylated metabolites of tamoxifen that control the proliferation of estrogen-responsive T47D breast cancer cells in vitro. *Mol. Pharmacol.* 38 737-743 (1990).

160 Hayakawa, Y. *et al.*, Acid/azole complexes as highly effective promoters in the synthesis of DNA and RNA oligomers via the phosphoramidite method. *J. Am. Chem. Soc.* 123 8165-8176 (2001).

161 Calculator Plugins were used for structure property prediction and calculation, Marvin 5.4.1.1, 2011, ChemAxon (Budapest, Hungary).

162 Johnson, R.J., McCoy, J.G., Bingman, C.A., Phillips, G.N., Jr., & Raines, R.T., Inhibition of human pancreatic ribonuclease by the human ribonuclease inhibitor protein. *J. Mol. Biol.* 368 434-449 (2007).

163 Kelemen, B.R. *et al.*, Hypersensitive substrate for ribonucleases. *Nucleic Acids Res.* 27 3696-3701 (1999).

164 Smith, B.D., Soellner, M.B., & Raines, R.T., Potent inhibition of ribonuclease A by oligo(vinylsulfonic acid). *J. Biol. Chem.* 278 20934-20938 (2003).

165 Thompson, J.E. *et al.*, Limits to catalysis by ribonuclease A. *Bioorg. Chem.* 23 471-481 (1995).

166 Serum contains both contaminating ribonucleases and albumin, which binds and thus sequesters HT. Bourassa, P.; Dubeau, S.; Maharvi, G. M.; Fauq, A. H.; Thomas, T. J.; Tajmir-Riahi, H. A. Binding of antitumor tamoxifen and its metabolites 4-hydroxytamoxifen and endoxifen to human serum albumin. *Biochimie 93*, 1089-1101 (2011).

167 Sorrentino, S. & Libonati, M., Human pancreatic-type and nonpancreatic-type ribonucleases: A direct side-by-side comparison of their catalytic properties. *Arch. Biochem. Biophys*. 312 340-348 (1994).

168 UpHT or its derivatives could provide exquisite control of gene expression in transgenic mice via the widely used Cre recombinase–estrogen receptor system. (a) Fell, R.; Brocard, J.; Mascrez, B.; LeMeur, M.; Metzger, D.; Chambon, P. Ligand-activated site-specific recombination in mice. *Proc. Natl. Acad. Sci. USA 93*, 10887-10890 (2002). (b) Hayashi, S.; McMahon, A. P. Efficient recombination in diverse tissues by a tamoxifen-inducible form of Cre: A tool for temporally regulated gene activiation/inactivation in the mouse. *Dev. Biol. 244*, 305-318 (2002).

169 Potenza, N. *et al*., Hybridase activity of human ribonuclease-1 revealed by a real-time fluorometric assay. *Nucleic Acids Res*. 34 2906-2913 (2006).

170 Weickmann, J.L., Olson, E.M., & Glitz, D.G., Immunological assay of pancreatic ribonuclease in serum as an indicator of pancreatic cancer. *Cancer Res*. 44 1682-1687 (1984).

171 Cormier, S.A. *et al*., Pivotal advance: Eosinophil infiltration of solid tumors is an early and persistent inflammatory host response. *J. Leukoc. Biol*. 79 1131-1139 (2006).

172 Lotfi, R., Lee, J.J., & Lotze, M.T., Eosinophilic granulocytes and damage-associated molecular pattern molecules (DAMPs): Role in the inflammatory response within tumors. *J. Immunother*. 30 16-28 (2007).

173 Munitz, A. & Levi-Schaffer, F., Eosinophils: 'New' roles for 'old' cells. *Allergy* 59 268-275 (2004).

174 Bosslet, K. *et al*., Elucidation of the mechanism enabling tumor selective prodrug monotherapy. *Cancer Res*. 58 1195-1201 (1998).

175 Rutkoski, T.J. & Raines, R.T., Evasion of ribonuclease inhibitor as a determinant of ribonuclease cytotoxicity. *Curr. Pharm. Biotechnol.* 9 185-189 (2008).

176 Leland, P.A., Schultz, L.W., Kim, B.M., & Raines, R.T., Ribonuclease A variants with potent cytotoxic activity. *Proc. Natl. Acad. Sci. USA* 95 10407-10412 (1998).

177 Zheng, A., Kallio, A., & Harkonen, P., Tamoxifen-induced rapid death of MCF-7 breast cancer cells is mediated via extracellularly signal-regulated kinase signaling and can be abrogated by estrogen. *Endocrinology* 148 2764-2777 (2007).

178 Grubbs, F.E., Procedures for Detecting Outlying Observations in Samples. *Technometrics* 11 1-21 (1969).

179 Maderuelo, C., Zarzuelo, A., & Lanao, J.M., Critical factors in the release of drugs from sustained release hydrophilic matrices. *J. Control. Release* 154 2-19 (2011).

180 Manzano, M., Colilla, M., & Vallet-Regi, M., Drug delivery from ordered mesoporous matrices. *Expert Opin. Drug Deli.v* 6 1383-1400 (2009).

181 Rong, X. *et al.*, Applications of polymeric nanocapsules in field of drug delivery systems. *Curr. Drug Discov. Technol.* 8 173-187 (2011).

182 Moodley, K. *et al.*, Oral drug delivery systems comprising altered geometric configurations for controlled drug delivery. *Int. J. Mol. Sci.* 13 18-43 (2012).

183 Pan, J., Chan, S.Y., Lee, W.G., & Kang, L., Microfabricated particulate drug-delivery systems. *Biotechnol. J.* 6 1477-1487 (2011).

184 Lipinski, C.A., Drug-like properties and the causes of poor solubility and poor permeability. *J. Pharmacol. Toxicol. Methods* 44 235-249 (2000).

185 Stegemann, S., Leveiller, F., Franchi, D., de Jong, H., & Linden, H., When poor solubility becomes an issue: From early stage to proof of concept. *Eur. J. Pharm. Sci.* 31 249-261 (2007).

186 Bergenheim, A.T. & Henriksson, R., Pharmacokinetics and pharmacodynamics of estramustine phosphate. *Clin. Pharmacokinet.* 34 163-172 (1998).

187 Sousa, F.J., The bioavailability and therapeutic effectiveness of prednisolone acetate vs. prednisolone sodium phosphate: A 20-year review. *CLAO J* 17 282-284 (1991).

188 Wire, M.B., Shelton, M.J., & Studenberg, S., Fosamprenavir : clinical pharmacokinetics and drug interactions of the amprenavir prodrug. *Clin. Pharmacokinet.* 45 137-168 (2006).

189 Ellis, G.A., McGrath, N.A., Palte, M.J., & Raines, R.T., Ribonuclease-activated cancer prodrug. *ACS Med. Chem. Lett.* 3 268-272 (2012).

190 Lofmark, S., Edlund, C., & Nord, C.E., Metronidazole is still the drug of choice for treatment of anaerobic infections. *Clin. Infect. Dis.* 50 Suppl 1 S16-23 (2010).

191 Metronidazole modified-release tablet multiple-dose bioequivalency study (fed/fasting). G.D. Searle & Co., Protocol No. S13-94-02-014; Report No. S13-95-06-014, 11 July 1995. Integrated clinical and statistical report for the treatment of bacterial vaginosis with metronidazole modified release tablet—a dose duration study. G.D. Searle & Co., Protocol No. N13-95-02-015; Report No. N13-96-06-015, 19 Nov 1996. Integrated clinical and statistical report for the treatment of bacterial vaginosis with metronidazole modified release tablet. G.D. Searle & Co., Protocol No. N13-95-02-017; Report No. N13-96-06-017, 11 Nov 1996.

192 Kasten, M.J., Clindamycin, metronidazole, and chloramphenicol. *Mayo Clin. Proc.* 74 825-833 (1999).

193 Chung, M.C., Bosquesi, P.L., & dos Santos, J.L., A prodrug approach to improve the physico-chemical properties and decrease the genotoxicity of nitro compounds. *Curr. Pharm. Des.* 17 3515-3526 (2011).

194 Ukita, T., Waku, K., Irie, M., & Hoshino, O., Research on pancreatic ribonuclease. I. The inhibition of cyclic phospho-diesterase activity of bovine pancreatic ribonuclease by several substrate analogues. *J. Biochem.* 50 405-415 (1961).

195 Kelemen, B.R., Schultz, L.W., Sweeney, R.Y., & Raines, R.T., Excavating an active site: the nucleobase specificity of ribonuclease A. *Biochemistry* 39 14487-14494 (2000).

196 C.L.S.I. Methods for Antimicrobial Susceptibility Testing of Anaerobic Bacteria; Approved Standard-Seventh Edition. CLSI document M47-A. (Wayne, PA, 2007).

197 Rediguieri, C.F. *et al*., Biowaiver monographs for immediate release solid oral dosage forms: metronidazole. *J. Pharm. Sci*. 100 1618-1627 (2011).

198 Varki, A. *et al*., *Essenstials of Glycobiology, 2nd edition*. (Cold Spring Harbor Laboratory Press, New York, 2009).

199 Ishiguro, M., Hisako, T., Sakakibara, R., Yamaguchi, J., & Aso, Y., A ricin B chain–ribonuclease A hybrid protein. A new tool for introduction of a foreign protein into targeted cells. *J. Fac. Agric. Kyushu Univ*. 46 367-379 (2002).

200 Kumar, A., Hozo, I., Wheatley, K., & Djulbegovic, B., Thalidomide versus bortezomib based regimens as first-line therapy for patients with multiple myeloma: a systematic review. *Am. J. Hematol*. 86 18-24 (2011).

201 Cuchillo, C.M., Nogués, M.V., & Raines, R.T. *Biochemistry* 50 7835-7841 (2011).

202 Marshall, G.R., Feng, J.A., & Kuster, D.J., Back to the future: Ribonuclease A. *Biopolymers* 90 259-277 (2008).

203 D'Alessio, G. & Riordan, J.F. eds., Ribonucleases: Structures and Functions. (Academic Press, New York, 1997).

204 Leland, P.A. & Raines, R.T., Cancer chemotherapy—ribonucleases to the rescue. *Chem. Biol*. 8 405-413 (2001).

205 Rutkoski, T.J., Kurten, E.L., Mitchell, J.C., & Raines, R.T., Disruption of shape-complementarity markers to create cytotoxic variants of ribonuclease A. *J. Mol. Biol*. 354 41-54 (2005).

206 Rutkoski, T.J. & Raines, R.T., Evasion of ribonuclease inhibitor as a determinant of ribonuclease cytotoxicity. *Curr. Pharm. Biotechnol.* 9 185-189 (2008).

207 Futami, J. *et al.*, Intracellular delivery of proteins into mammalian living cells by polyethylenimine-cationization. *J. Biosci. Bioeng.* 99 95-103 (2005).

208 Futami, J. *et al.*, Preparation of potent cytotoxic ribonucleases by cationization: enhanced cellular uptake and decreased interaction with ribonuclease inhibitor by chemical modification of carboxyl groups. *Biochemistry* 40 7518-7524 (2001).

209 Futami, J. *et al.*, Optimum modification for the highest cytotoxicity of cationized ribonuclease. *J. Biochem. (Tokyo)* 132 223-228 (2002).

210 Dube, D.H. & Bertozzi, C.R., Glycans in cancer and inflammation--potential for therapeutics and diagnostics. *Nat. Rev. Drug Discov.* 4 477-488 (2005).

211 Djanashvili, K., Frullano, L., & Peters, J.A., Molecular recognition of sialic acid end groups by phenylboronates. *Chem. Eur. J.* 11 4010-4018 (2005).

212 Otsuka, H., Uchimura, E., Koshino, H., Okano, T., & Kataoka, K., Anomalous binding profile of phenylboronic acid with N-acetylneuraminic acid (Neu5Ac) in aqueous solution with varying pH. *J. Am. Chem. Soc.* 125 3493-3502 (2003).

213 Springsteen, G. & Wang, B., A detailed examination of boronic acid-diol complexation. *Tetrahedron* 58 5291-5300 (2002).

214 Adamczyk-Wozniak, A., Cyranski, M.K., Zubrowska, A., & Sporzynski, A., Benzoxaboroles — Old compounds with new applications. *J. Organomet. Chem.* 694 3533-3541 (2009).

215 Snyder, H.R., Reedy, A.J., & Lennarz, W.J., Synthesis of aromatic boronic acids. Aldehydo boronic acids and a boronic acid analog of tyrosine. *J. Am. Chem. Soc.* 80 835-838 (1958).

216 Torssell, K. Zur kenntnis der arylborsauren .3. bromierung der tolylborsauren nach wohl-ziegler. *Arkiv. Kemi.* 10 507-511 (1957).

217 Bérubé, M., Dowlut, M., & Hall, D.G., Benzoboroxoles as efficient glycopyranoside-binding agents in physiological conditions: Structure and selectivity of complex formation. *J. Org. Chem.* 73 6471-6479 (2008).

218 Dowlut, M. & Dennis, G., An improved class of sugar-binding boronic acids, soluble and capable of complexing glycosides in neutral water. *J. Am. Chem. Soc.* 128 4226-4227 (2006).

219 Mahalingam, A., Geonnotti, A.R., Balzarini, J., & Kiser, P.F., Activity and safety of synthetic lectins based on benzoboroxole-functionalized polymers for inhibition of HIV entry. *Mol. Pharm.* 8 2465-2475 (2011).

220 Wlodawer, A., Svensson, L.A., Sjölin, L., & Gilliland, G.L., Structure of phosphate-free ribonuclease A refined at 1.26 Å. *Biochemistry* 27 2705-2717 (1988).

221 Malisan, F. & Testi, R., The ganglioside GD3 as the Greek goddess Hecate: several faces turned towards as many directions. *IUBMB Life* 57 477-482 (2005).

222 Deutscher, S.L., Nuwayhid, N., Stanley, P., Briles, E.I., & Hirschberg, C.B., Translocation across Golgi vesicle membranes: A CHO glycosylation mutant deficient in CMP-sialic acid transport. *Cell* 39 295-299 (1984).

223 The lost activity is attributable, at least in part, to the modification of the carboxyl group of aspartic acid 121, which is known to contribute to catalysis (Schultz, L. W.; Quirk, D. J.; Raines, R. T. *Biochemistry 37*, 8886–8898, 1998).

224 HOB of benzoxaborole has pK_a 7.34 ± 0.02 (Tomsho, J. W.; Pal, A.; Hall, D. G.; Benkovic, S. J. *ACS Med. Chem. Lett. 3*, 48-52, 2012), preserving most of the anionicity of a typical carboxyl group at pH 7.4.

225 Owens, D.E., 3rd & Peppas, N.A., Opsonization, biodistribution, and pharmacokinetics of polymeric nanoparticles. *Int. J. Pharm.* 307 93-102 (2006).

226 Venturoli, D. & Rippe, B., Ficoll and dextran vs. globular proteins as probes for testing glomerular permselectivity: effects of molecular size, shape, charge, and deformability. *Am. J. Physiol. Renal Physiol.* 288 F605 (2005).

227 Cheng, Y.F. *et al*., Carbohydrate biomarkers for future disease detection and treatment. *Sci. China. Chem*. 53 3-20 (2010).

228 Pal, A., Bérubé, M., & Hall, D.G., Design, synthesis, and screening of a library of peptidyl bis(boroxoles) as oligosaccharide receptors in water: Identification of a receptor for the tumor marker TF antigen disaccharide. *Angew. Chem. Int. Ed*. 49 1492-1495 (2010).

229 Smith, B.D., Soellner, M.B., & Raines, R.T., Potent inhibition of ribonuclease A by oligo(vinylsulfonic acid). *J. Biol. Chem*. 278 20934-20938 (2003).

230 Sela, M., Anfinsen, C.B., & Harrington, W.F., The correlation of ribonuclease activity with specific aspects of tertiary structure. *Biochim. Biophys. Acta* 26 502-512 (1957).

231 Roehrl, M.H., Wang, J.Y., & Wagner, G., A general framework for development and data analysis of competitive high-throughput screens for small-molecule inhibitors of protein-protein interactions by fluorescence polarization. *Biochemistry* 43 16056-16066 (2004).

232 Kelemen, B.R. *et al*., Hypersensitive substrate for ribonucleases. *Nucleic Acids Res*. 27 3696-3701 (1999).

233 Leland, P.A., Schultz, L.W., Kim, B.M., & Raines, R.T., Ribonuclease A variants with potent cytotoxic activity. *Proc. Natl. Acad. Sci. USA* 95 10407-10412 (1998).

234 Kehoe, J.W. *et al*., Tyrosylprotein sulfotransferase inhibitors generated by combinatorial target-guided ligand assembly. *Bioorg. Med. Chem. Lett*. 12 329-332 (2002).

235 Armstrong, J.I. *et al*., A library approach to the generation of bisubstrate analogue sulfotransferase inhibitors. *Org. Lett*. 3 2657-2660 (2001).

236 Armstrong, J.I. *et al*., Discovery of carbohydrate sulfotransferase inhibitors from a kinase-directed library. *Angew. Chem. Int. Ed*. 39 1303-1306 (2000).

237 Hang, H.C. *et al*., Small molecule inhibitors of mucin-type *O*-linked glycosylation from a uridine-based library. *Chem. Biol*. 11 337-345 (2004).

238 Sletten, E.M. & Bertozzi, C.R., From mechanism to mouse: A tale of two bioorthogonal reactions. *Acc. Chem. Res.* 44 666-676 (2011).

239 Boyce, M. & Bertozzi, C.R., Bringing chemistry to life. *Nat. Methods* 8 638-642 (2011).

240 Chang, P.V. *et al.*, Copper-free click chemistry in living animals. *Proc. Natl. Acad. Sci. USA* 107 1821-1826 (2010).

241 Abraham, S.A. *et al.*, The liposomal formulation of doxorubicin. *Methods Enzymol.* 391 71-97 (2005).

242 O'Brien, M.E. *et al.*, Reduced cardiotoxicity and comparable efficacy in a phase III trial of pegylated liposomal doxorubicin HCl (CAELYX/Doxil) versus conventional doxorubicin for first-line treatment of metastatic breast cancer. *Ann. Oncol.* 15 440-449 (2004).

243 Tomsho, J.W., Pal, A., Hall, D.G., & Benkovic, S.J., Ring structure and aromatic substituent dffects on the pK_a of the benzoxaborole pharmacophore. *ACS Med. Chem. Lett.* 3 48-52 (2012).

244 Lazarou, J., Pomeranz, B.H., & Corey, P.N., Incidence of adverse drug reactions in hospitalized patients: A meta-analysis of prospective studies. *JAMA* 279 1200-1205 (1998).

245 Lasser, K.E. *et al.*, Timing of new black box warnings and withdrawals for prescription medications. *JAMA* 287 2215-2220 (2002).

246 Weinstein, J.N., Yoshikami, S., Henkart, P., Blumenthal, R., & Hagins, W.A., Liposome-cell interaction: transfer and intracellular release of a trapped fluorescent marker. *Science* 195 489-492 (1977).

247 Szoka, F., Jacobson, K., Derzko, Z., & Papahadjopoulos, D., Fluorescence studies on the mechanism of liposome-cell interactions in vitro. *Biochim. Biophys. Acta* 600 1-18 (1980).

248 Friend, D.S., Papahadjopoulos, D., & Debs, R.J., Endocytosis and intracellular processing accompanying transfection mediated by cationic liposomes. *Biochim. Biophys. Acta* 1278 41-50 (1996).

249 Zhou, X. & Huang, L., DNA transfection mediated by cationic liposomes containing lipopolylysine: characterization and mechanism of action. *Biochim. Biophys. Acta* 1189 195-203 (1994).

250 Labat-Moleur, F. *et al*., An electron microscopy study into the mechanism of gene transfer with lipopolyamines. *Gene Ther*. 3 1010-1017 (1996).

251 Wrobel, I. & Collins, D., Fusion of cationic liposomes with mammalian cells occurs after endocytosis. *Biochim Biophys Acta* 1235 296-304 (1995).

252 Stegmann, T. & Legendre, J.Y., Gene transfer mediated by cationic lipids: lack of a correlation between lipid mixing and transfection. *Biochim. Biophys. Acta* 1325 71-79 (1997).

253 Noguchi, A., Furuno, T., Kawaura, C., & Nakanishi, M., Membrane fusion plays an important role in gene transfection mediated by cationic liposomes. *FEBS Lett*. 433 169-173 (1998).

254 Duzgune, scedil, & Nir, S., Mechanisms and kinetics of liposome-cell interactions. *Adv. Drug Deliv. Rev*. 40 3-18 (1999).

255 Szoka, F.C., Jr., Jacobson, K., & Papahadjopoulos, D., The use of aqueous space markers to determine the mechanism of interaction between phospholipid vesicles and cells. *Biochim. Biophys. Acta* 551 295-303 (1979).

256 Duzgunes, N., Straubinger, R.M., Baldwin, P.A., Friend, D.S., & Papahadjopoulos, D., Proton-induced fusion of oleic acid-phosphatidylethanolamine liposomes. *Biochemistry* 24 3091-3098 (1985).

257 Connor, J., Yatvin, M.B., & Huang, L., pH-sensitive liposomes: acid-induced liposome fusion. *Proc. Natl. Acad. Sci. USA* 81 1715-1718 (1984).

258 Ellens, H., Bentz, J., & Szoka, F.C., pH-induced destabilization of phosphatidylethanolamine-containing liposomes: role of bilayer contact. *Biochemistry* 23 1532-1538 (1984).

259 Straubinger, R.M., Duzgunes, N., & Papahadjopoulos, D., pH-sensitive liposomes mediate cytoplasmic delivery of encapsulated macromolecules. *FEBS Lett*. 179 148-154 (1985).

260 Connor, J. & Huang, L., Efficient cytoplasmic delivery of a fluorescent dye by pH-sensitive immunoliposomes. *J. Cell Biol*. 101 582-589 (1985).

261 Chu, C.J., Dijkstra, J., Lai, M.Z., Hong, K., & Szoka, F.C., Efficiency of cytoplasmic delivery by pH-sensitive liposomes to cells in culture. *Pharm. Res*. 7 824-834 (1990).

262 Straubinger, R.M., Hong, K., Friend, D.S., & Papahadjopoulos, D., Endocytosis of liposomes and intracellular fate of encapsulated molecules: encounter with a low pH compartment after internalization in coated vesicles. *Cell* 32 1069-1079 (1983).

263 Straubinger, R.M., Papahadjopoulos, D., & Hong, K., Endocytosis and intracellular fate of liposomes using pyranine as a probe. *Biochemistry* 29 4929-4939 (1990).

264 Lee, K.D., Nir, S., & Papahadjopoulos, D., Quantitative analysis of liposome-cell interactions in vitro: Rate constants of binding and endocytosis with suspension and adherent J774 cells and human monocytes. *Biochemistry* 32 889-899 (1993).

265 Wojcik, S.M. & Brose, N., Regulation of membrane fusion in synaptic excitation-secretion coupling: speed and accuracy matter. *Neuron* 55 11-24 (2007).

266 Borst, J.G. & Sakmann, B., Calcium influx and transmitter release in a fast CNS synapse. *Nature* 383 431-434 (1996).

267 Sabatini, B.L. & Regehr, W.G., Timing of neurotransmission at fast synapses in the mammalian brain. *Nature* 384 170-172 (1996).

268 McNew, J. *et al*., Close is not enough: SNARE-dependent membrane fusion requires an active mechanism that transduces force to membrane anchors. *J. Cell Biol*. 150 105 (2000).

269 Fasshauer, D., Structural insights into the SNARE mechanism. *Biochim. Biophys. Acta* 1641 87-97 (2003).

270 McNew, J.A., Weber, T., Engelman, D.M., Sollner, T.H., & Rothman, J.E., The length of the flexible SNAREpin juxtamembrane region is a critical determinant of SNARE-dependent fusion. *Mol. Cell* 4 415-421 (1999).

271 Wang, Y., Dulubova, I., Rizo, J., & Sudhof, T.C., Functional analysis of conserved structural elements in yeast syntaxin Vam3p. *J Biol Chem* 276 28598-28605 (2001).

272 Grote, E., Baba, M., Ohsumi, Y., & Novick, P.J., Geranylgeranylated SNAREs are dominant inhibitors of membrane fusion. *J. Cell Biol.* 151 453-466 (2000).

273 Stengel, G., Zahn, R., & Hook, F., DNA-induced programmable fusion of phospholipid vesicles. *J. Am. Chem. Soc.* 129 9584-9585 (2007).

274 Marsden, H.R., Korobko, A., & Kros, A., presented at the Protein and Peptide Engineering for Therapeutic and Functional Materials, Boston, MA, 2007 (unpublished).

275 Samad, A., Sultana, Y., & Aqil, M., Liposomal drug delivery systems: an update review. *Curr. Drug deliv.* 4 297-305 (2007).

276 Hobbs, S.K. *et al.*, Regulation of transport pathways in tumor vessels: role of tumor type and microenvironment. *Proc. Natl. Acad. Sci. USA* 95 4607-4612 (1998).

277 Maeda, H. & Matsumura, Y., Tumoritropic and lymphotropic principles of macromolecular drugs. *Crit Rev Ther Drug* 6 193-210 (1989).

278 Seymour, L.W., Passive tumor targeting of soluble macromolecules and drug conjugates. *Crit. Rev. Ther. Drug* 9 135-187 (1992).

279 Yuan, F. *et al.*, Microvascular permeability and interstitial penetration of sterically stabilized (stealth) liposomes in a human tumor xenograft. *Cancer Res.* 54 3352-3356 (1994).

280 Allen, T.M., Brandeis, E., Hansen, C.B., Kao, G.Y., & Zalipsky, S., A new strategy for attachment of antibodies to sterically stabilized liposomes resulting in efficient targeting to cancer cells. *Biochim. Biophys. Acta* 1237 99-108 (1995).

281 Zelphati, O. & Szoka, F.C., Liposomes as a carrier for intracellular delivery of antisense oligonucleotides: a real or magic bullet? *J. Control. Release* 41 99-119 (1996).

282 Park, J.W. *et al.*, Anti-HER2 immunoliposomes: Enhanced efficacy attributable to targeted delivery. *Clin. Cancer Res.* 8 1172-1181 (2002).

283 Park, J.W. *et al.*, Tumor targeting using anti-her2 immunoliposomes. *J. Control. Release* 74 95-113 (2001).

284 Sapra, P. & Allen, T.M., Ligand-targeted liposomal anticancer drugs. *Prog. Lipid Res.* 42 439-462 (2003).

285 Barenholz, Y., Liposome application: Problems and prospects. *Curr. Opin. Colloid In.* 6 66-77 (2001).

286 Harding, J.A., Engbers, C.M., Newman, M.S., Goldstein, N.I., & Zalipsky, S., Immunogenicity and pharmacokinetic attributes of poly(ethylene glycol)-grafted immunoliposomes. *Biochim. Biophys. Acta* 1327 181-192 (1997).

287 Koning, G.A., Kamps, J.A., & Scherphof, G.L., Interference of macrophages with immunotargeting of liposomes. *J. Liposome Res.* 12 107-119 (2002).

288 Lee, R.J. & Low, P.S., Folate-mediated tumor cell targeting of liposome-entrapped doxorubicin in vitro. *Biochim. Biophys. Acta* 1233 134-144 (1995).

289 Saul, J.M., Annapragada, A., Natarajan, J.V., & Bellamkonda, R.V., Controlled targeting of liposomal doxorubicin via the folate receptor in vitro. *J. Control. Release* 92 49-67 (2003).

290 Snyder, F., Blank, M.L., & Morris, H.P., Occurrence and nature of O-alkyl and O-alk-I-enyl moieties of glycerol in lipids of Morris transplanted hepatomas and normal rat liver. *Biochim. Biophys. Acta* 176 502-510 (1969).

291 Snyder, F. & Wood, R., Alkyl and alk-1-enyl ethers of glycerol in lipids from normal and neoplastic human tissues. *Cancer Res*. 29 251-257 (1969).

292 Brochez, V., Van Heuverswyn, D., Diniz, J.A., De Potter, C.R., & Van den Eeckhout, E.G., Cellular uptake and retention measurements of alkylphosphocholines in the SK-BR-3 breast cancer and Molt-4 leukemia cell line using capillary gas chromatography. *Lipids* 34 511-516 (1999).

293 Geilen, C.C. *et al*., Phospholipid analogues: side chain-and polar head group-dependent effects on phosphatidylcholine biosynthesis. *J. Lipid Res*. 35 625-632 (1994).

294 Kotting, J., Berger, M.R., Unger, C., & Eibl, H., Alkylphosphocholines: influence of structural variation on biodistribution at antineoplastically active concentrations. *Cancer Chemoth. Pharm*. 30 105-112 (1992).

295 Pinchuk, A.N. *et al*., Synthesis and structure-activity relationship effects on the tumor avidity of radioiodinated phospholipid ether analogues. *J. Med. Chem*. 49 2155-2165 (2006).

296 Available at http://cellectar.com/sciences/.

297 Micklefield, J., Backbone modification of nucleic acids: synthesis, structure and therapeutic applications. *Curr. Med. Chem*. 8 1157-1179 (2001).

298 Chernomordik, L.V. & Kozlov, M.M., Mechanics of membrane fusion. *Nat Struct Mol Biol* 15 675-683 (2008).

299 Hu, C. *et al*., Fusion of cells by flipped SNAREs. *Science* 300 1745-1749 (2003).

300 Burns, J.A., Butler, J.C., Moran, J., & Whitesides, G.M., Selective reduction of disulfides by tris(2-carboxyethyl)phosphine. *J. Org. Chem*. 56 2648-2650 (1991).

301 Cleland, W.W., Dithiothreitol, a new protective reagent for SH groups. *Biochemistry* 3 480-482 (1964).

302 Cline, D.J. *et al*., New water-soluble phosphines as reductants of peptide and protein disulfide bonds: reactivity and membrane permeability. *Biochemistry* 43 15195-15203 (2004).

303 Getz, E.B., Xiao, M., Chakrabarty, T., Cooke, R., & Selvin, P.R., A comparison between the sulfhydryl reductants tris(2-carboxyethyl)phosphine and dithiothreitol for use in protein biochemistry. *Anal. Biochem*. 273 73-80 (1999).

304 Gilbert, H.F., Thiol/disulfide exchange equilibria and disulfide bond stability. *Methods Enzymol*. 251 8-28 (1995).

305 Jocelyn, P.C., *Biochemistry of the SH Group: The Occurence, Chemical Properties, Metabolism and Biological Function of Thiols and Disulphides* (Academic Press, London, UK, 1972).

306 Lamoureux, G.V. & Whitesides, G.M., Synthesis of dithiols as reducing agents for disulfides in neutral aqueous-solution and comparison of reduction potentials. *J. Org. Chem*. 58 633-641 (1993).

307 Lees, W.J., Singh, R., & Whitesides, G.M., meso-2,5-dimercapto-N,N,N',N'-tetramethyladipamide: A readily available, kinetically rapid reagent for the reduction of disulfides in aqueous solution. *J. Org. Chem*. 56 7328-7331 (1991).

308 Ranganathan, S. & Jayaraman, N., Highly efficient propane-1,3-dithiol mediated thiol–disulfide interchange—a facile and clean methodology for S–S reduction in peptides. *Chem. Commun*. 934-936 (1991).

309 Singh, R., Lamoureux, G.V., Lees, W.J., & Whitesides, G.M., Reagents for rapid reduction of disulfide bonds. *Methods Enzymol*. 251 167-173 (1995).

310 Singh, R. & Whitesides, G.M., Reagents for rapid reduction of native disulfide bonds in proteins. *Bioorg. Chem*. 22 109-115 (1994).

311 Smith, D.J., Maggio, E.T., & Kenyon, G.L., Simple alkanethiol groups for temporary blocking of sulfhydryl groups of enzymes. *Biochemistry* 14 766-771 (1975).

312 Whitesides, G.M., Lilburn, J.E., & Szajewski, R.P., Rates of thiol-disulfide interchange reactions between mono- and dithiols and Ellmans reagent. *J. Org. Chem.* 42 332-338 (1977).

313 Shaked, Z., Szajewski, R.P., & Whitesides, G.M., Rates of thiol-disulfide interchange reactions involving proteins and kinetic measurements of thiol pK_a values. *Biochemistry* 19 4156-4166 (1980).

314 Keire, D.A., Strauss, E., Guo, W., Noszal, B., & Rabenstein, D.L., Kinetics and equilibria of thiol disulfide interchange reactions of selected biological thiols and related molecules with oxidized glutathione. *J. Org. Chem.* 57 123-127 (1992).

315 Rothwarf, D.M. & Scheraga, H.A., Equilibrium and kinetic constants for the thiol disulfide interchange reaction between glutathione and dithiothreitol. *Proc. Natl. Acad. Sci. USA* 89 7944-7948 (1992).

316 Fernandes, P.A. & Ramos, M.J., Theoretical insights into the mechanism for thiol/disulfide exchange. *Chem.—Eur. J.* 10 257-266 (2004).

317 Rosenfield, R.E., Parthasarathy, R., & Dunitz, J.D., Directional preferences of nonbonded atomic contacts with divalent sulfur .1. Electrophiles and nucleophiles. *J. Am. Chem. Soc.* 99 4860-4862 (1977).

318 Houk, J. & Whitesides, G.M., Structure reactivity relations for thiol disulfide interchange. *J. Am. Chem. Soc.* 109 6825-6836 (1987).

319 Snyder, J.P. & Carlsen, L., Lone pair-lone pair interactions in unsymmetrical systems: RSSR vs. RSOR *J. Am. Chem. Soc.* 99 2931-2942 (1977).

320 (Tris(2-carboxyethyl)phosphine) (TCEP) is more potent than DTT at reducing disulfide bonds between small molecules, but not within proteins.

321 Carbamate derivatives of DTBA are known. (a) Kessler, P.; Servent, D.; Hirth, C. *Tetrahedron Lett. 35*, 7237-7240 (1994). (b) Servent, D.; Ménez, A.; Kessler, P. *FEBS Lett. 360*, 261-265 (1995).

322 Mitsunobu, O. & Masahiko, E., Preparation of carboxylic esters and phosphoric esters by the activation of alcohols. *Bull. Chem. Soc. Jpn.* 44 3427-3430 (1971).

323 Jencks, W.P. & Salvesen, K. *J. Am. Chem. Soc.* 93 4433-4436 (1971).

324 Connett, P.H. & Wetterhahn, K.E., Reaction of chromium(VI) with thiols: pH dependence of chromium(VI) thio ester formation. *J. Am. Chem. Soc.* 108 1842-1847 (1986).

325 Lees, W.J. & Whitesides, G.M., Equilibrium constants for thiol-disulfide interchange reactions: A coherent, corrected set. *J. Org. Chem.* 58 642-647 (1993).

326 Woycechowsky, K.J., Wittrup, K.D., & Raines, R.T., A small-molecule catalyst of protein folding in vitro and in vivo. *Chem. Biol.* 6 871-879 (1999).

327 Benesch, R.E. & Benesch, R., The acid strength of the -SH group in cysteine and related compounds. *J. Am. Chem. Soc.* 77 5877-5881 (1955).

328 Singh, R., Blattler, W.A., & Collinson, A.R., An amplified assay for thiols based on reactivation of papain. *Anal. Biochem.* 213 49-56 (1993).

329 Roberts, D.D., Lewis, S.D., Ballou, D.P., Olson, S.T., & Shafer, J.A., Reactivity of small thiolate anions and cysteine-25 in papain toward methyl methanethiosulfonate. *Biochemistry* 25 5595-5601 (1986).

330 Schechter, I. & Berger, A., On the size of the active site in proteases. I. Papain. *Biochem. Biophys. Res. Commun.* 27 157-162 (1967).

331 Pickersgill, R.W., Harris, G.W., & Garman, E., Structure of monoclinic papain at 1.60 Å resolution. *Acta Crystallogr., Sect. B* 48 59-67 (1992).

332 Hurne, A.M., Chai, C.L.L., & Waring, P., Inactivation of rabbit muscle creatine kinase by reversible formation of an internal disulfide bond induced by the fungal toxin gliotoxin. *J. Biol. Chem.* 275 25202-25206 (2000).

333 Chen, L.H., Borders, C.L., Vasquez, J.R., & Kenyon, G.L., Rabbit muscle creatine kinase: consequences of the mutagenesis of conserved histidine residues. *Biochemistry* 35 7895-7902 (1996).

334 Putney, S. *et al*., Rabbit muscle creatine-phosphokinase - Cdna cloning, primary structure, and detection of human homologs. *J. Biol. Chem*. 259 4317-4320 (1984).

335 Rao, J.K.M., Bujacz, G., & Wlodawer, A., Crystal structure of rabbit muscle creatine kinase *FEBS Lett*. 439 133-137 (1998).

336 Woycechowsky, K.J., Hook, B.A., & Raines, R.T., Catalysis of protein folding by an immobilized small-molecule dithiol. *Biotechnol. Progr*. 19 1307-1314 (2003).

337 Bienvenu, C., Greiner, J., Vierling, P., & Di Giorgio, C., Convenient supported recyclable material based on dihydrolipoyl-residue for the reduction of disulfide derivatives. *Tetrahedron Lett*. 51 3309-3311 (2010).

338 Amos, R.A. & Fawcett, S.M., Reductive cleavage of aromatic disulfides using a polymer-supported phosphine reagent. *J. Org. Chem*. 49 2637-2639 (1984).

339 Kessler, P., Servent, D., & Hirth, C., Design and synthesis of a novel site-directed reducing agent for the disulfide bond involved in the acetylcholine binding site of the AChoR. *Tetrahedron Lett*. 39 7237-7240 (1994).

340 Ellman, G.L., Tissue sulfhydryl groups. *Arch. Biochem. Biophys*. 82 70-77 (1958).

341 Riddles, P.W., Blakely, R.L., & Zerner, B., Ellman's reagent: 5,5'-Dithiobis(2-nitrobenzoic acid)—a reexamination. *Anal. Biochem*. 94 75-81 (1979).

342 Riddles, P.W., Blakely, R.L., & Zerner, B., Reassessment of Ellman's reagent. *Methods Enzymol*. 91 49-60 (1983).

343 Simpson, R.J., *Purifying Proteins for Proteomics: A Laboratory Manual*. (Cold Spring Harbor Laboratory Press, Cold Spring Harbor, NY, 2004).

344 Singh, R. & Whitesides, G.M., A reagent for reduction of disulfide bonds in proteins that reduces disulfide bonds faster than does dithiothreitol. *J. Org. Chem.* 56 2332-2337 (1991).